

2007

Petrology, Structural Geology, and Significance of Mn-Andalusite from the Lower Ortega Quartzite, Tusas MTS., NM, USA

Nancy A. Price

University of Massachusetts Amherst

Follow this and additional works at: <https://scholarworks.umass.edu/theses>



Part of the [Geology Commons](#), and the [Other Earth Sciences Commons](#)

Price, Nancy A., "Petrology, Structural Geology, and Significance of Mn-Andalusite from the Lower Ortega Quartzite, Tusas MTS., NM, USA" (2007). *Masters Theses 1911 - February 2014*. 2578.

Retrieved from <https://scholarworks.umass.edu/theses/2578>

This thesis is brought to you for free and open access by ScholarWorks@UMass Amherst. It has been accepted for inclusion in Masters Theses 1911 - February 2014 by an authorized administrator of ScholarWorks@UMass Amherst. For more information, please contact scholarworks@library.umass.edu.

PETROLOGY, STRUCTURAL GEOLOGY, AND SIGNIFICANCE OF MN-ANDALUSITE FROM
THE LOWER ORTEGA QUARTZITE, TUSAS MTS., NM, USA

A Thesis Presented

by

NANCY A. PRICE

Submitted to the Graduate School of the
University of Massachusetts Amherst in partial fulfillment
of the requirements for the degree of

MASTERS OF SCIENCE

August 2007

Geosciences

PETROLOGY, STRUCTURAL GEOLOGY, AND SIGNIFICANCE OF MN-ANDALUSITE FROM
THE LOWER ORTEGA QUARTZITE, TUSAS MTS., NM, USA

A Thesis Presented

by

Nancy A. Price

Approved as to style and content by:

Michael L. Williams, Chair

Michael J. Jercinovic, Member

Sheila Seaman, Member

Michael L. Williams, Department Head
Department of Geosciences

ABSTRACT

PETROLOGY, STRUCTURAL GEOLOGY, AND SIGNIFICANCE OF MN-ANDALUSITE FROM THE LOWER ORTEGA QUARTZITE, TUSAS MTS., NM, USA

AUGUST 2007

NANCY A. PRICE, B.S., THE RICHARD STOCKTON COLLEGE OF NJ

M.S., UNIVERSITY OF MASSACHUSETTS AMHERST

Directed by: Professor Michael L. Williams

The Proterozoic syn-orogenic supra-crustal package exposed in the Tusas Mountain Range in northern New Mexico includes the anomalously thick, clean, ultramature Ortega Formation quartzite (Bauer and Williams, 1989). A unique Mn-bearing horizon spans the basal contact of the quartzite and contains Mn-andalusite, quartz, hematite, rutile, zircon, monazite, phyllosilicates, and locally kyanite and garnet in intermittent aluminous, hematite-bearing layers, on the surface of cross-beds, concentrated in high strain zones, and on cleavage planes. Large-scale Mn zoning in Mn-andalusite results from a decrease in Mn content away from localized Mn highs (X_{Mn} of up to 0.76) that commonly correspond with the location of high-Mn core regions. High Mn core regions are included in Mn-andalusite, preserve some of the earliest fabrics, and are associated with sedimentary structures (i.e. cross beds and graded beds). Both hematite and rutile from the Mn horizon are rich in trace elements, and hematite contains zones of rutile mineralization that create patchy/mottled, wormy, cross-hatched, and/or banded textures within the hematite that could be linked with oxidation-exsolution textures in ilmenite and spinel. The Mn horizon may be a result of (1) the formation of an Fe-Mn oxyhydroxide crust through extensive lateritic weathering of the metavolcanic units and/or (2) the chemical deposition of Fe and Mn phases in an oxygen stratified enriched basin environment.

Mn-andalusite preserves subtle textures in the Mn distribution and interference colors of the birefringence that can be used to understand mineral replacement and microstructural relationships in otherwise an well-annealed quartzite. A feathery texture that resembles the

crystal habit of a phyllosilicate, such as pyrophyllite, locally preserves crenulation cleavages. High-Mn halos around kyanite and localized areas of low Mn content in Mn-andalusite that mimic crystal shapes together represent areas of kyanite replacement.

The general tectonic histories preserved in the Mn-andalusite layer of the Hopewell Lake-Jawbone Mountain area, Quartzite Peak, and Kiowa Mountain of the Tusas Mountains include the growth of an M1 mineral assemblage in association with D1 (kyanite and/or pyrophyllite), the growth of an M2 assemblage post-D2 (kyanite and/or Mn-andalusite), and the growth of an M3 assemblage syn-D3 (a second generation of kyanite and/or Mn-andalusite). In the Hopewell Lake-Jawbone Mountain region, Mn-andalusite of the Hopewell anticline preserves phyllosilicate defined crenulation cleavages while the Jawbone syncline is dominated by a history of only kyanite growth suggesting a metamorphic divide between the anticline and syncline that could be a result of the movement along a late-stage D3 fault at or near Route 64. At Kiowa Mountain, high-Mn halos and low Mn regions suggest that Mn-andalusite replaced kyanite when changing P-T conditions during M2 lead to an Mn-andalusite-only M2 assemblage. Textures preserved in the Mn-distribution and interference colors of Mn-andalusite are an essential tool for understanding the structural and metamorphic histories of the Mn horizon and the Ortega Formation quartzite.

TABLE OF CONTENTS

	Page
DEDICATION.....	iii
ACKNOWLEDGEMENTS.....	iv
ABSTRACT.....	v
LIST OF TABLES.....	ix
LIST OF FIGURES.....	x
 CHAPTER	
1. INTRODUCTION.....	1
2. BACKGROUND.....	4
Stratigraphy of Proterozoic Supracrustal Rocks in the Tusas Mountains.....	4
The Vadito Group.....	6
The Ortega Formation Quartzite.....	7
Mn Horizon in the Tusas Mountains.....	8
Mineralogy, Crystal Chemistry, Petrology, and Occurrences of Mn-andalusite.....	9
Regional Structure.....	17
Regional Metamorphic Petrology.....	18
Interpreted Proterozoic Tectonic History of the Tusas Mountains.....	20
3. METHODS.....	24
Field Methods and Sample Collection.....	24
Thin Section Preparation and Analysis.....	25
Electron Microprobe X-Ray Mapping and Compositional Analysis.....	25
Pressure-Temperature Calculations.....	26
4. STRUCTURAL GEOLOGY.....	27
General Structure of the Tusas Mountains.....	27
Fabrics.....	27
S0.....	27
S1/F1/L1.....	29
S2/F2.....	29
S3/F3.....	31
S2/S3 - Composite Fabric.....	31
Hopewell Lake-Jawbone Mountain Area.....	36
Quartzite Peak.....	41
Kiowa Mountain.....	48
Map-Scale Folds.....	48
Anomalous Areas of Structural Importance.....	51
Discussion of the Structure	54

Hopewell Lake-Jawbone Mountain Area.....	54
Quartzite Peak.....	62
Kiowa Mountain.....	63
5. METAMORPHIC PETROLOGY.....	66
General Metamorphic History of the Tusas Mountains.....	66
Hopewell Lake-Jawbone Mountain Area.....	66
The Jawbone Syncline.....	67
The Hopewell Anticline.....	69
Discussion of the Hopewell Lake-Jawbone Mountain Area.....	75
Quartzite Peak and Kiowa Mountain.....	77
Pressure-Temperature Calculations.....	84
Summary of the Metamorphic Petrology of Quartzite Peak.....	84
6. MN HORIZON AND MN-ANDALUSITE MINERALIZATION	88
Field Observations.....	88
Manganese Zoning in Mn-andalusite.....	93
High-Mn Core Regions.....	95
Hematite and Rutile Mineralization.....	103
Variations Within the Mn-andalusite Layer.....	113
Origin of the Mn horizon	114
Textures Preserved in the Birefringence of Mn-Andalusite.....	118
Feathery Texture.....	118
High-Mn Halos and Low-Mn Shapes.....	123
Microstructural and Petrologic Analysis of the Mn-andalusite layer.....	128
Hopewell Lake-Jawbone Mountain Area.....	128
Kiowa Mt.....	135
7. CONCLUSIONS.....	138
APPENDICES	
A. SAMPLE LOCATIONS AND DESCRIPTIONS.....	144
B. PRESSURE-TEMPERATURE CALCULATIONS.....	145
C. QUARTZITE DEPOSITION AND STRATIGRAPHY.....	146
BIBLIOGRAPHY.....	154

LIST OF TABLES

Table	Page
2.1 Survey of Mn-andalusite and kanonaite compositions reported in the literature.....	14
2.2 Survey of Mn-andalusite and kanonaite occurrences from the literature.....	16
6.1 Composition of High-Mn Core Regions.....	97
6.2 Composition of hematite and rutile from the Mn-andalusite layer of the Ortega Formation.....	106
6.3 Composition of hematite from the Vadito Group transitional package.....	107
6.4 Mn-andalusite mineral reactions.....	124

LIST OF FIGURES

Figure	Page
1.1. Map of the southwestern USA showing the location of exposed Precambrian crust in relation to province boundaries.....	3
2.1 Map showing the Mn horizon in the Tusas Mountain range and other basement-cored uplifts of Paleoproterozoic age.....	10
2.2. Andalusite contains cross-linked single chains of edge-sharing Al octahedra (Al ₁) and double chains of alternating Al trigonal bipyramids	11
2.3. P-T diagram showing the effects Mn ³⁺ have on the placement of the kyanite + andalusite and andalusite + sillimanite reaction lines	13
2.4. Down plunge projection of a north/south transect of the Tusas Mountains showing the interpreted relationship between S1/F1, S2/F2	19
2.5. Isograd map of the Tusas Mountains showing an increase in metamorphic grade from the NW to SE (a), and a schematic drawing showing.....	21
2.6. P-T loops for Proterozoic rocks from the southwestern USA; paths highlighted in B specifically apply to the Tusas Mountains	22
4.1. A lithologic map of the Tusas Mountains showing the location of the Hopewell Lake-Jawbone Mountain area, Quartzite Peak, and Kiowa Mountain	28
4.2. F1 (a,b) and S1 (c) are preserved in the distribution of fine-grained hematite in samples from Mn-andalusite layer of the Hopewell anticline	30
4.3. Discrete Mn-andalusite-rich S2 cleavage planes disrupt the S0/S1 composite surface in this sample from the Hopewell Lake-Jawbone Mountain area	32
4.4. F3 crenulations of S2 in outcrop fold S2 in such a way as to maintain one limb in the NW-SE S2 orientation and transpose the other	33
4.5. F3 crenulation folds form on the grain scale through the reorientation of oxides into S3 (bottom right) and may lead to the transposition of S2 into S3	34
4.6. The S2/S3 composite fabric is defined in thin section by andalusite quadrilaterals with edges subparallel to S2 and S3 and the corners of which	35
4.7. Elongate hematite crystals aligned in S0/S1/S2 are crenulated by F3 (top) forming quadrilateral shaped islands (bottom) the edges of which	37
4.8. Lithologic map of the Hopewell Lake-Jawbone Mountain area showing the strike and dip of (a) S0/S1, (b) S2, and (C) S3.....	38
4.9. Hematite inclusion trails that define S1, S2, and S3 create a complex oxide pattern in samples from the Hopewell Lake-Jawbone Mountain area.....	42
4.10. Optically-continuous andalusite crystals (b) in P06NM12A preserve evidence for S2 development and F2 folding. Later D3 has strained andalusite.....	44

4.11. The progressive evolution of fabrics at Quartzite Peak produces a sigmoid shape from the combination of S1, S2, and S3 that can be.....	45
4.12. Quartzite Peak is dominated in outcrop by a steep to subvertical, northwest striking fabric that appears axial planar to tight to isoclinal folds	46
4.13. The S2/S3 composite fabric is composed of “waves” and incomplete quadrilateral-like shapes in thin section that are defined by.....	47
4.14. An attempt to interpret the evolution of the hematite-defined S1, S2, and S3 fabrics in a sample from the Mn-andalusite layer at Kiowa Mountain.....	49
4.15. Bedding in the Ortega Formation quartzite defines the core of the large map-scale Kiowa syncline and the transition from a northwest.....	52
4.16. This thin section from the D3 high strain zone in the Maquinita Formation granodiorite shows the interaction of S2 and S3 to create the	55
4.17. Map of the Hopewell Lake-Jawbone Mountain area showing the location of inferred structural features. D3 faults and high strain zones are shown.....	57
4.18. An interpreted structural history for the Hopewell Lake-Jawbone Mountain area (actual location of D1 thrust is unknown).....	58
4.19. The deformation of F2 during D3 created isoclinal upright folds and a wavy composite fabric that represents the folded axial plane of the F2 fold.....	64
4.20. D3 led to the steepening of S2 and F2 through the transposition of S2 into S3 (bottom) and the F3 crenulation folding of S2 (top).	65
5.1. The aluminous, hematite-bearing layers of the Jawbone syncline include quartz, kyanite, hematite, and chloritoid (blue mineral). F2 and F3 folds.....	68
5.2. Interpreted metamorphic history of Hopewell Lake-Jawbone Mountain area.....	70
5.3. The interpreted location of the Hopewell anticline and the Jawbone syncline in P-T space during M2 and M3 (left). At the end of D3, Jawbone.....	71
5.4. Lithologic map of the Hopewell Lake-Jawbone Mountain area showing the boundaries between metamorphic mineral zones.....	73
5.5. Late kyanite overgrows early kyanite in the samples from the kyanite + andalusite assemblage of Hopewell anticline suggesting more.....	74
5.6. A schematic diagram showing the timing of deformation and andalusite growth in the Ortega Formation quartzite of the Hopewell anticline.....	76
5.7. Hematite inclusions trails in kyanite preserve S1 in the cores of F2 folds (left) and in remnant kyanite crystals that are aligned subparallel to S0/S1.....	78
5.8. Mn-andalusite at Quartzite Peak displays a mottled texture (a,b) with only small, rare, localized zones of higher Mn (b). Textural relationships.....	79

5.9. Undeformed Mn-andalusite crystals overgrow F2 folds and include hematite and kyanite aligned in S2 (top) and in rare instances, Mn-andalusite.....	80
5.10. In places, kyanite and Mn-andalusite appear intergrown. The black bars in the Al X-ray map represent the traverses of EMP.....	82
5.11. Late kyanite overgrows early kyanite at Quartzite Peak (a) and Kiowa Mountain (b,c).....	83
5.12. Equation four and figure 15 of Grambling and Williams (1985) were used to calculate a P-T estimate for the conditions of M2 kyanite	85
5.13. The inferred tectonic history of the Mn-andalusite layer at the base of the Ortega Formation at Quartzite Peak (left) and Kiowa Mountain (right).....	86
6.1. Map of the Tusas Mountains showing the four areas of well-exposed and abundant Mn-andalusite focused on in this study	89
6.2. Mn-andalusite occurs with an abundance of hematite in aluminous, hematite-bearing layers (c), on the surface of cross beds (a), on cleavage planes.....	90
6.3. Lithologic map showing the location of the Mn horizon at Quartzite Peak. Bold, outlined, colored areas represent exposed outcrop and transparent.....	92
6.4. Zoning patterns preserved in the birefringence of Mn-andalusite crystals represent a decrease in Mn away from a localized high-Mn region (a,b,c).....	94
6.5. High-Mn core regions are areas of high Mn content as seen in the EMP Mn x-ray map shown in (b). Hematite aligned in the dominant foliation.....	96
6.6. The high-Mn core regions are most densely concentrated at the base of the aluminous, hematite-bearing layer and decrease in	99
6.7. High-Mn core regions can be found on the surface of cross beds in the Hopewell lake-Jawbone Mountain area.....	100
6.8 Mn-andalusite is concentrated in bands subparallel to bedding structures in the Hopewell Lake-Jawbone Mt area (right). In a sample.....	102
6.9. Abs-Wurmbach et al (1983) showed that Mn-andalusite will overgrown kanonaite cores at higher temperatures and pressures.....	104
6.10. Zones of rutile in hematite crystals produce textures that appear patchy or mottled (a,b), wormy (g), cross-hatched (c,d), or banded (e,f,h,i).....	108
6.11. The diagram above outlines three possible sources of the rutile-hematite textures in hematite from the transitional package of the Vadito.....	112
6.12. A bladed texture (a, b) preserved in the birefringence of Mn-andalusite crystals from the Mn horizon is a result of very subtle variations in Mn-content.....	119
6.13. The feathery texture preserves evidence for the existence of a crenulation cleavage overgrown by Mn-andalusite.....	121

6.14. The fold preserved in the feathery texture in the Mn-andalusite crystal (yellow) continues outside of the andalusite but is defined by aligned.....	122
6.15. A higher Mn “halo” in Mn-andalusite surrounding kyanite crystals suggests that kyanite expelled excess Mn to the edges of the growing.....	125
6.16. Areas of low order colors and low Mn content appear to mimic crystal shapes in some Mn-andalusite crystals (a). In some cases, the edges	126
6.17. Two types of Mn-andalusite crystals are identified at the Hopewell anticline. The first type (a & b) is characterized by localized highs of Mn.....	129
6.18. The heterogeneous distribution of D3 strain leads to the incomplete breakdown and regrowth of Mn-andalusite preserving both M2 (a) and M3.....	130
6.19. A schematic diagram showing the timing of deformation and Mn-andalusite growth in the Mn-andalusite layer of the Hopewell anticline.....	133
6.20. Mn-andalusite at Kiowa Mountain displays a mottled texture (a,b,c) and a kyanite-Mn-andalusite intergrowth texture.....	136
7.1. P/T diagram showing the difference in P-T paths for the Hopewell anticline and the Jawbone syncline from the Hopewell Lake-Jawbone Mountain.....	141
C.1. The stratigraphic section from the Hopewell Lake portion of the Hopewell Lake-Jawbone Mountain area showing the upper part of the Vadito.....	147
C.2. The stratigraphic section from the Jawbone Mountain portion of the Hopewell Lake-Jawbone Mountain area showing the upper part of the Vadito.....	148
C.3. The stratigraphic section from Quartzite Peak showing the upper part of the Vadito Group and the lower part of the Hondo Group. The Vadito.....	150
C.4. A lithologic map of the Kiowa Mountain showing the location of units in the transitional package along a traverse approximately perpendicular to.....	151
C.5. The stratigraphic section from Kiowa Mountain showing the upper part of the Vadito Group and the lower part of the Hondo Group The Vadito Group.....	152

CHAPTER 1

INTRODUCTION

The North American continent grew southward in the Proterozoic between 1.8 and 1.6 Ga through the addition of dominantly juvenile crustal material during subduction-related orogenic events (Fig. 1.1; Hoffman, 1988; Karlstrom and Bowring, 1987; Karlstrom et al, 2001). The juvenile material includes mafic and felsic metavolcanic rocks, a broad array of plutonic rocks, and a variety of metasedimentary rocks, most notably a thick, clean, ultramature (ca 1.7 Ga) quartzite that has been correlated across the southwestern USA and beyond (Bauer and Williams, 1989). The quartzite is interpreted to have been deposited in a shallow marine or fluvial environment at the continental margin or in a back-arc basin and is largely composed of locally derived sediment (Soegaard and Erikson, 1985; Condie and Chomaik 1992; Condie, 1992; Jessup et al, 2005). An anomalous Mn-bearing horizon can be found in Proterozoic rocks across the southwestern USA. It occurs near the base of the quartzite in many localities and is characterized by Mn-rich phases and distinctive trace element-rich oxides (Williams, 1987).

Understanding the depositional setting and deformational/metamorphic history of the thick Proterozoic quartzite(s) is a first order problem. The deposition of this distinctive unit may record changing conditions in the Precambrian Earth system. The structural character is important because the thick quartzite defines many of the largest and most important structures (e.g. folds and thrusts) that have been used to establish the tectonic history of the region. Although the quartzites have well preserved primary sedimentary structures, they tend to be metamorphosed and annealed, and thus primary minerals, microtextures, and microstructures are not well preserved. Consequently, there are still fundamental questions about the depositional setting (passive margin vs, syntectonic basin) and structural history, especially concerning the nature, number, and age of tectonic events preserved.

The Tusas Mountain range in northern New Mexico (Fig. 1.1) preserves extensive exposures of the Ortega Formation quartzite and superb exposures of the Mn horizon near the

base of the quartzite (Williams, 1987). The horizon is characterized by Mn-andalusite, which is related to primary structures and tends to preserve a rich microstructural record. The purpose of this research was (1) to investigate the setting and context of the Mn horizon in order to identify any defining petrogenetic characteristics of the layer and thus of the quartzite itself and (2) to describe and interpret the microstructures and microtextures that can be used to constrain the structural and metamorphic history of the Tusas Mountains. The Mn horizon may represent an invaluable tool for understanding the depositional and tectonic history of Ortega Formation and the Tusas Mountains and for correlating the quartzites and the tectonic events throughout the southwestern US and possibly to other once-connected Proterozoic continents.

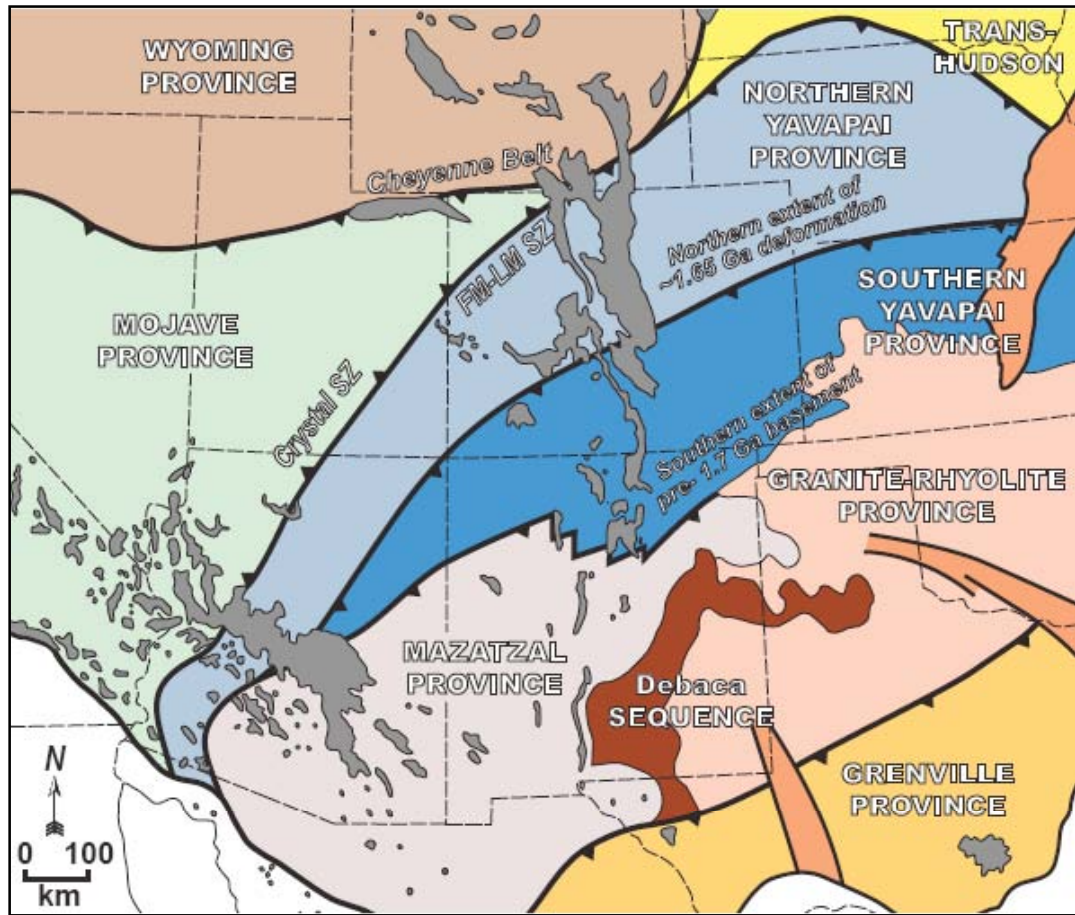


Figure 1.1. Map of the southwestern USA showing the location of exposed Precambrian crust in relation to province boundaries (Dumond, unpublished; based on map from Karlstrom et al, 2002).

CHAPTER 2

BACKGROUND

The cratonic interior of North America was assembled and stabilized by circa 1.80 Ga (Hoffman, 1988; Karlstrom and Bowering, 1988). The Cheyenne Belt shear zone in southern Wyoming represents the southernmost edge of the craton (Karlstrom and Houston, 1984). South of this shear zone, Proterozoic crust becomes progressively younger, with age domains of >1.8 Ga, 1.72-1.80 Ga, 1.65-1.72 Ga, and 1.1 to 1.2 Ga, with overlapping and overprinting geochronologic boundaries between these zones (Karlstrom et al, 1987). The age domains (labeled Mojave, Yavapai, Mazatzal, and Grenville respectively) are thought to represent different tectonic provinces with different lithologies, deformation styles, and metamorphic grade (Fig. 1.1; Karlstrom et al, 1987). The Yavapai and Mazatzal provinces are traditionally interpreted as individual terranes that were assembled and then added to the long-lived tectonic southern margin of Laurentia during subduction-related orogenic events in the Paleoproterozoic, namely the Yavapai and Mazatzal Orogenies (Condie, 1982; Karlstrom and Bowering, 1988; Jessup et al, 2005).

In the Tusas Mountains of the Mazatzal Province, a Paleoproterozoic supracrustal package of igneous, metasedimentary, and metavolcanic rocks preserves evidence for multiple deformational events and the growth of more than one metamorphic mineral assemblage during the Proterozoic (Williams, 1987; Bauer and Williams, 1989; Williams et al, 1999). These events have been placed in context regionally by previous researchers in an effort to understand the regional tectonic history of the southwestern US during the Proterozoic (e.g. Williams and Karlstrom, 1996; Williams et al, 1999; Karlstrom et al, 2005).

Stratigraphy of Proterozoic Supracrustal Rocks in the Tusas Mountains

The Tusas Mountains are one of a family of basement-cored uplifts that expose a Paleoproterozoic supracrustal package of igneous, metasedimentary, and metavolcanic rocks in northern New Mexico. Bauer and Williams (1989) divided this supracrustal package into three

parts: the Moppin Complex, the Vadito Group, and the Hondo Group. The stratigraphically lowest unit, the Moppin Complex, is interpreted to represent a sequence of metamorphosed and deformed, dominantly mafic volcanic, volcanoclastic, and epiclastic rocks (Bauer and Williams; 1989). These rocks include chlorite schist, amphibolite, and minor amounts of feldspathic schist and gneiss, muscovite-biotite schist, and banded iron formation. The Vadito Group unconformably overlies the Moppin Complex and is interpreted to represent a package of metavolcanic and immature metasedimentary rocks. The lower portion of the Vadito Group is dominated by feldspathic schists interpreted to be metarhyolites (including the Burned Mountain Formation) interlayered with metasedimentary units (including the Big Rock conglomerate). The upper portion of the Vadito Group is dominated by a sedimentary package of muscovite-biotite schist, muscovite-bearing quartzite, feldspathic quartzite, pelitic schist, and conglomerate with interlayered amphibolite. The overlying Hondo Group is dominated in the Tusas Mountains by the Ortega Formation, a thick, mature cross-bedded ortho-quartzite. The contact between the uppermost Vadito Group and the lowermost Ortega Formation has been described as both unconformable (Soegaard and Erikson, 1985) and gradational (Bauer and Williams, 1989). Mn-rich minerals (predominantly Mn-andalusite) define a manganiferous marker horizon that spans the uppermost 200m of the Vadito Group and the lowermost 100m of the Ortega Formation. Overlying sedimentary units of the Hondo Group include the Rinconada Formation and the Pilar Formation, neither of which are exposed in the Tusas Mountains (Bauer and Williams, 1989). The Rinconada Formation is a sequence of interlayered schists and quartzites that overlies the Ortega Formation (Williams, 1987; Bauer and Williams, 1989). The quartzites are thin and contain feldspar and ferromagnesian minerals. The Pilar Formation overlies the Rinconada Formation and includes graphitic slate, phyllite, and schist (Williams, 1987; Bauer and Williams, 1989).

This general large-scale stratigraphic sequence can be traced across the other Precambrian-cored uplifts of the southwestern US, including the Picuris Mountains, the Truchas Peaks Area, the Rio Mora-Pecos area, and the Taos Range (southern Sangre de Cristo Mountains) (Bauer and Williams, 1989). In addition, a similar and possibly contemporaneous

lithologic sequence can be found at localities in Arizona and southern Colorado but is classified under different nomenclature (e.g. the Mazatzal Group in Arizona; the Uncomphagre Formation and Vallecito Conglomerate in Colorado) (Tewksbury, 1989; Cox et al, 2002).

The Vadito Group

The Vadito Group represents a heterogeneous package of supracrustal immature metasedimentary and metavolcanic units (Williams, 1987). Metasedimentary units include quartz-muscovite-biotite schist, quartz-muscovite schist, feldspathic quartzite, and rarely metaconglomerate (Williams, 1987; Bauer and Williams, 1989). Felsic metarhyolite units (including the Burned Mountain Formation) are identified as feldspathic schists and gneisses with large euhedral quartz and feldspar crystals interpreted to be relict phenocrysts (Williams and Burr, 1994). Interlayered amphibolites are interpreted as metamorphosed mafic volcanic rocks (Soegaard and Eriksson, 1986). The thickness and relative proportions of the individual units in the Vadito Group vary between individual exposures across the southwest United States (Williams, 1987; Bauer and Williams, 1989). Within the Tusas Mountains, the thickness of the Vadito Group varies from several kilometers thick in the central and southern parts of the range to less than 100 meters thick in the northern part of the range (Williams, 1987).

The Vadito Group is best exposed at Kiowa Mountain and represents the most complete section of the Vadito Group in the Tusas Mountains (Bauer and Williams, 1987). In this section, the feldspathic schist and metarhyolite grade through impure metasediments and into the clean quartzite of the Ortega Formation (Bauer and Williams, 1987). The lowermost portion of the Vadito Group is marked by metarhyolite and associated metaconglomeritic units (i.e. the Big Rock Formation) (Williams, 1987). The immature metasedimentary sequence of the upper Vadito Group (feldspathic schist to muscovitic quartzite) includes one or more amphibolite layers (Bauer and Williams, 1987).

The Ortega Formation Quartzite

The Ortega Formation quartzite is the thick (>850m) meta-quartzarenite sedimentary unit in the Hondo Group. It is described as a dominantly clastic deposit with identifiable primary sedimentary structures and a lesser amount of interlayered pelites (Soegaard and Erikson, 1985). The interlayered pelites, referred to as aluminous, hematite-bearing layers in this study, are layers rich in oxides, particularly hematite, and aluminum silicates. They occur intermittently every meter or so and range in thickness from a few millimeters up to several centimeters. The aluminous, hematite-bearing layers were interpreted by Soegaard and Erikson (1986) to represent “kaolinitic mudstone drapes”. The sedimentary structures of the Ortega Formation include centimeter to meter-scale trough cross beds and coarse, pebbly conglomeritic layers (Soegaard and Erikson, 1985). The trough cross beds are commonly found with subhorizontal bottom-set beds, inclined foreset beds, and the subhorizontal topset beds, the surfaces of which are defined by hematite and aluminum silicates. Coarse conglomeritic layers are well-sorted zones of well-rounded quartz pebbles a few centimeters in diameter. At Jawbone Mountain in the Tusas range, quartz-pebbly conglomeritic layers are common in the bottom third of the Ortega Formation (Soegaard and Erikson, 1985). The majority of the sediment of the Ortega Formation was from a young, local source (1.80-1.70 Ga), presumably, the juvenile arc-related volcanic and plutonic rocks on which the quartzite was dominantly deposited (Condie, 1992; Jessup et al, 2005). A smaller proportion (~5-10%) of the sediment had an older source (3.2-2.2 Ga), such as the Archean rocks of the Wyoming craton, that could represent deeper pre-existing continental crust (Hill and Bickford, 2001; Jones, 2005; Koper, 2003; Bickford and Hill, 2007).

The depositional environment of the Ortega Formation has been interpreted as being a “north-east trending”, “shallow shelf basin environment” that was dominated by “tidal, wave, and storm processes” (Soegaard and Erikson, 1985; Trevena, 1979; Cox et al, 2002b; Medaris et al, 2003). Slight variation in sedimentary environments can be found between occurrences in different regions with some areas (i.e. the Mazatzal Group of Arizona) preserving evidence for alluvial fan and braided stream deposits (Cox et al, 2002b), while other areas (i.e. the Ortega

Formation of New Mexico) preserve evidence for dominantly subtidal shelf environments (Soegaard and Erikson, 1985). This variation could be indicative of variation along a single shoreline basin, perhaps at the continental margin, but could also provide evidence that separate sedimentary basins were preserved. Although deposition in a shoreline basin suggests a passive margin environment, the quartzite may have also been deposited in a syn-deformational basin. The stratigraphic association of the Ortega Formation quartzite with the bimodal volcanic deposits of the Vadito Group (metarhyolites and amphibolites) suggests deposition in a back-arc or intra-arc basin (Condie and Chomaik 1992; Dann, 1997; Hill and Bickford, 2001; Bickford and Hill, 2007).

The Ortega Formation and other thick, laterally extensive quartzites of the southwestern US are thought to represent first cycle quartz arenites and are unusual in their textural and compositional maturity (Cox et al, 2002a; Dott, 2003; Medaris et al, 2003). Extreme chemical weathering at the source may have contributed to the compositional maturity of the sediment (Dott, 2003; Medaris, 2003). The compositional maturity may also be a result of diagenetic alteration after deposition (Cox et al 2002a; 2000b). The textural maturity of the sediment, such as the rounded character of the grains, could be the result of extreme eolian abrasion associated with absence of land plants in the Proterozoic or intense mechanical weathering associated with tidal and wave action (Dott, 2003; Davis, 2006).

Mn Horizon in the Tusas Mountains

The manganiferous marker horizon dominantly spans the lowermost 100m of the Ortega Formation in the Tusas Mountains and is characterized by the occurrence of Mn-rich phases (Fig. 2.1; Williams, 1987). When hosted by schist, the Mn is contained in Mn-andalusite, piemontite, muscovite, and spessartine with local trace amounts of staurolite and gahnite, whereas in quartzite, Mn-andalusite is the main Mn-bearing mineral (Williams, 1987). Rutile, found in association with Mn-rich phases, has been reported to contain anomalous concentrations of trace elements, such as Nb, Ta, Sb, and W, whereas rutile found outside of the Mn horizon is composed of essentially pure TiO₂ (Grambling and Williams, 1985; Williams,

1987). In the nearby uplifts, particularly in the Rio Mora and the Picuris uplifts, the combined weight percent of $\text{Nb}_2\text{O}_5 + \text{Ta}_2\text{O}_5 + \text{Sb}_2\text{O}_5$ in rutile from the Mn horizon has been recorded to reach as high as 30 percent (Grambling and Williams, 1985).

Mineralogy, Crystal Chemistry, Petrology, and Occurrences of Mn-andalusite

Mn-rich andalusite, formerly called “viridine”, is classified by the IMA Commission on New Minerals and Mineral Names as a member of the andalusite-kanonaite series (Gunter and Bloss, 1982). This series ranges from pure andalusite (Al_2SiO_5) to kanonaite (MnAlSiO_5) with increasing substitution of Mn^{3+} for Al^{3+} . Intermediate members are included under the names manganian andalusite and aluminous kanonaite, and the prefix ferrian- is added when a significant amount of Fe^{3+} also substitutes for Al^{3+} . For the sake of simplicity, all Mn-bearing andalusite included in this study is simply referred to as manganese andalusite or Mn-andalusite unless stated otherwise.

The andalusite crystal structure contains cross-linked single chains of edge-sharing Al octahedra (AlO_6) and double chains of alternating Al trigonal bipyramids (AlO_5) and silica tetrahedra (SiO_4) that extend along the c-axis (Fig. 2.2; Kerrick, 1990). The 6-coordinated Al defines the M1 site and the 5-coordinated Al defines the M2 site. When substitution occurs, Al is commonly replaced by Mn^{3+} and Fe^{3+} at the M1 site, although Mössbauer studies of andalusite in which Mn^{3+} and Fe^{3+} substitutions have occurred have also shown minimal substitution (10-15%) of Fe (and possibly Mn) on the M2 site (Abs-Wurmbach et al, 1981; Gunter and Bloss, 1982). Cation ordering on the M1 site can be largely explained by the ability of the larger M1 site to accommodate the larger Fe and Mn cations (Griggen, 1992).

Gunter and Bloss (1982) showed that there was a direct relationship between the lengthening of the Mn-O bonds of the M1 site and the amount of Mn and Fe substituted on the M1 site. With an increase in cation substitution, there is an increased distortion in the optical properties of the mineral. This causes the refractive index parallel to each optic axial to increase disproportionately relative to each other and the interference colors of Mn-andalusite to increase (white to brown to blue to green) with increased cation substitution. The mineral will

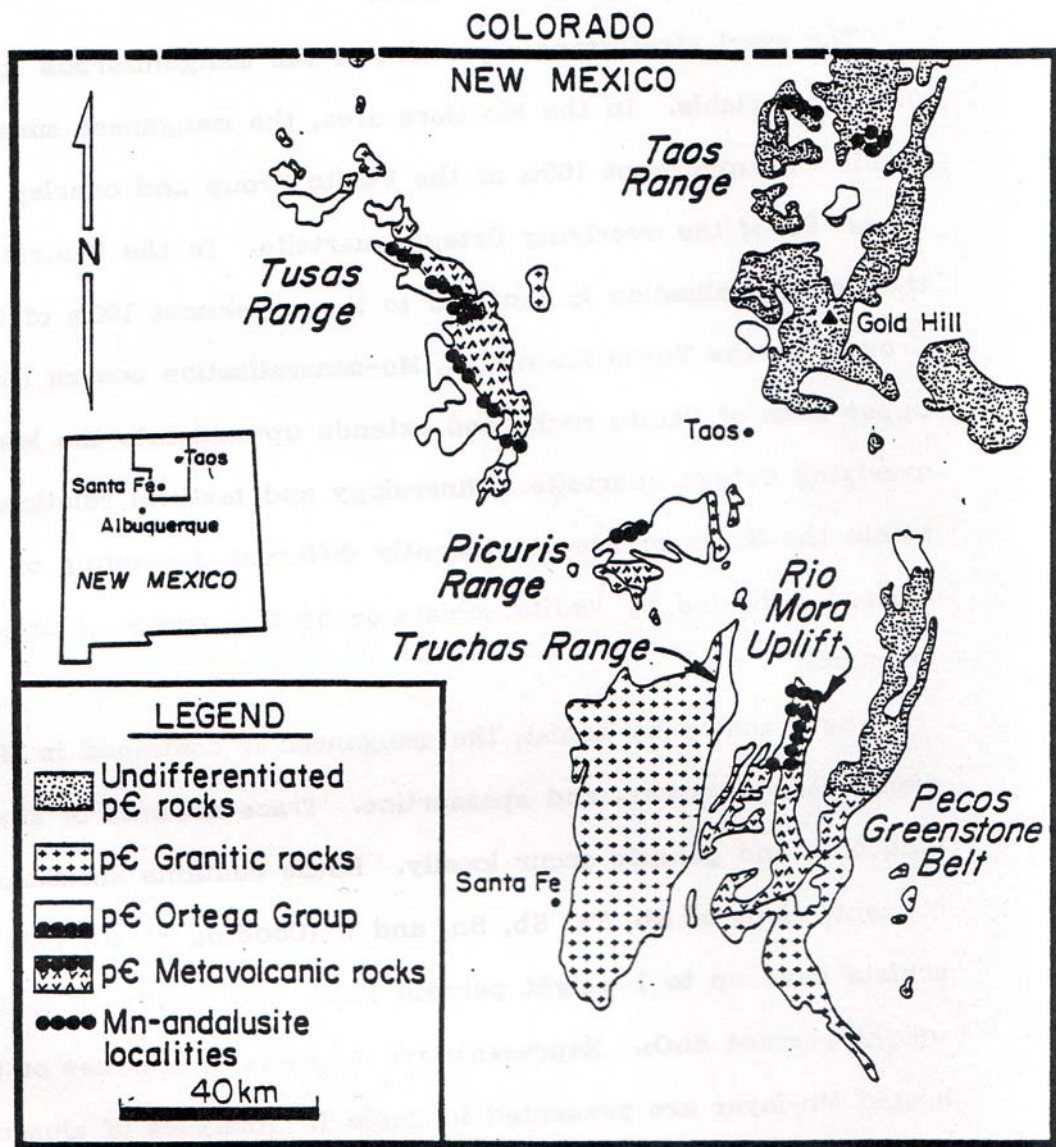


Figure 2.1. Map showing the Mn horizon in the Tusas Mountain range and other basement-cored uplifts of Paleoproterozoic age (from Williams, 1987).

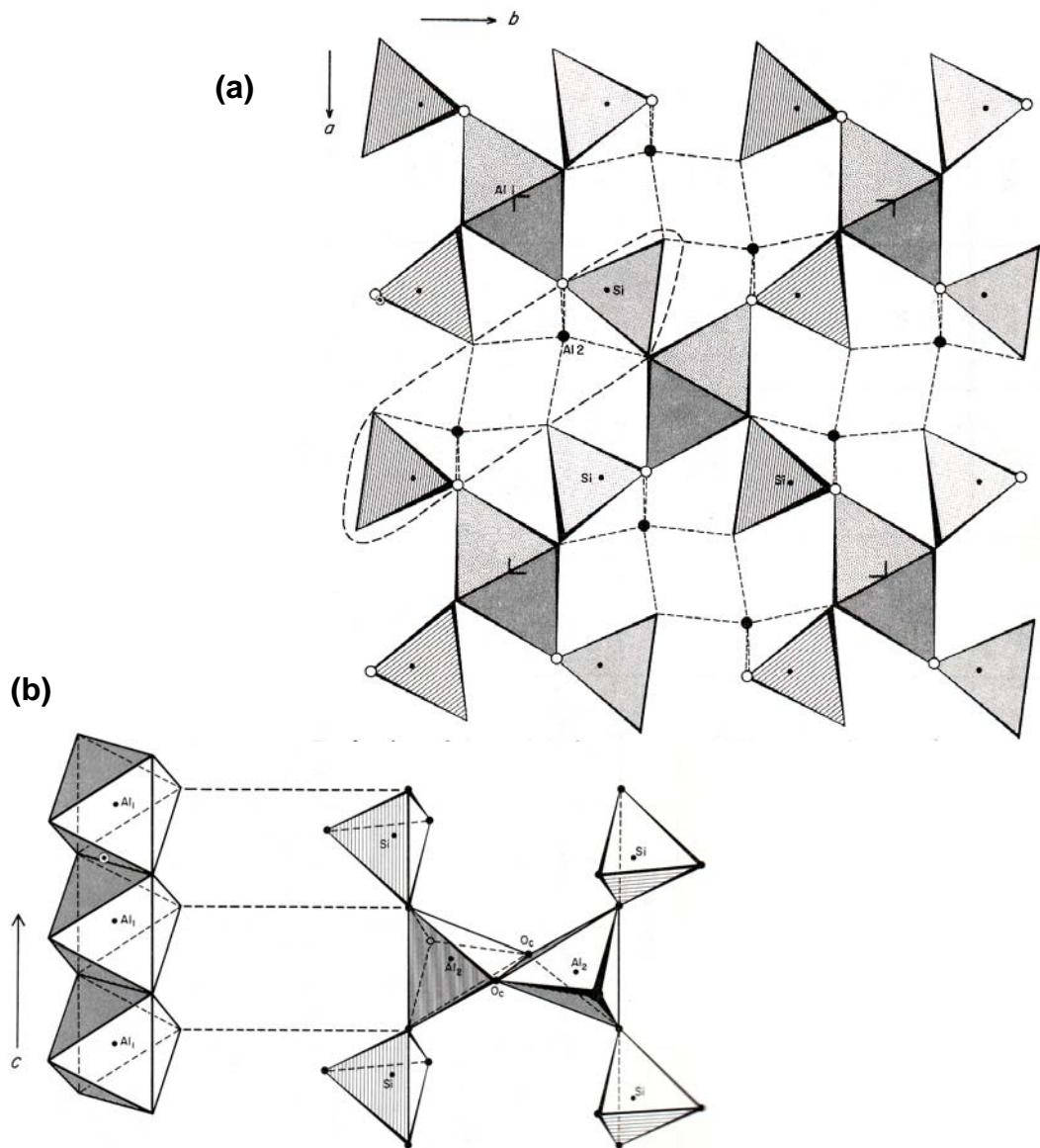


Figure 2.2. Andalusite contains cross-linked single chains of edge-sharing Al octahedra (Al_1) and double chains of alternating Al trigonal bipyramids (Al_2) and silica tetrahedra (Si) that extend along the c-axis. The crystal structure is shown in (a) looking down the c-axis and the dotted area shown in (b) is a view normal to the c-axis chains looking down the a-axis (from Kerrick, 1990).

appear optically isotropic when the refractive indices of all three optic axes are equal. This isotropic point is reached when the molar proportion of Mn + Fe per 5 oxygens approaches 0.066 (Gunter and Bloss, 1982; Grambling and Williams, 1985). Grambling and Williams (1985) point out that this effect can be seen in some areas of the Tusas Mountains where Mn-andalusite grains appear to be zoned due to a change in interference colors that correspond with a change in the abundance of Mn. They identified the isotropic region in those grains as areas where the Mn + Fe proportion reached 0.08-0.09.

Experimental studies (Freer, 1981; Abs-Wurmbach et al, 1983) have attempted to document the effects of Mn cation substitution on andalusite stability. Mn-andalusite is only stable at high oxygen fugacities where Mn³⁺ is the main cation species. At low oxygen fugacities, Mn-andalusite is no longer stable, and the assemblage "spessartine + corundum + pure Al₂SiO₅" dominates (Abs-Wurmbach et al, 1983). Spessartine (Mn-garnet) is stable when oxygen fugacity is low and when Mn²⁺ is the main cation species. The addition of Mn³⁺ into the andalusite crystal structure has the effect of expanding the stability of Mn-andalusite at low temperatures pushing it into the stability ranges of hydrous phases (pyrophyllite & kaolinite) and at higher pressures and temperatures bringing it well into the stability fields of both kyanite and sillimanite (Fig. 2.3; Freer, 1981; Abs-Wurmbach et al, 1983). This leads to a condition where Mn-andalusite can coexist with kyanite and/or sillimanite in a rock at conditions that are outside of those for univariant equilibrium. When Mn-andalusite coexists with other aluminum silicate polymorphs, andalusite is greatly enriched in Mn³⁺ relative to kyanite or sillimanite (Abs-Wurmbach et al, 1983). Kanonaite, the high Mn end-member of the Mn-andalusite series, was shown by Abs-Wurmbach et al (1983) to be stable only at temperatures below 500°C and at low fluid pressures. Evidence from later petrographic studies supports this observation (Kramm, 1979; Schreyer et al, 2001; Schreyer et al, 2004). The observations made in experimental studies of the stability of Mn-andalusite and kanonaite have been reflected in other studies (Kramm, 1979; Grambling and Williams, 1985; Schreyer et al, 2001, 2004; Kugimiya et al, 2004).

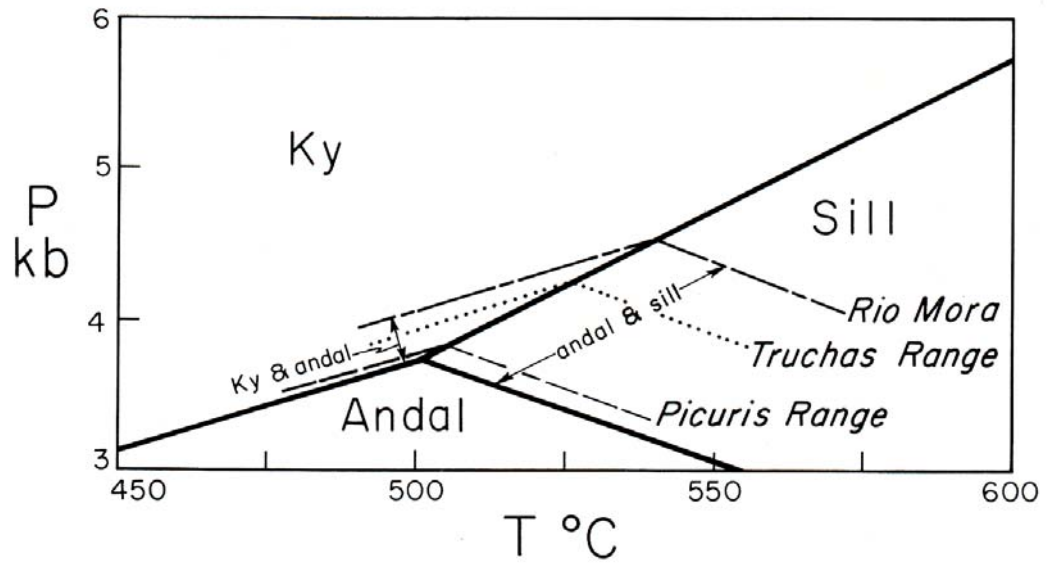


Figure 2.3. P-T diagram showing the effects Mn^{3+} have on the placement of the kyanite + andalusite and andalusite + sillimanite reaction lines in Proterozoic rocks from North-Central New Mexico (from Grambling and Williams, 1985).

Table 2.1. Survey of Mn-andalusite and kanonaite compositions reported in the literature

	Salmchateau Belgium*	Ardennes Mts. Belgium*	Rio Mora N. Mexico*	Rio Mora N. Mexico*	Darmstadt Germany*	Darmstadt Germany*	Darmstadt Germany*	Yakutia Russia*	Aldan Shield Russia*	Ultevis N. Sweden*	Vestana S. Sweden*
SiO ₂	33.00	35.41	36.12	34.50	33.47	35.30	34.09	31.52	39.50	36.72	
TiO ₂	1.32	-	0.00	0.05	-	1.04	-	0.40	0.07	-	
Al ₂ O ₃	43.70	46.95	61.55	50.45	40.98	55.52	45.60	41.41	51.80	56.99	
Fe ₂ O ₃	4.89	0.82	2.13	3.10	6.08	4.16	10.01	12.03	3.30	-	
FeO	-	-	-	-	-	-	-	2.16	-	-	
Mn ₂ O ₃	19.81	16.75	0.45	12.52	17.96	4.77	11.46	8.71	3.63	6.91	
MgO	-	-	0.00	0.00	-	-	-	0.42	0.33	-	
CaO	-	-	-	-	-	-	-	2.48	0.40	trace	
Na ₂ O	0.05	-	-	-	-	-	-	0.23	0.18	-	
K ₂ O	-	-	-	-	-	-	-	0.22	0.33	-	
Cr ₂ O ₃	-	0.03	-	-	-	-	-	-	-	-	
H ₂ O (+)	-	-	-	-	-	-	-	1.23	0.31	-	
H ₂ O (-)	-	-	-	-	-	-	-	-	0.37	-	
F	-	-	-	-	-	-	-	-	0.10	-	
Total	102.77	99.96	100.25	100.62	98.49	100.79	101.16	100.81	100.32	100.62	
Si	0.963	4.072	0.980	0.980	1.003	1.000	0.984	0.950	1.000	1.000	
Al	1.503	6.365	0.000	0.001	1.448	1.850	1.552	1.472	1.550	1.830	
Fe ₃₊	0.107	0.071	1.970	1.690	0.137	0.090	0.217	0.273	0.060	-	
Fe ₂₊	-	-	-	-	-	-	-	0.054	-	-	
Mg	-	-	0.044	0.066	-	-	-	0.019	0.010	-	
Ti	-	-	0.009	0.271	-	0.020	-	0.009	0.000	-	
Mn ₃₊	0.440	1.466	0.000	0.000	0.410	0.100	0.252	0.200	0.070	0.140	
Na	-	-	-	-	-	-	-	0.013	0.010	-	
Ca	-	-	-	-	-	-	-	0.080	0.010	-	
K	-	-	-	-	-	-	-	0.008	0.010	-	
(Herbosh, 1968)	(Kramm, 1973)	(Grambling and Williams, 1985)	(Abraham & Schreyer, 1975)	(Klemm, 1911)	(Serdyuch- enko 1949)	(Kulish, 1961)	(Odman, 1950)	(Odman, 1950)	(Odman, 1950)		

* denotes Mn-andalusites

** denotes kanonaite

~ cations recalculated to 5 oxygens

Table 2.1. (continued)

	Mt Ragged W. Australia*	Beach sand W. Australia*	Hidaka Japan*	synthetic mn-and*	synthetic mn-and*	Kanona Zambia**	Salmchateau Belgium**	Le Coreux Belgium**	Le Coreux Belgium**	Le Coreux Belgium**
SiO2	35.71	27.30	34.88	34.57	33.12	32.20	33.25	31.34	31.73	32.33
TiO2	0.17	-	0.30	-	-	0.01	0.07	-	-	0.01
Al2O3	58.38	58.70	41.48	49	42.3	33.90	33.25	30.68	26.56	32.33
Fe2O3	2.21	3.70	4.76	6.21	5.81	0.66	2.97	1.73	3.79	3.17
FeO	-	-	-	-	-	-	-	-	-	-
Mn2O3	3.67	9.50	14.57	9.33	18.48	32.20	30.32	34.55	38.28	31.88
MgO	-	-	0.67	-	-	0.04	0.01	-	0.04	0.02
CaO	-	-	2.23	-	-	-	-	-	0.05	0.03
Na2O	-	-	-	-	-	-	-	-	-	-
K2O	-	-	-	-	-	-	-	-	-	-
Cr2O3	-	-	-	-	-	-	-	0.03	-	-
H2O (+)	-	-	0.92	-	-	-	-	-	-	-
H2O (-)	-	-	0.65	-	-	-	-	-	-	-
F	-	-	-	-	-	-	-	-	-	-
Total	100.14	99.2	100.46	99.11	99.71	99.21	99.87	98.33	100.46	99.77
Si			1.000	1.004	0.982	0.994	1.012	0.990	1.001	0.999
Al			1.380	1.665	1.478	1.234	1.209	1.142	0.988	1.178
Fe3+			0.100	0.135	0.13	0.015	0.068	0.042	0.090	0.074
Fe2+			-	-	-	-	-	-	-	-
Mg			0.030	-	-	0.002	-	-	0.002	0.001
Ti			0.010	-	-	-	0.001	-	-	-
Mn3+			0.320	0.205	0.417	0.757	0.703	0.830	0.919	0.750
Na			-	-	-	-	-	-	-	-
Ca			0.070	-	-	-	-	-	0.002	0.001
K			-	-	-	-	-	-	-	-
	(Prider, 1960)	(Lairrett, 1970)	(Suzuki et al, 1965)	(Freer, 1981)	(Freer, 1981)	(Vrana et al, 1978)	(Kramm, 1979)	(Schreyer et al, 2001)~	(Schreyer et al, 2004)~	(Schreyer et al, 2004)~

* denotes Mn-andalusites
 ** denotes kanonaites
 ~ cations recalculated to 5 oxygens

Table 2.2. Survey of Mn-andalusite and kanonaite occurrences from the literature

Location	Rock Type	Age	Reference
New Mexico- Rio Mora Tusas Uplift Picuris Uplift	metasediments (schists and quartzites) and metavolcanics	Proterozoic	(Heinrich and Cory, 1959 ; Grambling and Williams, 1985)
Arizona- Squaw Peak	metasediments and metavolcanics	Proterozoic	(Thorpe and Burt, 1978)
Colorado- Wet Mountians	mica schists	Proterozoic	(Goodge and Siddoway, 1997)
W. Australia- Mt Ragged & Mica Hills	metasediments (schists and quartzites)	Precambrian (Proterozoic?)	(Prider, 1960)
Coastal beach sand	sand sourced from Mt Ragged	modern deposit, precambrian source	(Larrett, 1970)
Germany- Darmstadt	hornfels	-	(Abraham and Schreyer, 1975)
Netherlands- near Enschede, Sibculo, Hellendoorn and Hoenderlo	pre-glacial sand, source unknown	Pleistocene deposit, source unknown	(Crommelin and Van Der Plas, 1961)
Belgium- Le Coreux	phyllite and quartz veins	Ordovician and younger	(Kramm, 1979; Schreyer et al, 2001; Schreyer et al, 2004)
Turkey- Asigedigi Formation, Nigde Massif	quartzite	Paleozoic	(Whitney and Dilek, 1998)
Japan- Chisaka Area, Hidaka Province, Hokkaido	metasediments (sericite quartz schist)	-	(Suzuki et al, 1968)
Africa- Kongwa, Mpwapa district, Tanzania	quartzites and dolomites	Proterozoic	(Basu and Hamisi, 1984)
Kanona, Zambia	-	-	(Vrana et al, 1978)
Russia- Yakutia and Aldan Shield	quartzite	Precambrian	(Serdyuchenko 1949; Kulish 1961)
Sweden- Ultevis and Vestana	-	-	(Odman, 1950)
United Arab Emirates- Oman Ophiolite	metachert pebble	-	(Kugimiya et al, 2004)
Brazil- Serra das Bicas, Carrancas, Minas Gerais (and others)	-	-	(Pires et al, 2000)

Mn-andalusite and kanonaite are known to occur only at a limited number of localities around the world (Table 2.1; Table 2.2). Mn-andalusite and/or kanonaite porphyroblasts are known from Russia (Serdyuchenko 1949; Kulish 1961; Kulish and Kulish, 1981), Germany (Abraham and Schreyer, 1975), Belgium (Kramm, 1979; Schreyer et al, 2001; Schreyer et al, 2004), Sweden (Odman, 1950), Turkey (Whitney and Dilek, 1998), Australia (Prider, 1960; Larrett, 1970), Japan (Suzuki et al, 1968), Brazil (Pires et al, 2000), Africa (Vrana et al, 1978; Basu and Hamisi, 1984), the United Arab Emirates (Kugimiya et al, 2004), and Colorado, New Mexico, and Arizona of the southwestern US (Heinrich and Cory, 1959; Grambling and Williams, 1985; Goodge and Siddoway, 1997). Traces of Mn-andalusite were also found as a component of beach sands from the southern coast of western Australia (Larrett, 1970) and pre-glacial Pleistocene sands from the Netherlands (Crommelin and Van Der Plas, 1961). A large majority of Mn-andalusite and kanonaite occurrences were found in or associated with high Al, manganese-rich metasediments, particularly quartzites, schists, and carbonates, that can be interbedded/intercalated in nature with Mn-rich and Mn-poor zones (e.g. Kramm, 1979). More rarely they have been found in hornfels (Abraham and Schreyer, 1975) and quartz veins (Schreyer et al, 2001 & 2004). Mn-andalusite and kanonaite commonly occur with hematite (due to the high oxygen fugacity) and have been shown to occur with rutile, braunite, zircon, spessartine, piemontite, pyrophyllite, muscovite, and/or sillimanite and kyanite. Many workers reported compositional zoning within Mn-andalusite and kanonaite porphyroblasts (Grambling and Williams, 1985; Goodge and Siddoway, 1997; Pedrick and Thompson, 1998; Schreyer et al, 2004) and some reported porphyroblasts with a composite, or “blebby”, nature (Goodge and Siddoway, 1997; Schreyer et al, 2004).

Regional Structure

The Tusas Mountain Range preserves evidence for three periods of deformation (D1, D2, D3) that are respectively associated with three generations of fabric (S1, S2, S3) and fold (F1, F2, F3) formation (Williams, 1991; Williams et al, 1999). D1 involved the formation of a bedding-parallel fabric (S1), recumbent F1 folds, and stratigraphic discontinuities related to

stacked sections and bedding parallel thrusts (Williams, 1991; Williams et al, 1999). Specifically, in the Ortega Formation, bedding-parallel shearing was accommodated in the weaker aluminous, hematite-bearing layers (Williams, 1991). D2 involved the formation of centimeter- to kilometer-scale tight to isoclinal, reclined F2 folds and fold-thrust structures with NW-striking, SW dipping axial plane cleavage (S2) and south-over-north shear sense (Williams, 1991; Williams et al, 1999). D2 also involved the reactivation of S1 surfaces, including the aluminous hematite-bearing layers within the quartzite (Williams, 1991). D3 involved the formation of upright and open F3 folds, an E-NE striking cleavage (S3), and a broadly spaced crenulation cleavage (Williams, 1991; Williams et al, 1999).

Large map-scale synclines, namely the Jawbone syncline, the Kiowa syncline, and the La Madera syncline, are interpreted as F2 (or late F1) folds, the upper limbs of which have been truncated by south-dipping ductile shear zones with a south over north shear sense (Fig. 2.4 & 4.1; Grambling et al, 1989; Williams, 1991). The location of a number of faults, or shear zones, have been postulated, including one south of the Jawbone syncline and one north of the Kiowa syncline (the Spring Creek Shear Zone) (Fig. 4.1; Williams, 1991; Davis, 2003; Kopera, 2003).

Regional Metamorphic Petrology

Three distinct metamorphic mineral assemblages have been identified in the Tusas Mountains (M1, M2, M3). M1 was associated with D1 and involved the growth of a low-grade assemblage that included kyanite, muscovite, oxides, and locally hornblende (Williams, 1991). Minerals in the M2 assemblage (garnet, kyanite, and locally staurolite) overgrew D2 structures and are interpreted to have grown syn- to dominantly post-D2 (Williams et al, 1999). The growth of the low-P, high-T M3 assemblage was associated with D3 and includes andalusite, sillimanite, garnet, staurolite, and cordierite (Bishop, 1997; Lombardi, 1997; Williams et al, 1999). The M3 mineral assemblage is interpreted to have grown syn-D3 and involved the growth of M3 rims on M2 garnet and plagioclase crystals (Bishop, 1997; Williams et al, 1999).

The large-scale metamorphic trend is one of increasing grade from north (450°C, 2 kbar) to south (550°C, 4.5 kbar) and was interpreted to represent the sequential southward

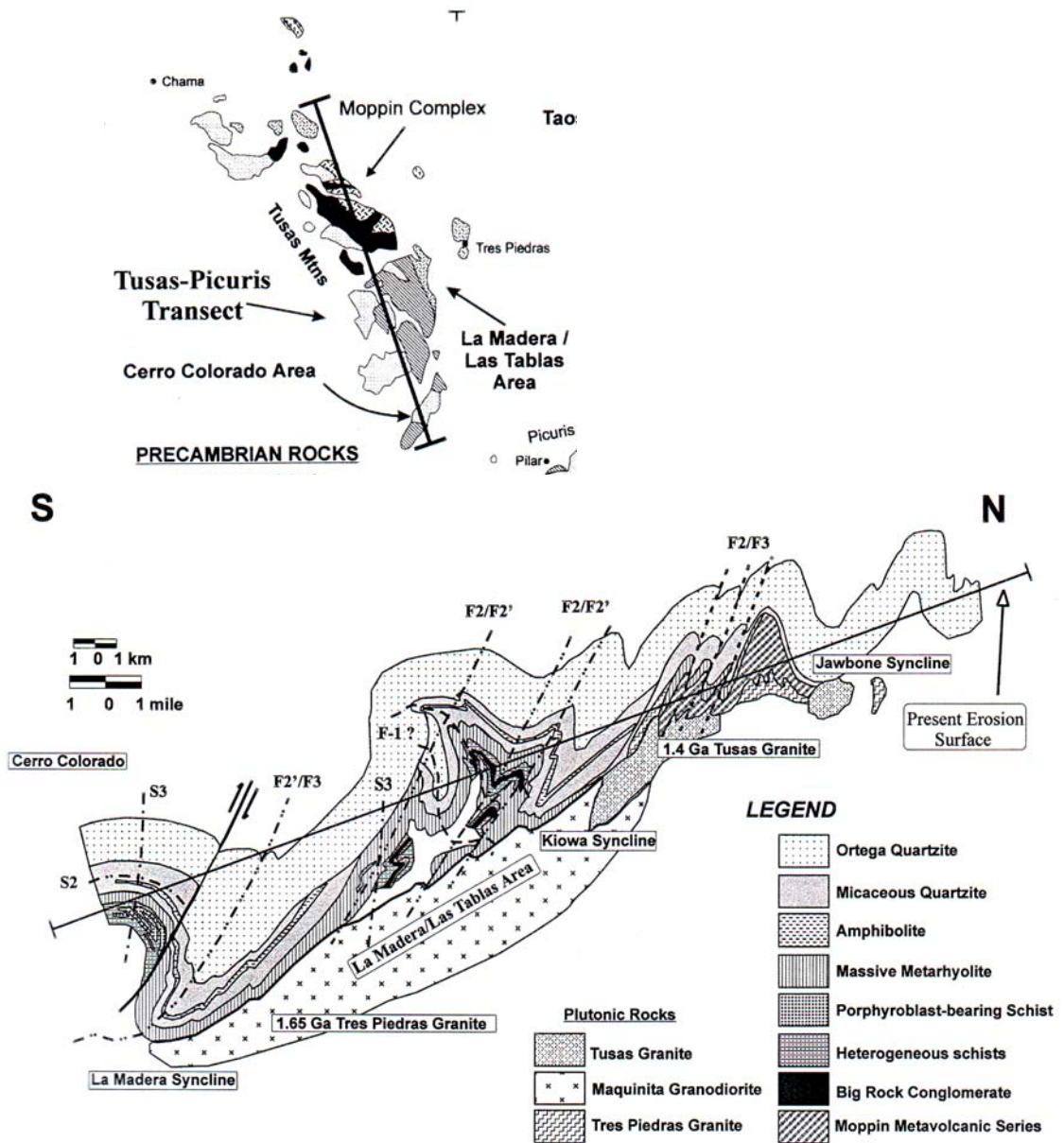


Figure 2.4. Down plunge projection of a north/south transect of the Tusas Mountains showing the interpreted relationship between S1/F1, S2/F2, and S3/F3 structures (from Williams et al, 1999).

exposure of shallowly dipping, subhorizontal isograds (Fig. 2.5; Bishop, 1997; Lombardi, 1997; Grambling et al, 1989; Williams et al, 1999). The isograds overprint the regional D1 and D2 structures and are associated with the growth of the M2 and/or M3 metamorphic mineral assemblages. The overall metamorphic path is interpreted to have a clockwise geometry with a counterclockwise character that results from cooling isobarically at a higher pressure than that interpreted from the prograde path (Fig. 2.6; Williams and Karlstrom, 1996).

Interpreted Proterozoic Tectonic History of the Tusas Mountains

Researchers have debated the placement of D1, D2, and D3 and growth of the M1, M2, and M3 metamorphic assemblages within a tectonic context. Traditionally, a multiphase history has assigned each respective generation of deformation and metamorphism to a single distinct tectonic event, but a more recent theory links D1, D2, D3 and the growth of M1, M2, and M3 to one protracted orogenic event. The multiphase history states that three distinct tectonic events are responsible for each generation of deformation and metamorphic mineral growth (Williams et al, 1999). D1 is thought to represent the burial of rock by thrusting before 1.65 Ga and was associated with the growth of the M1 assemblage (Williams, 1991). D2 and the growth of the M2 assemblage are thought to have occurred at circa 1.65 Ga during the crustal shortening and localized magmatic activity of the Mazatzal Orogeny (Williams et al, 1999). The Mazatzal Orogeny was associated with the assembly and addition of lithosphere at the continental margin (Karlstrom et al, 2005). A regional transpressional tectonic event associated with variable heating and localized magmatism at circa 1.45 Ga was thought to be responsible for D3 and the growth of the M3 assemblage (Nelson and DePaolo, 1985; Nyman et al, 1994). A more recent theory states that D1, D2, and D3 and the growth of the M1, M2, and M3 assemblages occurred during one protracted regional orogenic event at circa 1.45 Ga (Daniel and Pyle, 2005). This orogenic event occurred after the burial and thrusting associated with the Mazatzal Orogeny at 1.65 Ga.

Differences between theories stem from efforts to use geochronology to date fabrics and time mineral growth. Attempts to date M2 minerals, the growth of which are thought to be

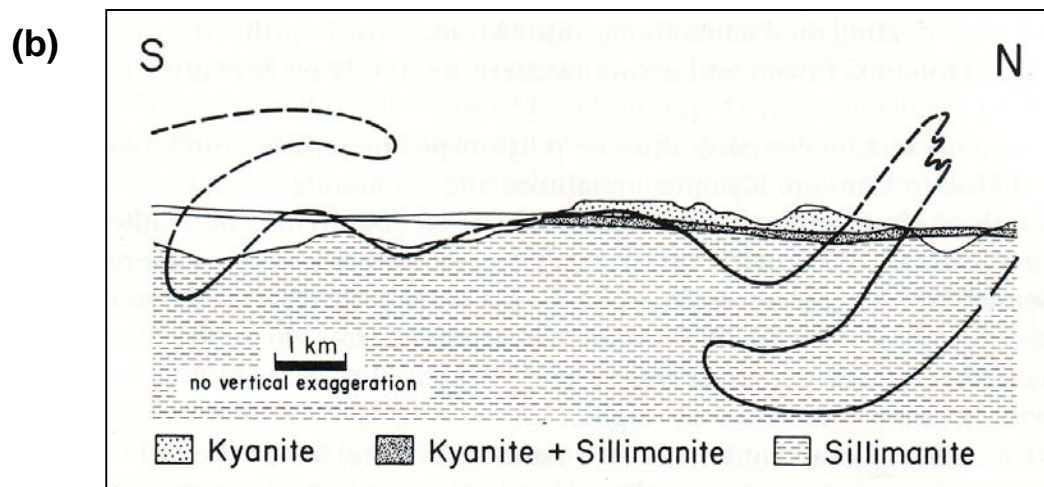
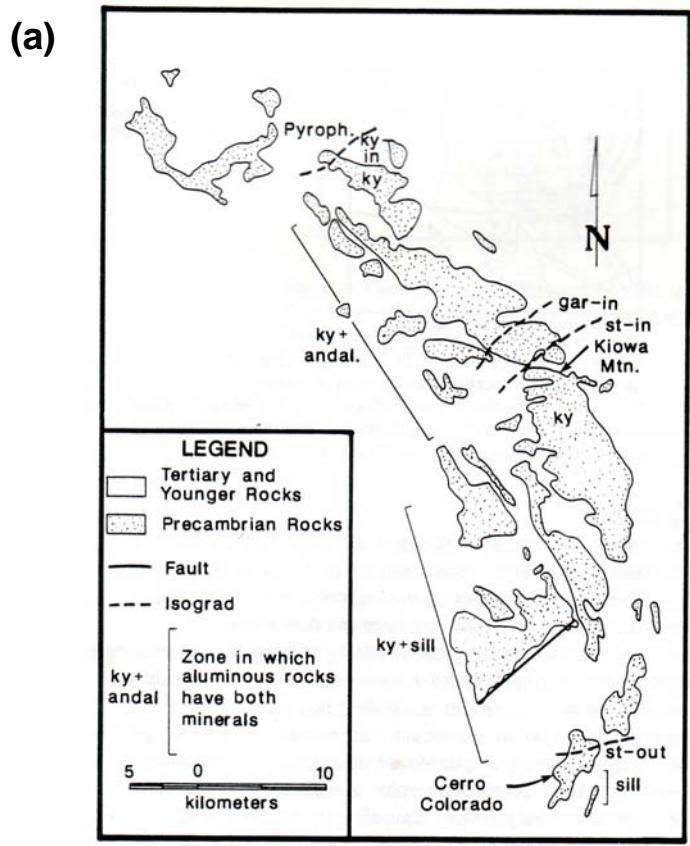


Figure 2.5. Isograd map of the Tusas Mountains showing an increase in metamorphic grade from the NW to SE (a), and a schematic drawing showing the relationship between the sub-horizontal metamorphic overprint and large map-scale folds at the Rio Mora Uplift (b) (from Grambling and Williams, 1985).

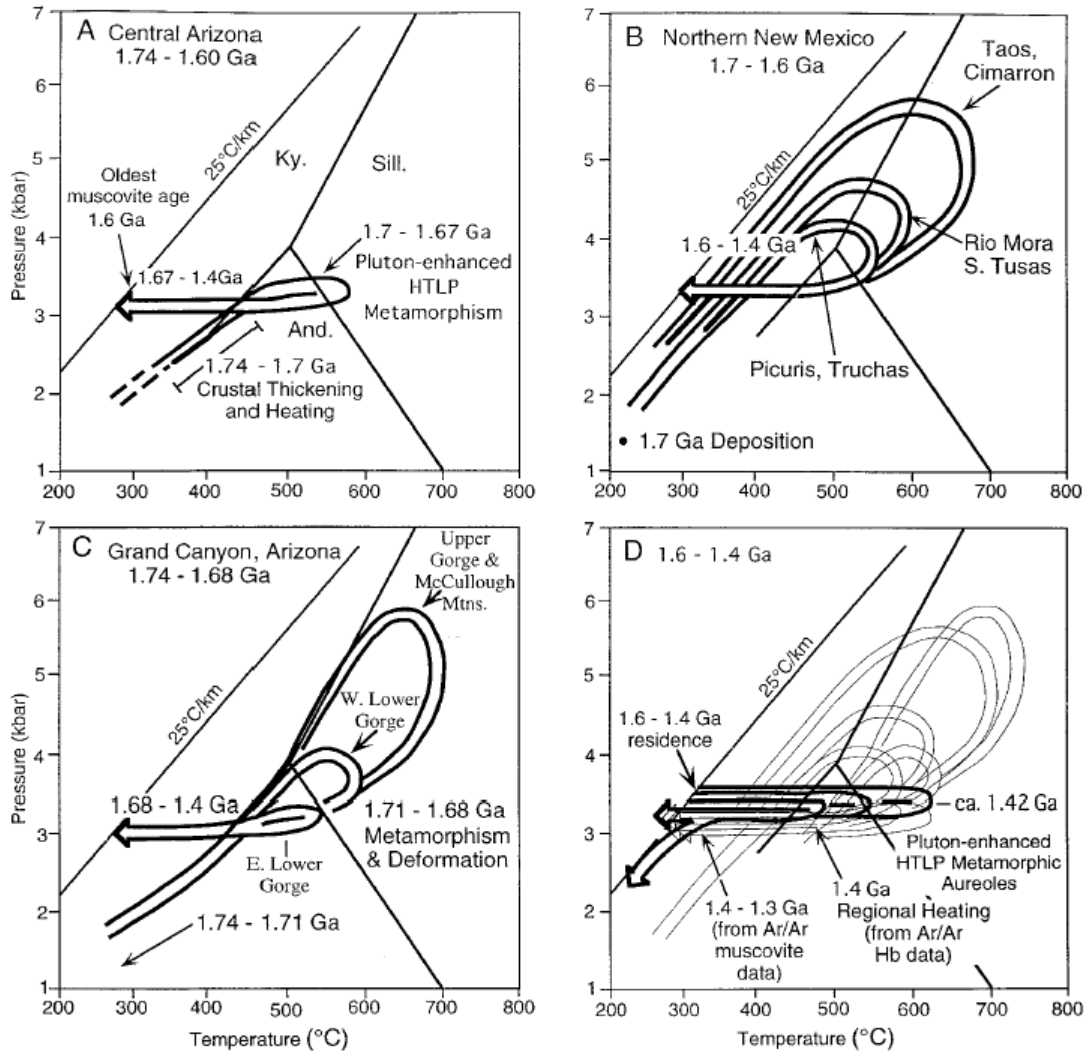


Figure 2.6. P-T loops for Proterozoic rocks from the southwestern USA; paths highlighted in B specifically apply to the Tusas Mountains (from Williams and Karlstrom, 1996).

associated with D2, have provided ages of both circa 1.6 and 1.4 Ga (U-Pb in monazite and zircon and $^{40}\text{Ar}/^{39}\text{Ar}$ in hornblende and mica) (Bishop, 1997; Karlstrom et al, 1997; Wingsted, 1997; Davis, 2003; Kopera, 2003). M3 minerals, which are thought to be associated with D3, provide ages of circa 1.4 Ga. Supporters of the single event theory state that because M2 and M3 minerals date to 1.4 Ga, all the minerals grew at roughly the same time (Daniel and Pyle, 2005). Proponents of the traditional polyphase history suggest that recrystallization of M2 minerals during the 1.4 Ga orogeny reset time sensitive minerals to a younger age (Williams et al, 2003).

CHAPTER 3

METHODS

Field and laboratory techniques were applied in this study in order to characterize the Mn horizon and to use Mn-andalusite as a tool to compare the metamorphic and structural histories of the Hopewell Lake-Jawbone Mountain area, Quartzite Peak, and Kiowa Mountain. Fieldwork focused on identifying the location and extent of Mn-andalusite mineralization in the areas studied and placing the Mn horizon in context stratigraphically. Microscale observations were focused on characterizing the Mn horizon and interpreting microstructural and metamorphic mineral relationships. The electron microprobe (EMPA) was used to obtain compositional analyses of hematite and Mn-andalusite and to create compositional x-ray maps to observe textures in the Ti and Fe distribution in hematite and the Mn distribution in Mn-andalusite. EMPA compositional data were used to calculate an estimated metamorphic pressure and temperature for Quartzite Peak and Kiowa Mountain.

Field Methods and Sample Collection

Five weeks of fieldwork conducted over the summer of 2006 focused on identifying and characterizing Mn-mineralization in the field and placing the Mn horizon in a stratigraphic context. Contact and structural mapping in the Hopewell Lake-Jawbone Mountain area was concentrated on identifying the extent of Mn-andalusite mineralization and constraining the relationship between the Jawbone syncline and the Hopewell anticline. A traverse across the Vadito-Hondo contact in the Hopewell Lake-Jawbone Mountain area, at Quartzite Peak, and at Kiowa Mountain helped to constrain the stratigraphic context of the Mn horizon in each of those areas. Samples were collected across each traverse and include samples from the metasedimentary and metavolcanic units of the Vadito Group and the Ortega Formation (Appendix 1). Whenever possible, an oriented sample was taken. A few unoriented samples were collected near their suspected point of origin. A total of 40 oriented samples and 13

unoriented samples were collected from across the Vadito-Hondo contact from the Hopewell Lake-Jawbone Mountain area, Quartzite Peak, and Kiowa Mountain

Thin Section Preparation and Analysis

A collection of both old and new thin sections was compiled for use in microstructural and petrologic analysis of samples from across the Vadito-Hondo contact in the Hopewell Lake-Jawbone Mountain area, Quartzite Peak, and Kiowa Mountain. Existing thin sections prepared by previous researchers (Michael L. Williams, Joe Kopera, and Catherine Lombardi) containing Mn-phases, particularly Mn-andalusite, were selected for use in this study. New thin sections, both covered and polished sections, were prepared from samples collected in the field. When structures and fabrics could be confidently identified, thin section billets were cut perpendicular to the main foliation and, if possible, parallel to the main lineation. Many sections were prepared from billets cut perpendicular to the horizontal in “map view” to show the relationship between more than one fabric generation.

Microstructural and petrologic observations were made using a WILD polarizing microscope and a standard transmitted-light petrographic microscope. Microstructural observations documented the alignment of minerals, the orientation of mica grains, the composition of fabrics, growth-timing relationships between the fabric and porphyroblast, and textures preserved in Mn-andalusite. A reflected-light petrographic microscope was used to identify textures in hematite. Petrologic observations documented the mineral assemblage, relationships between minerals, and mineral inclusions. The electron microprobe was also used to image textures and identify phase relationships.

Electron Microprobe X-Ray Mapping and Compositional Analysis

The Cameca SX50 electron microprobe (EMP) at the University of Massachusetts was used to make compositional x-ray maps for Ti, Fe, Al, and Mn, generate BSE images, and to obtain compositional point analyses on selected carbon coated polished sections.

Compositional x-ray maps were obtained using a 15kV accelerating voltage, 100nA current, 50-

100 ms count time, and 0-5um beam and analyzed for the $K\alpha$ x-ray line for Ti, Fe, Mn, or Al. BSE images and X-ray maps were used to image textures in Mn-andalusite and hematite. Point analyses were run at 15kV accelerating voltage and 15nA current and analyzed for the following oxides: MgO, Mn₂O₃, CaO, K₂O, TiO₂, Fe₂O₃, Al₂O₃, SiO₂, ZnO, Cr₂O₃, BaO, V₂O₃, Ce₂O₃, SO₂, Nb₂O₃, ZrO₂, Ta₂O₅, Sb₂O₃, NiO, and CuO. Corrections were made to V₂O₃ values to resolve the interference between Ti and V x-rays. Aluminum silicate formulas were calculated using 5 oxygens and Al, Mn, and Fe as cations. Quantitative point analyses were used to obtain compositional data specifically for Mn-andalusite, kyanite, hematite, and rutile, and data from Mn-andalusite and kyanite were used to calculate estimated P-T conditions.

Pressure-Temperature Calculations

Pressure-temperature estimates are based on the calculations presented in Grambling and Williams (1985). The calculations used compositional values obtained from spaced quantitative point analyses across a kyanite-andalusite contact in intergrown Mn-andalusite and kyanite from the Mn-andalusite layer in the Ortega Formation at Quartzite Peak and Kiowa Mountain. A reasonable estimated temperature range was extrapolated for an $X_{FeAlSiO_5}$ value in Mn-andalusite from Figure 15 of Grambling and Williams (1985). This temperature range was applied to equation four of Grambling and Williams (1985) to obtain a pressure offset for the kyanite-andalusite reaction line based on the $X_{Al_2SiO_5}$ values for kyanite and Mn-andalusite. The offset is caused by the stabilizing effects Mn has on andalusite. ΔV values were calculated from an andalusite value of 51.45cm³ (Gunter and Bloss, 1982) and a kyanite value of 44.60 cm³ (Holdaway, 1971).

CHAPTER 4

STRUCTURAL GEOLOGY

General Structure of the Tusas Mountains

The Tusas Mountain Range preserves evidence for three periods of deformation (D1, D2, D3) that are associated with three generations of fabric (S1, S2, S3) and fold (F1, F2, F3) formation (Williams, 1991; Williams et al, 1999). D1 involved the formation of a bedding parallel fabric (S1), recumbent F1 folds, and stratigraphic discontinuities related to stacked sections and bedding parallel thrusts. D2 involved the formation of centimeter- to kilometer-scale tight to isoclinal, reclined F2 folds with NW-striking, SW dipping axial plane cleavage (S2). D3 involved the formation of upright and open F3 folds, an E-NE striking cleavage (S3), and a broadly spaced crenulation cleavage. Large, map-scale synclines, namely the Jawbone syncline, the Kiowa syncline, and the La Madera syncline, are interpreted as F2 (or late F1) folds. The southern limbs of the synclines have been truncated by south-dipping ductile shear zones with a south over north shear sense (Fig. 2.4 & 4.1; Grambling et al, 1989; Williams, 1991). The location of a number of faults or shear zones have been postulated, including one south of the Jawbone syncline and one north of the Kiowa syncline (the Spring Creek Shear Zone) (Fig. 4.1; Williams, 1991; Davis, 2003; Koper, 2003).

Fabrics

S0

Aluminous, hematite-bearing layers (“kaolinitic mudstone drapes” of Soegaard and Erikson, 1986) and cross-beds define S0 in the Ortega Formation. The aluminous, hematite-bearing layers are characterized by concentrations of hematite, rutile, zircon, monazite, and aluminum silicates, such as kyanite and andalusite. In the Mn horizon, S0 is additionally characterized by the occurrence of distinct high-Mn core regions (see Chapter 6). S0 is defined by primary sedimentary structures, such as cross beds, in the metasediments of the

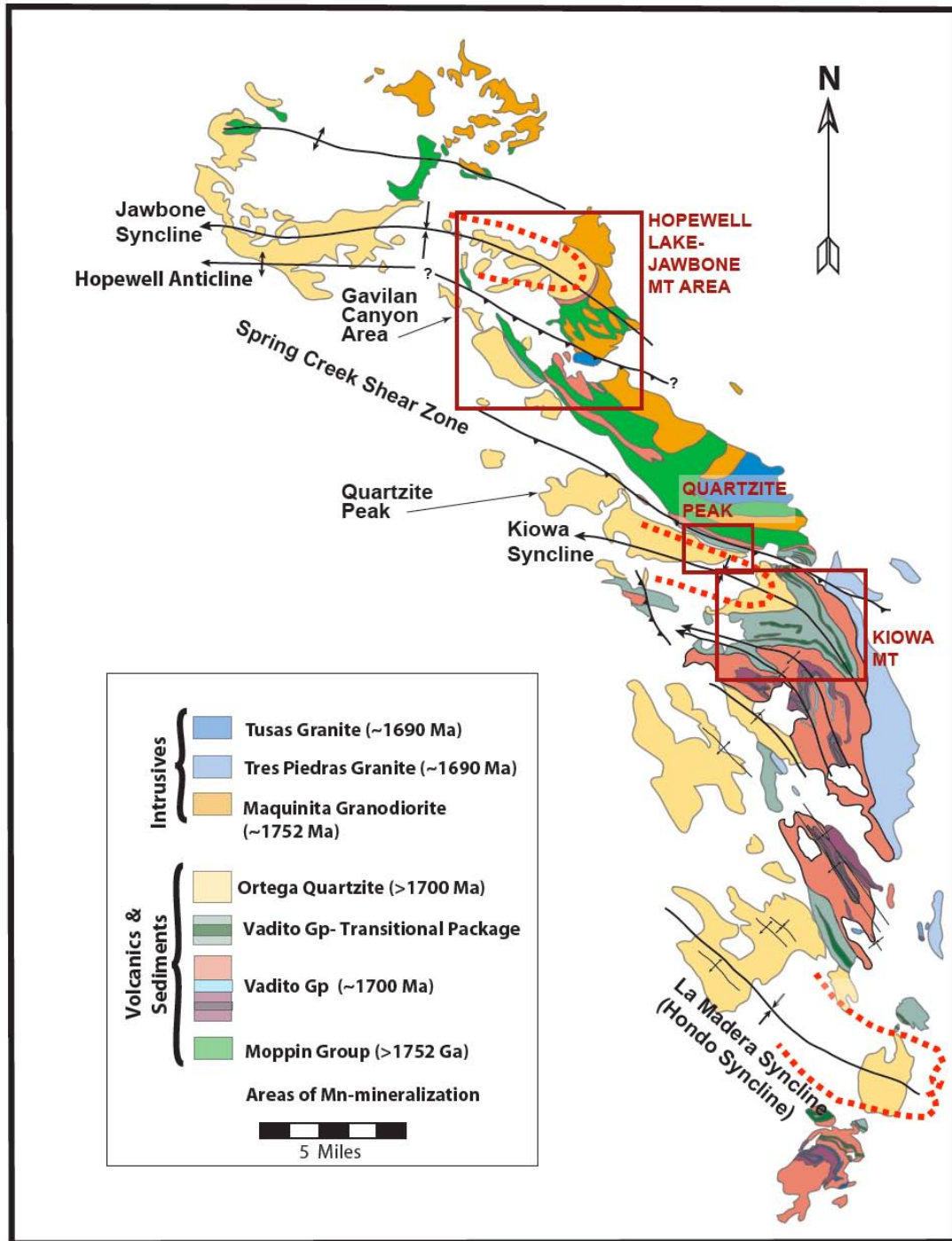


Figure 4.1. A lithologic map of the Tusas Mountains showing the location of the Hopewell Lake-Jawbone Mountain area, Quartzite Peak, and Kiowa Mountain field areas relative to map-scale synclines and shear zones (adapted from Kopera, 2003 and Williams, 1991).

Vadito Group and by light colored feldspar-rich lenses and elongate pods in the amphibolites. In the Burned Mountain Formation metarhyolite, S0 is defined by visually distinct layers, pods, and lenses that are interpreted to represent primary compositional and/or textural banding.

S1/F1/L1

S1 is a bedding-parallel cleavage that is axial planar to rare, recumbent centimeter-scale F1 folds. An L1 stretching lineation is defined by the long axis of “oriented kyanite crystals”, “hematite aggregates”, and “stretched quartz” (Kopera, 2003). In the Ortega Formation, S1 is defined by alignment of hematite crystals, winnowed quartz pebbles, and bands of aluminum silicates (Mn-andalusite and kyanite). S1 and F1 are best preserved in the alignment of fine hematite inclusions in aluminum silicate crystals within the aluminous, hematite-bearing layers (Fig. 4.2c). In the Mn horizon, hematite aligned in S1 can commonly be found wrapping high Mn-core regions (see Chapter 6). Rare recumbent F1 folds are preserved in the alignment of very fine-grained hematite and rutile crystals in the high Mn-core regions of the Mn horizon (Fig. 4.2a,b). In the Burned Mountain Formation metarhyolite, S1 is subparallel to primary compositional and/or textural banding (S0) and is defined by aligned muscovite and elongate feldspar and quartz crystals. In the metasediments of the Vadito Group, S1 is defined by the alignment of minerals, such as hematite, and is variably preserved. Commonly, S1 has been overprinted and incorporated into an S0/S1/S2 composite fabric.

S2/F2

S2 is a ubiquitous northwest striking, moderate to steeply southwest dipping cleavage that is axial planar to tight to isoclinal, reclined, centimeter to kilometer-scale F2 folds of S0/S1. S2 varies in character across the Tusas range and F2 folds range from mild crenulations to overturned, isoclinal folds. In the Ortega Formation, S2 is defined by quartz pebbles flattened parallel to S2, the alignment of elongate hematite, kyanite, and Mn-andalusite crystals, and flattened, discrete planes of massive aluminum silicates in outcrop (Fig. 4.3). F2 crenulations

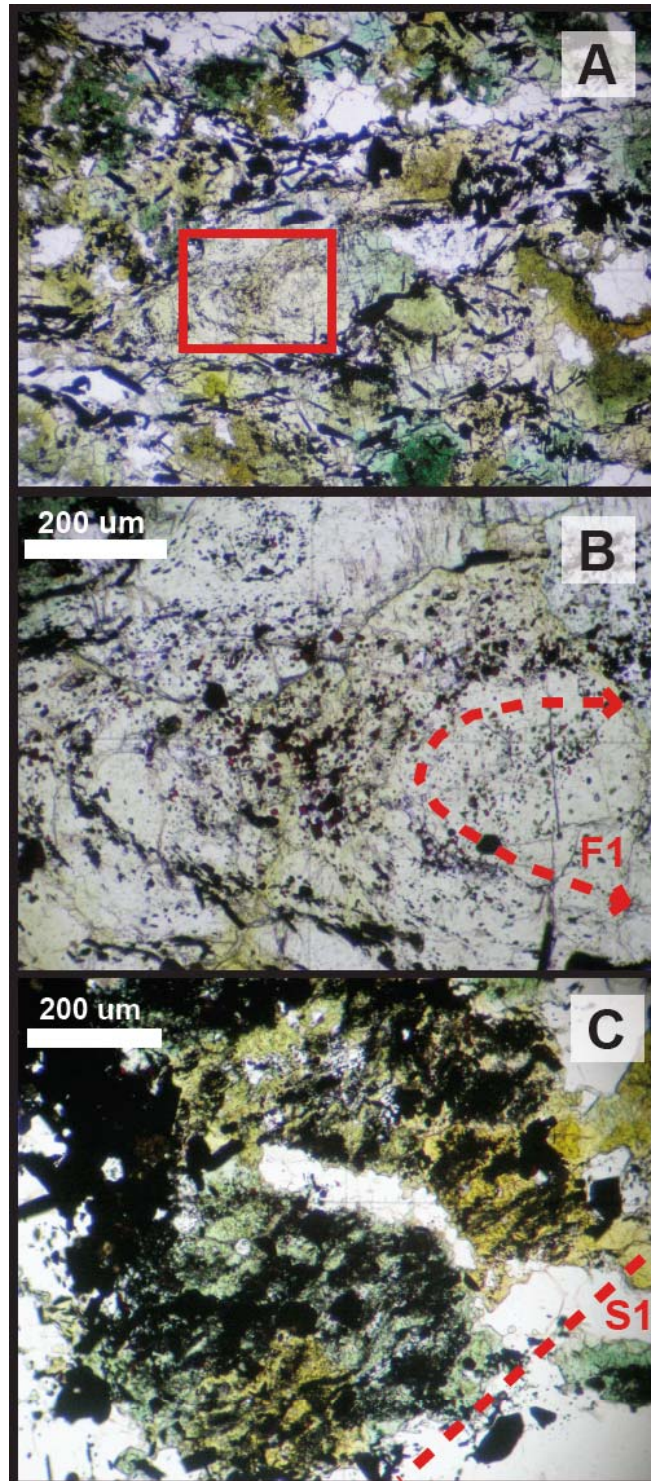


Figure 4.2. F1 (a,b) and S1 (c) are preserved in the distribution of fine-grained hematite in samples from Mn-andalusite layer of the Hopewell anticline (a,b- MLW1C; c-P06NM20C).

of S1 are preserved within the alignment of hematite inclusions in the cores of aluminum silicate crystals. In the Mn horizon of the Ortega Formation, hematite aligned in S2 commonly wraps high Mn-core regions (Fig. 6.5d). In the Burned Mountain Formation metarhyolite, S2 is primarily defined by aligned muscovite as well as some quartz and feldspar “phenocrysts” with edges that have been flattened in the direction parallel to S2. Elongate quartz and feldspar crystals and muscovite aligned in S1 are reoriented and folded by F2 folds. In the Vadito Group, S2 is defined by the alignment of phyllosilicates, elongate hematite, feldspar, quartz, and/or epidote in the metasediments and in the alignment of hornblende, hematite, phyllosilicates, and feldspar in the amphibolites.

S3/F3

S3 is an east-west striking, subvertical to steeply north dipping cleavage that is axial planar to upright F3 folds. F3 folds include centimeter-scale crenulations, open to tight meter-scale axial planar folds, and millimeter to meter-scale open crenulation folds. F3 open crenulation folds are found at all scales and are formed when one limb of the fold maintains an original orientation (dominantly NW-SE) and the other is transposed into an orientation that is parallel to S3 (dominantly E-W) (Fig. 4.4 & 4.5). F3 crenulation folds gently warp and/or steepen S2 and F2 folds in outcrop and include the transposition of aluminum silicate and hematite-rich S2 cleavage into an S3 orientation on the microscale (Fig. 4.5). In the Ortega Formation, S3 is defined by quartz pebbles flattened parallel to S3, aligned, elongate hematite, and rarely flattened, discrete planes of massive aluminum silicates. In the Vadito Group, S3 is defined by the alignment of hematite, phyllosilicates, and/or hornblende.

S2/S3 - Composite Fabric

The combination of S2 and S3 cleavages contribute to the formation of a scale-dependent “fabric” that is in an orientation intermediate between S2 and S3. At the outcrop scale, the composite fabric is defined by elongate quartz pebbles and discrete aluminum silicate and hematite-rich planes (Fig. 4.6). In thin section, the composite fabric is defined by

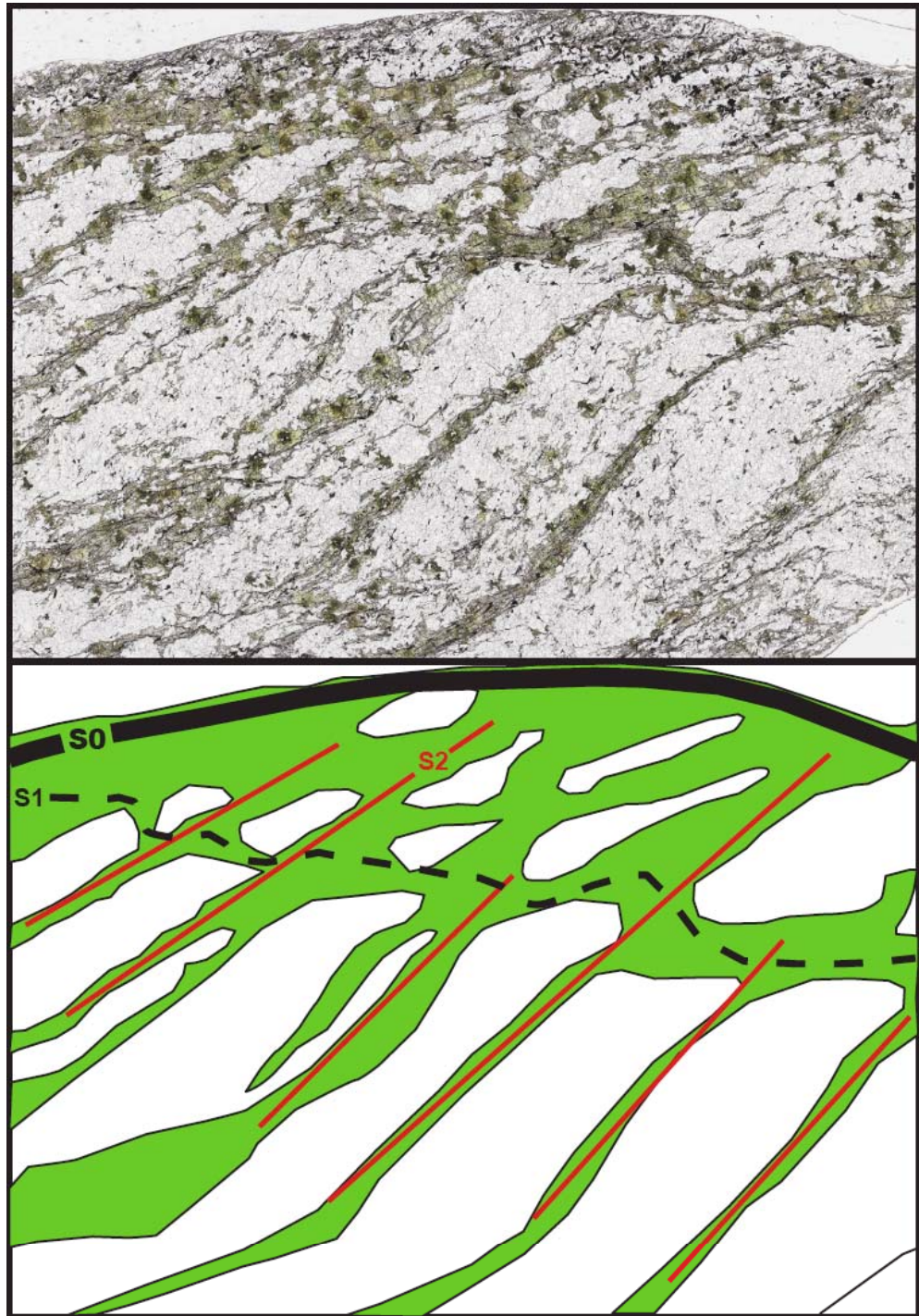


Figure 4.3. Discrete Mn-andalusite-rich S2 cleavage planes disrupt the S0/S1 composite surface in this sample from the Hopewell Lake-Jawbone Mountain area (sample-P06NM15A).

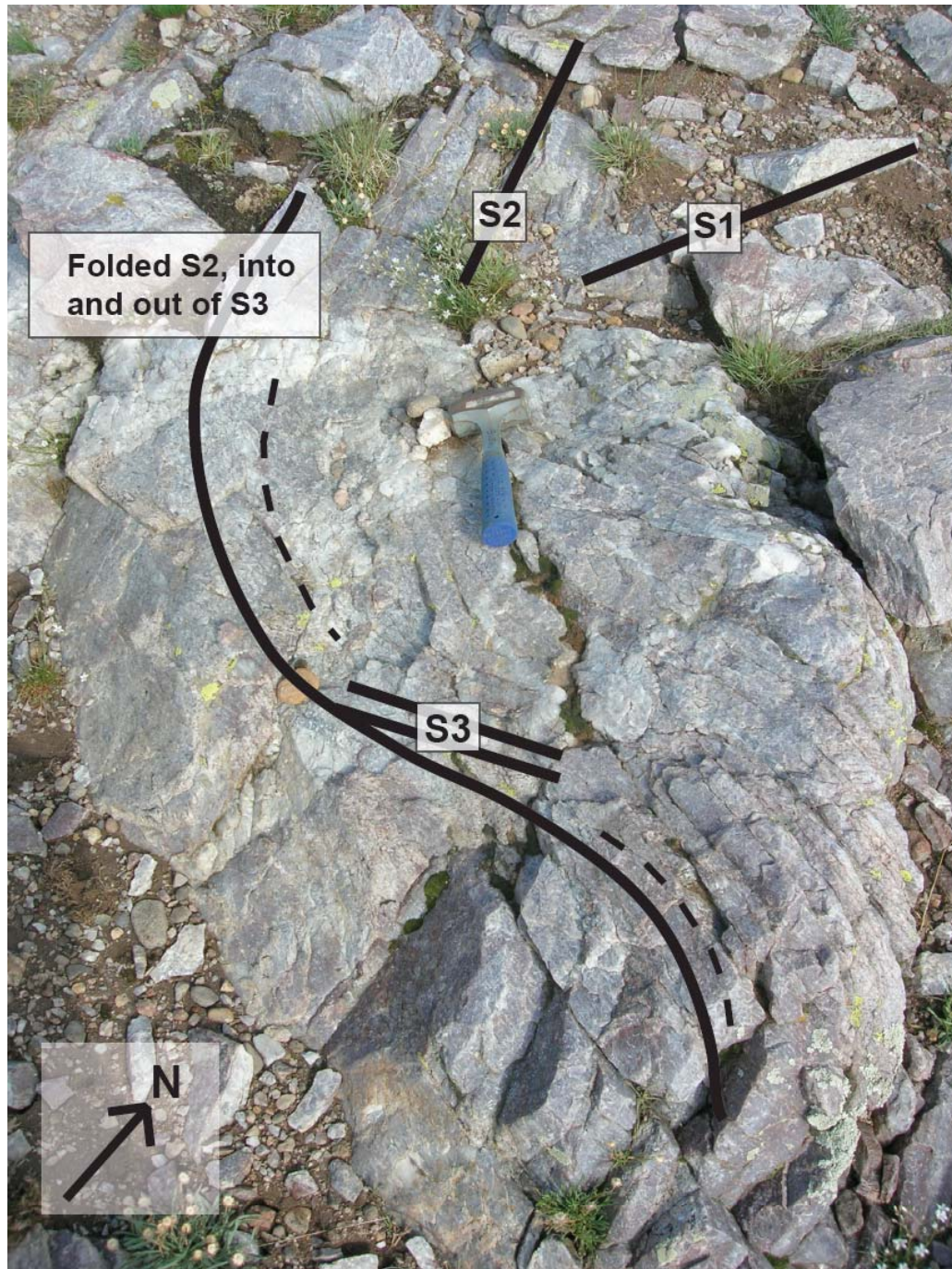


Figure 4.4. F3 crenulations of S2 in outcrop fold S2 in such a way as to maintain one limb in the NW-SE S2 orientation and transpose the other into the E-W S3 orientation.

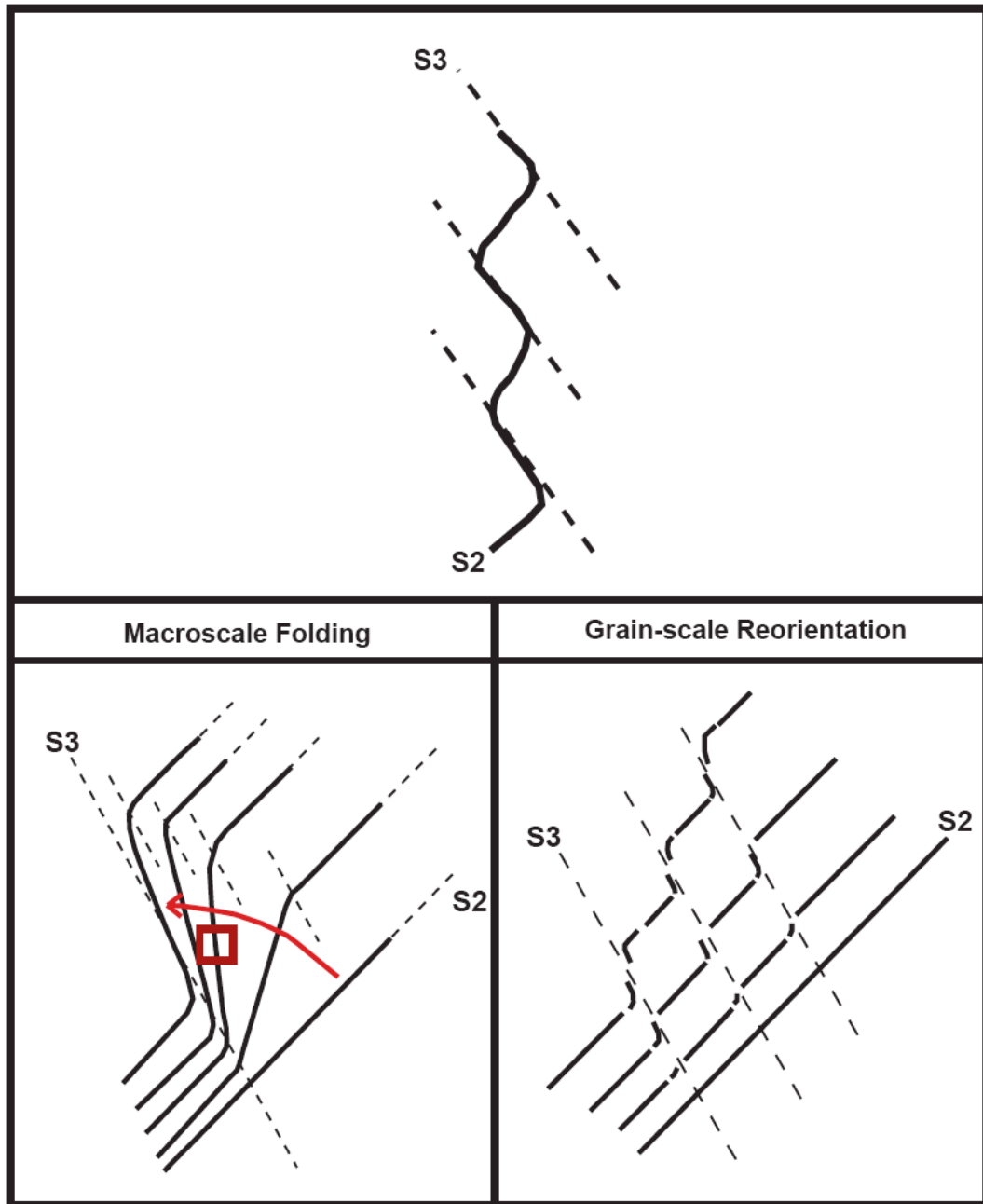


Figure 4.5. F3 crenulation folds form on the grain scale through the reorientation of oxides into S3 (bottom right) and may lead to the transposition of S2 into S3 on the macroscale (bottom left).

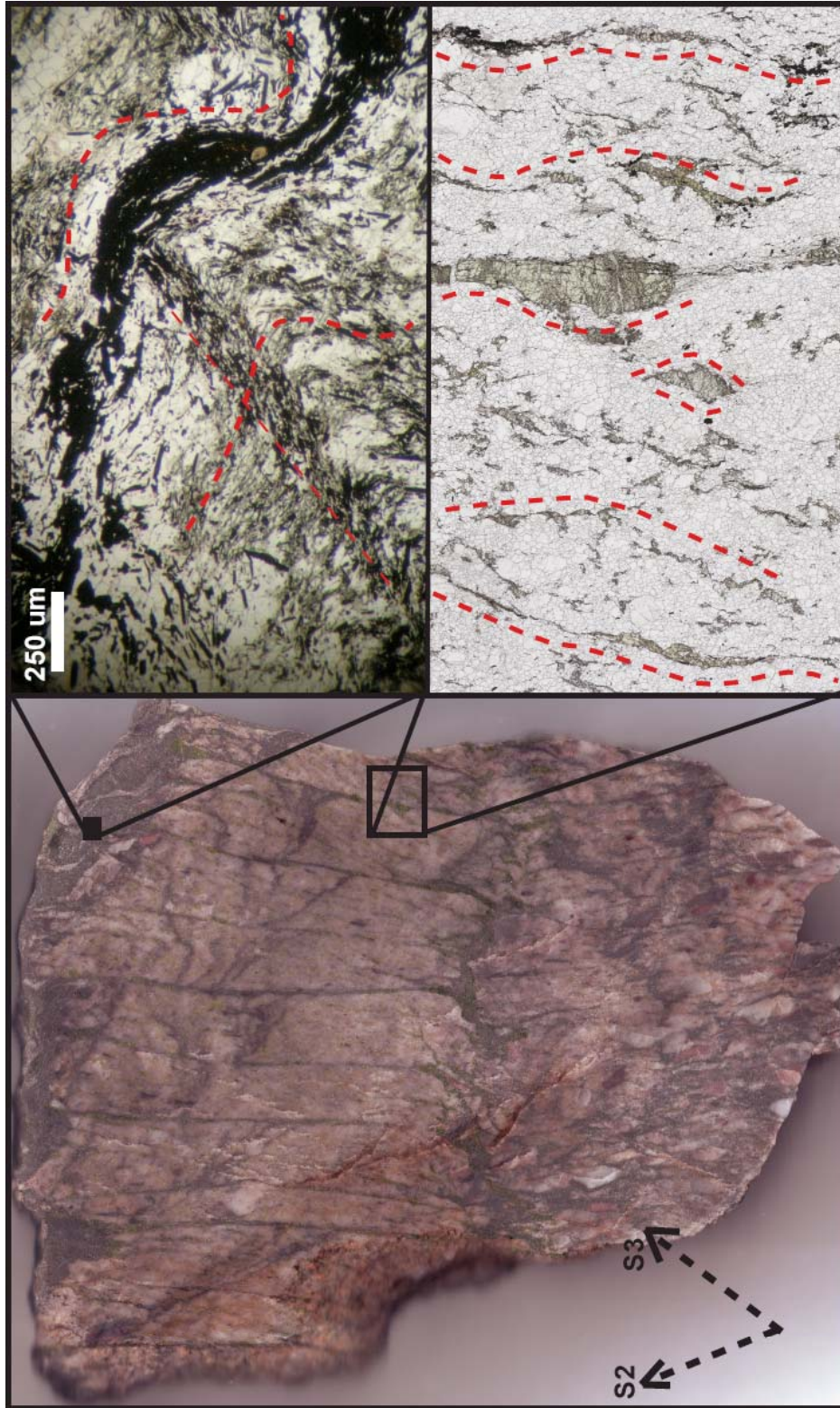


Figure 4.6. The S2/S3 composite fabric is defined in thin section by andalusite quadrilaterals with edges subparallel to S2 and S3 and the corners of which connect in a line parallel to the composite fabric.

quadrilateral-shaped islands, the opposite corners of which connect to form a line intermediate between S2 and S3 (Fig. 4.6 & 4.7). The sides of the quadrilateral-shaped islands are defined by two sets of parallel lines, one set aligned in S2 and the other aligned in S3. The islands are formed by the flattening of quartz pebbles in both S2 and S3. They are also formed from the combination of hematite aligned in both S2 and S3, such as when S2 is crenulated and reoriented into S3 (Fig. 4.7). When defined by planes of aluminum silicates, the composite fabric is composed of elongate islands of aluminum silicate that have been flattened in S2 and S3 (Fig. 4.6). When discrete hematite and aluminum silicate rich S2 cleavage planes are crenulated by F3 folds, the hinge of the fold will be aligned between S2 and S3 and can also help define the composite fabric (Fig. 4.7).

The composite fabric can be characterized as a scale dependent cleavage that is discrete in outcrop but is defined by S2/S3-sided quadrilaterals in thin section. There are several possible explanations for the formation of the composite fabric. It is possible, although unlikely, that the composite fabric is a result of the progressive change in stress orientation from northeast-southwest to north-south compression. The WNW-ESE composite fabric may represent one point of fabric formation during a progressive fabric-forming event between the formation of the penetrative NW-SE S2 and E-W S3 cleavages. It is also possible that the composite fabric is a result of the transposition of S2 into S3 during D3 (Fig. 4.5). The reorientation of aligned minerals on the microscale from S2 to S3 could lead to F3 folding in thin section but the incomplete reorientation of S2 into S3 on the macroscale. The intermediate orientation represents the incomplete transposition of S2 into S3.

Hopewell Lake-Jawbone Mountain Area

Strain is heterogeneously concentrated in the aluminous, hematite-bearing layers and in high strain zones within the Ortega Formation quartzite of the Hopewell Lake-Jawbone Mountain area (Fig. 4.8). S1, S2, S3 are best developed in the aluminous, hematite-bearing layers and primary sedimentary structures (S0), such as cross beds, are preserved outside of

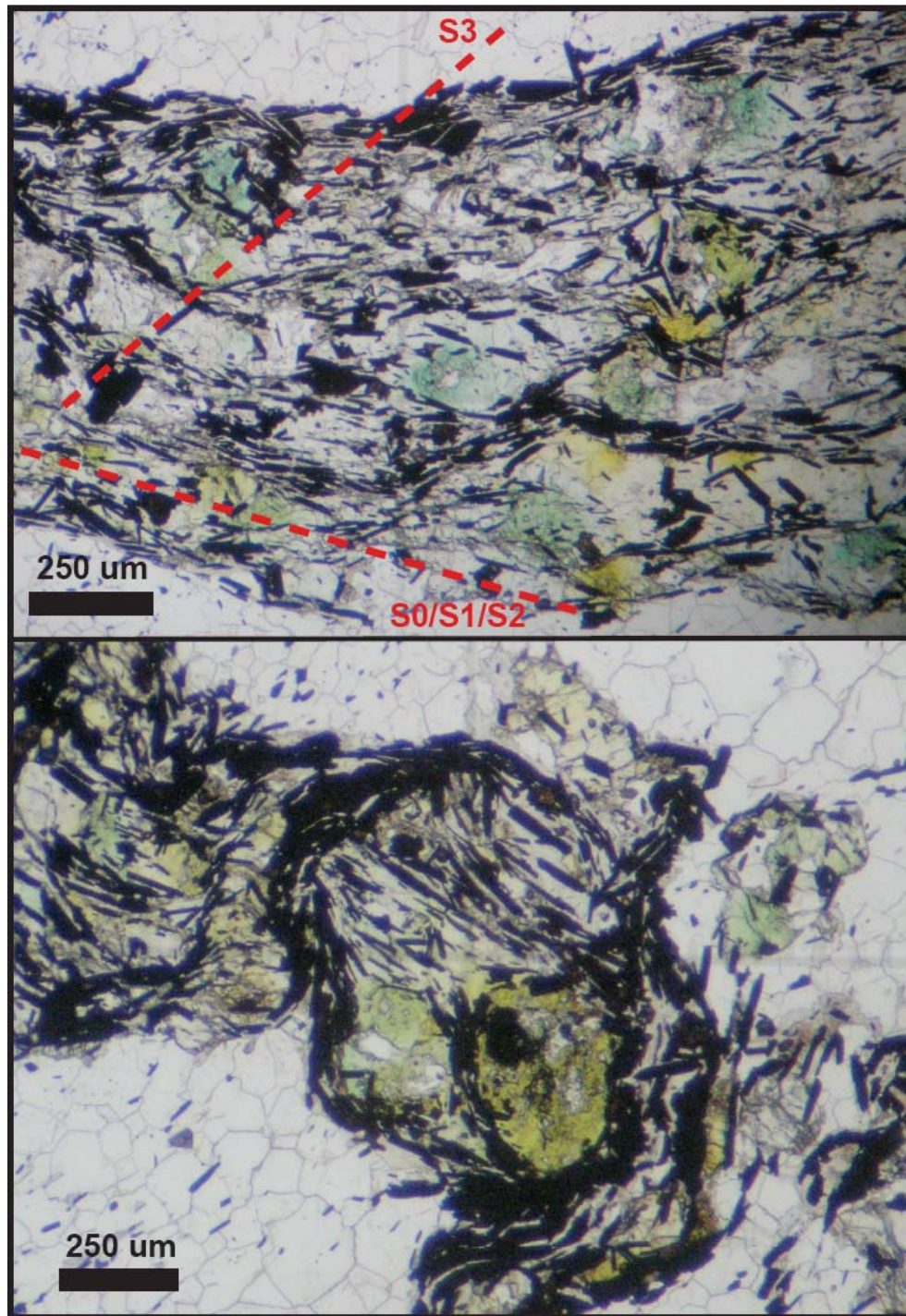


Figure 4.7. Elongate hematite crystals aligned in S0/S1/S2 are crenulated by F3 (top) forming quadrilateral shaped islands (bottom) the edges of which are subparallel to S2 and S3 (sample-P06NM21).

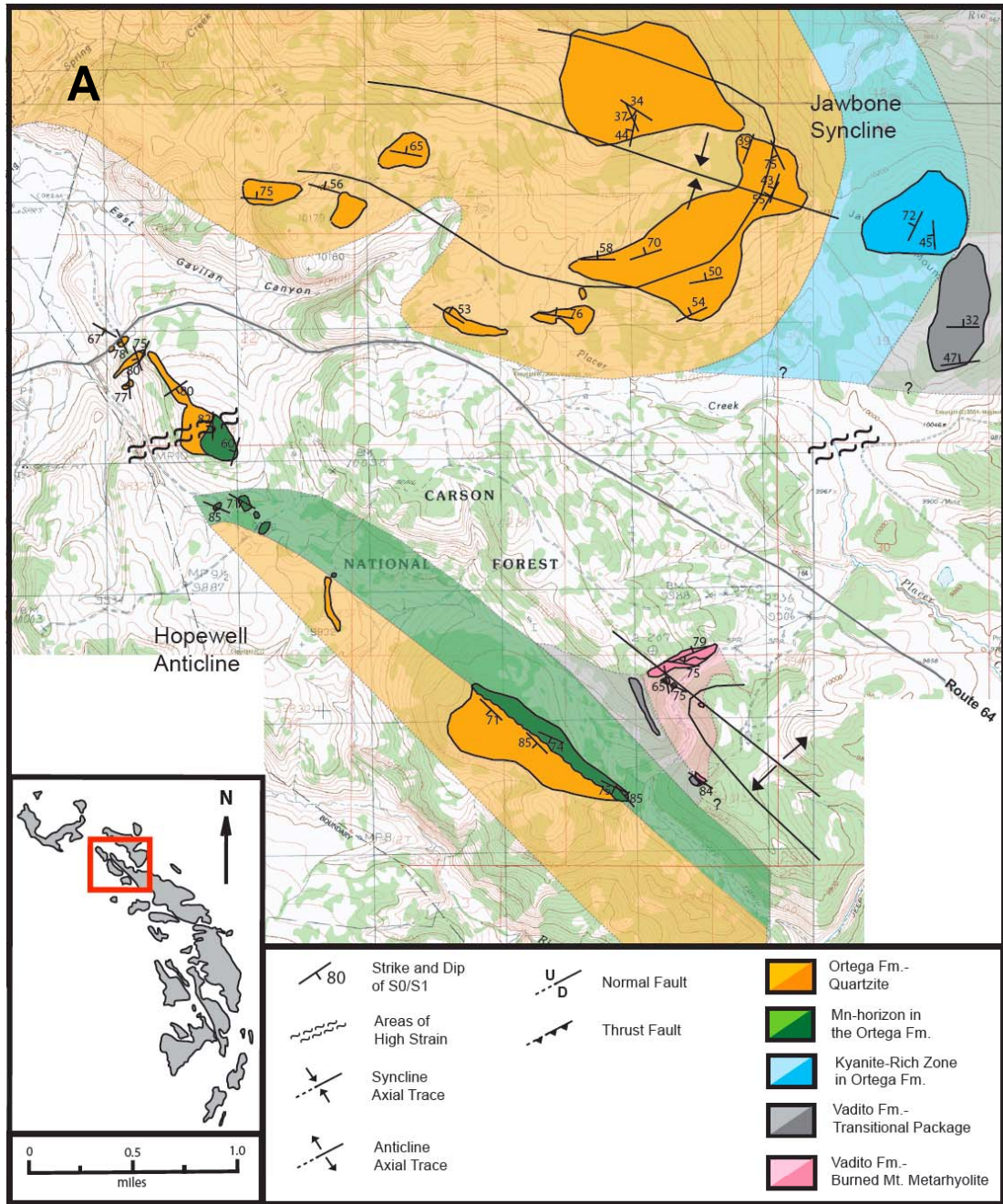


Figure 4.8. Lithologic map of the Hopewell Lake-Jawbone Mountain area showing the strike and dip of (a) S0/S1, (b) S2, and (c) S3.

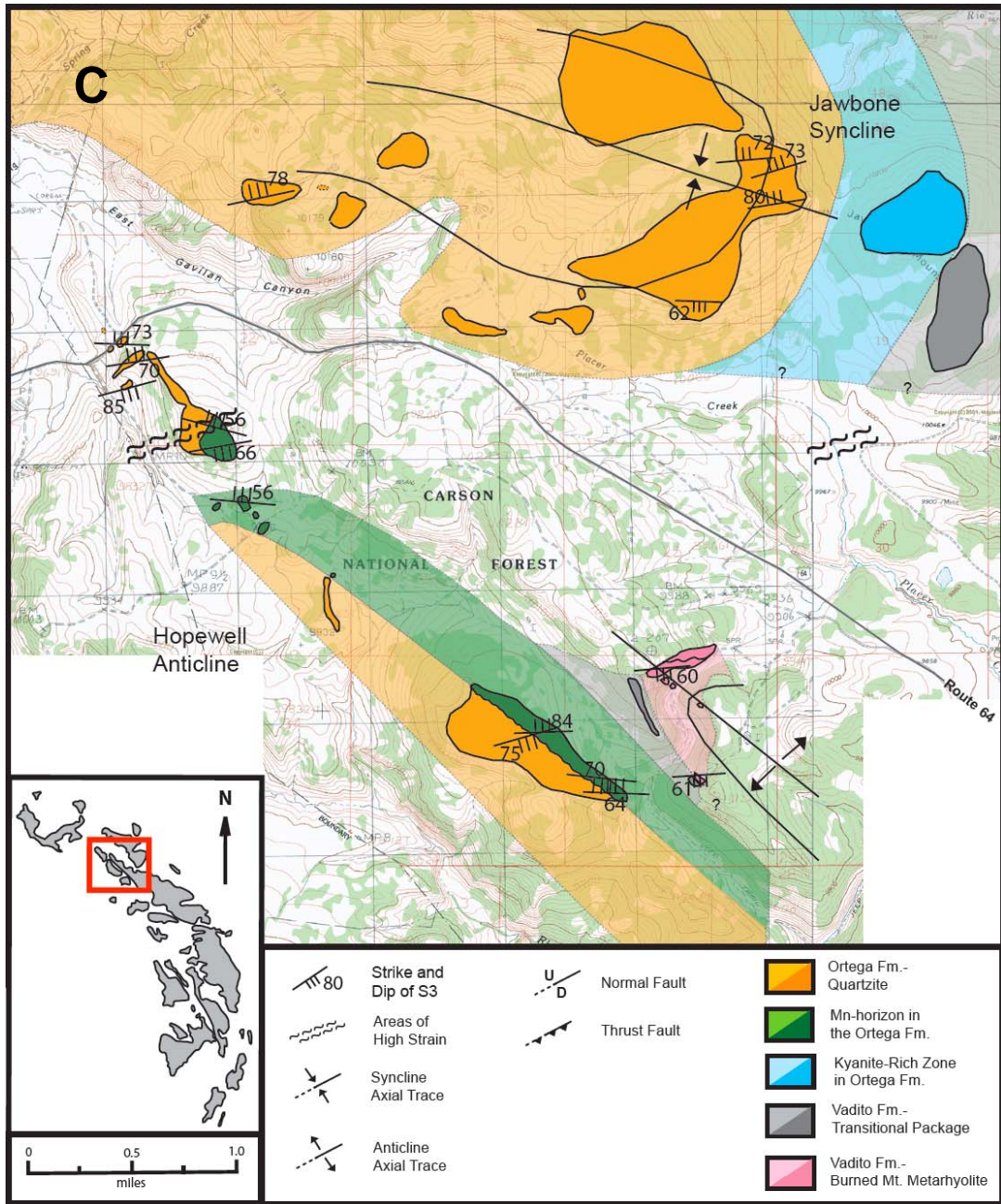


Figure 4.8. (continued).

the aluminous layers and high strain zones. The interaction between S1, S2, and S3 at the thin section scale within the aluminous, hematite-bearing layers in the Hopewell Lake-Jawbone Mountain region is diagrammed in Figure 4.9.

S2 varies in intensity and character across the Hopewell Lake-Jawbone Mountain area. When poorly developed, S2 is defined by aligned hematite and mild F2 crenulations within the aluminous, hematite-bearing layers, but when well developed, S2 is defined by aligned hematite and flattened, discrete planes of massive aluminum silicates that cut S0/S1 (Fig. 4.3). In places, S0/S1 shale drape layers are folded by centimeter-scale tight, reclined F2 folds with aluminum silicate filled axial planar S2 cleavage planes that originate at and extend outward from the hinge zone of the folds (Fig. 4.10).

F3 crenulation folds are common across the Hopewell Lake-Jawbone Mountain area. At the map-scale, S0/S1/S2 varies in strike between $\sim 090^{\circ}$ - 135° on the southern limb of the Hopewell anticline and between ~ 240 - 290° on the southern limb of the Jawbone syncline due to gentle, meter-scale F3 crenulation folds (Fig. 4.4). Intense S3 development and F3 folding was particularly concentrated in localized map-scale high strain zones in the Hopewell Lake-Jawbone Mountain area. An extensive S3 fracture cleavage, tight, upright F3 folds, and discrete planes of massive aluminum silicates subparallel to S3 are exclusively found in the high strain zones.

Quartzite Peak

S0 is defined in thin section as a concentrated zone of hematite, rutile, and aluminum silicate clusters composed of Mn-andalusite and kyanite. S1, S2, and S3 are preserved as hematite defined inclusions trails within the clusters. F2 and F3 crenulation folds combine S1, S2, and S3 in such a way as to create an "S-shaped" inclusion trail in the aluminum silicate clusters (Fig. 4.11). S2 and F2 are extensively folded by open F3 crenulation folds, particularly at the microscale, with one limb of the fold maintained in the S2 orientation and the other limb transposed into the S3 orientation. A scale-dependent S2/S3 composite fabric is ubiquitous at Quartzite Peak. It appears penetrative in outcrop (290 - 302° , dips 74 - 89°) but is defined by

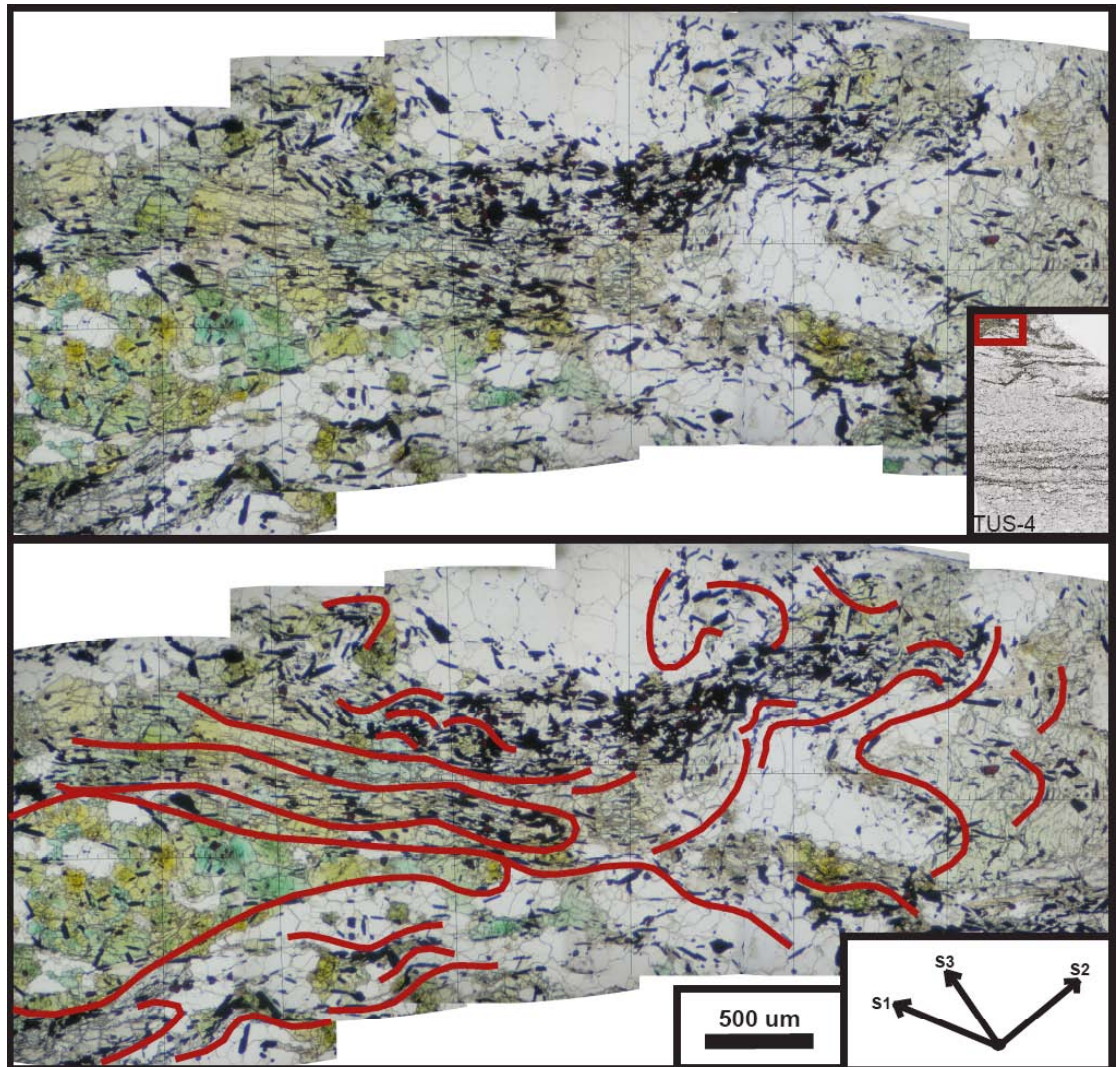


Figure 4.9. Hematite inclusion trails that define S1, S2, and S3 create a complex oxide pattern in samples from the Hopewell Lake-Jawbone Mountain area and an attempt to interpret the evolution of fabrics in sample Tus4 is shown.

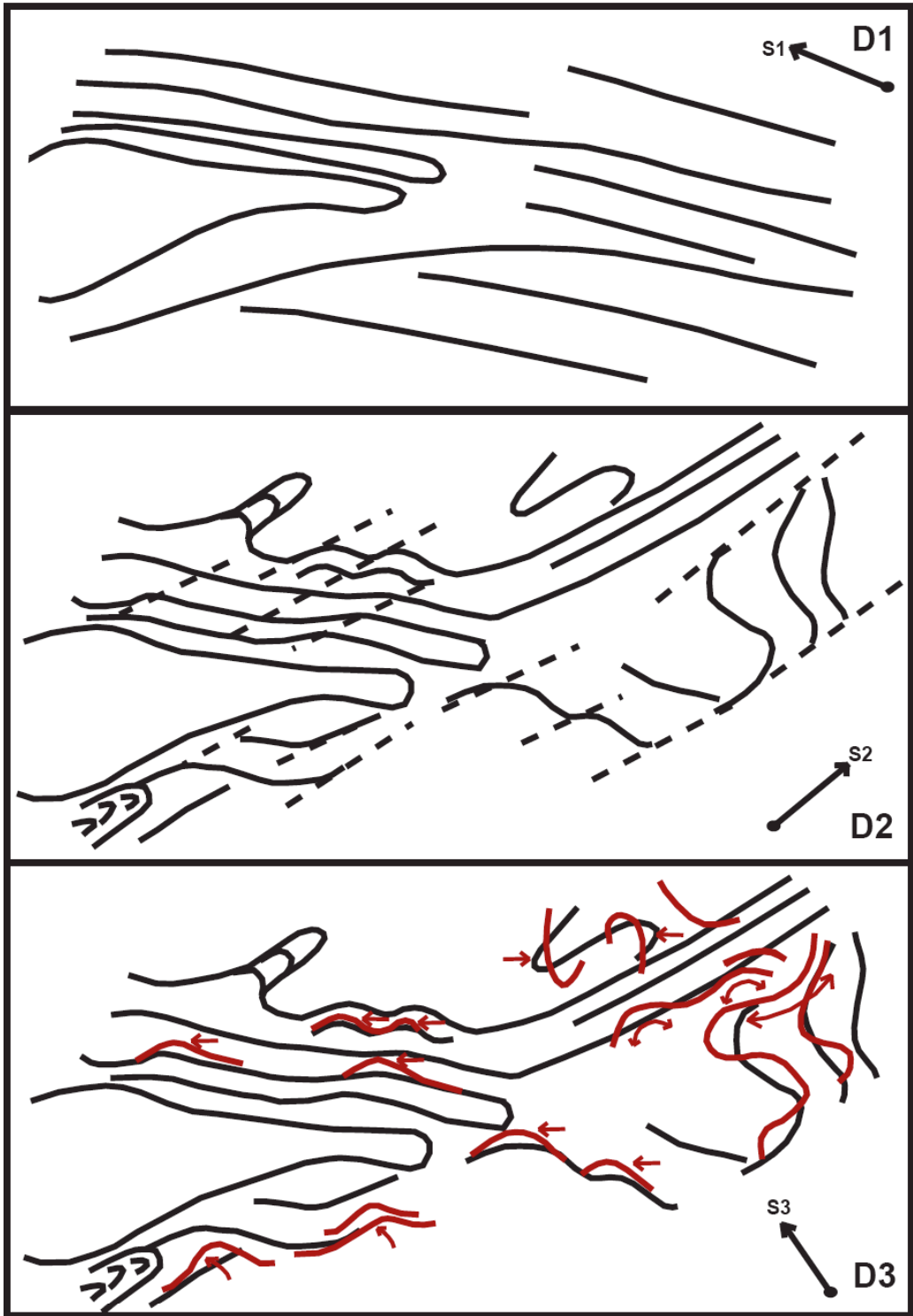


Figure 4.9. (continued).

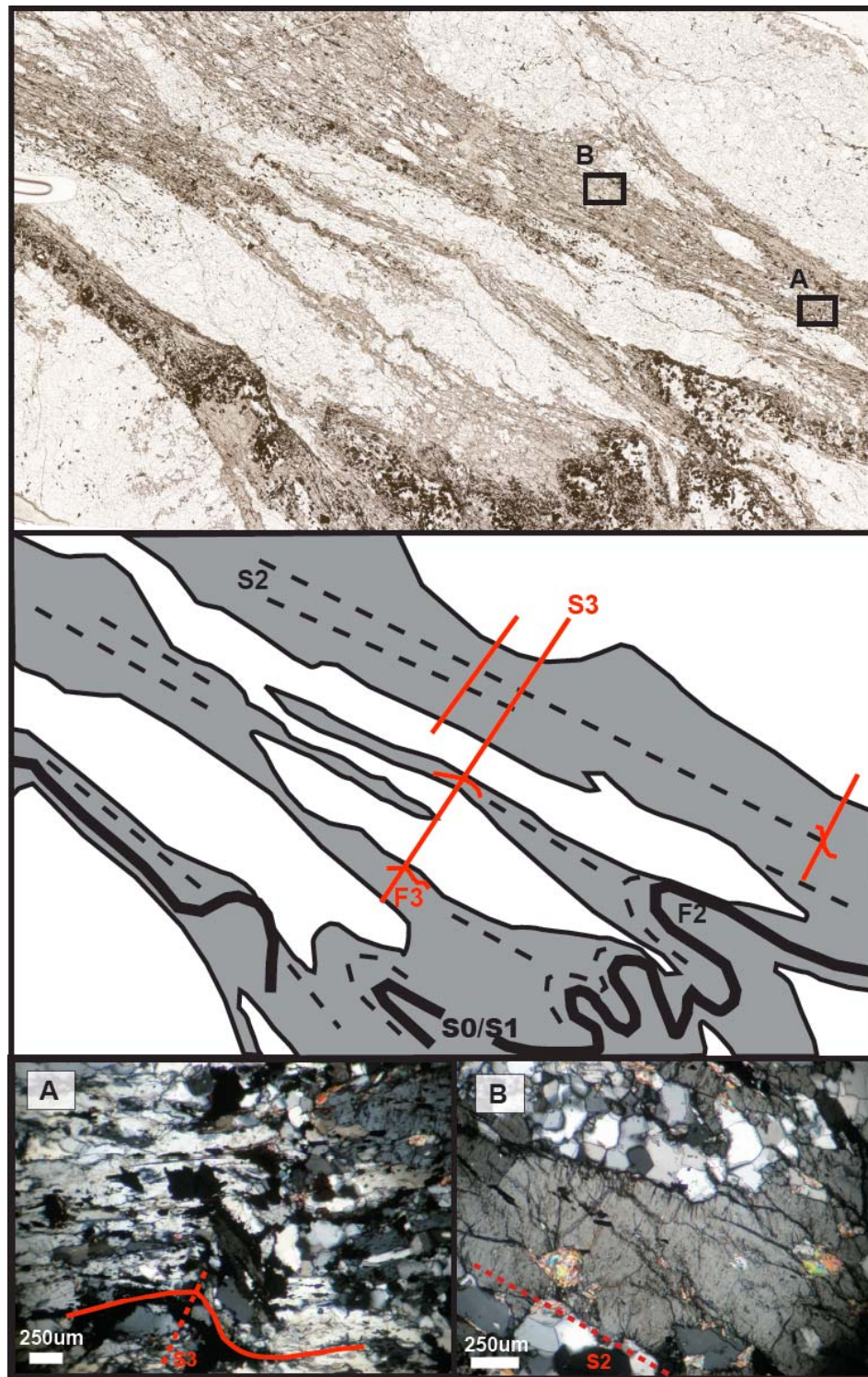


Figure 4.10. Optically-continuous andalusite crystals (b) in P06NM12A preserve evidence for S2 development and F2 folding. Later D3 has strained andalusite crystals (a) leading to localized S3 development and F3 folding.

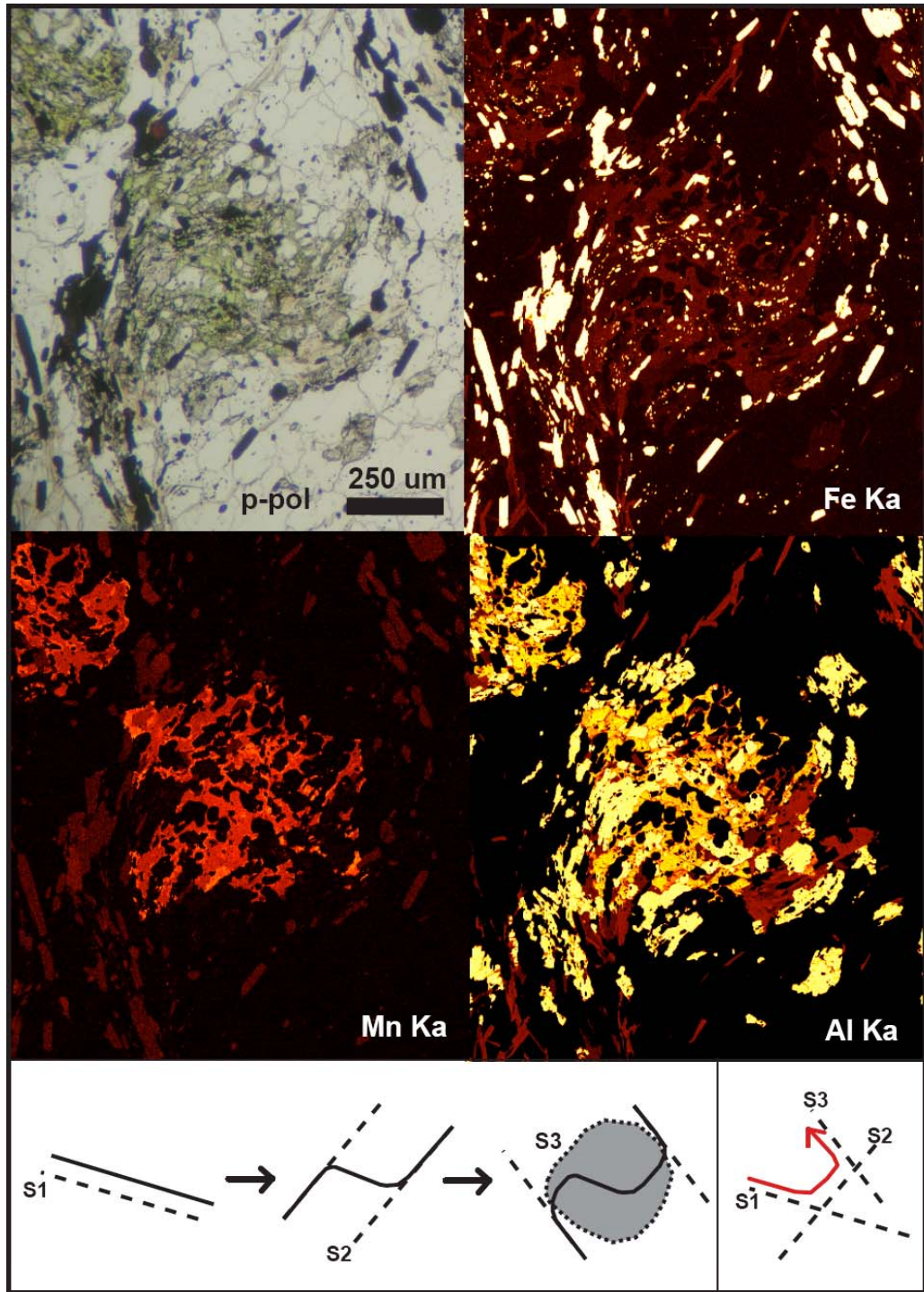


Figure 4.11. The progressive evolution of fabrics at Quartzite Peak produces a sigmoid shape from the combination of S1, S2, and S3 that can be mistaken as evidence of shear (EMP x-ray maps of Fe, Mn, and Al are shown; sample- P06NM40).



Figure 4.12. Quartzite Peak is dominated in outcrop by a steep to subvertical, northwest striking fabric that appears axial planar to tight to isoclinal folds that plunge to the northwest.

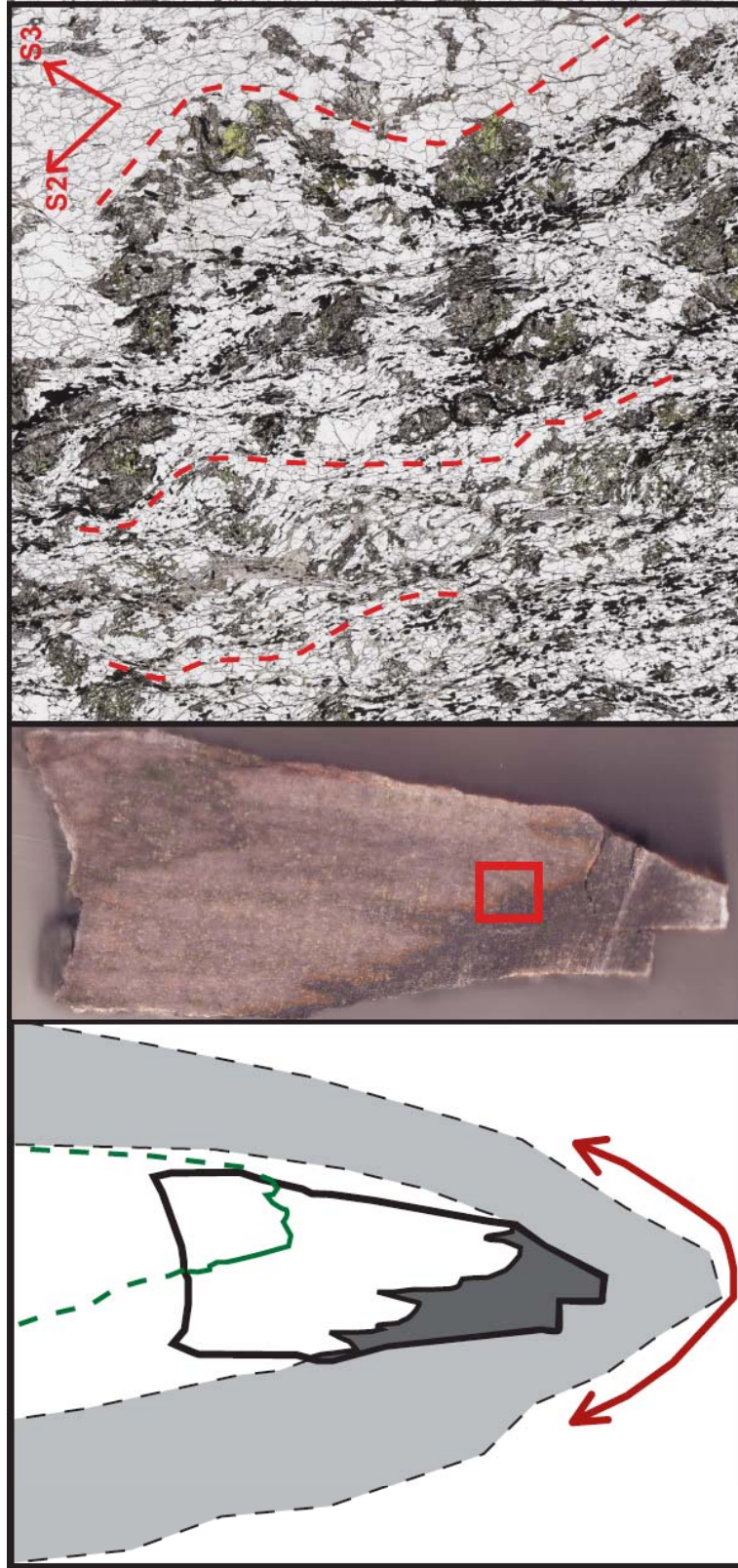


Figure 4.13. The S2/S3 composite fabric is composed of “waves” and incomplete quadrilateral-like shapes in thin section that are defined by elongate hematite aligned in both S2 and S3 (sample-P06NM40).

waves and lozenges of elongate hematite aligned in both S2 and S3 in thin section (Fig. 4.12 & 4.13).

Kiowa Mountain

F2 folds and the S2 cleavage are prevalent in outcrop at Kiowa Mountain. Folds and fabrics, particularly S2 and F2, are generally better developed and tighter in the transitional package of the Vadito Group than in the Ortega Formation quartzite. F2 folds in the Ortega Formation are open to tight, reclined, and upright to slightly overturned, whereas F2 folds in the Vadito Group are generally tight, reclined, and overturned to recumbent. S2 and F2 were steepened and refolded by F3. The interaction between S2 and S3 at the thin section scale within the aluminous, hematite-bearing layers of the Ortega Formation quartzite at the summit of Kiowa Mountain is diagrammed in Figure 4.14.

It is important to note that outcrop of the Mn-andalusite layer in the Ortega Formation is limited. Many of the Mn-andalusite-rich samples are unoriented float samples collected at the summit of Kiowa Mountain. One oriented sample (P06NM29) was obtained from the Mn-andalusite layer and observations regarding fabric relationships are based on that sample.

Map-Scale Folds

The map-scale Jawbone syncline and what has been interpreted to be the Hopewell anticline are present in the Hopewell Lake-Jawbone Mountain area (Fig. 4.8; Williams, 1983; Williams, 1991; Williams et al, 1999; Kopera, 2003). Bedding in the Ortega Formation quartzite defines the Jawbone syncline as well as one limb of the Hopewell anticline. The core of the Hopewell anticline is defined by the Burned Mountain Formation metarhyolite in the map area shown in Figure 4.8. The Jawbone syncline is a tight to isoclinal, upright fold with an axis plunging 23 to 285° (Kopera, 2003). Near the hinge of the Jawbone syncline, S0/S1 (198, 43NE) is cut by S2 (115, 69S) and both S0/S1 and S2 are obliquely cut by S3 (261, 80N). The Hopewell anticline is a tight, reclined fold with a steeply plunging fold axis and northwest striking

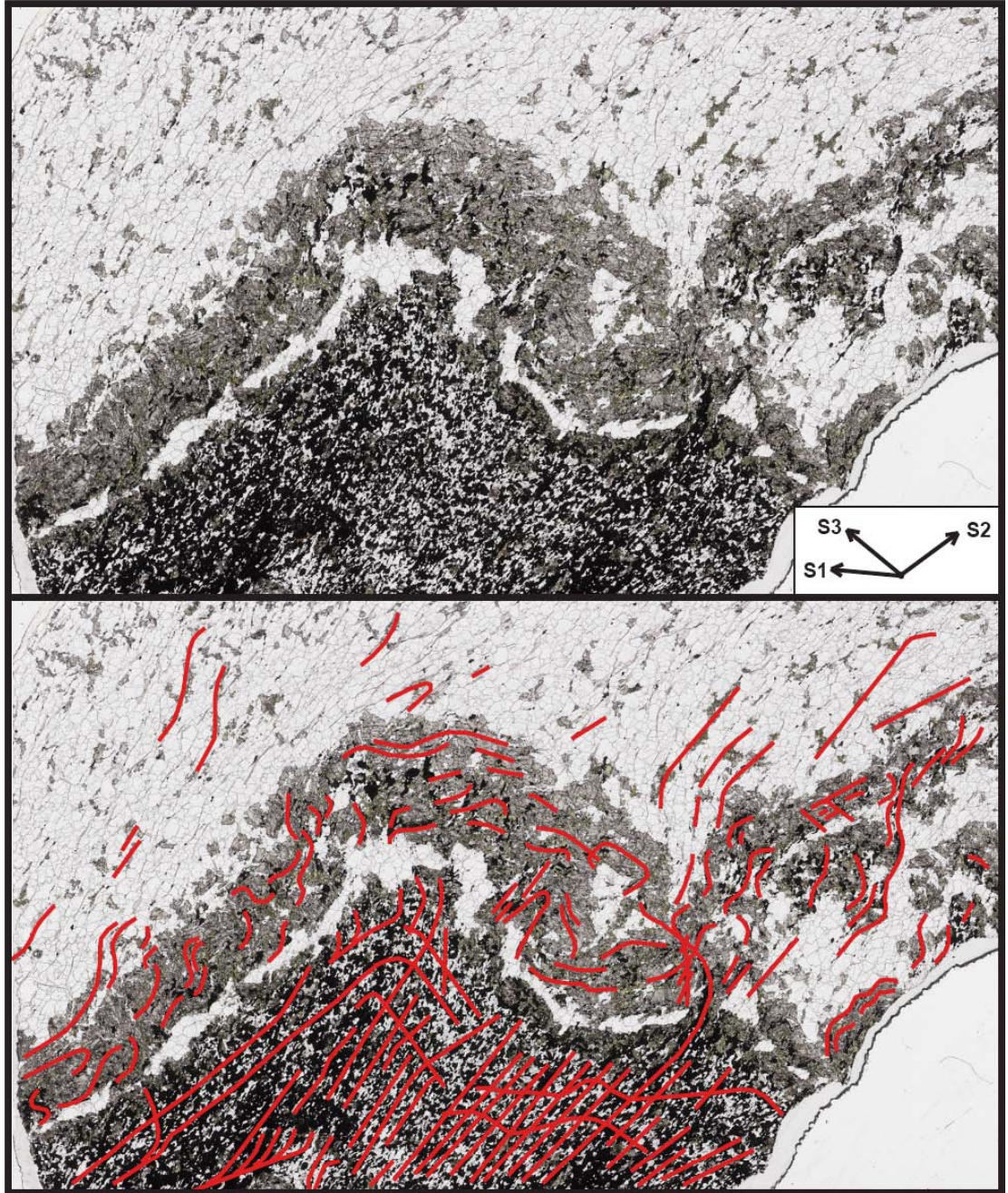


Figure 4.14. An attempt to interpret the evolution of the hematite-defined S1, S2, and S3 fabrics in a sample from the Mn-andalusite layer at Kiowa Mountain is shown (unoriented sample P06NM59FB; cut perpendicular to S2).

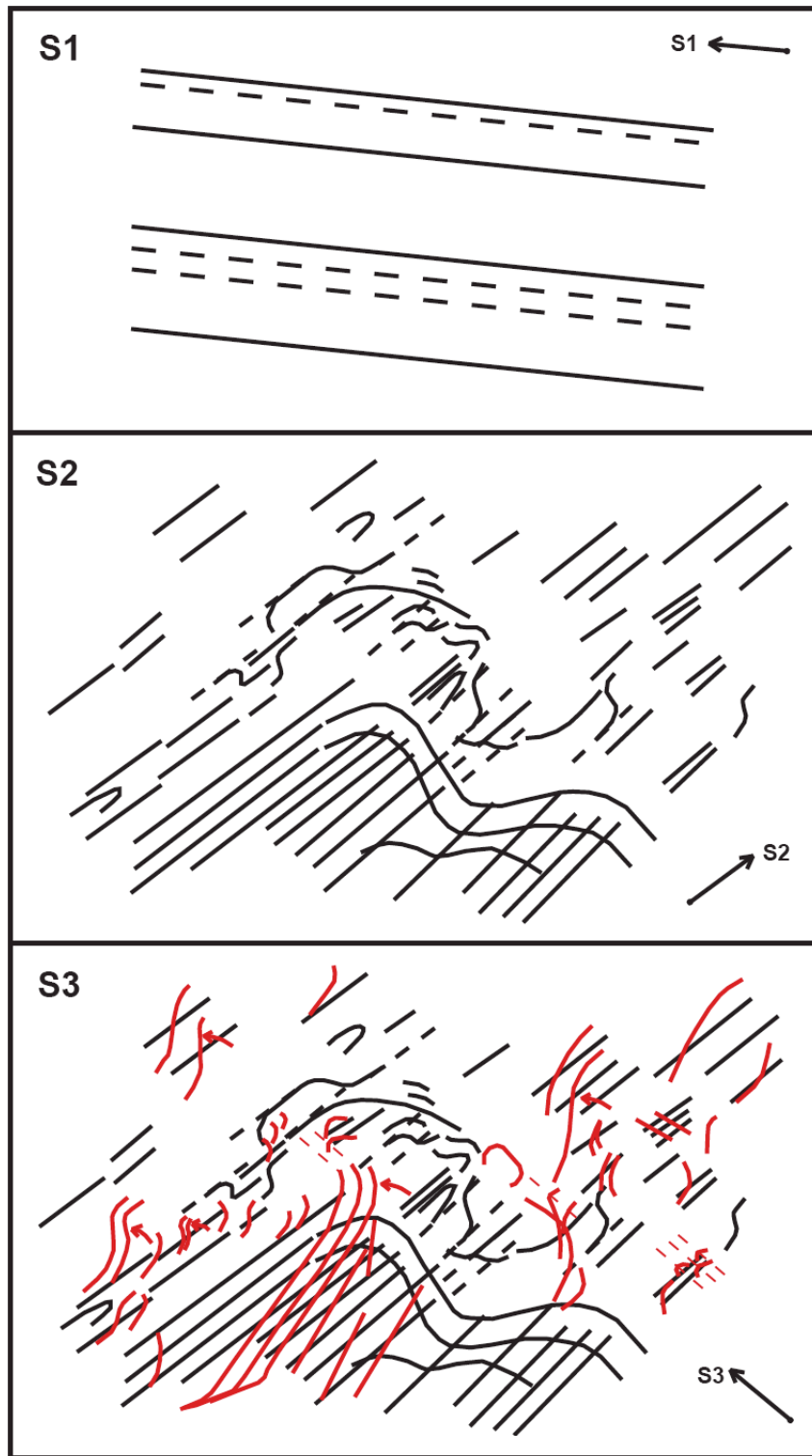


Figure 4.14. (continued).

and steeply southwest dipping axial surface. Only the southern limb of the Hopewell anticline axial trace is preserved in the Ortega Formation. A Proterozoic thrust is postulated between the Jawbone syncline and the Hopewell anticline in the Hopewell Lake-Jawbone Mountain area (Fig. 4.1; Williams, 1991).

Bedding in the Ortega Formation quartzite defines the core of the large map-scale Kiowa syncline at Kiowa Mountain (Fig. 4.15). The orientation of the Kiowa syncline changes from the southeast to northwest from a moderately plunging (59 to 283°) fold with a northwest striking, southwest dipping axial plane (171, 67W) to a shallowly west plunging (26 to 281°) slightly overturned fold with an east striking, south dipping axial plane (093,76S) (Kepes, 1984; Williams, 1991; Kopera, 2003). The transition in the fold geometry and axial plane orientation corresponds with the contact between the Ortega Formation quartzite and the transitional package of the Vadito Group (Kepes, 1984; Williams, 1991; Kopera, 2003).

The timing of the large, map-scale folds, particularly the Jawbone and Kiowa synclines, has been uncertain (Kepes, 1984; Williams, 1987; Williams et al, 1999; Kopera, 2003). The upright character and east-west strike of the axial plane of the Jawbone syncline and parts of the Kiowa syncline suggest an association with the F3 folds (Kepes, 1984; Williams, 1987). Williams (1991) suggested that the map-scale synclines formed early in the history during D1 and helped to establish a heterogeneity that controlled strain partitioning.

Anomalous Areas of Structural Importance

Three areas of structural importance within the Hopewell Lake-Jawbone Mountain map area will be specifically highlighted and discussed below (Fig. 4.8a): (1) a D3 high strain zone in the Ortega Formation with a break in the mapped Ortega Formation/Mn horizon contact, (2) a D3 high strain zone in the Maquinita Formation granodiorite, and (3) a stratigraphic variation in metasedimentary units near the Burned Mountain Formation/transitional package contact.

The outcrops of the Ortega Formation at the northernmost exposure of the southern limb of the Hopewell anticline represents a D3 high strain zone within the Ortega Formation (intense S3 fracture cleavage and tight, upright F3 folding) and also involves a discordant break

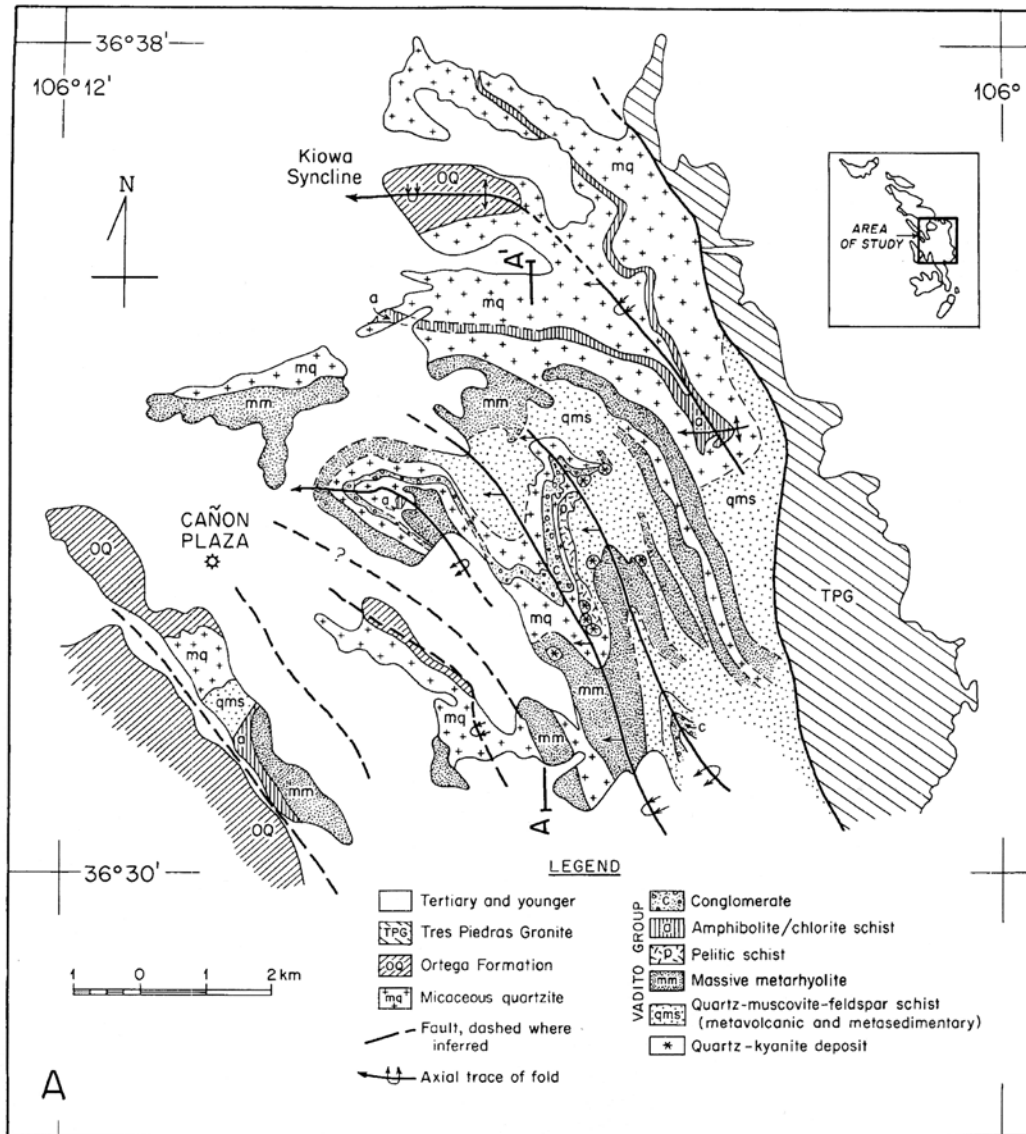


Figure 4.15. Bedding in the Ortega Formation quartzite defines the core of the large map-scale Kiowa syncline and the transition from a northwest striking to an east striking axial plane corresponds with the contact between the Ortega Formation and the transitional package of the Vadito Group (from Williams, 1991).

in the mapped Ortega Formation/Mn horizon contact. The discordant break in the map pattern involves the westward turn of the contact of the lower Mn-andalusite absent Ortega Formation with the upper Mn-andalusite rich Ortega Formation that ran consistently NW along strike along the southern limb of the anticline (~134 for S0/S1/S2) (Fig. 4.8a). The westward turn does not involve a drastic change in orientation for S0/S1/S2, with only a slight shift (~20 degrees) from a NW orientation to a W-NW orientation (~113°). It is the contact that appears to turn westward and does not directly connect with the reciprocal contact just north of the break. S3 is well-developed in the outcrops that represent the westward turn. The discordant break in the mapped Ortega Formation/Mn horizon contact is thought to represent a D2 and/or D3 structure. The westward turn of the contact and the fact that S3 well developed suggest a D3 structure, such as an F3 fold, but it is also possible that a preexisting D2 structure, such as an F2 fold or D2 fault, served to later concentrate D3 strain.

A localized D3 high strain zone can be found in the Maquinita Granodiorite south of the hinge of the Jawbone syncline (Fig. 4.8a). In outcrop, a subvertical fabric strikes 265° and dips 84N. The subvertical fabric represents the S2/S3 composite fabric discussed previously and is defined by quadrilateral lozenges of unstrained rock, the edges of which are composed primarily of muscovite, biotite, chlorite, and/or quartz and that are elongate and aligned in both S2 and S3 (Fig. 4.16). Strained feldspars with stepped and offset twins and the localized offset of a few chlorite crystals (vertical shear planes and south side up motion) associated with S3 formation supports a high degree of strain and possibly even some degree of shear in this zone during D3. Kopera (2003) hypothesized that the intense fabric development of this zone represents a “mylonitic fabric”. However, there is no evidence for the grain size reduction and fine-grained matrix that would be characteristic of a mylonite (Passchier and Trouw, 2005).

A small outcrop near the contact between the Burned Mountain Formation metarhyolite and the transitional package metasediments exposes metasedimentary units that are markedly different from any other unit in the Hopewell Lake-Jawbone Mountain area (Fig. 4.8a). The outcrop reveals the contact between a highly-weathered, schistose metarhyolite and a medium to large pebble conglomerate. The conglomerate is unlike the small dominantly quartz pebble

conglomerate in the transitional package and is more similar in clast type, clast size, and matrix color to the large pebble conglomerate from the base of the Vadito Group exposed at Kiowa Mountain. The conglomerate has pebbles flattened and aligned in S2 and an S2 fracture cleavage that displayed gentle F3 crenulation folds. The metarhyolite preserves S2 and S3 fabrics.

The stratigraphic variations in the metasedimentary units near the Burned Mountain Formation/transitional package contact may indicate the structural juxtaposition of units in the Hopewell Anticline. As was previously discussed, the metasedimentary units do not correlate directly with other metasedimentary units in the area. It is possible that these units represent simple stratigraphic variation in the transitional package in the Hopewell Lake-Jawbone Mountain area and are just not exposed elsewhere. However, given the similarity with units from the base of the Vadito Group in the Kiowa Mountain area, these units may come from a part of the stratigraphic section that is not present in the Hopewell Anticline. Bedding parallel thrusts may have juxtaposed units in the Hopewell anticline that are not stratigraphically continuous. The stratigraphic variation in the metasedimentary units may thus represent a tectonically placed sliver of crust within a complex bedding-parallel thrust zone.

Discussion of Structure

The Hopewell Lake-Jawbone Mountain Area

The main variations in character between fabric and fold generations within the Hopewell Lake-Jawbone Mountain area are interpreted to be due to differences in strain intensity. Differing strain intensity is the main factor between the formation of the F3 crenulation folds (low strain) and the tight, upright F3 folds (high strain). Similarly, differences in D2 strain intensity most likely influenced the formation of distinct S2 cleavage planes and centimeter-scale reclined folds in some areas (high strain) and not others (low strain).

Variations in character between fabric and fold generations within the Hopewell Lake-Jawbone Mountain area can also be attributed to the partitioning of strain into less competent



Figure 4.16. This thin section from the D3 high strain zone in the Maquinita Formation granodiorite shows the interaction of S2 and S3 to create the composite S2-S3 fabric (sample P06NM22; vertical section perpendicular to main foliation: 269, 84N).

units. Williams (1991) interpreted that strain partitioning led to the map-scale concentration of strain into high strain domains and the preservation of primary structures in low strain domains. Strain partitioning had a similar effect in the Hopewell Lake-Jawbone Mountain area. There is a large competency contrast between the more competent quartzite layers and the less competent aluminous, hematite-bearing layers in the Ortega Formation. Bedding parallel, high strain zones concentrate strain into the less competent layers leading to intense fabric formation subparallel to S_0 (particularly S_1 and S_2) in the less competent aluminous, hematite-bearing layers and the preservation of primarily bedding structures, such as cross-beds, in the more competent and less deformed quartzite layers.

The large map-scale folds are preserved in the orientation of S_0/S_1 in the Hopewell Lake-Jawbone Mountain area. The Jawbone syncline is a tight, upright, west plunging fold with an isoclinal geometry. Kopera (2003) determined a regional fold axis plunging $23 \rightarrow 285^\circ$ and an axial surface oriented $275^\circ, 90$ for the Jawbone syncline. Both limbs of the syncline have similar moderate to steep dips of 50° - 75° to the north. The Hopewell Anticline is a tight reclined fold with a steep fold axis and northwest striking and steeply southwest dipping axial plane. The limbs of the anticline strike to the northwest and dip steeply to the southwest. The hinge zone of the anticline is not exposed in the Ortega Formation. At first glance the map pattern suggests that the Hopewell anticline and the Jawbone syncline represent an anticline-syncline pair, but the differences in the character and geometries between the two structures may indicate diverging or even different formation histories.

The large map-scale folds are thought to have nucleated early in the deformational history, perhaps as D_1 structures, and then to have continued to evolve through D_2 (Williams, 1991; Williams et al, 1999; Kopera 2003). Figure 4.18 shows an interpreted structural history for the Hopewell Lake-Jawbone Mountain area (Fig. 4.17). By this scenario, D_1 involved top to the north, layer-parallel shearing and folding as evidenced by bedding-parallel high strain zones and shear zones, mineral stretching lineations along S_0/S_1 , and recumbent F_1 folds (Williams, 1991; Kopera 2003). Map-scale folds nucleated during D_1 . In the Jawbone syncline, S_2 overprints the map-scale fold providing evidence that the syncline formed prior to

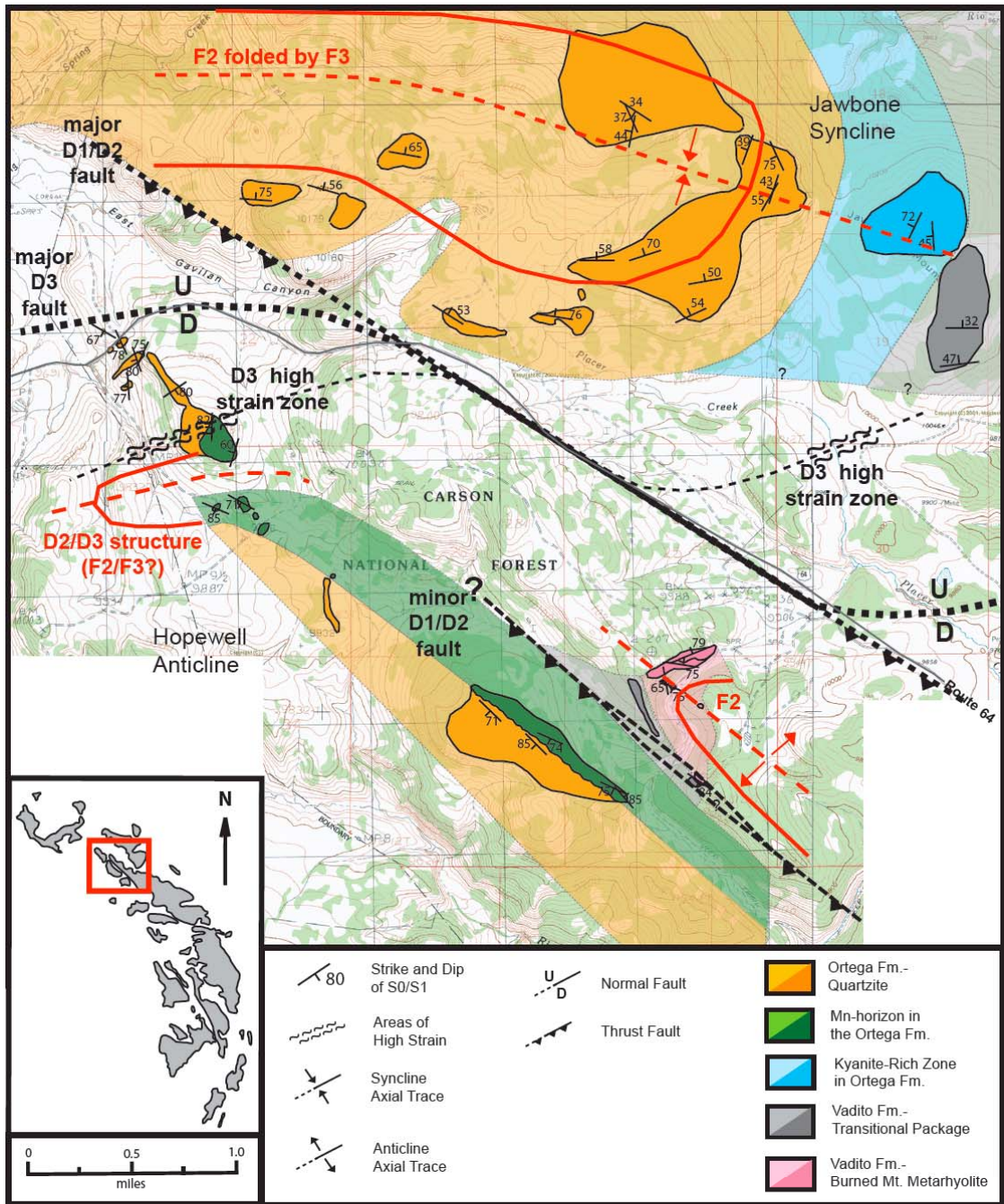


Figure 4.17. Map of the Hopewell Lake-Jawbone Mountain area showing the location of inferred structural features. D3 faults and high strain zones are shown to merge with D1/D2 structures reflecting the reactivation of earlier structures by later structures.

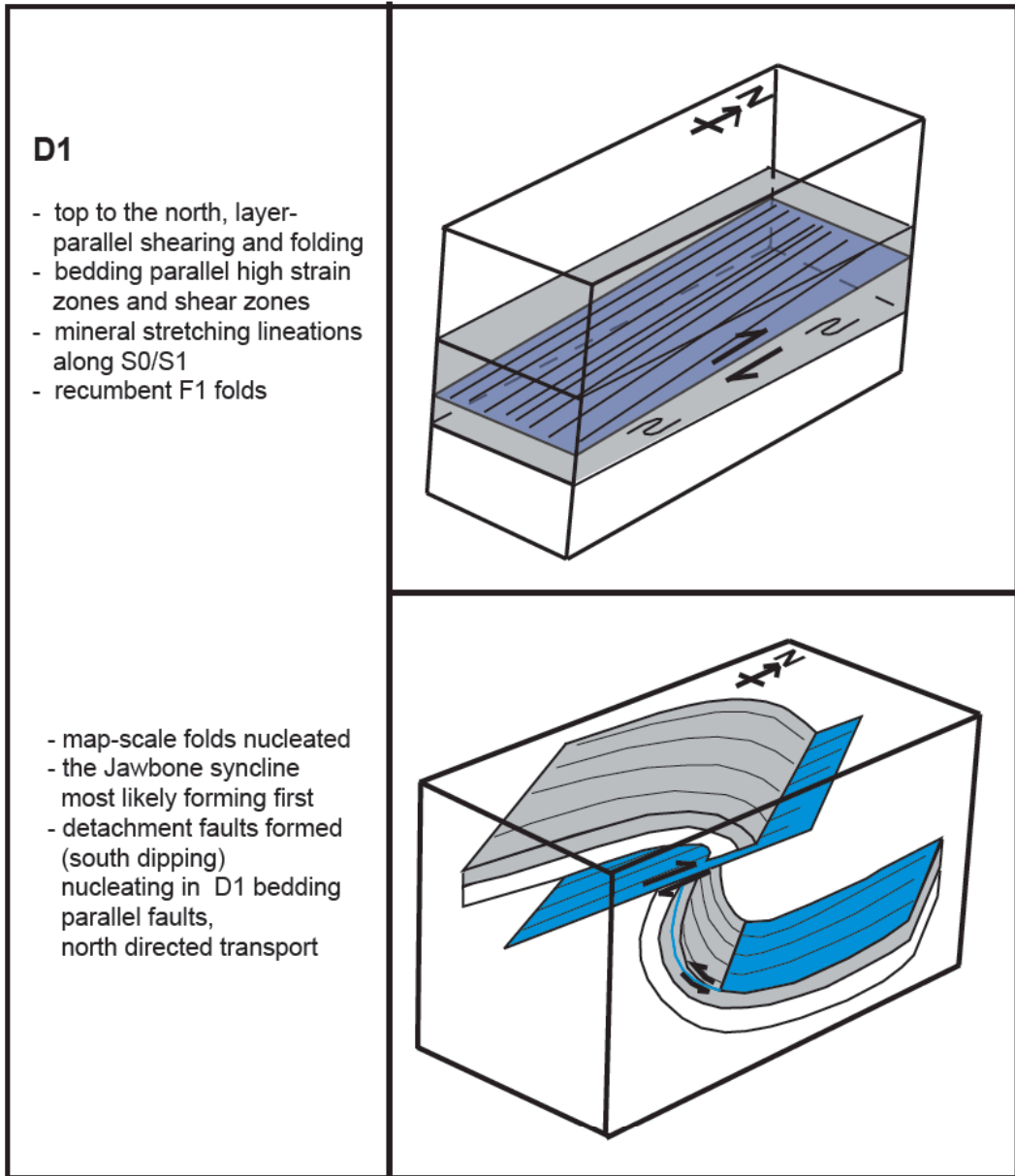


Figure 4.18. An interpreted structural history for the Hopewell Lake-Jawbone Mountain area (actual location of D1 thrust is unknown).

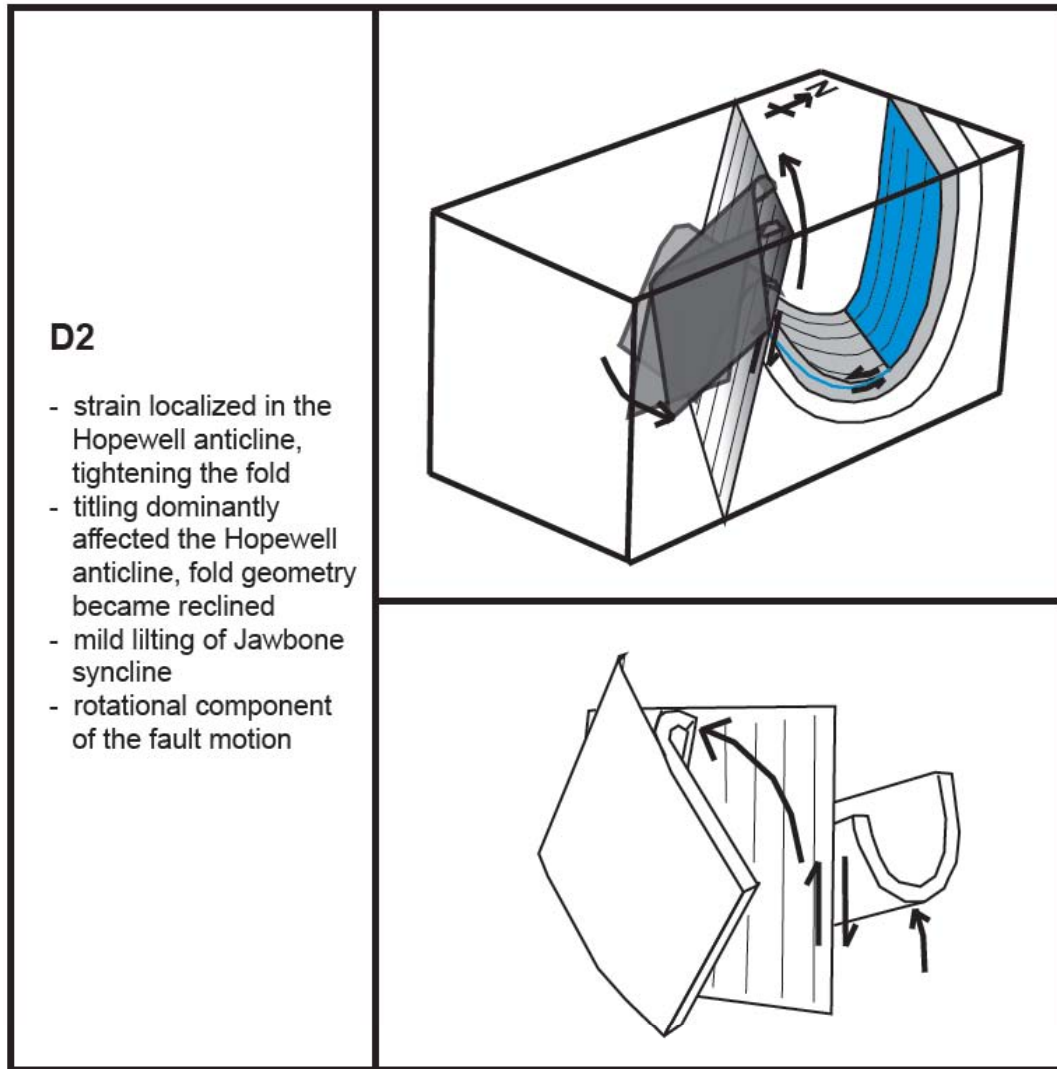


Figure 4.18. (continued).

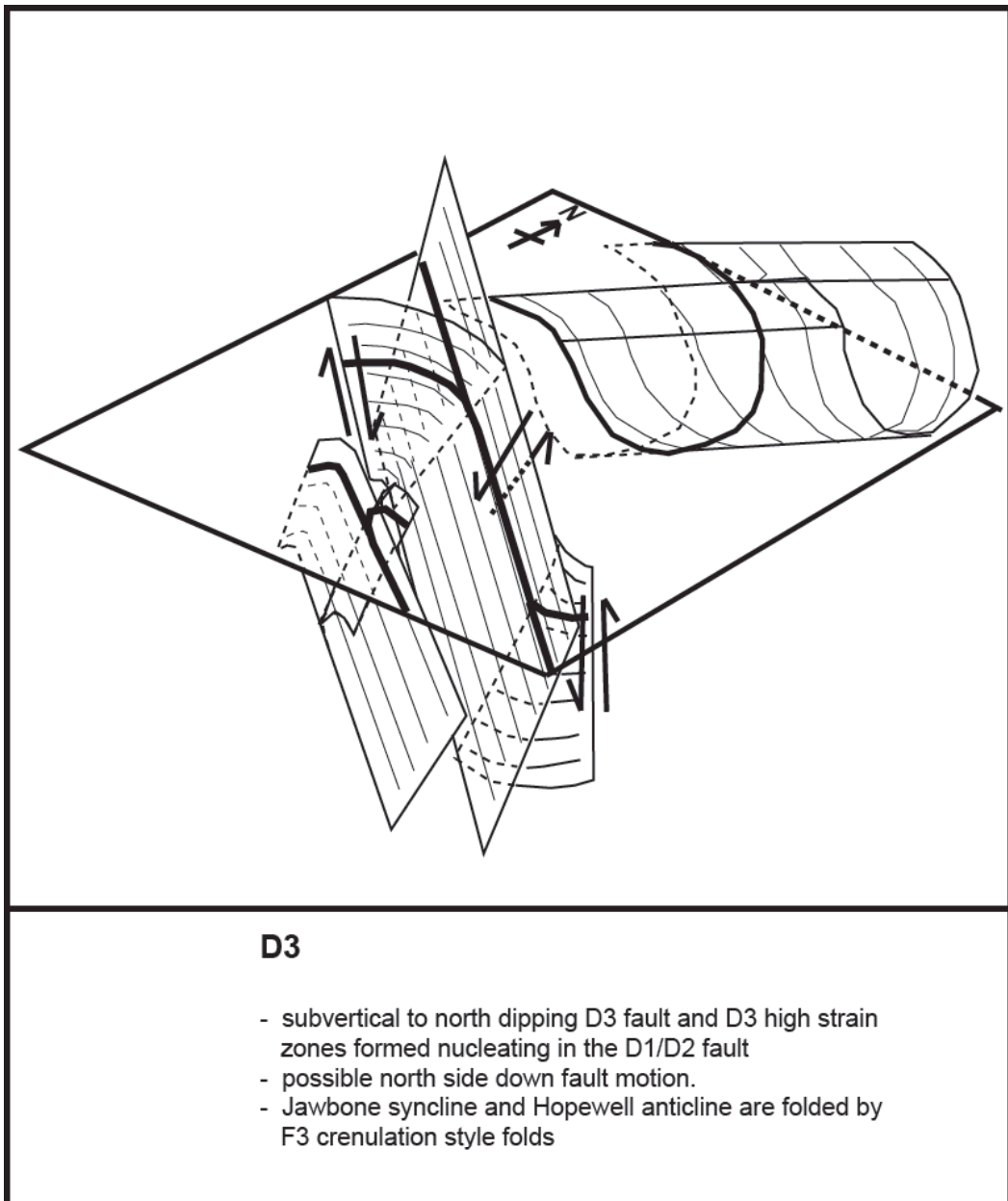


Figure 4.18. (continued).

D2. Preexisting D1 shear zones may have served as the nucleation point for D2 extensional structures. A D2 thrust fault with a top to the northeast vergence is interpreted between the Hopewell anticline and the Jawbone syncline based on mineral lineations in the Hopewell Lake-Jawbone Mountain area and elsewhere in the Tusas range (Kopera 2003; Davis, 2003). D2 strain may have concentrated in the anticline tightening the fold and may have led a greater amount of offset along the shear zone, preserving the syncline from further deformation. The timing of the westward tilt and increased plunge of the map-scale synclines is still unconstrained. However, if tilting occurred during D2, then differences in the anticline and syncline geometry (gently vs. steeply plunging) could indicate a rotational component to the movement along the D2 fault preventing the Jawbone syncline from experiencing as high a degree of westward tilting as the Hopewell anticline.

It is possible that the Jawbone syncline and the Hopewell anticline represent two different generations of folds. The Jawbone syncline and Hopewell anticline appear to represent a syncline anticline pair, but the anticline may not directly correlate with the syncline. If the Jawbone anticline is a D1 structure, then the D1 anticline that corresponds with it may not be present in the Hopewell Lake-Jawbone Mountain area or may be preserved at a different level in the crust. The Hopewell anticline could have formed separately as a map scale F2 fold and its placement near the Jawbone syncline would create the appearance that they are a fold pair. The differences between the geometry of the Jawbone syncline and Hopewell anticline may in this case indicate that they formed at different times in the history of the Hopewell Lake-Jawbone Mountain area.

The Hopewell anticline and the Jawbone syncline have been affected by F3 folding. Meter-scale F3 crenulation folds have warped the limbs (S0/S1) of both the anticline and the syncline. Similar F3 folds have also folded S2 in outcrop. Kopera (2003) described the Jawbone syncline as an east-west trending structure. At the map-scale, however, the Jawbone syncline trends northwest-southeast near the hinge and east-west further west along the axial trace. Given that both S0/S1 on the fold limbs and S2 are folded by F3 crenulation folds, it is may be possible that F3 crenulation folding affected the map-scale structure as well. The

Jawbone syncline itself may have been folded in a similar way during D3 with the limbs of the syncline folded into an east-west orientation from an originally northwest orientation.

The heterogeneous distribution of D3 strain led to the formation of D3 high strain zones and may be indicative of a larger map-scale D3 structure located between the Hopewell anticline and the Jawbone syncline. The location of the two D3 high strain zones (in the Ortega Formation quartzite and in the Maquinita Formation Granodiorite) generally fall on a hypothetical east-west to northeast striking line that cuts across the Hopewell Lake-Jawbone Mountain area and separates the Jawbone syncline from the Hopewell anticline (Fig. 4.17). This hypothetical line could represent the trace of a large east-west striking D3 structure such as shear zone or fault that cuts across the area. However, the D3 high strain zones also appear to be areas of high D2 strain, with distinct S2 cleavage planes and reclined centimeter-scale F2 folds. Because preexisting D2 structures can serve as areas where additional D3 strain partitions, it is possible that a previous D2 structure, such as a large D2 thrust fault, served to localize further D3 strain. Instead of an entirely new east-west D3 fault, D3 may have reactivated a D2 fault and lead to small localized areas of higher D3 strain. The map in Figure 4.17 shows such a fault. The D3 fault structure on the map has been postulated as following the style of the F3 crenulation folds with part of the fault reactivating the D2 structure in a northwest orientation and part of the fault in a new east-west orientation.

Quartzite Peak

The progressive formation of new fabrics at Quartzite Peak creates what appear to be sigmoid-shaped hematite inclusion trails (Fig. 4.11). Such a sigmoid shape would otherwise indicate intense shear or rotation, but there is no evidence to support such a high degree of strain. The sigmoid shape evolved through three consecutive generations of fabric formation (Fig. 4.11; Bell, Rubenach, and Fleming, 1986). The alignment of very fine hematite grains define S1. S1 has been reoriented into S2, and S2 has been reoriented into S3, both of which are defined by the alignment of elongated hematite. The sigmoid shape is an artifact of the

similarity between the S1 and S3 orientations and the incomplete overprint of earlier fabrics by newer ones.

D3 strain is dominantly accommodated on the microscale by open F3 crenulation folds of S2, without extensive F3 folding on the macroscale. At the outcrop scale, F2 folds that had once had NW striking, SW dipping axial planes have been transposed into folds that now appear to be tight to isoclinal with subvertical axial planes that strike WNW (290-302). Only more rarely do F3 folds directly fold S2 in outcrop. In thin section, S2 is strongly folded by F3 crenulation folds (Fig. 4.13). The transposition of F2 folds into an intermediate more upright orientation in outcrop appears to be similar in effect to the tilting of a deck of cards, where deformation occurs on the small scale in between each individual card (which in this case is the folding of S2 into S3) and the picture on the cards edge is distorted but preserved intact (the F2 folds) (Fig. 4.19). If D3 strain was to progress past the point that is preserved at Quartzite Peak, then it is highly probable that the surface of the F2 folds would begin to appear much more deformed and the S3 cleavage would be more defined at the outcrop scale.

Kiowa Mountain

The distribution of D3 strain is relatively uniform throughout the Kiowa syncline and involved the steepening of S2 and F2 folds (Fig. 4.20). With the exception of the difference in D3 intensity between the Vadito Group and Ortega Formation, D3 strain does not appear to be concentrated in any known D3 high strain zones. D3 led to the steepening of S2 through the transposition of S2 into S3 and the F3 crenulation folding of S2. The “unusual box shaped geometry” of folds described by Kopera (2003) may be a result of the steepening and folding of the limbs of F2 folds making a fold that had been slightly overturned appear upright (Fig. 4.14 & 4.20).



Figure 4.19. The deformation of F2 during D3 created isoclinal upright folds and a wavy composite fabric that represents the folded axial plane of the F2 fold.

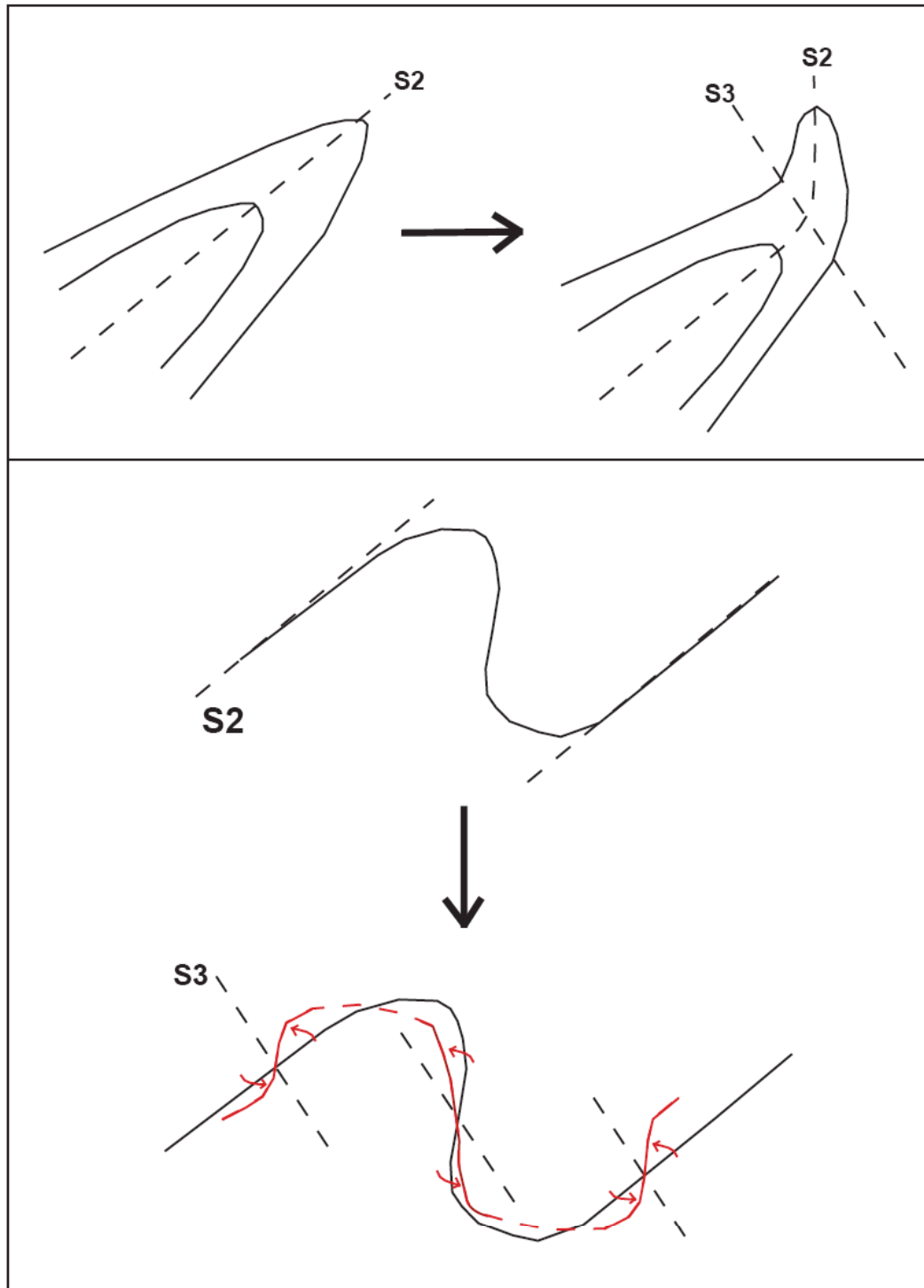


Figure 4.20. D3 led to the steepening of S2 and F2 through the transposition of S2 into S3 (bottom) and the F3crenulation folding of S2 (top).

CHAPTER 5

METAMORPHIC PETROLOGY

General Metamorphic History of the Tusas Mountains

Three distinct metamorphic mineral assemblages have been identified in the Tusas Range (M1, M2, M3) (Williams, 1991; Bishop, 1997; Lombardi, 1997; Williams et al, 1999). The M1 assemblage was associated with D1 and involved the growth of a low-grade assemblage that included kyanite, muscovite, oxides, and locally hornblende (Williams, 1991). Minerals in the M2 assemblage overgrew D2 structures, involved the growth of garnet, kyanite, and local staurolite, and are interpreted to have grown syn- to dominantly post-D2 (Williams et al, 1999). The growth of the low-P, high-T M3 assemblage included andalusite, sillimanite, garnet, staurolite, and cordierite (Bishop, 1997; Lombardi, 1997; Williams et al, 1999). The M3 mineral assemblage is interpreted to have grown syn-D3 and involved the growth of M3 rims on M2 garnet and plagioclase crystals (Bishop, 1997; Williams et al, 1999). It is important to note that at this time it is unclear whether the growth of each metamorphic assemblage was part of one single P-T loop or multiple P-T loops and the discussion of M1, M2, and M3 in this study is to be considered independent of such interpretations.

The large-scale metamorphic trend is one of increasing grade from north (450°C, 2 kbar) to south (550°C, 4.5 kbar) and was interpreted to represent the sequential southward exposure of shallowly dipping subhorizontal isograds (Fig. 2.5; Bishop, 1997; Lombardi, 1997; Grambling et al, 1989; Williams et al, 1999). The isograds overprint the regional D1 and D2 structures and are associated with the growth of the M2 and/or M3 metamorphic mineral assemblages.

Hopewell Lake-Jawbone Mountain Area

The mineral assemblage in the Ortega Formation quartzite in the Hopewell Lake-Jawbone Mountain area includes quartz, aluminum silicate, rutile, hematite, phyllosilicates (dominantly pyrophyllite), monazite, and zircon. Hematite and aluminum silicate minerals are

concentrated in the aluminous, hematite-bearing layers in the Ortega Formation quartzite. Kyanite is the stable aluminum silicate at the Jawbone syncline and both kyanite and andalusite are stable at the Hopewell anticline. For this reason, the Jawbone syncline and the Hopewell anticline will be discussed separately below.

The Jawbone Syncline

The mineral assemblage of the aluminous, hematite-bearing layers of the Jawbone syncline includes quartz, kyanite, hematite, chloritoid, rutile, zircon, and monazite (Fig. 5.1). Kopera (2003) also reported rare fibrolite and some andalusite at the Jawbone syncline.

Both kyanite and aligned hematite define S0/S1, S2, and S3. The long axis of kyanite blades are aligned with S1 and define L1 on S0/S1 planes (Kopera, 2003). Kyanite crystals are commonly kinked, fractured, display undulose extinction, and in places are reduced in size to a mass of smaller grains (Fig. 5.1). Aligned hematite inclusions in undeformed areas of kyanite define S0/S1 and in rare instances S2. S0/S1-parallel kyanite crystals and hematite inclusions are kinked and folded by both F2 and F3 folds. All kyanite crystals that include hematite aligned in S3 or are aligned subparallel to S3 display undulose extinction or are fractured and kinked. Undeformed chloritoid crystals display hexagonal growth zoning and include hematite inclusion trails aligned in S1 and S2. Chloritoid is uncommon relative to kyanite, but where present chloritoid is concentrated in S0/S1 along with kyanite. Like kyanite, some chloritoid crystals are fractured and display undulose extinction.

The Jawbone syncline was within the kyanite stability field for the majority of its history. Much of the kyanite of the Jawbone syncline formed during the growth of the M1 assemblage post-D1. Undeformed kyanite that includes hematite aligned in S1 and kyanite crystals that are aligned in S1 and L1 support this interpretation. Later periods of deformation (D2 and D3) lead to the deformation of M1 kyanite. This is supported by the kinking and fracturing of M1 kyanite during the formation of both F2 and F3 folds. A second period of kyanite growth is suggested by the inclusion of hematite aligned in S2 in undeformed kyanite crystals and may indicate the

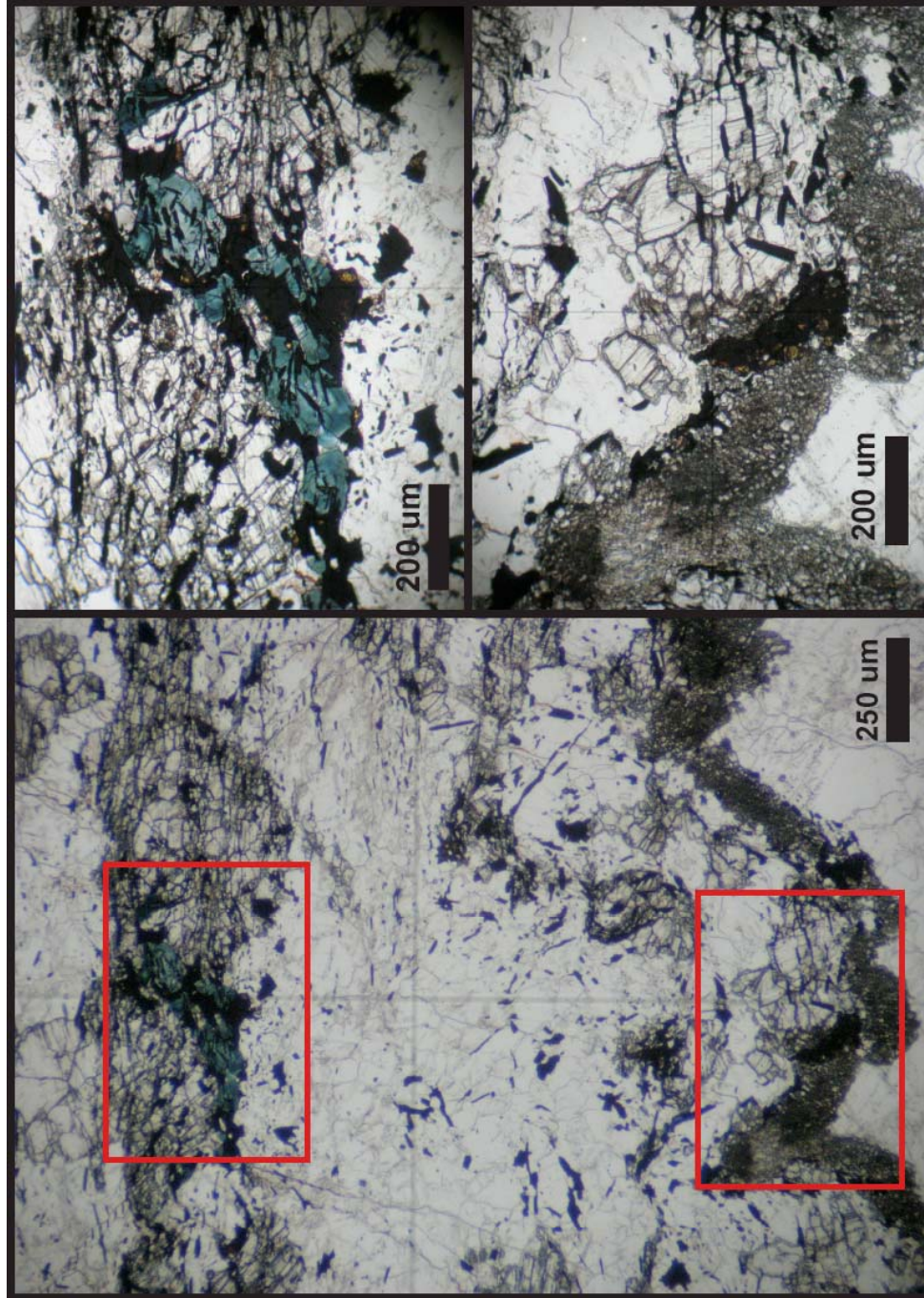


Figure 5.1. The aluminous, hematite-bearing layers of the Jawbone syncline include quartz, kyanite, hematite, and chloritoid (blue mineral). F2 and F3 folds fractured and folded kyanite (sample- P06NM26).

growth of an M2 assemblage syn- to post-D2. The inclusion of S1 and S2 aligned hematite in chloritoid suggests that the M2 assemblage may have included the growth of chloritoid. A lack of undeformed kyanite associated with S3 or F3 suggests that the M3 assemblage did not include new kyanite growth (or kyanite with S3/F3 inclusion trails). Koper (2003) reported that fibrolite sillimanite replaces kyanite crystals that define all fabrics (S1, S2, S3) suggesting that sillimanite grew syn- to post-D3. Koper (2003) reported andalusite in the Ortega Formation and the Burned Mountain Formation in association with deformational fabrics that post-date D2. No andalusite was observed in the aluminous, hematite-bearing layers in this study.

The P-T-D history of the Jawbone syncline involves (1) D1 deformation was associated with the early growth of M1 kyanite, (2) D2 deformation and the growth of M2 kyanite and chloritoid, and (3) D3 deformation and M3 sillimanite growth (Fig. 5.2). M1 and M2 were dominated by kyanite growth suggesting a pressure and temperature at or above the kyanite-andalusite reaction line for much of its history. The replacement of kyanite by sillimanite during growth of the M3 assemblage suggests a drop in pressure, an increase in temperature, or both during D3 (Fig. 5.3).

The Hopewell Anticline

The mineral assemblage of the aluminous, hematite-bearing layers at the base of the Ortega Formation of the Hopewell Anticline includes quartz, andalusite, hematite, rutile, pyrophyllite, zircon, monazite, in some places kyanite, and locally pennantite and gahnite. Andalusite occurs as Mn-andalusite within the Mn horizon and Mn-poor andalusite in the Mn-poor aluminous, hematite-bearing layers stratigraphically overlying the Mn horizon (Appendix 3). Andalusite is the dominant aluminum silicate throughout most of the Hopewell Anticline, but there is a transition to an andalusite + kyanite assemblage on the southern limb of the anticline.

Massive, optically continuous andalusite crystals within the andalusite dominated assemblage define discrete S2 cleavage planes and include hematite aligned with S0/S1, F2 folds and crenulations of S0/S1, and S2 (Fig. 4.3). Andalusite-filled axial planar S2 cleavage planes originate at and extend outward from the hinge zone of some tight, reclined, cm-scale F2

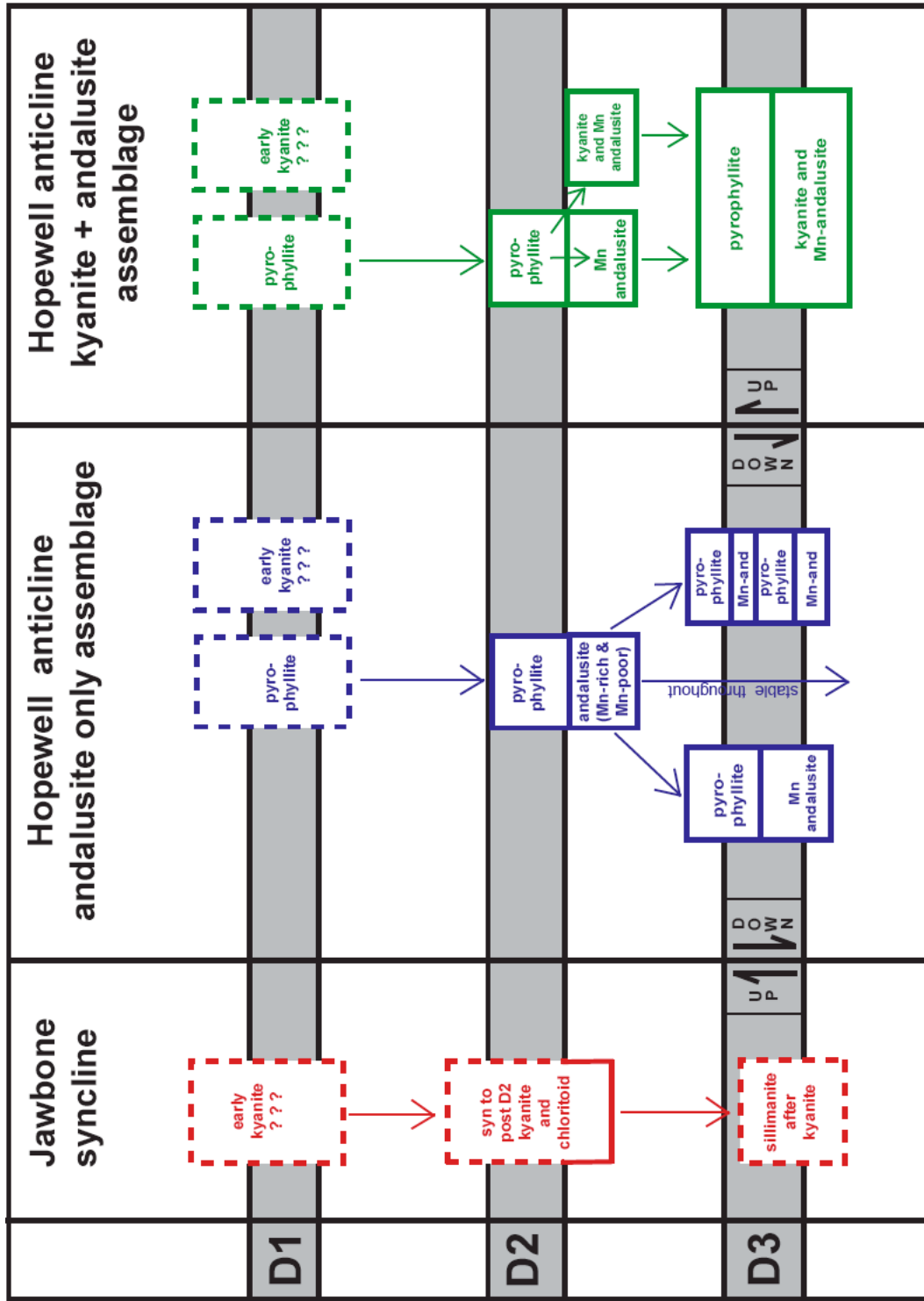


Figure 5.2. Interpreted metamorphic history of Hopewell Lake-Jawbone Mountain area.

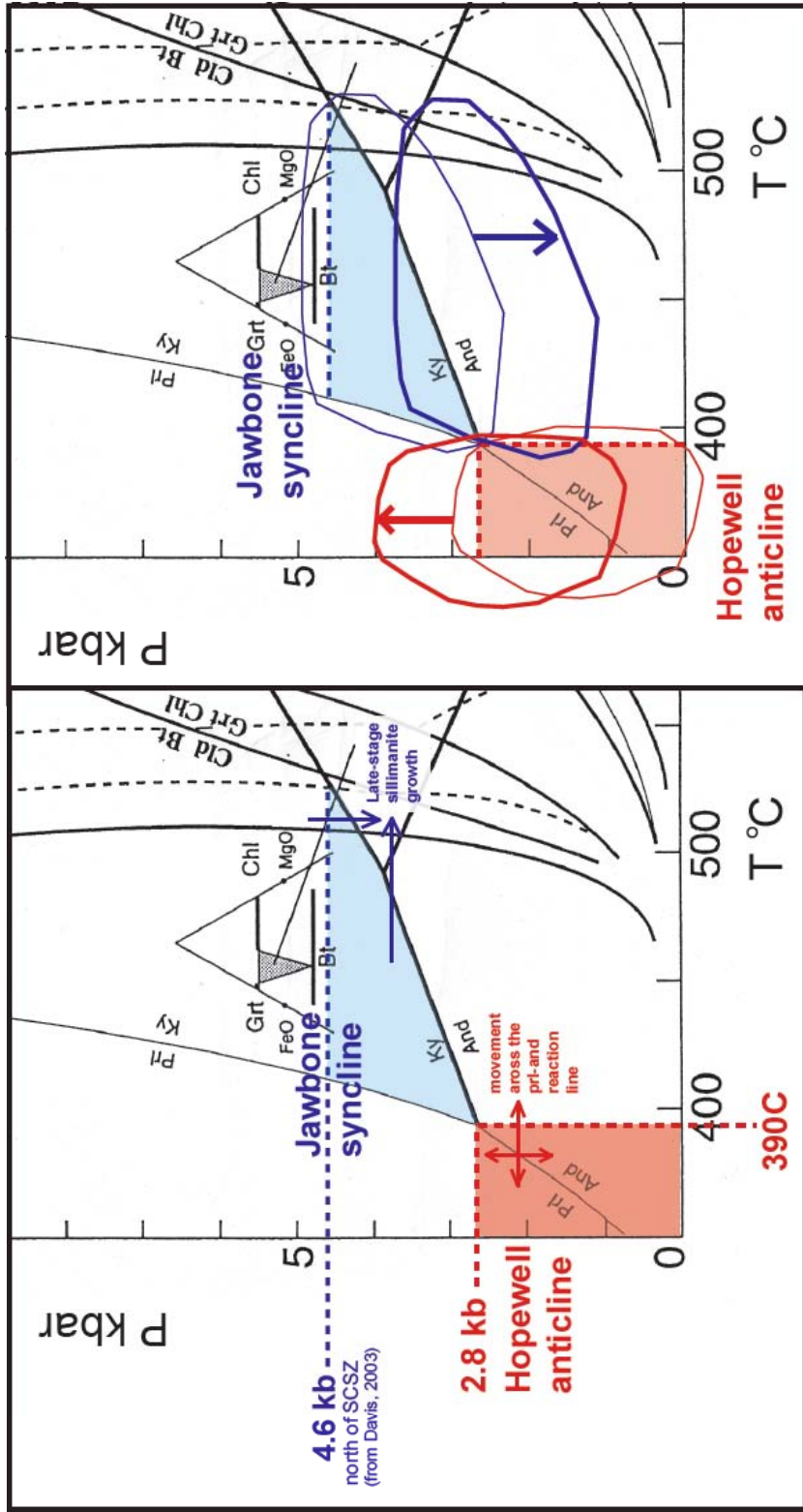


Figure 5.3. The interpreted location of the Hopewell anticline and the Jawbone syncline in P-T space during M2 and M3 (left). At the end of D3, Jawbone-syncline-down motion on a D3 fault juxtaposed the Jawbone syncline and the Hopewell anticline (right) (P-T diagram from Spear, 1993).

folds (Fig. 4.10). Andalusite displays undulose extinction and new grain boundaries in areas that have been folded by F3 folds (4.10a). Patchy areas of pyrophyllite can be found within andalusite crystals and near grain boundaries. Pyrophyllite also cuts andalusite crystals in planes parallel to S3 and in areas associated with F3 folds. Andalusite crystals that include hematite aligned in S3 or are aligned subparallel to S3 are also deformed.

There is an abrupt transition from the andalusite dominant mineral assemblage to the kyanite + andalusite assemblage on the southern limb of the Hopewell anticline near Placer Creek in the Hopewell Lake-Jawbone area (Fig. 5.4). The timing of kyanite growth relative to andalusite growth and the timing of fabric formation in the kyanite + andalusite field near Placer Creek in southern part of the Hopewell anticline is difficult to determine. In the samples where both kyanite and andalusite are present, kyanite includes hematite aligned in both S0/S1 and S2 and kyanite crystals display kinking that is related to S3 and F3 fold development. There is no indication that the strain that caused the kinking in the kyanite was associated with D2 fabric formation in the samples collected placing kyanite growth at post-D2 or pre- to syn-D3. In some samples, small blades of kyanite appear to overgrow existing larger blades of kyanite suggesting more than one period of kyanite growth (Fig. 5.5).

The Hopewell Anticline was near the andalusite-pyrophyllite reaction line throughout much of its history. Andalusite grew after D2 during the growth of the M2 assemblage but before D3. The lack of andalusite deformation associated with D2 and the presence of undulose extinction and new grain boundaries associated with D3 supports this interpretation. The massive habit of the andalusite crystals and the lack of remnant M1 minerals suggest that M2 andalusite replaced a phyllosilicate precursor, such as pyrophyllite. The formation S2 cleavage planes rich in andalusite is likely to be a result of the replacement of early phyllosilicates that were concentrated into discrete zones parallel to S2. M3 mineral growth was associated with the break down of andalusite to pyrophyllite as evidenced by zones of pyrophyllite that are parallel to S3 and are associated with F3 folding.

The P-T-D history of the andalusite-rich regions of the Hopewell Anticline involves (1) D1 deformation and M1 phyllosilicate growth, (2) D2 deformation followed by the growth of the

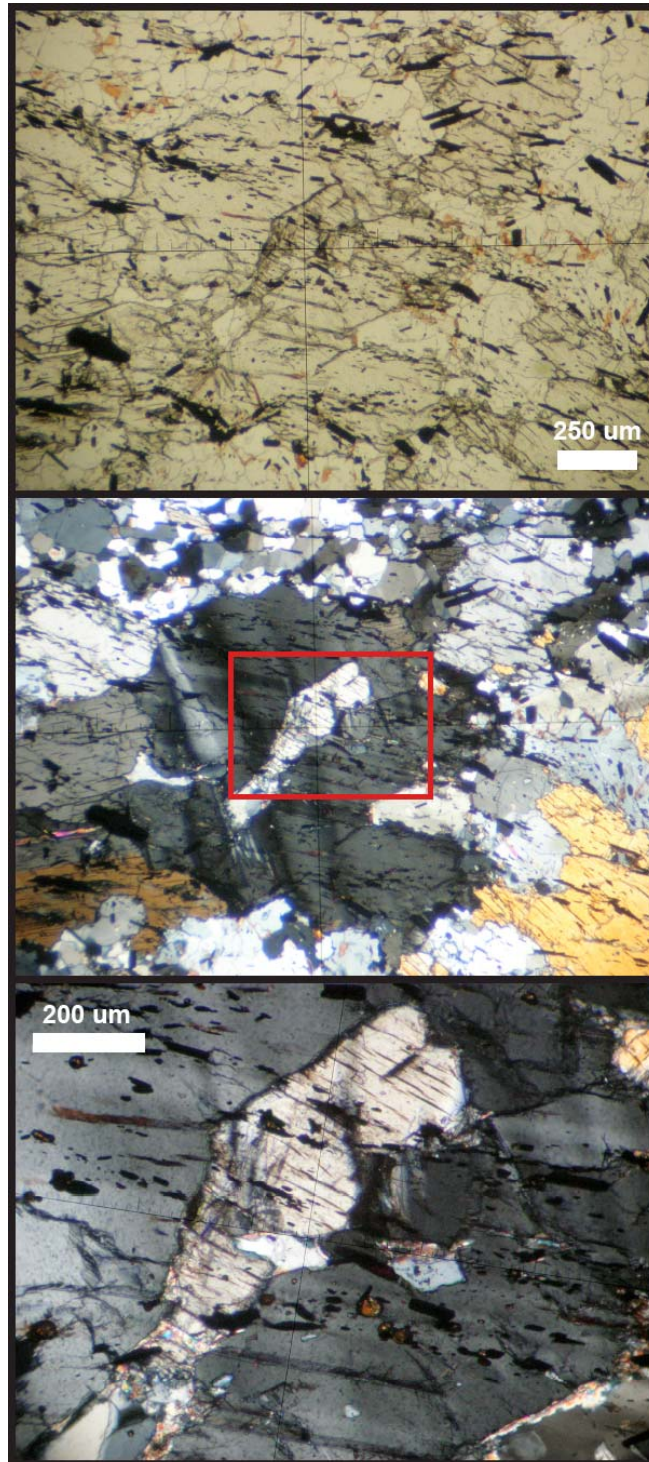


Figure 5.5. Late kyanite overgrows early kyanite in the samples from the kyanite + andalusite assemblage of Hopewell anticline suggesting more than one period of my kyanite growth (sample- Tus3).

dominant M2 andalusite assemblage, and (3) D3 deformation, syn-deformational andalusite breakdown, and M3 pyrophyllite growth (Fig. 5.2 & 5.6). The growth of M3 pyrophyllite after M2 andalusite suggests a pressure and temperature near the pyrophyllite-andalusite univariant reaction but below the kyanite-andalusite reaction line at some point during its history (Fig. 5.4)

Discussion of the Hopewell Lake-Jawbone Mountain Area

The metamorphic mineral assemblages of the Hopewell Lake Jawbone Mountain region are interpreted to correlate with the three regional metamorphic mineral assemblages of the Tusas Mountain Range both in the timing of mineral growth relative to fabric formation and folding and in overall metamorphic grade. The M1 assemblage included kyanite growth in the Jawbone syncline syn- to post-D1. Mn-andalusite crystals in the Hopewell anticline preserve a D2 crenulation cleavage in the habit phyllosilicates in the Mn-distribution and birefringence of the andalusite crystal (see Chapter 6). This crenulation cleavage suggests that the M1 assemblage included phyllosilicates at the Hopewell anticline. The M1 assemblage may have also included early kyanite at the Hopewell anticline, but if early M1 kyanite was present, then it was completely removed via a reaction to pyrophyllite prior to D2. Growth of the M2 assemblage included kyanite and chloritoid at the Jawbone syncline syn to post-D2 and both andalusite and Mn-andalusite post-D2. Most evidence suggests that the growth of the M2 assemblage postdates D2, particularly in the Hopewell Anticline. Growth of the M3 assemblage involved the reaction of kyanite to sillimanite syn- to post-D3 at the Jawbone syncline and the breakdown of andalusite to phyllosilicate and local regrowth of Mn-andalusite in the Hopewell Anticline (see Chapter 6). Evidence suggests that growth of the M3 assemblage was synchronous with D3, particularly in the Mn-andalusite layer (see Chapter 6).

A large metamorphic divide occurs in the approximate location of Route 64 (i.e. separating the Hopewell anticline from the Jawbone syncline). North of Route 64 the Jawbone syncline displays a history dominated by kyanite where as south of Route 64 the Hopewell anticline displays a history dominated by andalusite (Fig. 5.2 & 5.4). The differences in P-T


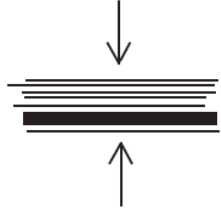



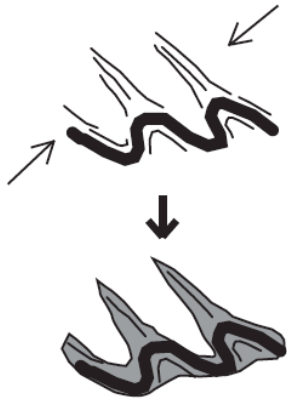


Deformation History	Schematic Fold Model	Thin Section View
<p>1. D1- S1 development</p> <p>alignment of phyllosilicates and hematite subparallel to S0</p>		
<p>2. start of D2</p> <p>S1 buckles</p>		
<p>3. F2, S2 formation</p> <p>realignment of phyllosilicates and hematite</p> <p>↓</p> <p>end of D2</p> <p>phyllosilicates replaced by andalusite</p>		
<p>4. start of D3</p> <p>F3 folding, S3 formation,</p> <p>andalusite crystals strained, formation of undulous extinction and new grain boundaries</p>		

Figure 5.6. A schematic diagram showing the timing of deformation and andalusite growth in the Ortega Formation quartzite of the Hopewell anticline.

conditions of the Hopewell Anticline and the Jawbone syncline may suggest some degree of vertical offset with a north-side-up motion sense near or along Route 64 (Fig. 5.3).

The transition from an andalusite-dominated assemblage to a kyanite + andalusite assemblage on the limb of the Hopewell anticline near Placer Creek represents a discontinuity in the mineral assemblage (Fig. 5.4). This transition involves a change in the metamorphic mineral assemblage without a significant change in the bulk composition of the rock and may represent the location of the kyanite isograd in the Hopewell Lake-Jawbone Mountain area and the Tusas Range (Williams, 1987).

Quartzite Peak and Kiowa Mountain

The mineral assemblage at Quartzite Peak and Kiowa Mountain includes quartz, kyanite, Mn-andalusite, hematite, rutile, zircon, monazite, ± pyrophyllite. Gahnite is locally present at Kiowa Mountain. Mn-andalusite and kyanite are found within the aluminous, hematite-bearing layers and form aluminum silicate clusters at Quartzite Peak.

S1, S2, and S3 are preserved as hematite inclusion trails in the aluminum silicates of Quartzite Peak and Kiowa Mountain. At Kiowa Mountain, rare hematite aligned in S1 is included in kyanite preserved in the cores of F2 folds and in remnant kyanite crystals that define L1 (Fig. 5.7). The kyanite preserved in the cores of F2 folds display undulose extinction associated with F2 folding. At Quartzite Peak, hematite inclusions in Mn-andalusite in the cores of aluminum silicate clusters define S1 (Fig. 4.11). At both Quartzite Peak and Kiowa Mountain, Mn-andalusite and kyanite include hematite aligned in S2 and S3. Kyanite and Mn-andalusite crystals display undulose extinction, kinking, and/or new grain boundaries, which commonly are associated with F3 and rarely F2 folds (Fig. 5.8f). Kyanite with hematite inclusion trails aligned in S3 can be found overgrowing existing kyanite crystals with hematite aligned in S2. At Kiowa Mountain, Mn-andalusite crystals overgrow F2 folds that are later deformed by F3, and in rare instances, Mn-andalusite includes hematite and kyanite aligned in S3 (Fig. 5.9).

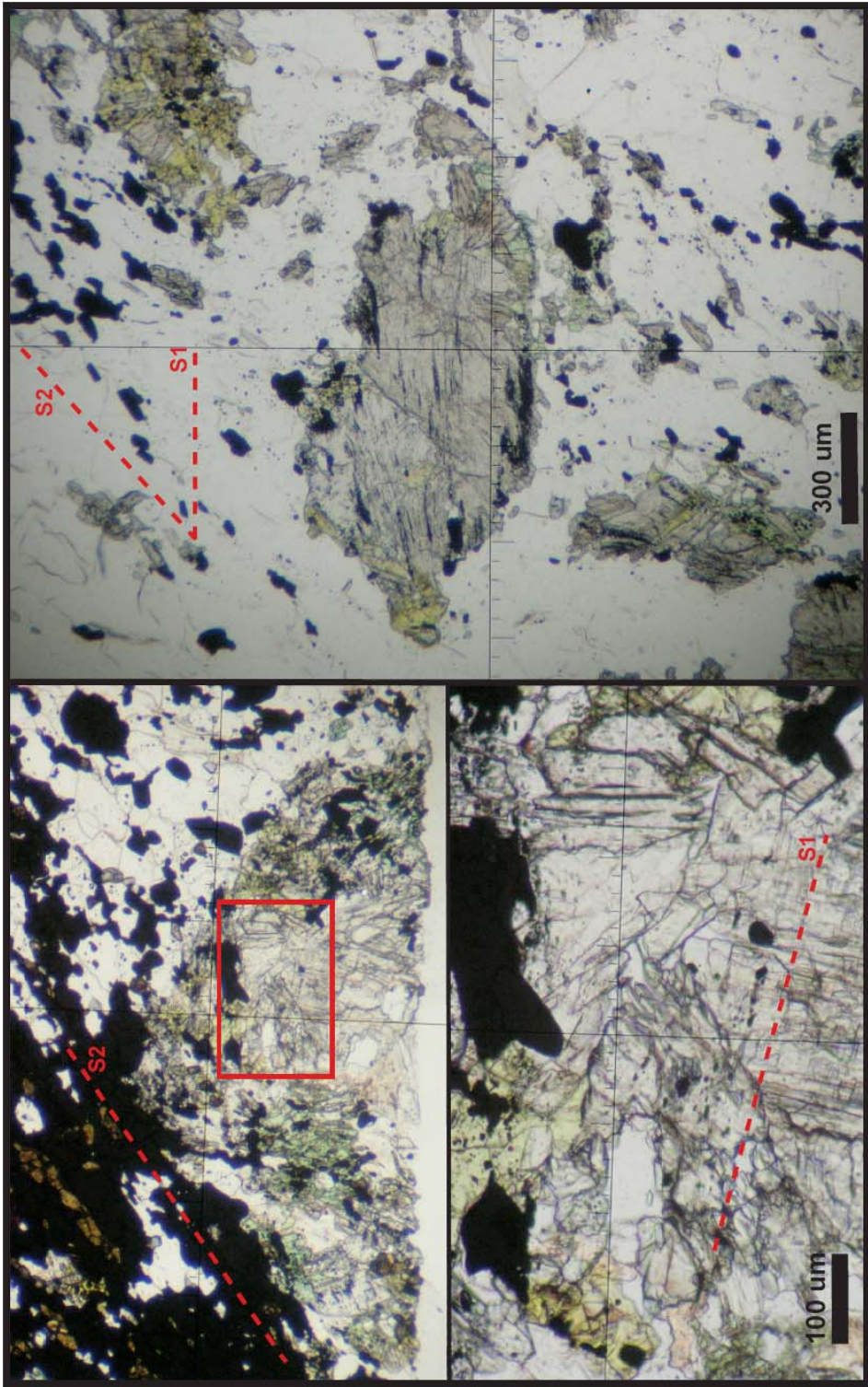


Figure 5.7. Hematite inclusions trails in kyanite preserve S1 in the cores of F2 folds (left) and in remnant kyanite crystals that are aligned subparallel to S0/S1 in a layer otherwise dominated by S2 (right).

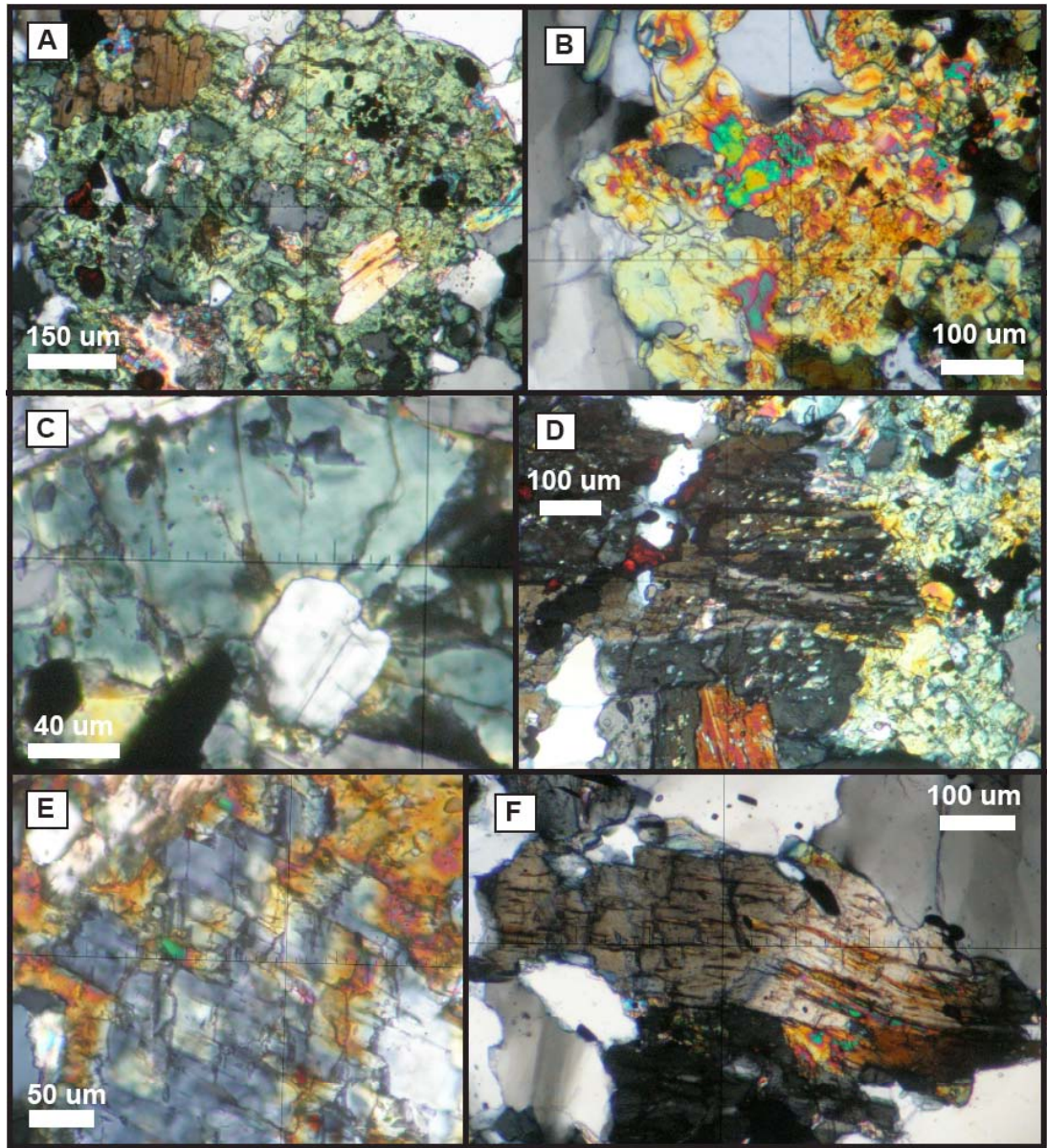


Figure 5.8. Mn-andalusite at Quartzite Peak displays a mottled texture (a,b) with only small, rare, localized zones of higher Mn (b). Textural relationships between kyanite and Mn-andalusite include: (c) high Mn-halos around kyanite included in Mn-andalusite, (d) Mn-andalusite inclusions in kyanite, (e) the Mn-andalusite replacement of kyanite, and (f) intergrown kyanite and Mn-andalusite. Kyanite and Mn-andalusite crystals were deformed and display kinking and undulose extinction (f) (sample-P06NM40).

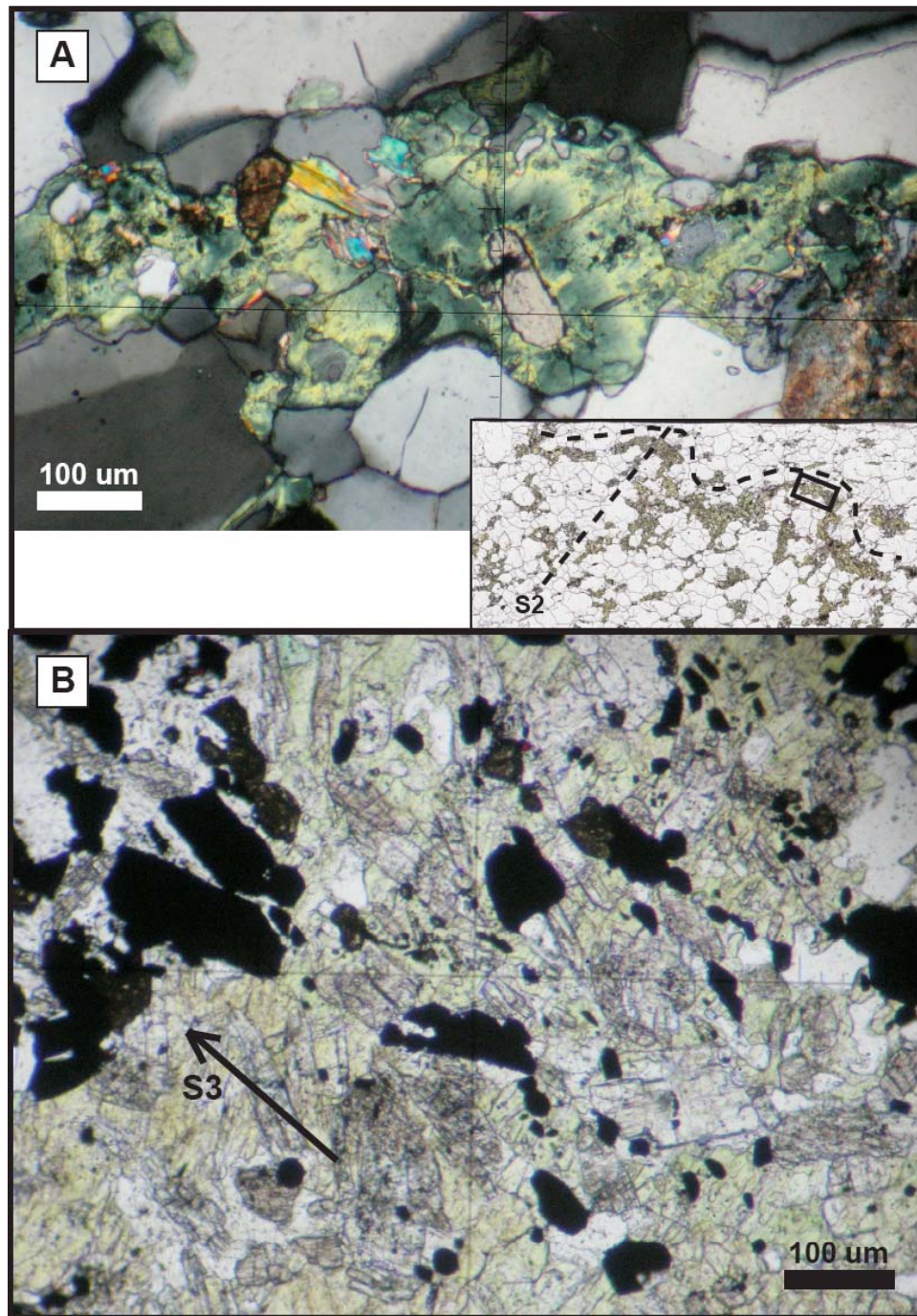


Figure 5.9. Undeformed Mn-andalusite crystals overgrow F2 folds and include hematite and kyanite aligned in S2 (top) and in rare instances, Mn-andalusite includes hematite and kyanite aligned in S3 (bottom).

Mn-andalusite-kyanite timing relationships are contradictory in the Mn-andalusite layer at Quartzite Peak and to some degree at Kiowa Mountain. Mn-andalusite inclusions can be found in optically continuous kyanite crystals suggesting andalusite growth after kyanite (Fig. 5.8d). In some cases, Mn-andalusite and kyanite appear intergrown with Mn-andalusite concentrated along zones subparallel to the C-axis of the kyanite crystal suggesting that both aluminum silicates were contemporaneous (Fig. 5.8f & 5.10). Mn-andalusite appears to have replaced kyanite in places where an otherwise continuous kyanite crystal had broken down (Fig. 5.8e). Evidence for all possible growth relationships are, therefore, preserved: the replacement of kyanite by Mn-andalusite, the replacement of Mn-andalusite by kyanite, and the growth of both minerals simultaneously. Commonly, these growth relationships are all preserved in close proximity. The evidence that suggests kyanite growth occurred after Mn-andalusite (Mn-andalusite inclusions in kyanite) is at odds with the evidence that suggests Mn-andalusite replaced kyanite. More than one period of Mn-andalusite mineral growth would explain conflicting timing relationships.

Evidence for more than one period of kyanite and Mn-andalusite growth is preserved at Quartzite Peak and Kiowa Mountain. An early period of kyanite growth at Kiowa Mountain was associated with D1 and formed during the growth of the M1 mineral assemblage. This early period of M1 kyanite growth is supported by the preservation of kyanite crystals aligned subparallel to S0/S1 and L1 and crystals that include hematite aligned in S1. M1 kyanite was folded by F2 folds causing undulose extinction in the kyanite. The first period of kyanite growth at Quartzite Peak, the second period of kyanite growth at Kiowa Mountain, and the first period of Mn-andalusite growth in both areas occurred during the growth of the M2 mineral assemblage syn- to post-D2 as is evidenced by kyanite and Mn-andalusite crystals that have been folded by F3 but also include hematite trails aligned in S2. A lack of evidence of strained kyanite crystals associated with S2 and F2 fabric development and the fact that most of the deformed crystals also overgrow hematite that is aligned in S3 both support a post-D2 period of kyanite growth. The M2 assemblage, particularly the M2 kyanite, has been overgrown by an additional generation of kyanite during the growth of the M3 metamorphic assemblage syn- to

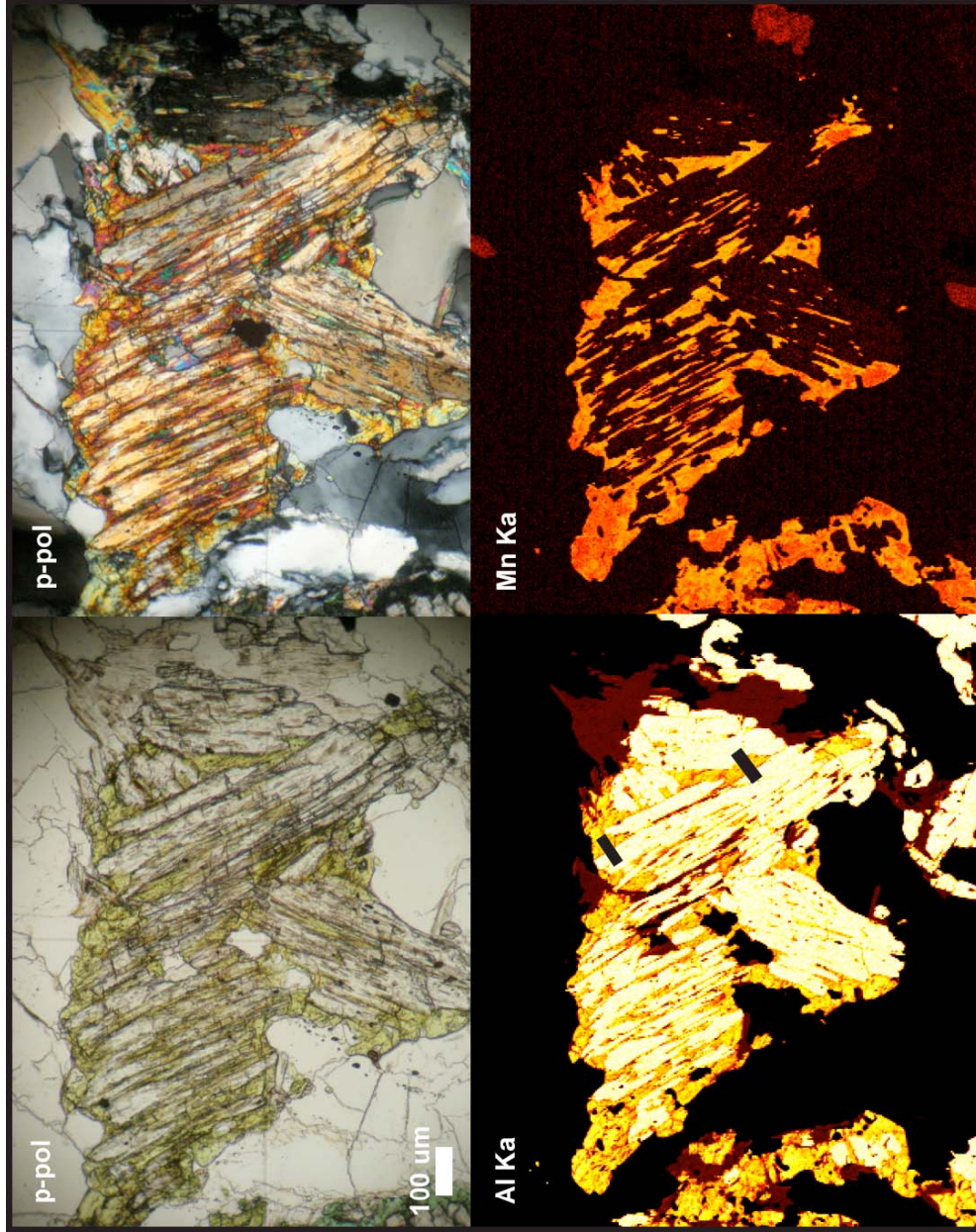


Figure 5.10. In places, kyanite and Mn-andalusite appear intergrown. The black bars in the Al X-ray map represent the traverses of EMP point analyses used for the geobarometry calculations (EMP x-ray maps of Al and Mn; sample- P06NM40).

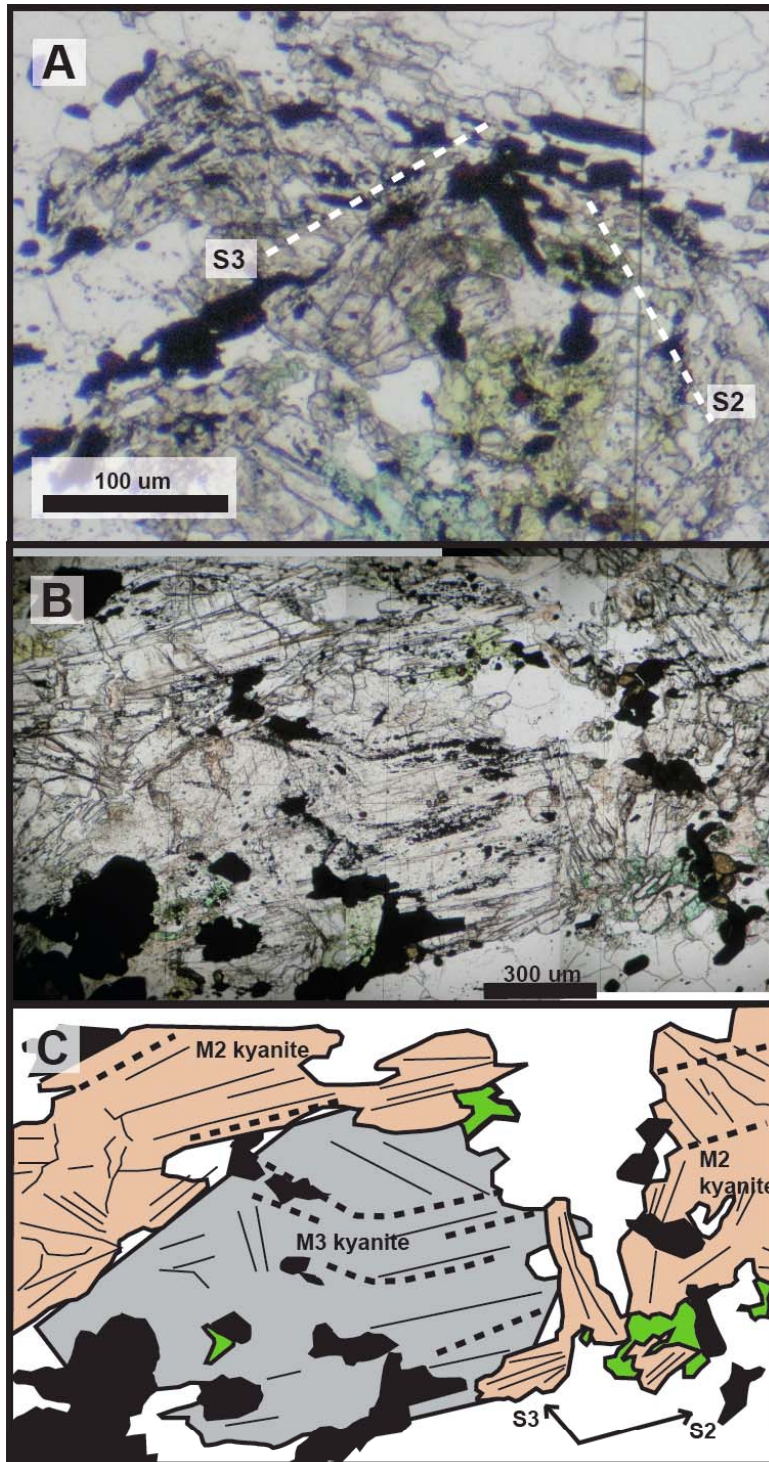


Figure 5.11. Late kyanite overgrows early kyanite at Quartzite Peak (a) and Kiowa Mountain (b,c). (samples-P06NM40 and P06NM59FB).

post-D3. This is largely supported by the fact that M2 kyanite with hematite aligned in S2 is overgrown by a different generation of kyanite with hematite aligned with S3 (Fig 5.11). The deformation of kyanite at Quartzite Peak is dominantly associated with S3 and F3 folding suggesting syn-D3 mineral growth and there is no evidence for unstrained kyanite crystals supporting a lack of post-D3 kyanite growth. Mineral inclusion and reaction relationships between kyanite and Mn-andalusite and the presence of hematite and kyanite inclusions aligned in S3 in Mn-andalusite both suggest a second period of Mn-andalusite growth during the growth of the M3 assemblage at Quartzite Peak and Kiowa Mountain.

Pressure-Temperature Calculations

The compositions of Mn-andalusite and kyanite from the Mn-andalusite layer at Quartzite Peak and Kiowa Mountain were used to calculate a pressure-temperature estimate for each area during the growth of the M2 assemblage. Calculations were based on compositional analyses from intergrown kyanite and Mn-andalusite thought to represent the simultaneous growth of both minerals early during the growth of the M2 assemblage (Fig. 5.12; Appendix 2). An estimated temperature range of 400-450°C and pressure offset of ~0.85 kb for the kyanite-andalusite line lead to a P-T estimate of ~3.2kb and 430°C for Quartzite Peak. An estimated temperature range of 400-440°C and pressure offset of ~ 0.68 kb for the kyanite-andalusite line lead to a P-T estimate of ~2.7kb and ~415°C for Kiowa Mountain. P-T estimates are thought to represent the conditions of M2 at the point of kyanite and Mn-andalusite growth in each area.

Summary of Quartzite Peak and Kiowa Mountain

Two major periods of metamorphism (M2, M3) lead to the growth of a kyanite + Mn-andalusite assemblage in the Mn-andalusite layer at the base of the Ortega Formation at Quartzite Peak and Kiowa Mountain (Fig. 5.13). The first metamorphic assemblage (M1) included the growth of kyanite at Kiowa Mountain and may have included the growth of low-grade minerals, such as kyanite and pyrophyllite, at Quartzite Peak. The growth of the second

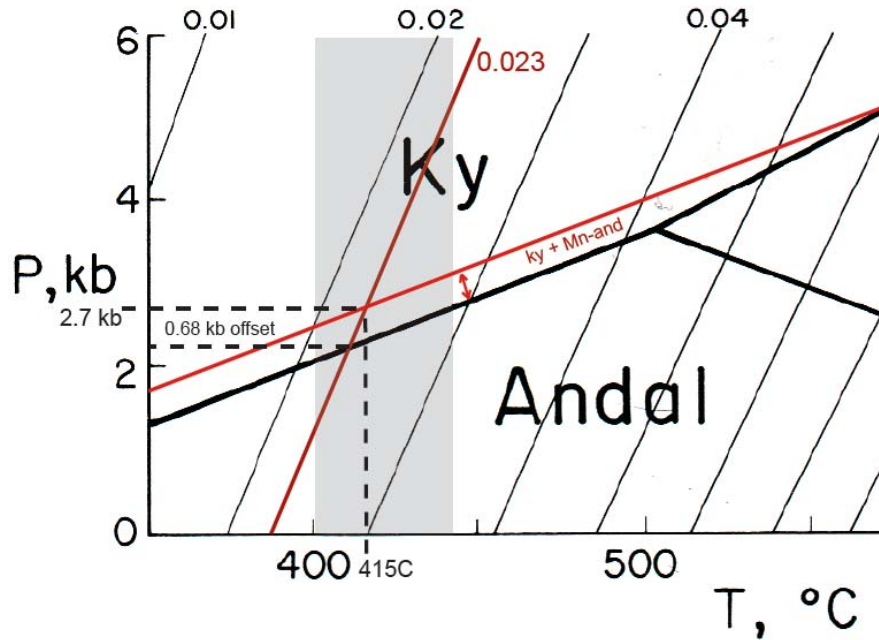
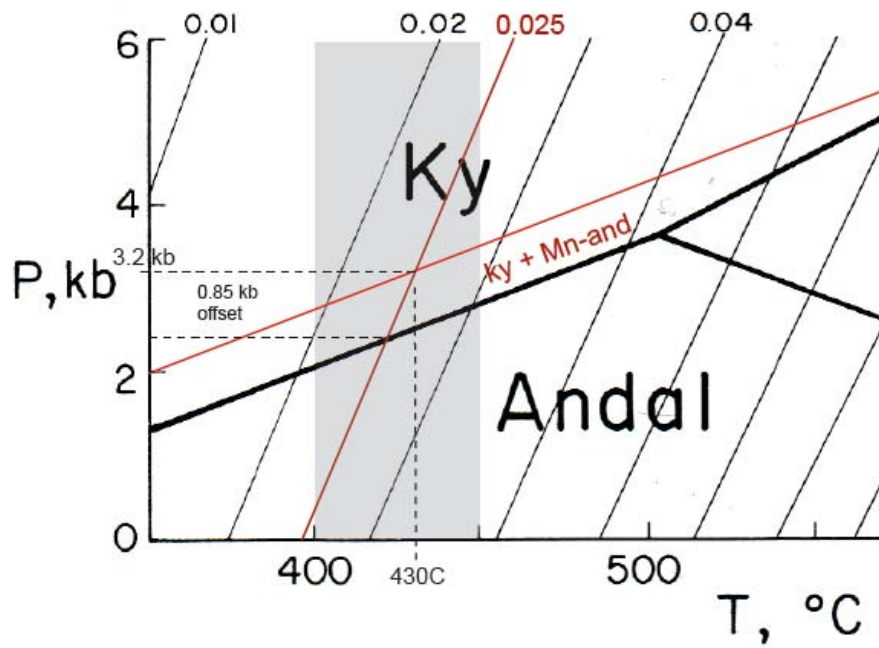


Figure 5.12. Equation four and figure 15 of Grambling and Williams (1985) were used to calculate a P-T estimate for the conditions of M2 kyanite and Mn-andalusite growth at Quartzite Peak (top) and Kiowa Mountain (bottom).

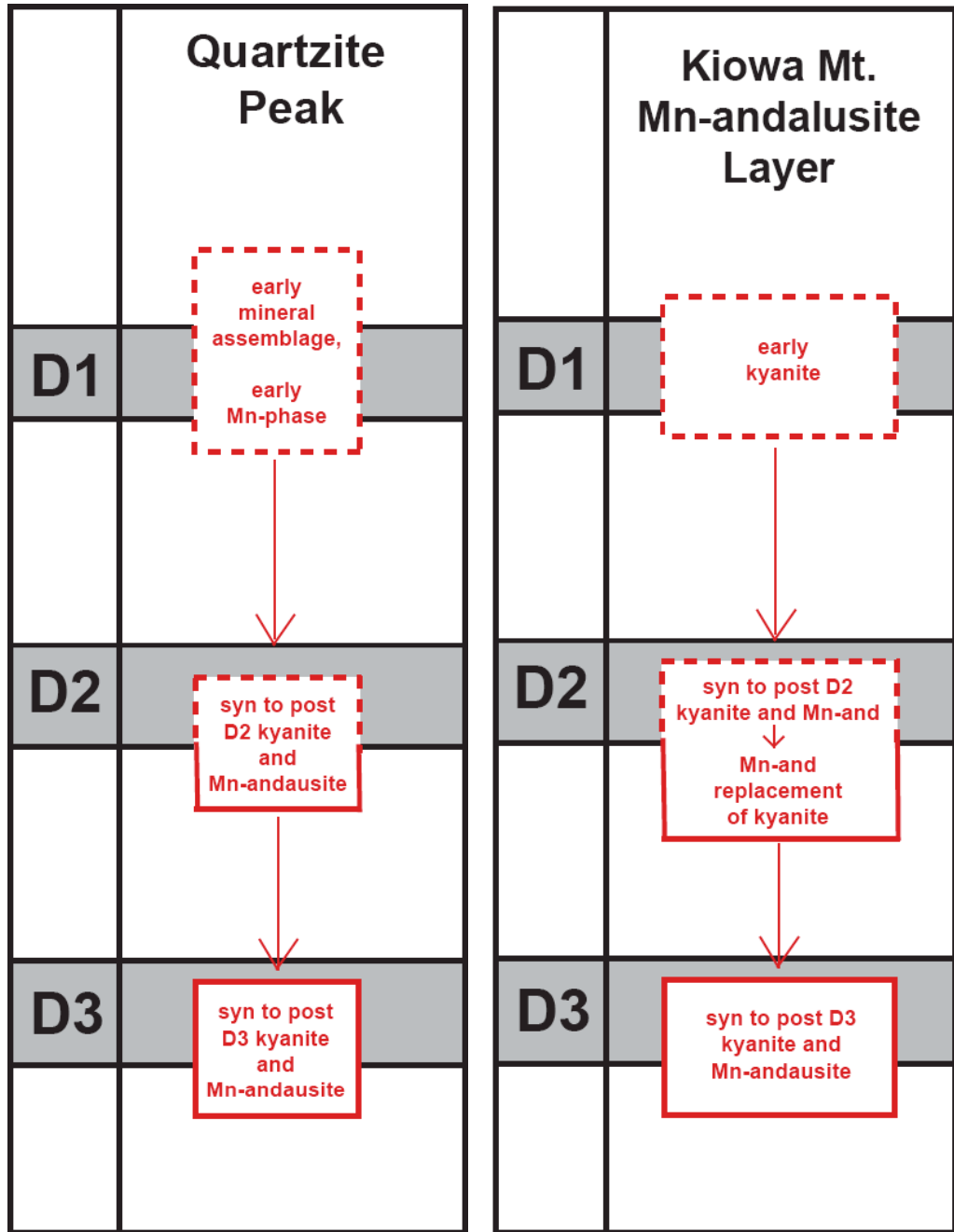


Figure 5.13. The inferred tectonic history of the Mn-andalusite layer at the base of the Ortega Formation at Quartzite Peak (left) and Kiowa Mountain (right).

metamorphic assemblage (M2) followed D2 deformation and included the growth of kyanite and Mn-andalusite. The growth of M2 Mn-andalusite and kyanite was followed by a period of solely Mn-andalusite growth at Kiowa Mountain (Chapter 6). The growth of the M3 assemblage occurred syn to post D3 deformation and included the growth of a second kyanite and Mn-andalusite assemblage.

The timing of kyanite and Mn-andalusite growth relative to fabric formation is difficult to decipher in thin section because not all hematite and Mn-andalusite crystals preserve clear fabric relationships in hematite inclusion trails. Without preserved inclusion trails or the deformation of mineral grains, it is highly difficult to determine to which generation (M2 or M3) a given Mn-andalusite or kyanite crystal belongs. Given the similarity of the two metamorphic assemblages, it is easy to mistakenly attribute all the mineral growth to one single metamorphic event.

CHAPTER 6

MN HORIZON AND MN-ANDALUSITE MINERALIZATION

The Mn horizon is can be found within the first few hundred meters of the Ortega Formation quartzite in the Tusas Mountains in most places where the Vadito-Ortega contact is exposed. The Mn horizon includes an assemblage of Mn-andalusite, quartz, hematite, rutile, zircon, monazite, phyllosilicates (dominantly pyrophyllite and some pennantite) ± kyanite and gahnite. This study focuses on three areas with well-exposed and abundant Mn-andalusite in the Tusas Mountains: the Hopewell Lake-Jawbone Mountain area, Quartzite Peak, and Kiowa Mountain (Fig. 6.1).

Field Observations

Mn-andalusite at the base of the Ortega Formation area occurs primarily in association with abundant hematite in the aluminous, hematite-bearing layers (“kaolinitic mudstone drapes” of Soegaard and Erikson, 1986; Fig. 6.2c), on the surface of cross-beds (Fig. 6.2a), concentrated in high strain zones (Fig 6.2c), and on cleavage planes (Fig 6.2d). Quartzite hosted Mn-andalusite crystals are rarely larger than a few millimeters where as Mn-andalusite in schistose layers are up to a centimeter in size. Mn-andalusite crystals are the most concentrated within the aluminous, hematite bearing layers and the high strain zones. High strain zones typically occur within the aluminous, hematite-bearing layers. Thin layers of Mn-andalusite and hematite can be found defining the surface of cleavage planes and the bottom-set, foreset, and topset beds of cross-beds. These planes are rarely thicker than several millimeters and can make the cleavage planes and cross-beds bright green in outcrop. Mn-andalusite typically is not recognized and may not be present in the conglomeritic layers where the sediment is coarser.

The Mn horizon in the Hopewell Lake-Jawbone Mountain area is exposed along a number of erosion resistant quartzite outcrops at the base of the Ortega Formation south of Route 64 that define the NW striking SW dipping southern limb of the Hopewell anticline

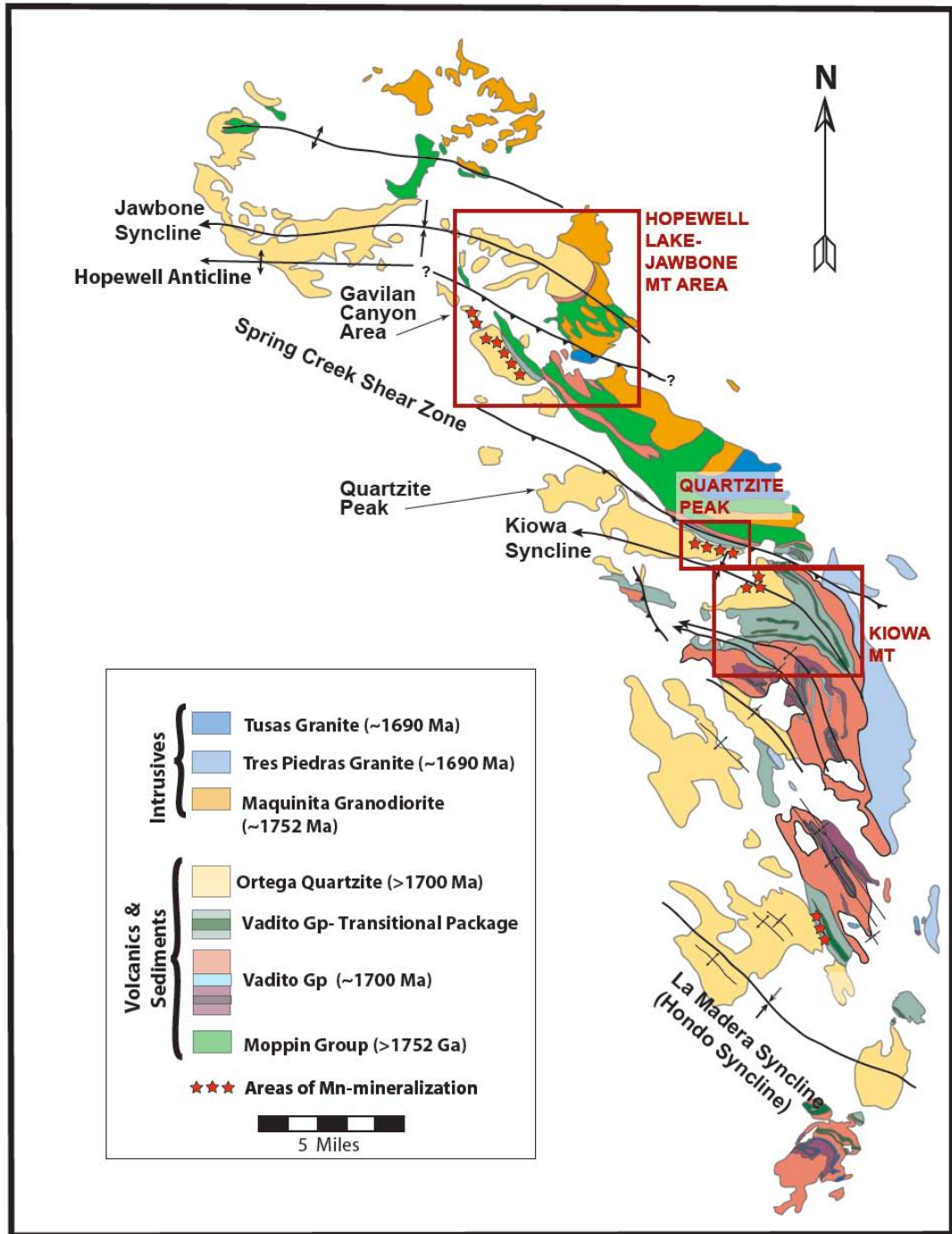


Figure 6.1. Map of the Tusas Mountains showing the four areas of well-exposed and abundant Mn-andalusite focused on in this study (adapted from Williams, 1991 and Kopera, 2003).

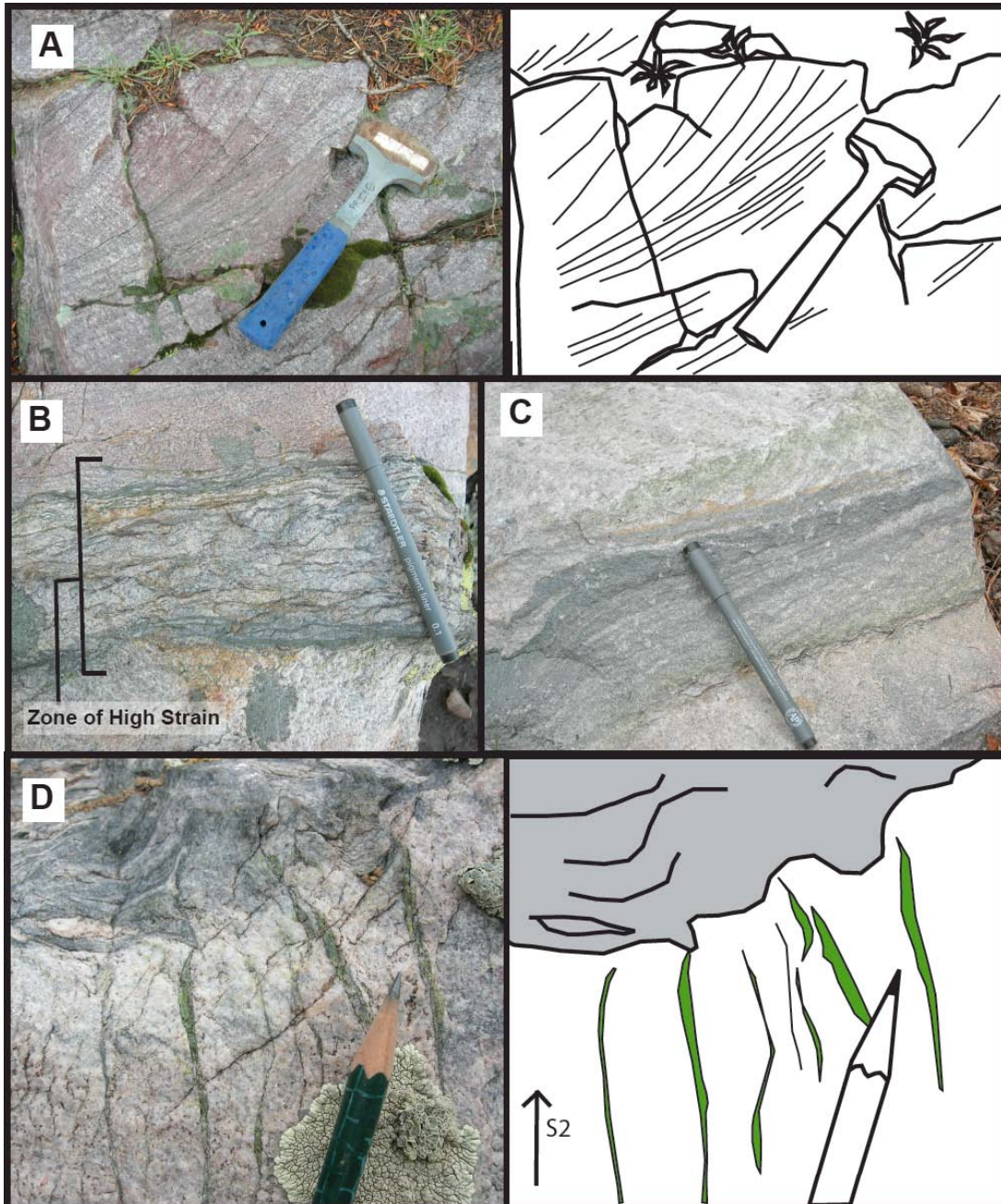


Figure 6.2. Mn-andalusite occurs with an abundance of hematite in aluminous, hematite-bearing layers (c), on the surface of cross beds (a), on cleavage planes (d), and in high strain zones (b).

(Fig. 4.8). In the Hopewell-Lake Jawbone Mountain area, distinct Mn-andalusite-rich cleavage planes are common, and Mn-andalusite crystals are usually rich in color with dark green specks seen at the center of many of the crystals under hand lens magnification.

The Mn horizon is exposed at the base of the Ortega Formation where it outcrops along the northeast side of the Quartzite Peak just south of Spring Creek (Fig. 6.3) and at the summit of Kiowa Mountain. Very few of the Mn-andalusite containing rocks at the summit of Kiowa Mountain are still in place and exposure is mostly limited to unoriented blocks of Mn-andalusite-rich quartzite float. The distribution of Mn-andalusite within the aluminous, hematite-bearing layers is variable at both Quartzite Peak and Kiowa Mountain. Mn-andalusite may be concentrated at the top-most part of a hematite-rich layer, concentrated into layers with little to no hematite, or even be absent from hematite-rich layers all together. Mn-andalusite also forms individual layers within the quartzite with little or no hematite, and the Mn-andalusite-only layers spatially overlap hematite-rich layers and display similar types of sedimentary structures (Fig. 6.2c). Unlike the Hopewell Lake Jawbone Mountain area, Mn-andalusite rich high strain zones, cross-beds, and cleavage planes are less common at Quartzite Peak and Kiowa Mountain. Differences in Mn-andalusite between the Hopewell Lake-Jawbone Mountain area, Quartzite Peak, and Kiowa Mountain suggest some degree of variability in the Mn horizon from area to area. Both Quartzite Peak and Kiowa Mountain display significant variability in the distribution of Mn-andalusite within the aluminous, hematite-bearing layers whereas the Hopewell Lake-Jawbone Mountain area is more homogenous.

Mn-andalusite consistently occurs in association with hematite (and to a lesser degree rutile) throughout all the areas studied in the Tusas Mountains. Mn-andalusite occurs with hematite on primary structures such as in the aluminous, hematite-bearing layers and on the surface of cross beds as well as in deformational structures, such as in high-strain zones and on cleavage planes. This association suggests that hematite and Mn-andalusite are genetically related.

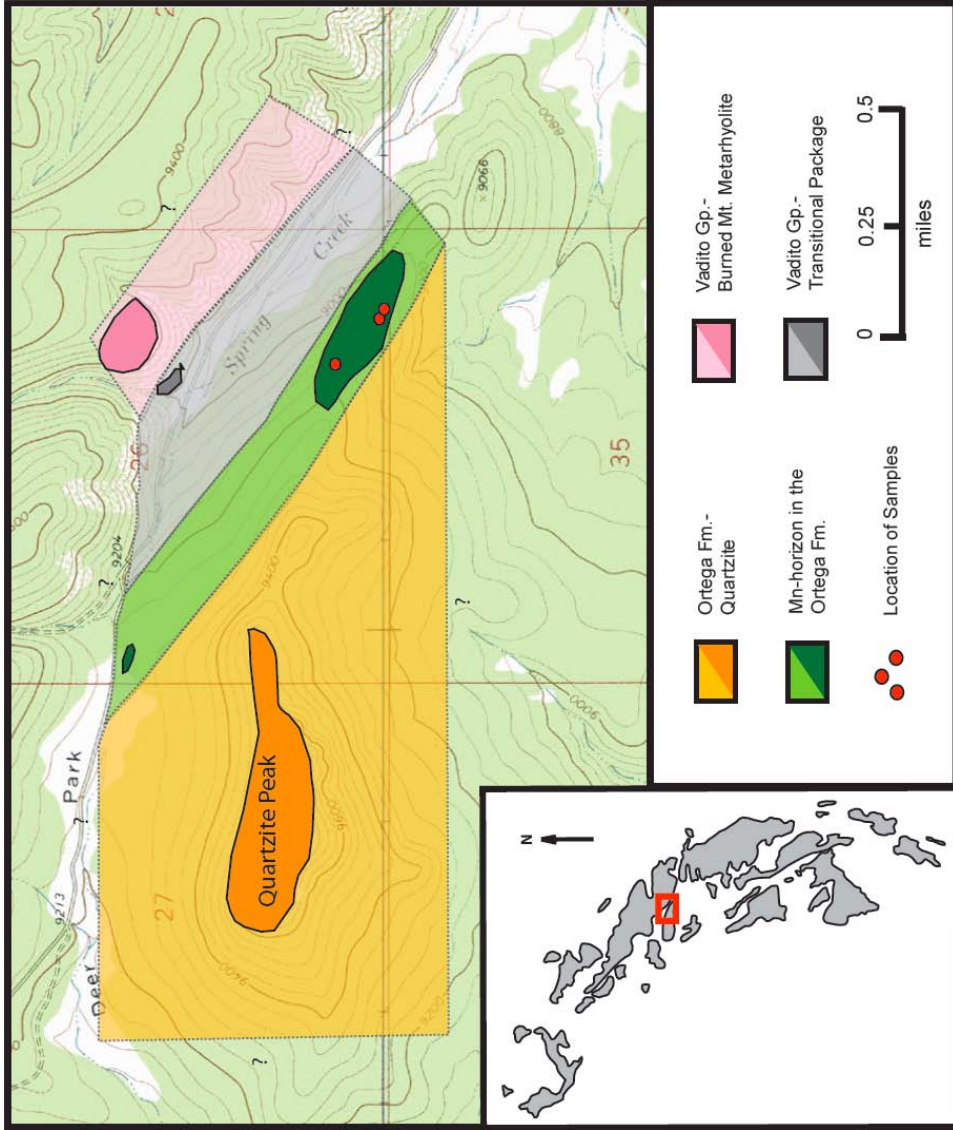


Figure 6.3. Lithologic map showing the location of the Mn horizon at Quartzite Peak. Bold, outlined, colored areas represent exposed outcrop and transparent colored areas represent the inferred extent of Proterozoic units.

Mn-andalusite also occurs on both primary and deformational structures throughout the areas studied in the Tusas Mountains. It occurs on the surface of primary cross-beds and is dominantly concentrated in aluminous, hematite-bearing layers. Mn-andalusite also occurs with deformational structures such on cleavage planes and in high strain zones. The presence of Mn-andalusite on primary depositional structures suggests a link between Mn-andalusite and depositional processes and may indicate that the Mn horizon is syn-sedimentary. The association of the aluminous, hematite-bearing layers and the high strain zones suggests that strain may have concentrated the aluminous, hematite-bearing layers during deformation. In addition, the association of Mn-andalusite on cleavage planes could be a result of the remobilization and concentration of Mn onto cleavage planes during deformation.

Manganese Zoning in Mn-andalusite

The crystal chemistry of Mn-andalusite dictates that as Mn^{3+} substitutes for Al^{3+} in the andalusite crystal structure, the crystal lattice expands changing the refractive index and thus the birefringence of the mineral (Gunter and Bloss, 1982). Because of the effect Mn substitution has on the refractive indices of the mineral, there is a direct relationship between changes in birefringence and the amount of Mn incorporated into the crystal structure. The relationship between Mn content and birefringence color is such that as the amount of Mn incorporated into the andalusite crystal structure increases, the birefringence correspondingly increases to higher order colors.

Some Mn-andalusite crystals display large-scale zoning patterns that reflect significant differences in Mn content across a single Mn-andalusite crystal (Fig. 6.4). Typically, Mn-andalusite crystals contain localized zones of high Mn content that display high order colors (e.g. yellow, pink, orange, and light green). Mn-content decreases away from the localized Mn highs, and the remainder of the crystal has a relatively low Mn-content (less than 5 weight percent Mn_2O_3) and displays lower order colors (e.g. grey, indigo, and blue green). Grambling and Williams (1985) reported similar zoning patterns that show a decrease in Mn across an Mn-andalusite crystal from a localized high at the edge of the crystal or a concentric zoning pattern

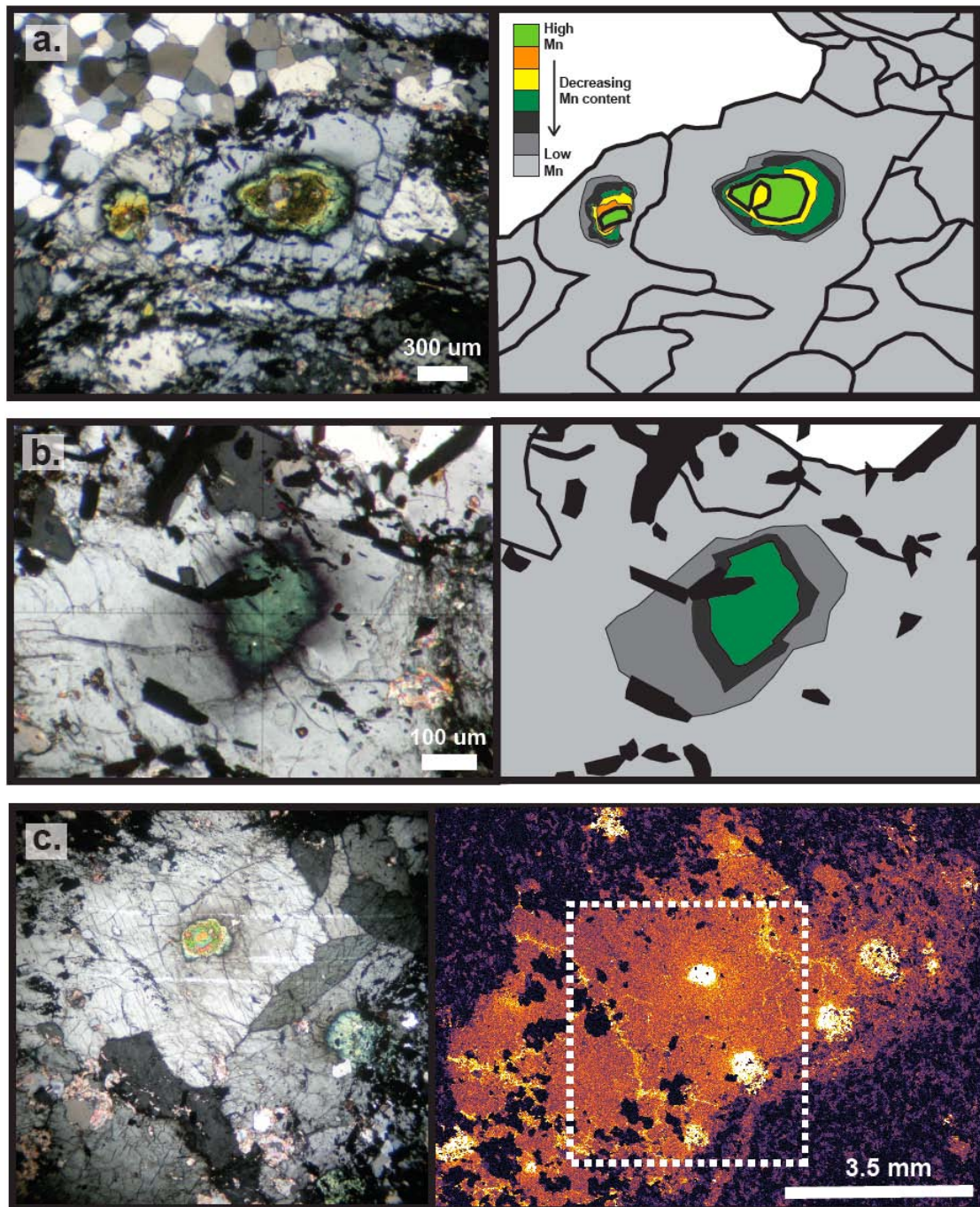


Figure 6.4. Zoning patterns preserved in the birefringence of Mn-andalusite crystals represent a decrease in Mn away from a localized high-Mn region (a,b,c). EMP x-ray map of Mn shows the concentration of Mn in localized high-Mn regions (brighter color = higher Mn) (a, b- MLW2; c- JK01-58-H1).

when the high is found within the center of the crystal. In most Mn-andalusite crystals, the zoning pattern appears sharp and tight near the localized high.

The large-scale zoning patterns in Mn-andalusite crystals are interpreted to reflect the original large-scale distribution of Mn in the rock at the time of Mn-andalusite growth (Grambling and Williams, 1985). The large-scale zoning could represent the type of growth zoning associated with Rayleigh fractionation, but the evidence present does not support such an interpretation. Commonly there is more than one zoning pattern in a single crystal without any evidence of crystal twinning. The zoning consistently decreases in Mn content away from the localized high in all samples studied without any evidence of oscillation. The zoning pattern also does not display a crystal shape as is commonly seen in porphyroblasts that display growth zoning. Instead, the decrease in Mn-content away from localized highs appears to represent a gradient of Mn content from areas of high Mn to areas of low Mn. The gradients may be caused by the diffusion of Mn away from the high Mn areas and the localized areas of Mn-highs may be the remnants of an earlier Mn-rich phase.

High-Mn Core Regions

Localized regions of extremely elevated Mn content in the Mn-andalusite crystals of the Hopewell Lake-Jawbone Mountain region have a distinctly different character than the crystals that contain them. Mn-andalusite crystals from the Hopewell Lake-Jawbone Mountain area are characterized by extreme localized highs of Mn content within a crystal of an otherwise low, relatively homogenous Mn distribution. The concentrated Mn regions are areas of markedly high birefringence (bright green, yellow, and pink) dotting a crystal that has a low, uniform birefringence (grey or dark blue) (Fig. 6.4 & 6.5). The high Mn-regions are andalusite in composition and include X_{Mn} of up to 0.76 (Table 6.1). They have a composite texture and include fine rounded crystals of hematite and rutile, the alignment of which can preserve early fabric and fold structures (specifically S1 and F1) (Fig. 6.5c). The high-Mn regions have a distinct textural boundary with the surrounding andalusite crystal and there is a difference in relief between the two, but they also appear optically continuous with the surrounding crystal

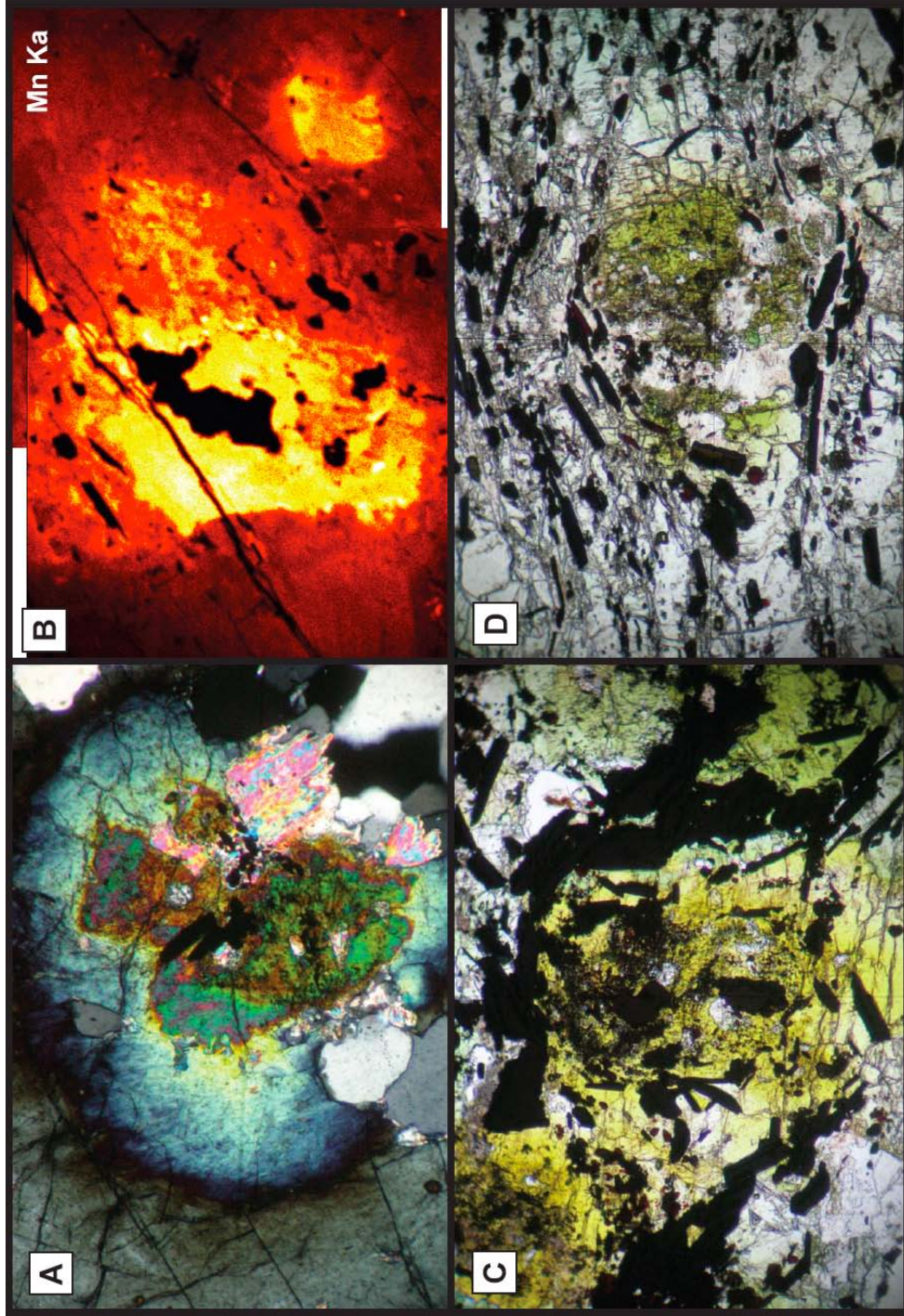


Figure 6.5. High-Mn core regions are areas of high Mn content as seen in the EMP Mn x-ray map shown in (b). Hematite aligned in the dominant foliation wraps the core regions (d), and the core regions have distinct textural boundaries with the surrounding Mn-andalusite crystal (a). Hematite included in Mn is fine grained (c).

Table 6.1. Composition of High-Mn Core Regions

	MLW2C	MLW2C	MLW2C	MLW2C	P06NM15A	P06NM20A	MLW2C
SiO ₂	33.93	34.43	34.59	34.06	32.86	33.37	
TiO ₂	0.00	0.00	0.01	0.00	0.00	0.00	
Al ₂ O ₃	33.36	36.55	38.36	38.17	42.07	44.35	
Fe ₂ O ₃	1.04	1.37	1.06	1.60	1.03	1.57	
Mn ₂ O ₃	30.56	28.08	24.88	22.43	20.33	18.53	
MgO	0.00	0.02	0.01	0.00	0.01	0.00	
Total	99.27	100.69	99.11	96.26	96.30	97.84	
Si	1.118	1.099	1.099	1.076	1.048	1.094	
Al	1.296	1.375	1.436	1.421	1.582	1.420	
Fe ³⁺	0.026	0.033	0.025	0.038	0.025	0.036	
Mn ³⁺	0.767	0.682	0.601	0.658	0.494	0.619	

under crossed polarizers (Fig. 6.5a). The high-Mn regions are generally ellipsoidal in shape and do not have a specific crystal habit. Hematite inclusions within the high-Mn region are finer and lack a crystal habit whereas the hematite inclusions within the surrounding crystal are larger, elongate, and display a tabular crystal habit. Elongate hematite crystals aligned in the direction of foliation wrap the high-Mn regions and the high Mn-regions typically have edges flattened in a direction parallel to foliation (Fig. 6.5d).

The high-Mn regions found in the Mn-andalusite of the Hopewell Lake-Jawbone Mountain area are optically continuous with the surrounding andalusite crystal but differ in appearance and in Mn-content. In addition, elongate hematite wraps the high-Mn region but is included in the mantle indicating that deformation has affected the high-Mn regions prior to the growth of the surrounding crystal. These differences suggest that the high-Mn region was present prior to the growth of the surrounding crystal. The surrounding crystal may have nucleated on and incorporated the high-Mn region as it grew. The high-Mn regions, therefore, appear to display a core-rim relationship with the surrounding Mn-andalusite crystal and will, therefore, be referred to as high-Mn core regions.

The high Mn-core regions in the Hopewell Lake-Jawbone Mountain area are dominantly found on cross-beds and in the aluminous, hematite-bearing layers, and the pattern of their distribution suggests a connection with sedimentary structures. High-Mn core regions are dominantly concentrated within the aluminous, hematite-bearing layers. They can be seen in outcrop as dark green specks. Within the least deformed samples, the high-Mn core regions are most densely concentrated at the base of the aluminous, hematite-bearing layer and decrease in abundance up section within the layer (Fig. 6.6). This vertical gradation appears similar to a sedimentary graded bed with the high-Mn core regions representing what would be the coarsest material concentrated at the bottom of the bed and then decreasing in abundance upward. When present outside of the aluminous, hematite-bearing layers, they are located on the surface of cross beds or what are interpreted to have been cross beds prior to deformation (Fig. 6.7).

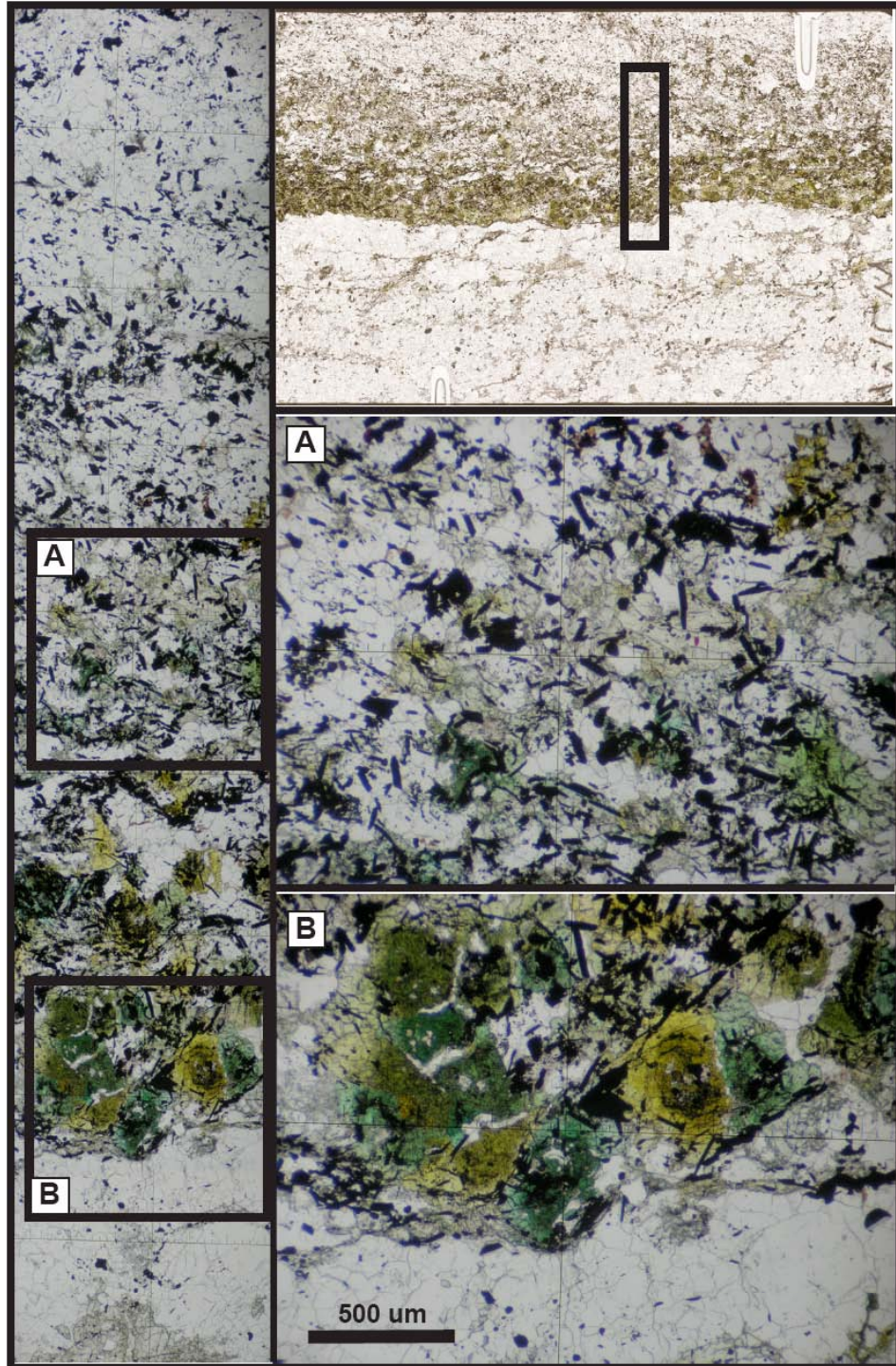


Figure 6.6. The high-Mn core regions are most densely concentrated at the base of the aluminous, hematite-bearing layer and decrease in abundance up section within the layer. This gradation appears similar to a sedimentary graded bed.

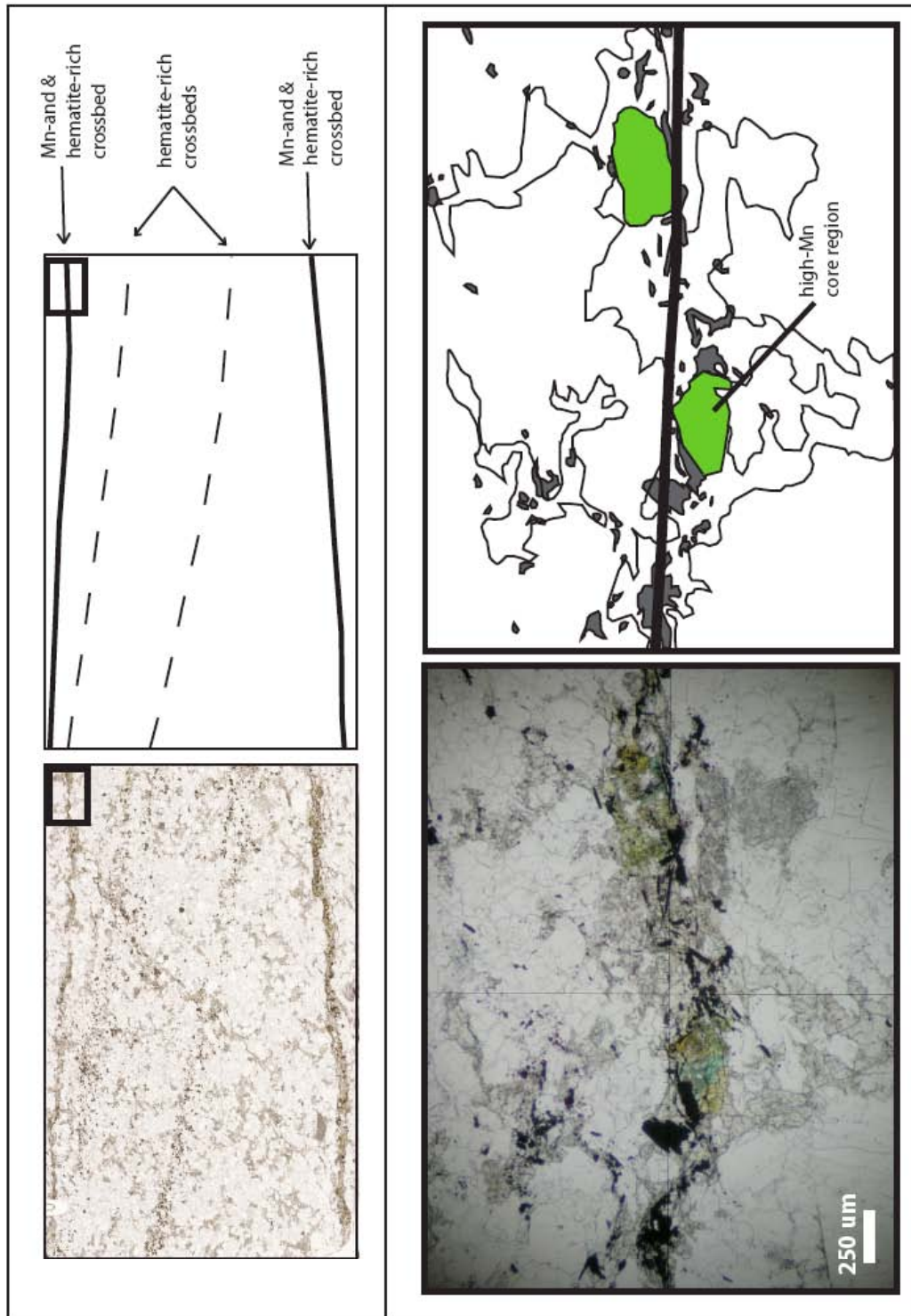


Figure 6.7. High-Mn core regions can be found on the surface of cross beds in the Hopewell lake-Jawbone Mountain area.

High-Mn core regions are best exposed at the Hopewell Lake-Jawbone Mountain area in the andalusite-only rocks, but similar Mn-concentrations in the kyanite + Mn-andalusite rocks from the Hopewell Lake-Jawbone Mountain area and Quartzite Peak may be related to high-Mn core regions. Because Mn stabilizes andalusite outside of its stability field, areas of higher Mn content can exist as andalusite in aluminous rocks otherwise dominated by kyanite. Areas of Mn-andalusite stability in kyanite rich rocks are the areas of the highest Mn content and may correspond the high Mn-core regions. In a kyanite-rich rock from the Hopewell Lake-Jawbone Mountain area, Mn-andalusite occurs as isolated ball-like “islands” within a sea of kyanite and the distribution of those islands is concentrated in bands subparallel to bedding structures (Fig. 6.8). In a sample from Quartzite Peak, kyanite and Mn-andalusite occur together in aluminum silicate clusters. Mn-andalusite is typically found at the center of these clusters and is the place where early fabrics (S1) are preserved (Fig. 4.2). These Mn-andalusite rich areas and islands may be the remnants of high-Mn core regions.

High-Mn core regions preserve some of the earliest fabrics and the highest amounts of Mn in the andalusite crystals. The high Mn-core regions preserve hematite inclusion trails of the earliest fabric (S1) and the core regions are wrapped by later fabrics (S1, S2, & S3). This suggests that they were present during and perhaps even prior to the earliest deformation. The high Mn-core regions also contain the highest amount of Mn in the andalusite. They are the only areas where Mn is so highly concentrated and large-scale zoning shows that Mn decreases outward from the high-Mn core regions. The Mn-distribution suggests that a source of Mn in Mn-andalusite may be associated with the high Mn-core regions. Textural evidence and Mn distribution patterns, therefore, suggest the high-Mn core regions were present early in the history of the Mn-andalusite layer and that they reflect the replacement of an earlier Mn-phase that may have been a source of Mn in the Mn-andalusite layer.

Mn-andalusite was probably not stable early in the history of the Mn-andalusite layer and the high-Mn core regions may have replaced an earlier Mn-containing precursor phase. The identity of this precursor phase is unknown but was probably a lower grade, high Mn-phase such as pennantite, Mn-chlorite, or kanonaite, the high-Mn end member of the andalusite

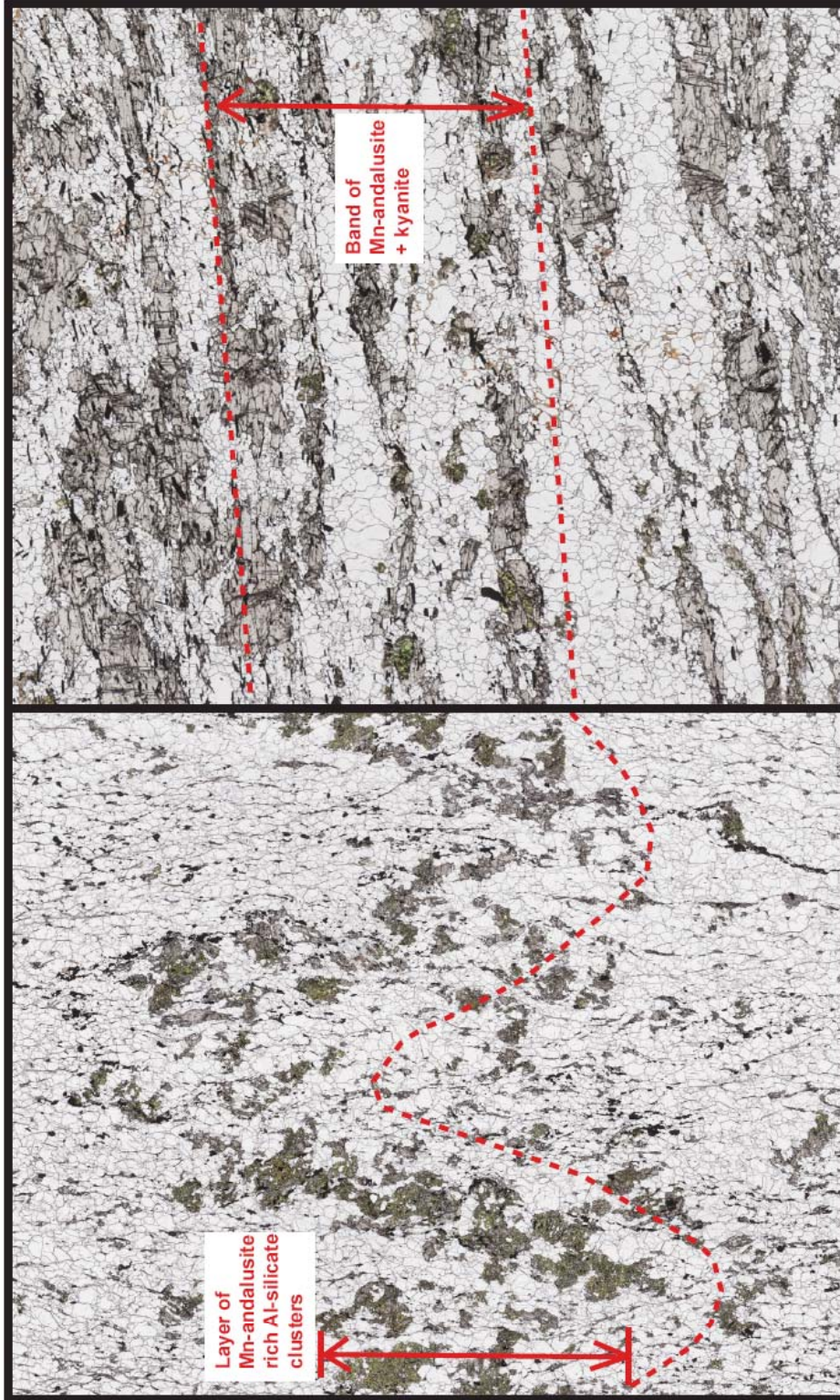


Figure 6.8. Mn-andalusite is concentrated in bands subparallel to bedding structures in the Hopewell Lake-Jawbone Mt area (right). In a sample from Quartzite Peak, kyanite and Mn-andalusite occur together in aluminum silicate clusters (left).

kanonaite series. Abs-Wurmbach et al (1983) have shown that kanonaite is only stable at low temperatures and pressures and that Mn-andalusite will overgrow kanonaite cores at higher temperatures and pressures (Fig. 6.9). Additionally, Schreyer et al (2004) showed kanonaite from Coreux, Belgium to have a composite texture. This may explain why the high-Mn core regions appear to have an andalusite crystal structure, serve as the nucleation point for Mn-andalusite growth, and have a composite texture.

The association of high Mn-core regions with sedimentary structures suggests that the source of the Mn-precursor phase is linked to sedimentary processes. The high Mn-core regions are present on the surface of cross-beds in the same way as a pebble or coarse hematite grain would be suggesting that the precursor phase was deposited on the surface of the cross beds. Additionally, in the graded bed structure, high-Mn core regions decrease in concentration upward in the same way pebbles would grade upward in a graded bed suggesting that the high-Mn precursor phase was deposited in a similar way. Both of these observations not only suggest that the precursor phase of the high-Mn core regions was deposited, but that it may have served as a competent particle during deposition.

Hematite and Rutile Mineralization

Mn-andalusite is closely associated with hematite in most localities. Mn-andalusite occurs with hematite in the aluminous, hematite-bearing layers and on the surface of cross beds. This association suggests that the mineral-scale observations of hematite may be important for understanding the origin of the Mn horizon. Observations made from the transitional package of the Vadito Group and the Mn-andalusite layer from the base of the Ortega Formation are considered below.

Hematite consistently occurs in association with rutile in the Mn-andalusite-rich rocks of the Mn horizon, but without rutile in the metasedimentary and metavolcanic units that comprise the transitional package of the Vadito Group. Hematite and rutile also occur together in the Mn-poor aluminous, hematite-bearing layers at the base of the Ortega Formation (i.e. in the Hopewell Lake-Jawbone Mountain area). Hematite can be found as elongate tabular crystals,

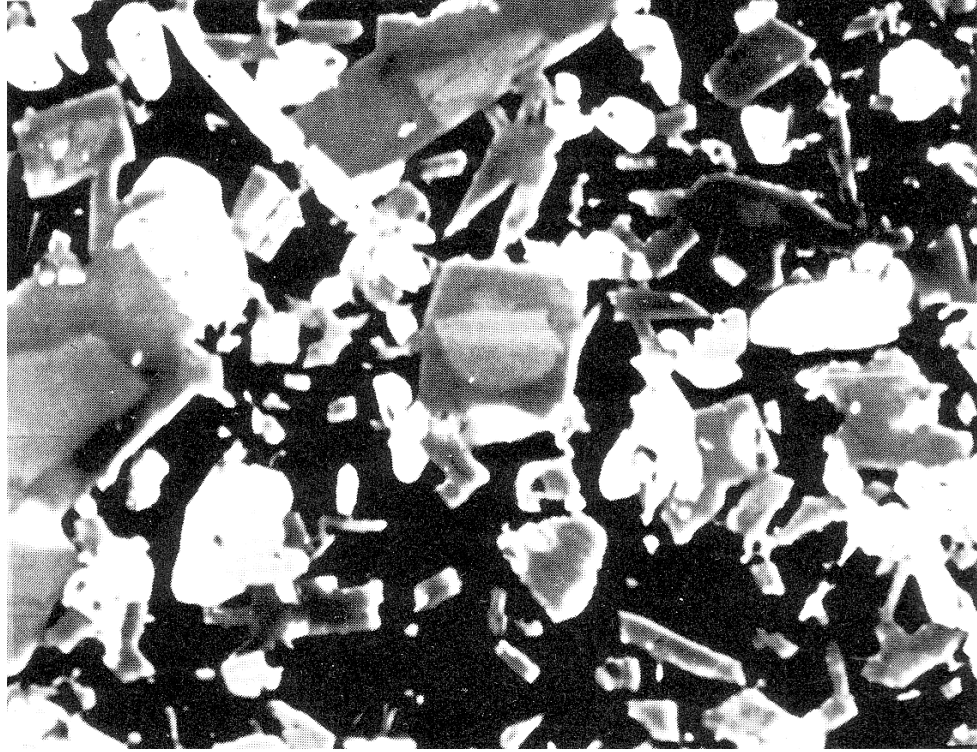


Figure 6.9. Abs-Wurmbach et al (1983) showed that Mn-andalusite will overgrown kanonaite cores at higher temperatures and pressures.

small rounded granular crystals, or large euhedral to rounded grains in the Ortega Formation. Rutile occurs as red-brown grains of varying size that typically have rounded or ellipsoidal shapes. Hematite abundance does not greatly vary between the three areas studied, but the Mn-andalusite layer at Kiowa Mountain has a notably greater abundance of rutile than either the Hopewell Lake-Jawbone Mountain area or Quartzite Peak. In the metasedimentary units of the Vadito Group, hematite occurs both as elongate rectangular shaped crystals and as euhedral to rounded grains that vary in size. In the metarhyolite and amphibolite units, hematite dominantly occurs as medium to large euhedral crystals with a smaller degree of broken and elongate crystals occurring in areas of high strain.

Both hematite and rutile from the Mn-andalusite layer at the base of the Ortega Formation and the hematite of the metasedimentary, metarhyolite, and/or amphibolite units of the Vadito Gp. are rich in trace elements (Table 6.2 & 6.3). Trace elements include less than one weight percent of one or more of the following: Mn, Al, Mg, Ca, Si, Zn, Cr, Ba, V, Ce, S, Nb, Zr, Ta, Sb, Ni, Cu, K (Table 6.2). Hematite typically contains higher levels of Ti and Mn, and rutile typically contains higher levels of Mn, Fe, and to a lesser degree Ba, V, and Nb. The amount and type of trace elements included in both rutile and hematite inconsistently vary from sample to sample and commonly vary between hematite crystals within a single thin section. The Mn-andalusite layer of the Hopewell Lake-Jawbone Mountain area displays the greatest amount of variation in trace element content and abundance between samples. In general, there is little difference in the trace element content between the Hopewell Lake-Jawbone Mountain area, Quartzite Peak, and Kiowa Mountain. Variations in the trace element content are limited to the a slightly higher amount of Mn in the hematite and rutile of Quartzite Peak and a greater variety of trace elements in the hematite and rutile from Kiowa Mountain (Table 6.2). There is less Mn and significantly higher Ti in the hematite from the transitional package than in the hematite from the Mn-andalusite layer (Table 6.3).

The large euhedral to rounded hematite grains of both the Mn-andalusite layer and the units of the transitional package in the Vadito Group commonly preserve textures related to zones of rutile within the hematite crystal in all three of the areas studied (Fig. 6.10).

Table 6.2. Composition of hematite and rutile from the Mn-andalusite layer of the Ortega Formation

	Hopewell anticline		Hopewell anticline		Quartzite Peak		Quartzite Peak		Kiowa Mt.		Kiowa Mt.	
	Mn-and layer hematite P06NM20A	Mn-and layer rutile P06NM20A	Mn-and layer hematite P06NM40A	Mn-and layer rutile P06NM40A	Mn-and layer hematite P06NM56B	Mn-and layer rutile P06NM56B	Mn-and layer hematite P06NM40A	Mn-and layer rutile P06NM40A	Mn-and layer hematite P06NM56B	Mn-and layer rutile P06NM56B	Mn-and layer hematite P06NM56B	Mn-and layer rutile P06NM56B
MgO	0.03	-	0.01	-	0.08	-	-	-	0.08	-	-	2.00
MnO	0.54	-	0.70	-	0.84	-	-	-	0.84	-	-	-
CaO	-	-	0.02	-	0.02	-	-	-	0.02	-	-	0.78
K2O	-	-	-	-	-	-	-	-	0.02	-	-	0.05
TiO2	0.27	98.55	0.25	97.45	0.40	97.45	0.04	97.45	0.40	0.04	0.04	0.04
Fe2O3	99.04	0.35	99.30	0.79	97.35	0.79	-	97.35	97.35	97.85	97.85	97.85
Al2O3	0.07	0.06	0.19	-	-	-	-	-	-	0.92	0.92	0.92
SiO2	-	0.01	-	-	0.04	-	-	0.04	0.04	-	-	-
ZnO	-	-	-	-	0.20	-	-	0.20	0.20	0.07	0.07	0.07
Cr2O3	0.02	-	0.01	-	0.12	-	-	0.12	0.12	0.35	0.35	0.35
BaO	0.05	-	0.04	-	-	-	-	-	-	0.04	0.04	0.04
V2O3	-	-	0.01	-	0.05	-	-	0.05	0.05	0.03	0.03	0.03
Ce2O3	0.11	0.16	0.03	0.04	-	0.04	-	-	-	-	-	-
SO2	-	-	0.01	-	0.03	-	-	0.03	0.03	0.33	0.33	0.33
Nb2O3	-	0.10	-	-	0.05	-	-	0.05	0.05	0.04	0.04	0.04
ZrO2	-	-	-	-	0.13	0.01	-	0.13	0.13	0.23	0.23	0.23
Ta2O5	-	-	-	-	0.45	-	-	0.45	0.45	0.12	0.12	0.12
Sb2O3	-	-	0.06	-	0.13	-	-	0.13	0.13	0.64	0.64	0.64
NiO	0.03	-	0.04	-	0.06	-	-	0.06	0.06	0.33	0.33	0.33
CuO	-	-	-	-	0.21	-	-	0.21	0.21	0.08	0.08	0.08
	-	-	-	-	-	-	-	-	-	0.25	0.25	0.25
Total	100.16	99.23	100.67	98.29	100.18	98.29	100.18	98.29	100.18	102.15	102.15	102.15

Table 6.3. Composition of hematite from the Vadito Group transitional package

	Hopewell anticline metarhyolite hematite P06NM03	Kiowa Mt. amphibolite hematite P06NM54B	Kiowa Mt. Trans. metased. hematite P06NM32A	Quartzite Peak Trans. metased. hematite P06NMF50A	Jawbone syncline Trans. metased. hematite P06NM24A
MgO	-	-	-	0.06	0.01
MnO	0.01	0.07	0.02	0.08	0.07
CaO	0.07	0.02	-	0.02	0.02
K2O	0.01	-	-	0.04	0.02
TiO2	13.18	10.15	6.97	6.53	1.63
Fe2O3	84.07	90.00	92.59	92.62	98.85
Al2O3	0.02	0.05	0.03	0.10	-
SiO2	0.74	0.09	0.01	0.06	-
ZnO	-	-	-	-	0.06
Cr2O3	0.03	0.06	0.06	0.10	0.06
BaO	0.36	0.29	0.04	0.31	-
V2O3	0.49	0.81	0.33	0.44	0.12
Ce2O3	-	0.01	0.01	-	-
SO2	-	-	-	0.03	-
Nb2O3	0.19	-	-	0.08	0.03
ZrO2	-	0.07	0.06	0.06	0.04
Ta2O5	-	-	-	0.05	-
Sb2O3	-	0.05	0.17	0.20	-
NiO	-	0.08	0.02	0.04	-
CuO	-	0.02	0.05	0.10	0.03
Total	99.16	101.76	100.36	100.91	100.93

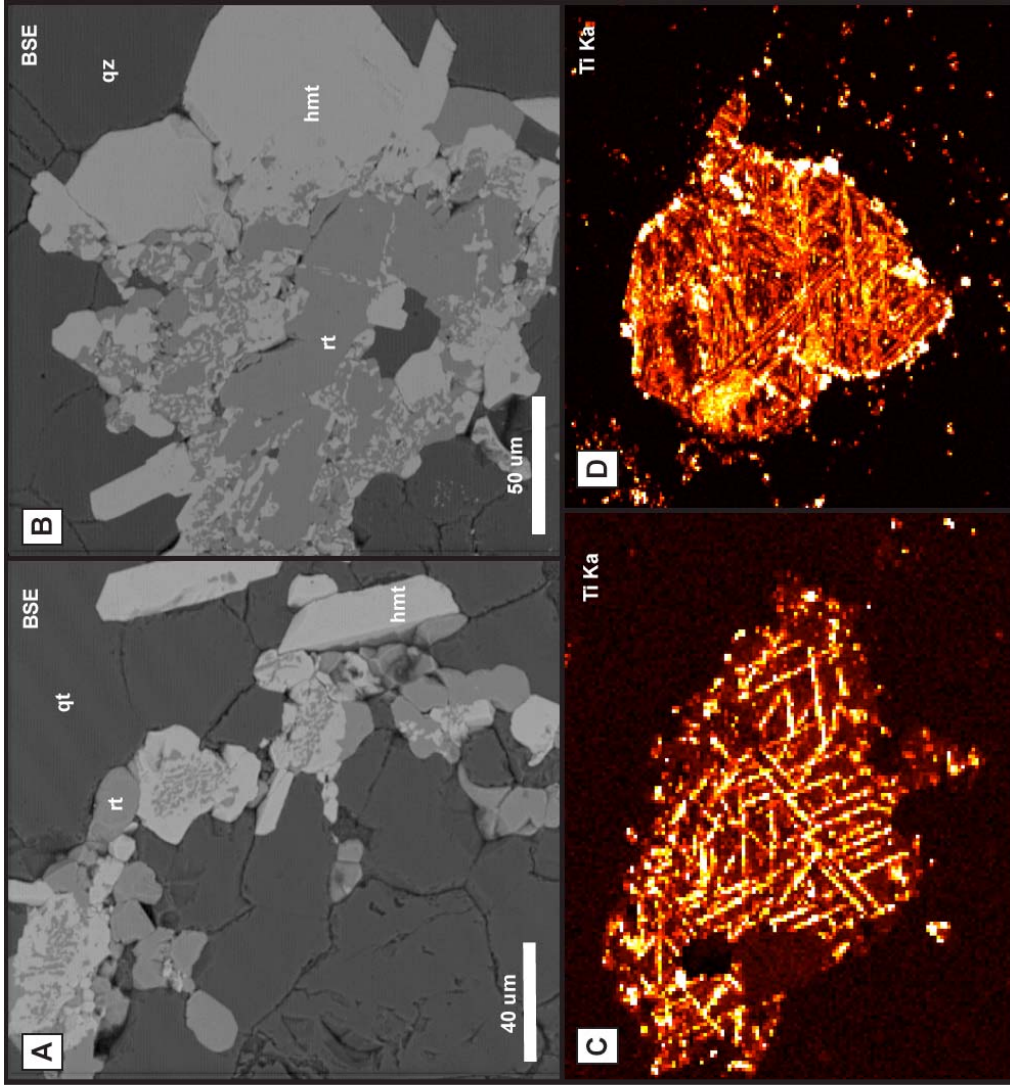


Figure 6.10. Zones of rutile in hematite crystals produce textures that appear patchy or mottled (a,b), wormy (g), cross-hatched (c,d), or banded (e,f,h,i) (Ortega Formation - a,b,c,d,g; Vadito Group- e,f,h,i; samples- a,b-MLW2D; c,d-P05NM51A; e,f-P06NM54B; g-P06NM58A; h,i-P06NM35).

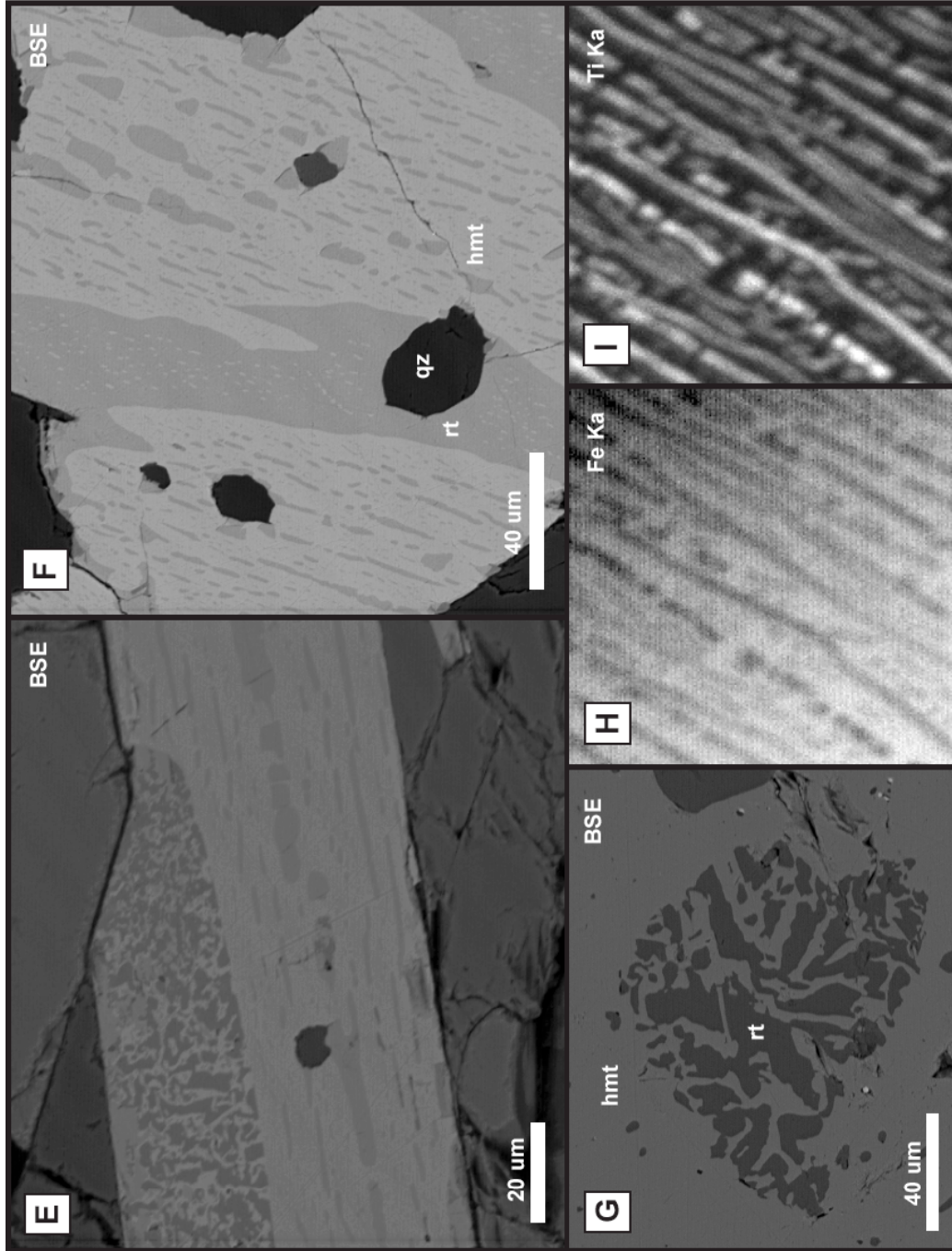


Figure 6.10. (continued).

The pattern of rutile zones can appear patchy and mottled (Fig. 6.10a,b), wormy (Fig. 6.10e, g), cross-hatched (Fig. 6.10c,d,e,f,h,i), or as bands within the hematite. The texture can cover the entire hematite grain or in small distinct areas at the center or edges of the crystal. In the Ortega Formation, the hematite portions of the large textured crystals have a higher Ti content than the more common and more uniform elongate hematite crystals. Textures can be found in the metarhyolite and metasediments of the transitional package of the Vadito Group but are most abundant in the euhedral hematite crystals of the amphibolite layers. More than one texture pattern can be found in a single hematite crystal (Fig. 6.10e)

A number of trends can be observed when comparing the hematite of the Mn-andalusite layer in the Ortega Formation with the hematite from outside the later. First, the Mn content in the hematite is highest in the Mn-andalusite layer (up to 2.5 weight percent Mn_2O_3 ; ~0.7 average) and is significantly lower in hematite from outside of the Mn horizon (up to 0.23 weight percent Mn_2O_3 ; ~0.08 average). This suggests that Mn-andalusite is not the only Mn-containing mineral and that hematite may act as a reservoir for Mn in the Mn horizon. Secondly, although the mineral assemblage of the transitional package metasediments does not include rutile, the hematite in the metasedimentary units has a higher Ti content relative to the hematite from the rutile-bearing Mn-andalusite layer. Third, the textures seen in the hematite of the metavolcanic units of the Vadito Group are similar to the textures seen in some hematite from the Mn-andalusite layer of the Ortega Formation and the metasedimentary units of the Vadito Group.

The association of rutile with the Mn-andalusite layer suggests a relationship between the Mn horizon and the presence of rutile. The aluminous, hematite-bearing layers of the Ortega Formation contain rutile and have a lower Ti content in hematite, whereas the metasediments of the Vadito Group do not contain rutile but have a higher Ti content in hematite. The conditions that lead to the crystallization of rutile in the aluminous, hematite-bearing layers of the Ortega Formation and in the Mn horizon were probably also linked with the decrease in Ti in the hematite. A high oxygen fugacity in the Ortega Formation, which is required for the stability of Mn^{3+} and Fe^{3+} in Mn-andalusite and hematite, might explain the Ti-

rutile relationship. Rutile is stable at high oxygen fugacities and Fe-Ti oxide phases may break down to hematite and rutile under such conditions. A lack of rutile and a higher Ti content may indicate lower oxygen fugacities in units of the Vadito Group outside of the Ortega Formation.

Textures formed by zones of rutile in hematite crystals that were identified in metavolcanic and metasedimentary units of the Vadito Group and the aluminous, hematite-bearing layers of the Ortega Formation could be a clue to the origin of hematite and rutile in the Mn-andalusite layer. The textures can be mottled and patchy, banded, wormy, and/or crosshatched. The crosshatched texture is similar to the trellis texture that Haggerty (1991) links to the oxidation-exsolution of spinels in basalt. The trellis texture is formed by the concentration of Ti in laminae along the octahedral {111} spinel planes in high-Fe hosts. In addition, the banded texture is similar to the texture produced by exsolved ilmenite lenses parallel to the {0001} ilmenite planes in a hematite host (Haggerty, 1991). The similarity of the textures observed with the exsolution textures of Haggerty (1991) suggests that perhaps the observed textures may be related to the oxidation of original Fe-Ti phases. This oxidation could have occurred anytime during the life of the hematite crystals (Fig. 6.11-2). The fact that the textures can be observed in primary metavolcanic units suggests that oxidation may have occurred during igneous processes. Primary volcanic hematite displaying exsolution textures could have been extracted from the source during weathering and deposited in the metasedimentary units perhaps linking nearby metavolcanic units with the quartzite (Fig. 6.11-3).

Although the textures within the hematite appear similar to documented oxidation-exsolution textures, it is possible that they may have formed through other ways as well, such as through the amalgamation of smaller rutile and hematite grains into one large crystal or the direct deposition of Fe and Ti oxides and/or oxyhydroxides in a depositional basin (Fig. 6.11-1). In the Mn-andalusite layer, hematite and rutile both occur as small rounded granular crystals and these small grains may have been concentrated together to form what would appear to be a single hematite crystal with mottled or patchy zones of rutile. In addition, iron oxyhydroxides, such as goethite, have been shown to co-precipitate with titanium oxides to produce intergrowth

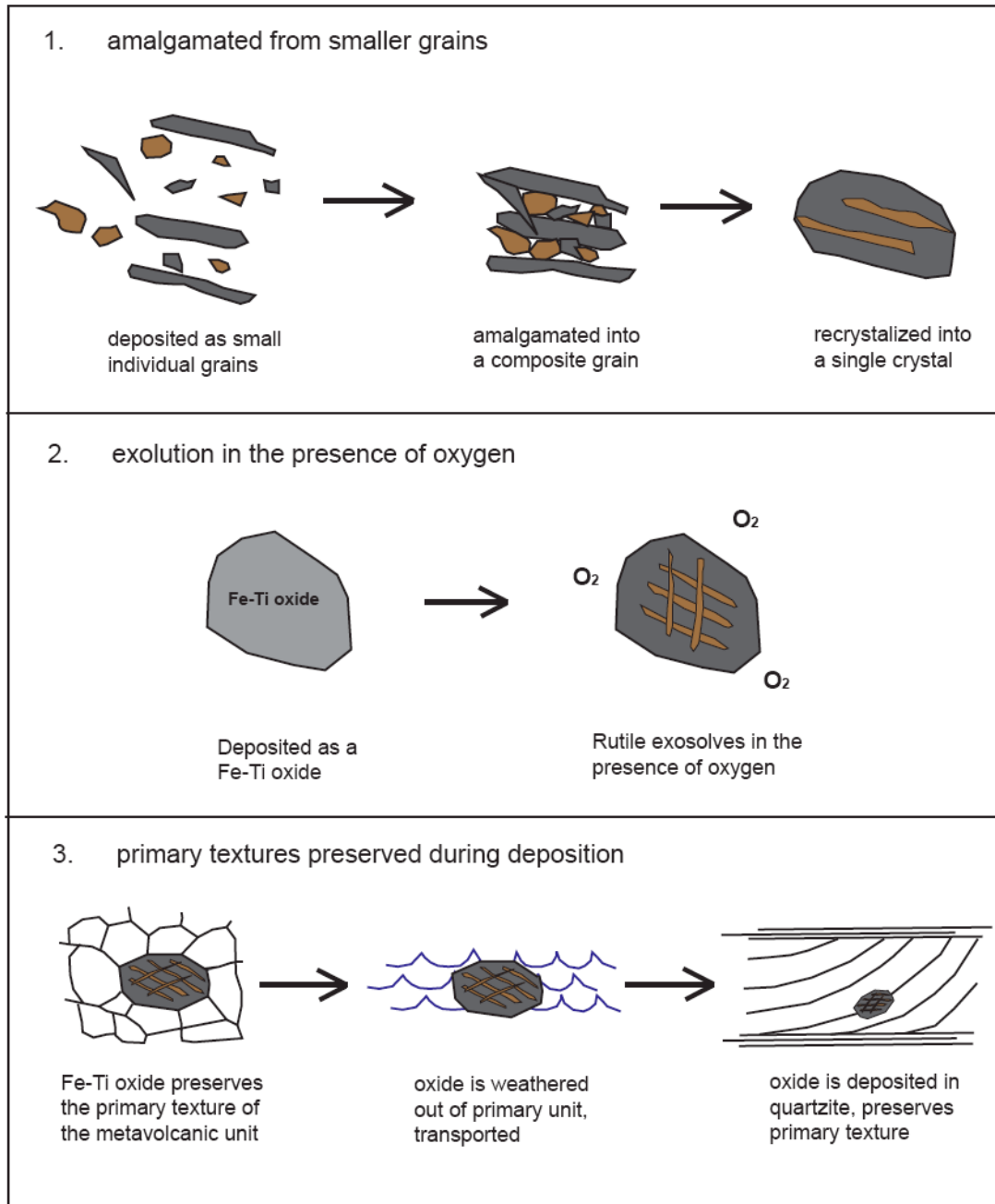


Figure 6.11. The diagram above outlines three possible sources of the rutile-hematite textures in hematite from the transitional package of the Vadito Group and the aluminous, hematite-bearing layers of the Ortega Formation quartzite.

textures that could have formed during the precipitation of Fe and Ti in basin waters within a sedimentary environment (e.g. Grey et al, 1983; Nakayma et al, 2005).

Variations Within the Mn-andalusite Layer

Samples taken from the Hopewell Lake-Jawbone Mountain area, Quartzite Peak, and Kiowa Mountain were compared in an effort to document any variation in Mn content, trace element content, and mineral content both stratigraphically within the Mn horizon and between study areas.

A number of spaced samples taken stratigraphically across the Mn-andalusite layer in the Ortega Formation of the Hopewell Lake-Jawbone Mountain area shows little to no consistent variation in trace element content, mineral content, or Mn content across the layer. Quartz, Mn-andalusite (and/or kyanite), hematite, rutile, and pyrophyllite are present in all samples. Variations do exist between individual aluminous, hematite-bearing layers, but there was no consistent increase or decrease in Mn-andalusite, hematite, and/or rutile abundance across the layer. The type and abundance of trace elements in hematite and rutile inconsistently varies between and within the samples collected. Nothing in the compositional data suggests a trend in the trace element content across the section. The Mn-content of Mn-andalusite also varies to some degree from sample to sample, but that variation also is not consistent enough or variable enough to represent a trend in Mn-content between samples. Within the Ortega Formation, rocks with Mn-poor andalusite are very similar in mineral content and trace element content to the rocks with Mn-rich andalusite but differ almost exclusively in Mn content. The contact between Mn-rich and Mn-poor rocks within the Ortega Formation is relatively abrupt and only involves a decrease in Mn.

There are no stark differences between samples from the Mn-andalusite layer of the Hopewell Lake-Jawbone Mountain area, Quartzite Peak, and Kiowa Mountain, but subtle differences in Mn and trace element content and rutile abundance distinguish each area. The Hopewell Lake-Jawbone Mountain area is the only area that is characterized by such extreme localized Mn highs (X_{Mn} of up to 0.76). Hematite and rutile crystals of the Mn-andalusite layer

at Quartzite Peak have a slightly higher Mn content than those of the Hopewell Lake-Jawbone Mountain area or Kiowa Mountain. Hematite and rutile from Kiowa Mountain consistently have the greatest variety in trace elements, and Kiowa Mountain has a higher abundance of rutile in the aluminous, hematite-bearing layers of the Mn-andalusite layer when compared to the Hopewell Lake-Jawbone Mountain area and Quartzite Peak.

Origin of the Mn horizon

Any model addressing the origin of the Mn horizon must explain the following observations:

- Mn-andalusite occurs with hematite and rutile in aluminous, hematite-bearing layers and on the surface of cross beds.
- Mn-andalusite is less abundant or absent in the hematite-poor areas and conglomeritic layers of the quartzite where the sediment is coarser.
- Not all hematite-rich layers have Mn-andalusite and not all Mn-andalusite-rich layers have hematite. Hematite only and Mn-andalusite only layers can be found in the Mn-andalusite layer.
- High-Mn core regions were present in the Hopewell Lake-Jawbone Mountain area early in the tectonic history and are characterized by a high-Mn content and a composite texture and are associated with fine hematite and rutile grains.
- High-Mn core regions are concentrated in the aluminous, hematite-bearing layers, on the surface of cross beds, and in structures similar to a graded-bed.
- High-Mn core regions represent localized Mn-highs in Mn-andalusite crystals and are associated with zoning patterns that reflect a decrease in Mn-content away from the core region.
- The aluminous, hematite-bearing layers of the Ortega Formation are rich in aluminum silicates (andalusite and/or kyanite) and rutile while the units of the transitional package of the Vadito Group are not.

- The Mn-rich and Mn-poor andalusite layers in the Ortega Formation are similar in trace element and mineral content but differ significantly in Mn-content.
- Hematite-rutile textures preserved within some hematite crystals can be found in the Mn-andalusite layer of the Ortega formation and in the metavolcanic and metasedimentary units of the transitional package of the Vadito Group

Williams (1987) suggested three possible sources for the Mn in the marker horizon: (1) Mn was introduced along low angle faults near the Vadito-Hondo contact, (2) Mn was concentrated during extensive lateritic weathering of the underlying metarhyolite or similar source areas away from the basin, or (3) Mn was deposited, either on the surface of clay grains or as a chemical precipitate, from hydrothermal solutions or enrichment of basin waters related to the end of volcanism in the area. Aspects of sources two and three are supported by many of the observations listed above. Hematite-rutile textures may link the metavolcanic units of the Vadito Group with the Ortega Formation quartzite suggesting a weathering connection between the Ortega Formation and the metarhyolite of the Vadito Group (or similar metavolcanic units elsewhere) as was proposed in source two. Extensive weathering is also supported by the concentration of only hematite, rutile, aluminum silicates, and quartz in the aluminous, hematite-bearing layers of the quartzite because all elements except for Si, Mn, Al, Ti, and Fe are absent and have presumably been removed through weathering. The depositional source postulated in source three may be supported by the presence of Mn-andalusite on the surface of cross-beds. The association of Mn with a concentration of Al may suggest a connection with the accumulation of clay material as well as the concentration of Al through weathering supporting both source two and three. Hematite and rutile contain a variety of trace elements, which could have been incorporated during chemical deposition as source three suggests or could also reflect the trace element content of the hematite and rutile inherited from weathered metavolcanic units as source two suggests. Source one does not explain most of the observations listed above. In addition, the presence of Mn-andalusite on bedding planes and cross beds and the lateral continuity of the Mn horizon along the Vadito-Hondo contact would

require a bedding parallel fault network to have existed at Vadito-Hondo contact across the entire Tusas range. Such a fault network has not been identified.

Evidence suggests that the best explanation for the origin of the Mn horizon either involves the lateritic weathering of the metavolcanic units (such as in the Vadito Group or similar units elsewhere) and/or the chemical deposition of Fe and Mn phases in an enriched basin environment. In an effort to consider each hypothesis, a lateritic weathering model and a chemical deposition model are presented below. Discussion of each model will attempt to explain aspects of the observations presented above or will address inconsistencies between the model and the observations.

Lateritic weathering may have lead to the formation of the Mn horizon through the mobilization and concentration of Mn and Fe within the lateritic profile. Lateritic weathering leads to the chemical breakdown of most minerals leaving aluminum-rich clays and quartz in a saprolite layer. This could explain the increased Al and Si content at the base of the quartzite and the removal of most common elements. Fe and Mn would be reduced, mobilized, and then concentrated and deposited in oxidized crusts above the saprolite as Fe oxyhydroxides, Mn-Al oxyhydroxides, and Mn-oxides (Parc et al, 1989; Valetton, 1994). Fe and/or Mn crusts are areas where Ti, Zn, Cu, Co, Ni, REE including Ce, and other heavy metals accumulate (Gilkes et al, 1973; Braun et al, 1990; Valetton, 1994; Maynard, 2003). The concentration of Mn and Fe in a crust could explain the concentration of Mn and Fe in the Mn-andalusite layer. The concentration of elements in a weathered profile, particularly Ti and Zn, can explain the variability of trace elements in hematite and rutile of the Mn-andalusite layer and the occurrence of rutile and rarely gahnite. Mn crusts have been associated with the development of Paleoproterozoic paleosols elsewhere the world (e.g. Hekpoort paleosol of the Transvaal Supergroup in southern Africa; Beukes et al, 2002).

The development of a lateritic crust alone does not explain the concentration of Fe and Mn on the surface of cross-beds or in aluminous, hematite-bearing layers, and it does not explain the existence of high-Mn core regions. A depositional component is missing from the lateritic weathering model. It is possible that additional mechanical weathering lead to the

breakup and reworking of the Fe-Mn rich crusts. Broken pieces of the crust could act as sediment and could be deposited on the surface of cross beds and in aluminous, hematite-bearing layers. The high-Mn core regions may represent evidence of such sediment. The mechanical reworking of laterites may also explain the lack of a lateritic profile at the base of the Ortega Formation. Reworked laterites have been specifically identified as part of the Hekpoort paleosol of the Transvaal Supergroup in southern Africa (Beukes et al, 2002) and in the Ziemougoula area on the Ivory Coast (Nahon and Parc, 1990).

The chemical deposition of Fe and Mn phases in an enriched basin environment may have led to the formation of the Mn horizon through the oxidation of Mn and Fe in oxygen stratified waters. The influx of hydrothermal fluids would have enriched the waters of the Paleoproterozoic basin in Fe, Mn, Co, Ni, Cu and other heavy metals (Maynard, 2003). Hydrothermal fluids have also been associated with an increase in Ce (Maynard, 2003). The hydrothermal enrichment of basin waters would explain the variety of trace elements found in the hematite and rutile crystals of the Mn-andalusite layer. Changes in atmospheric composition during the Precambrian are thought to have resulted in oxygen stratified ocean basins with a thin oxic layer above an otherwise anoxic ocean (Roy, 2006). If anoxic waters rich in dissolved Mn^{2+} and Fe^{2+} were to upwell into the oxic layer, the Mn and Fe would become oxidized and precipitate from solution as Fe and Mn oxyhydroxides (Roy, 2006). The Fe and Mn oxyhydroxides could precipitate onto suspended particles, such as clays, to be deposited or transported or could accumulate directly on depositional surfaces, such as cross beds (Williams, 1987; Roy, 2006). The precipitation of Fe and Mn phases would explain the presence of Mn-andalusite and hematite on depositional surfaces. In addition, the high-Mn core regions may represent a complex of Fe, Mn, and/or Al oxyhydroxide phases that were deposited on cross beds and in the aluminous, hematite-bearing layers. Goethite, an Fe-oxyhydroxide has been shown to incorporate Mn, Ti, Al, and other heavy metals into its crystal structure and may also serve as a vector for the deposition of Mn into the Mn-andalusite layer (Grey et al, 1983; Manceau et al, 2000; Scheinost et al, 2001; Nakayama et al, 2005). Since Mn is more soluble than Fe, changes in the basin environment (changes in Mn concentration or

oxygen level) would more easily lead to a cessation of Mn precipitation but not Fe precipitation (Roy, 2006). This may explain the existence of both Mn-poor and Mn-rich zones at the base of the Ortega Formation

Both lateritic weathering and the chemical deposition of Fe and/or Mn phases can result in many of the observations presented. Lateritic weathering could explain the concentration of Fe and Mn and the presence of high-Mn core regions, and extreme chemical weathering has already been proposed as a factor for the formation of the Ortega Formation quartzite and similar quartzites in the southwestern United States (Dott, 2003; Medaris, 2003). Yet, the chemical deposition of Fe and Mn phases could also result in the concentration of Mn and Fe and better explains the presence of both elements on the surface of cross-beds and in aluminous, hematite bearing layers. It is possible that a combination of both processes played a role in the formation of the Mn-horizon in the Tusas Mts. Other processes, such as the biogenic production of Mn, may have also played a role in the formation of the Mn horizon, but both the lateritic weathering and the chemical deposition best explain the observations presented and have been previously used to explain similar Precambrian deposits elsewhere in Africa and India (Beukes et al, 2002; Roy, 2006).

Textures Preserved in the Birefringence of Mn-Andalusite

Subtle variations in the birefringence of Mn-andalusite reflect localized variations in Mn content that overprint the larger-scale Mn zoning pattern previously discussed. In some cases, variations in birefringence produce shapes and patterns that resemble a mineral habit or that define a texture. These localized variations may be a result of Mn localization and/or displacement during metamorphic mineral reactions and/or replacement.

Feathery Texture

Subtle variations in the birefringence of some Mn-andalusite crystals preserve a feathery texture. The feathery texture is produced by very small variations in Mn content (less than a weight percent Mn_2O_3) that are best seen in EMP x-ray maps for Mn (Fig. 6.12d). The

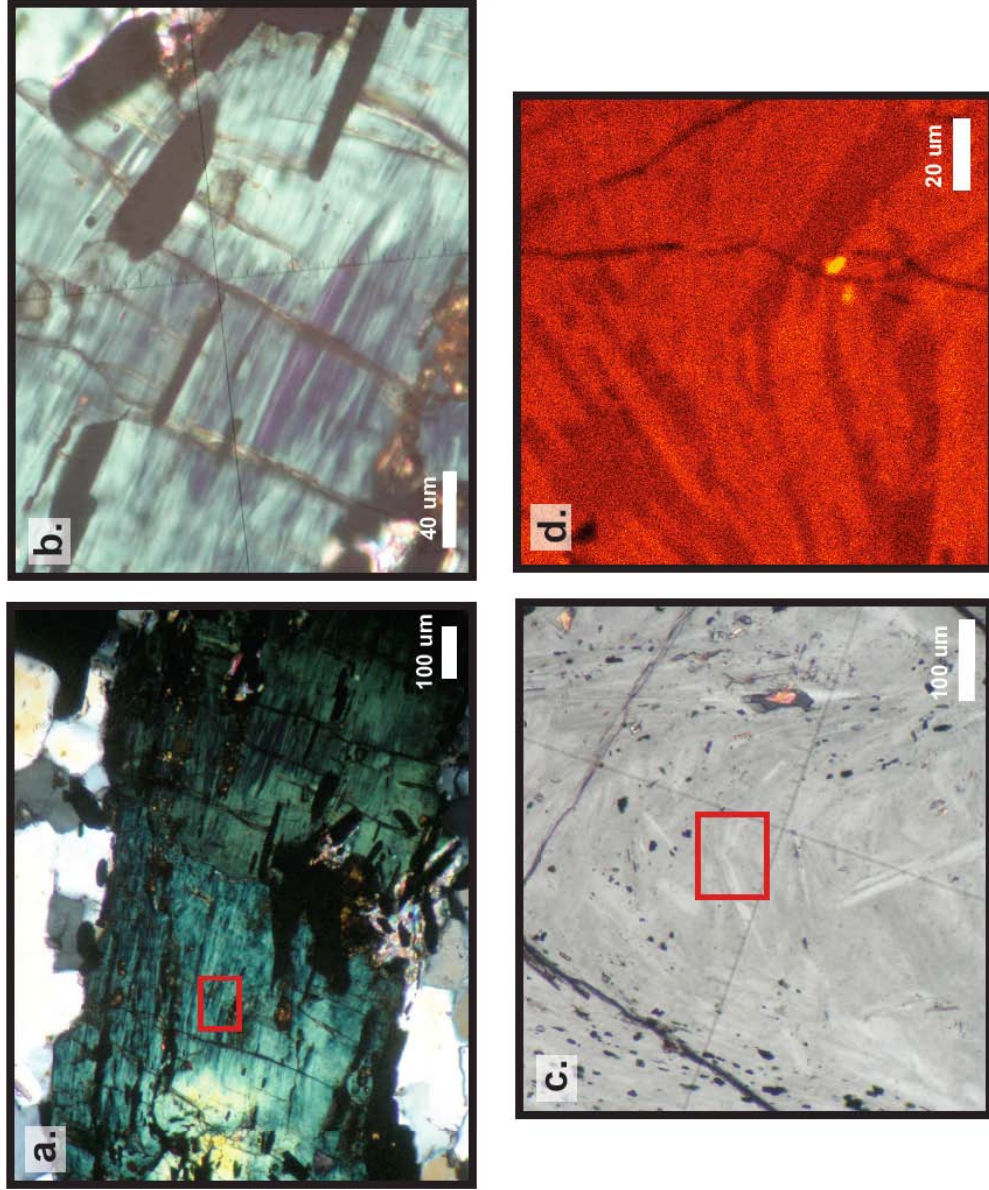


Figure 6.12. A bladed texture (a, b) preserved in the birefringence of Mn-andalusite crystals from the Mn horizon is a result of very subtle variations in Mn-content (c,d) (EMP x-ray map- Mn) (a, b- JK01-57-2; c- P06NMF51-A; d- P06NM16).

variations are produced by the juxtaposition of elongate, needle-shaped areas of slightly higher or lower relative Mn-content. The feathery texture typically defines a “fabric” that is subparallel to the dominant foliation and to aligned hematite crystals. Both aligned hematite inclusions and the feathery birefringence texture preserve a crenulation cleavage fabric in some samples (Fig. 6.13). Where the feathery texture defines a crenulation cleavage, the needle-like shapes change orientation around the hinge of the crenulation fold and appear folded in places (Fig. 6.12c). Folds and fabrics that are preserved in the feathery texture in the Mn-andalusite may continue to be defined in other ways outside of the andalusite crystal. For example, the fold shape preserved in the feathery texture in the Mn-andalusite crystal in Figure 6.14 continues to be defined outside of the andalusite crystal by aligned hematite and pyrophyllite inclusions in adjacent quartz crystals.

The feathery texture preserved in the birefringence of Mn-andalusite crystals is interpreted to be inherited from phyllosilicate precursor minerals. The feathery texture has an appearance that is similar to the fibrous, elongate habit of aligned phyllosilicates. In addition, the crenulations that are defined by the feathery texture are similar in appearance to common examples of phyllosilicate-defined crenulations. Given that the feathery texture represents a phyllosilicate crystal habit, the preservation of the texture in the birefringence suggests that Mn-andalusite directly replaced phyllosilicate precursor minerals preserving their mineral habit in the Mn distribution. Furthermore, the presence of a crenulation cleavage in the feathery texture suggests that a phyllosilicate-defined crenulation cleavage was present at the time of Mn-andalusite growth and was preserved in the Mn distribution.

The identity of the phyllosilicate precursor(s) is not known, but pyrophyllite $[\text{Al}_2\text{Si}_4\text{O}_{10}(\text{OH})_2]$ and pennantite $[\text{Mn}_5\text{Al}_5\text{Si}_3\text{O}_{10}(\text{OH})_8]$ are strong candidates. Both pennantite and pyrophyllite have been identified in the Mn-andalusite layer in direct association with Mn-andalusite and both have an abundance of Al and Si in their crystal structure. A lack of significant amounts of K, Ca, or Mg in the Mn-andalusite layer suggests that other phyllosilicates, such as muscovite or biotite, would not have been present. Pennantite is an Mn-containing mineral and could have served as the source of Mn for the Mn-andalusite.

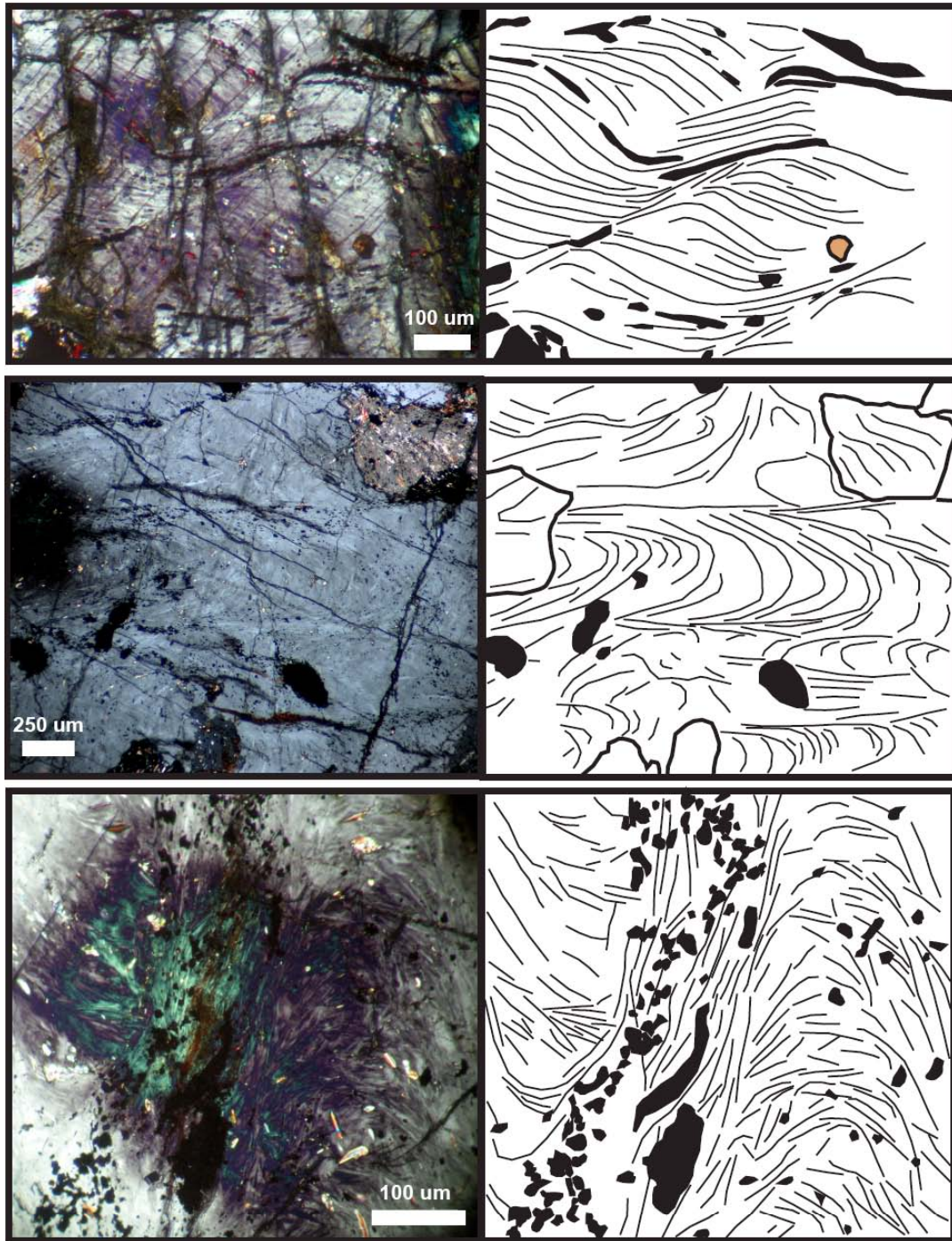


Figure 6.13. The feathery texture preserves evidence for the existence of a crenulation cleavage overgrown by Mn-andalusite (black- hematite; brown- rutile) (top- JK01-57-2; middle & bottom- P06NMF51A).

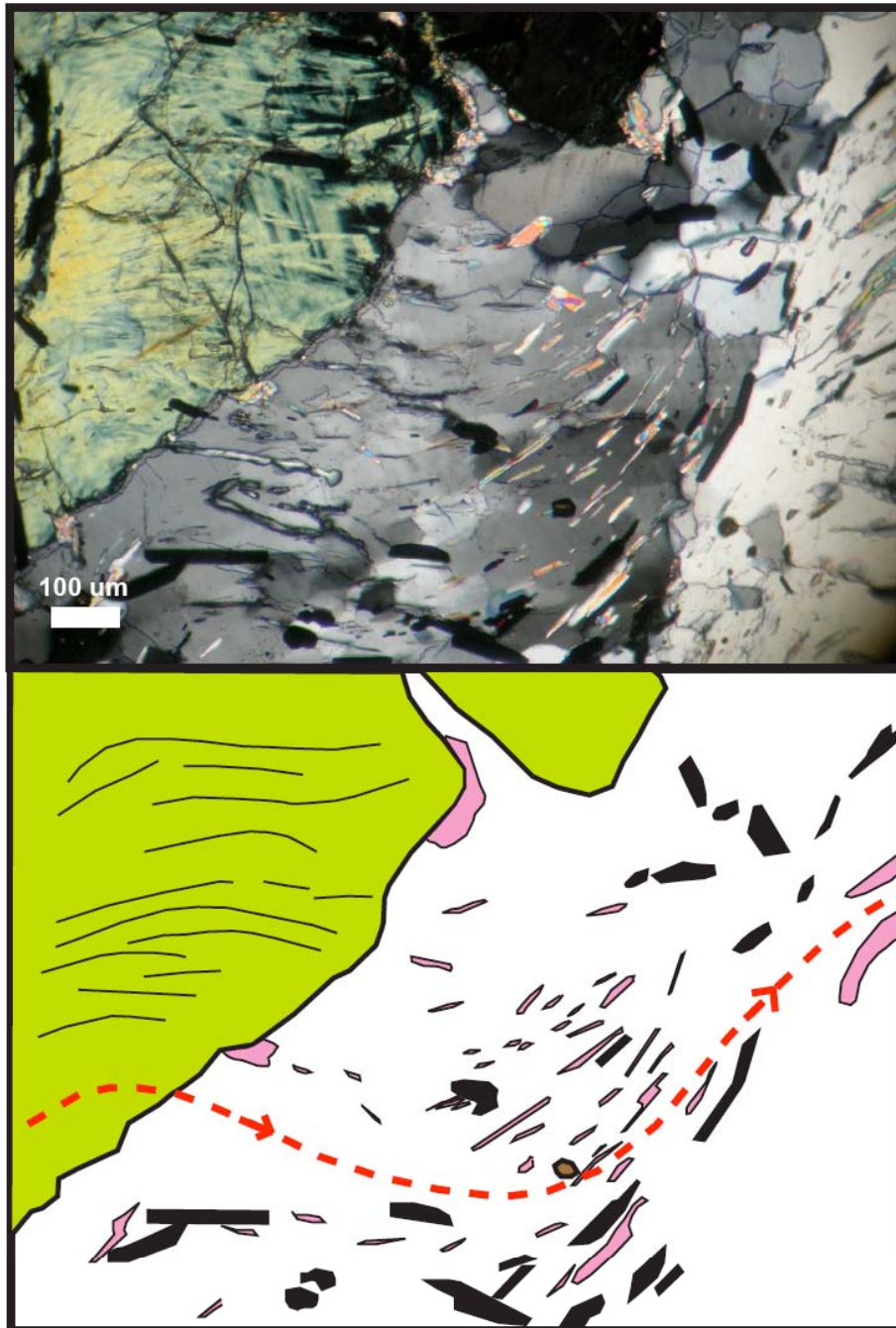


Figure 6.14. The fold preserved in the feathery texture in the Mn-andalusite crystal (yellow) continues outside of the andalusite but is defined by aligned hematite (black) and pyrophyllite (pink) inclusions in the adjacent quartz crystals (white) (rutile-brown; sample- P06NM16-B).

However, pennantite has a high Mn-content and if Mn-andalusite directly replaced only pennantite, then the Mn content of the andalusite would be close to a kanonaite composition in the areas preserving the feathery texture (Table 6.4). Because this is not the case, pennantite is not interpreted to have been the sole precursor mineral. A combination of both pyrophyllite and pennantite as precursor minerals would provide the right element abundances to produce the composition of Mn-andalusite seen. Yet, if Mn-andalusite directly replaced a mixture of pennantite and pyrophyllite, then that mixture should be reflected in the distribution of Mn with extreme highs of Mn where pennantite would have been and extreme lows where pyrophyllite would have been. Such extreme variations are not seen at the level observed in thin section, but may have been altered during later diffusion. If pyrophyllite were the only precursor mineral, then the source of Mn becomes an issue because pyrophyllite does not typically incorporate Mn into its crystal structure (Deer, Howe, and Zussman, 1992). The Mn could have been supplied by an Mn-bearing reservoir phase, such as braunite or pennantite, or could have accumulated as a film on the surface of pyrophyllite crystals (Churakov, 2007).

High-Mn Halos and Low-Mn Shapes

Mn concentration increases around kyanite crystals included in Mn-andalusite producing Mn-halos of higher order colors in the birefringence of the Mn-andalusite crystal. The increase in Mn content around the kyanite crystals is no more than a few weight percent Mn_2O_3 . The halos are typically smooth and mimic the shape of the kyanite crystal, but can also appear jagged around the perimeter of the kyanite crystal (Fig. 6.15). The width of the halo varies, but is on average only a few tens of microns wide. Not all kyanite included in Mn-andalusite is surrounded by halos of higher order colors and higher Mn-content.

Areas of low order colors and low Mn content appear to mimic crystal shapes in some Mn-andalusite crystals (Fig. 6.16a). The crystal shapes appear splintery, elongate, blocky, and/or bladed. The shapes are typically outlined by areas of markedly higher order colors and Mn-content. The crystals shapes are defined solely by differences in the birefringence, but in rare cases, the edges of the crystal shapes are defined by what appears to be crystal

Table 6.4. Mn-andalusite mineral reactions

$2 \text{Mn}_5\text{Al}_5\text{Si}_3\text{O}_{10}(\text{OH})_8 + 4 \text{SiO}_2 + 11 \text{O}_2 \rightarrow 10 \text{MnAlSiO}_5 + 16 \text{OH}$ <p style="text-align: center;"> pennantite quartz kanonaite (cation ratio-1:1) </p>
$20 \text{Al}_2\text{Si}_4\text{O}_{10}(\text{OH})_2 + 2 \text{Mn}_5\text{Al}_5\text{Si}_3\text{O}_{10}(\text{OH})_8 + 21 \text{O}_2 \rightarrow 10 \text{MnAl}_5\text{Si}_3\text{O}_{15} + 56 \text{SiO}_2 + 56 \text{OH}$ <p style="text-align: center;"> pyrophyllite pennantite Mn-andalusite quartz (cation ratio-1:5) </p>
$5 \text{Al}_2\text{Si}_4\text{O}_{10}(\text{OH})_2 + 2 \text{Mn} + 4 \text{O}_2 \rightarrow 2 \text{MnAl}_5\text{Si}_3\text{O}_{15} + 14 \text{SiO}_2 + 10 \text{OH}$ <p style="text-align: center;"> pyrophyllite Mn-andalusite quartz (cation ratio-1:5) </p>

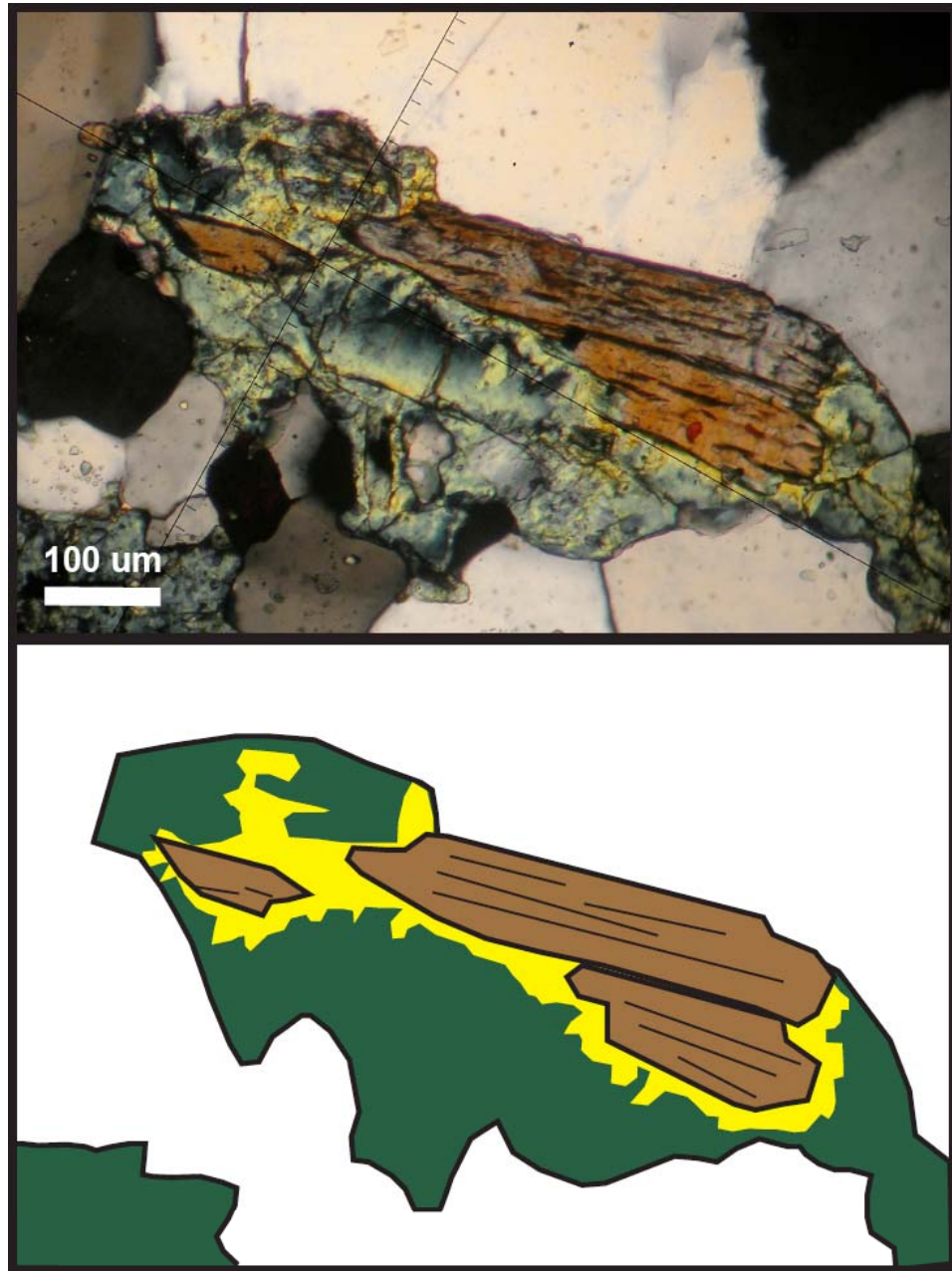


Figure 6.15. A higher Mn “halo” in Mn-andalusite surrounding kyanite crystals suggests that kyanite expelled excess Mn to the edges of the growing kyanite crystal (Mn-andalusite- blue-green and yellow; kyanite- brown) (sample- KTH4-12002).

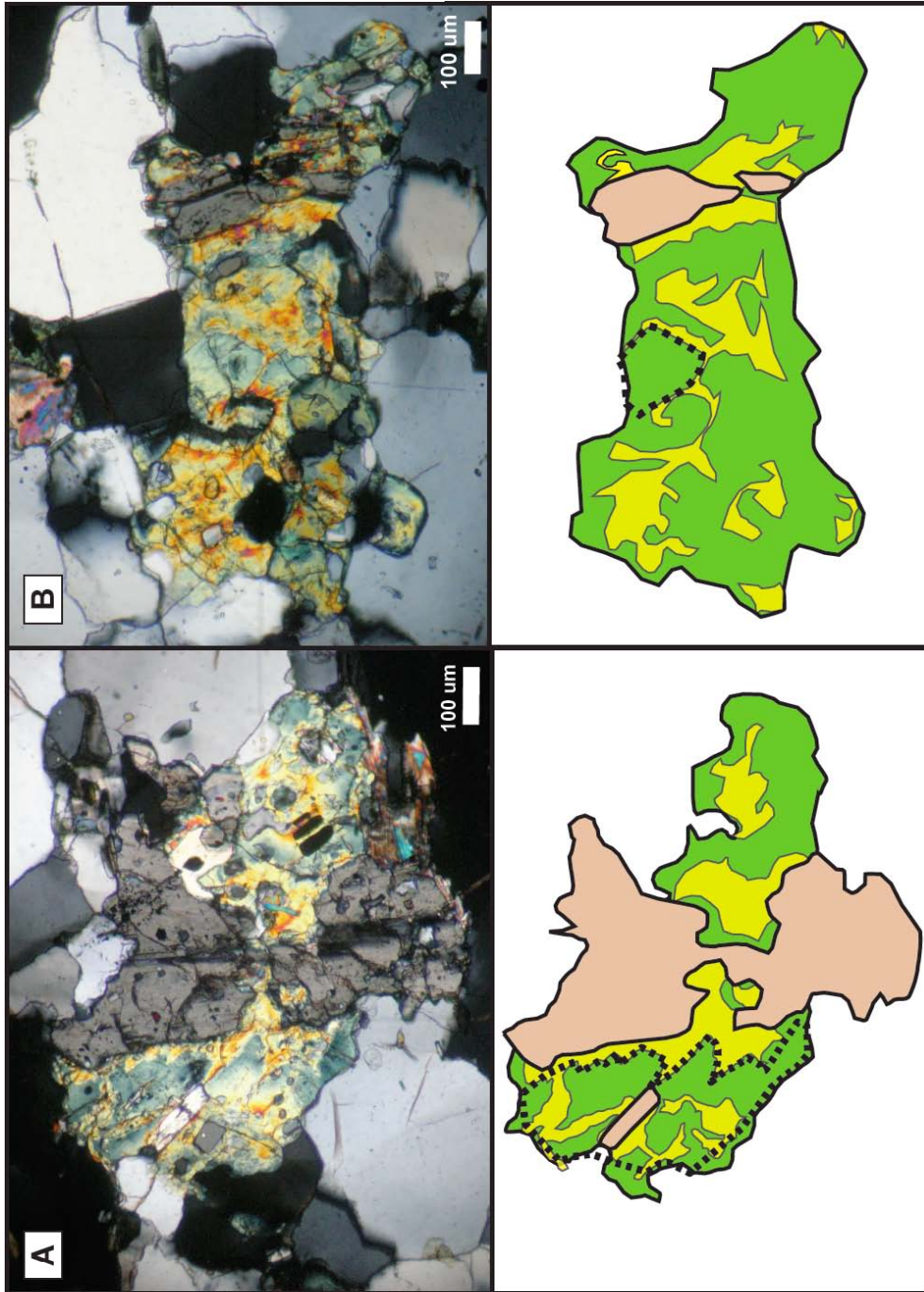


Figure 6.16. Areas of low order colors and low Mn content appear to mimic crystal shapes in some Mn-andalusite crystals (a). In some cases, the edges of the crystal shapes are defined by what appears to be crystal boundaries in optically continuous Mn-andalusite crystals (b).

boundaries in optically continuous Mn-andalusite crystals (Fig. 6.16b). The crystal shapes are commonly associated with inclusions of kyanite.

The high-Mn halos that surround kyanite inclusions in Mn-andalusite are interpreted to represent the displacement of Mn during kyanite growth. Kyanite has been documented to accommodate only limited amounts of Mn in its crystal structure (Gunter and Bloss, 1982). If kyanite replaces an Mn-bearing phase, then it would be expected that some amount of Mn will be rejected and accumulate at the edge of the growing crystal. Such an accumulation would account for high amounts of Mn at the edge of the kyanite crystal. It is unclear whether the Mn-bearing phase that kyanite replaced would have been an Mn-bearing phyllosilicate, Mn-andalusite, or some other Mn-phase.

The areas of low order colors that mimic crystal shapes are interpreted to represent areas where Mn-andalusite has replaced kyanite. The crystal shapes are similar in appearance to the crystal habit of kyanite and they are commonly associated with existing kyanite inclusions. The crystal shapes are also outlined and defined by areas of higher order colors. The outlines may directly correspond to the high-Mn halos present around existing kyanite inclusions (Fig. 6.20). The presence of the crystal shapes suggest that Mn-andalusite has overgrown kyanite inclusions preserving their crystal habit in areas of low Mn-content.

The concept of high-Mn halos can be combined with the existence of areas of low Mn-content to help understand kyanite and Mn-andalusite paragenesis. The areas of low Mn-content that resemble the shape of a crystal may represent areas where Mn-andalusite replaced kyanite. The area of markedly higher Mn content that surrounds the crystal shape could be the remnants of a high-Mn halo that had surrounded the once present kyanite crystal. If kyanite grew during or just prior to Mn-andalusite and created the high-Mn halo around kyanite, then when Mn-andalusite growth dominated and replaced kyanite, the area where kyanite once had been would be left as an area of low Mn-content. Considered together, the textures seen in the birefringence of Mn-andalusite may represent the growth of kyanite during or shortly prior to Mn-andalusite followed by Mn-andalusite growth and replacement of kyanite.

Microstructural and Petrologic Analysis of the Mn-andalusite layer

Careful petrography of Mn-andalusite can allow for the identification of unique textures developed through subtle variations in Mn concentrations that otherwise might not have been preserved. Such textures preserved in the birefringence of Mn-andalusite help in the identification and understanding of deformational textures and metamorphic paragenesis. Textures identified in Mn-andalusite from the Mn horizon in the Hopewell Lake-Jawbone Mountain area and at Kiowa Mountain in the Tusas Mountains are used to interpret aluminum silicate timing relative to fabric formation.

Hopewell Lake-Jawbone Mountain Area

There is evidence for at least two main generations of Mn-andalusite in the Mn-andalusite only assemblage in the Hopewell anticline in the Hopewell Lake-Jawbone Mountain area. The first generation of Mn-andalusite is characterized by large-scale Mn zoning that corresponds with high-Mn core regions. The zoning is a result of extreme localized highs of Mn within an otherwise low, relatively homogenous Mn distribution (Fig. 6.17a,b & 6.18a). Concentric zoning around the high-Mn core regions reflects the steep Mn gradient between high Mn at the center and low Mn in the rest of the crystal (Fig. 6.4). A feathery texture is preserved within the birefringence of the first generation of Mn-andalusite reflecting very subtle variations in Mn distribution. This feathery texture helps to define a tight D2 crenulation cleavage (Stage 3-4 of Bell & Rubenach, 1983; Fig. 6.17a & 6.18a). Zones of higher Mn-content subparallel to S3 that cut the Mn-andalusite crystals are interpreted to be areas of dissolution associated with D3 (Fig. 6.18a).

The second generation of Mn-andalusite is has a more uniform Mn-distribution. High Mn-core regions and associated large-scale Mn zoning are uncommon (Fig. 6.17c,d & Fig. 6.18b). The second generation of Mn-andalusite has on overall higher Mn content when compared to the low birefringence of the uniform areas of the first generation (Fig. 6.17). A feathery texture is preserved within the birefringence in some places, but the variations in Mn distribution and birefringence are less subtle making the texture more defined under crossed

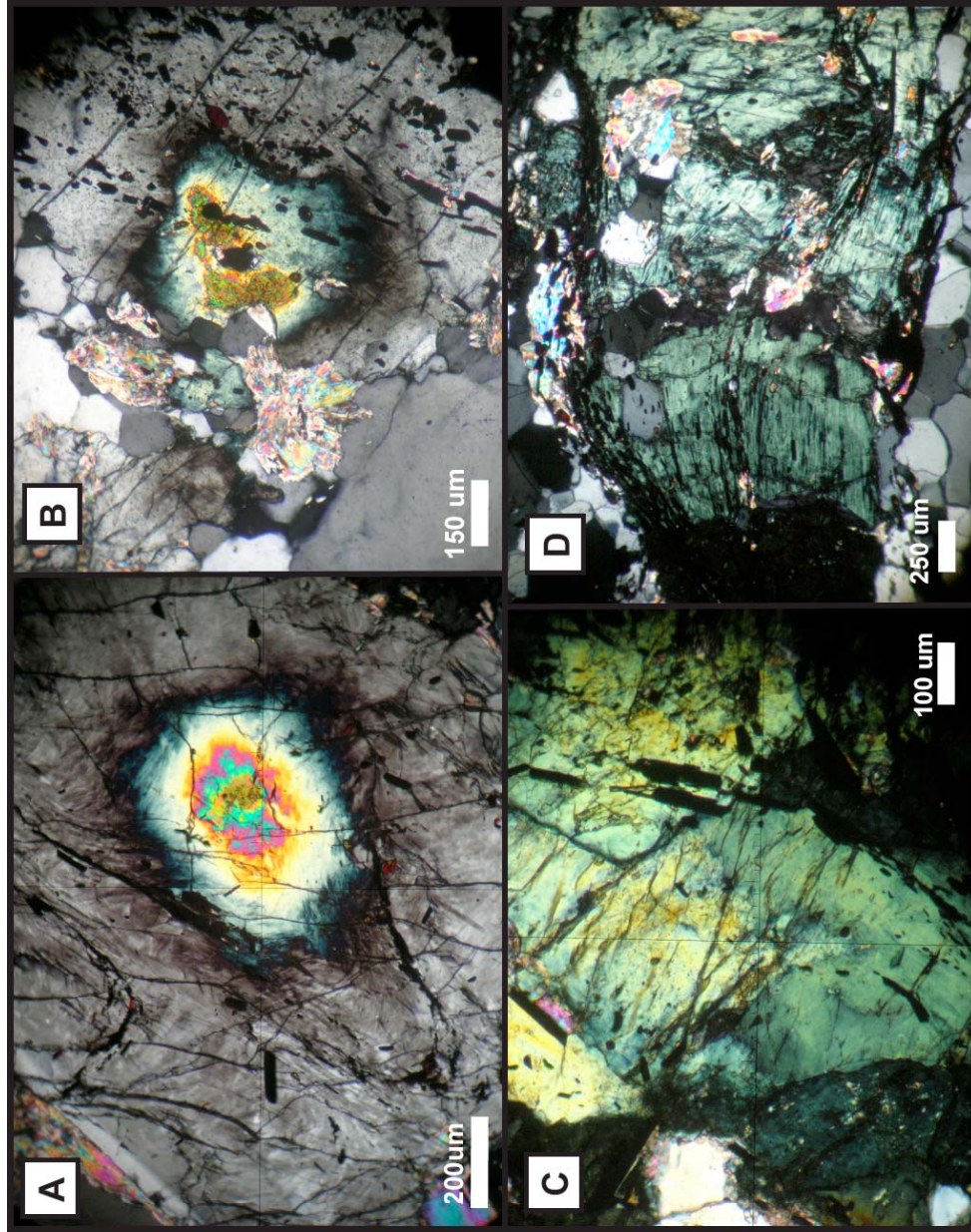


Figure 6.17. Two types of Mn-andalusite crystals are identified at the Hopewell anticline. The first type (a & b) is characterized by localized highs of Mn content and the preservation of a tight D2 crenulation cleavage. The second type (c,d) is characterized by a more uniform Mn-distribution and an open D3 crenulation cleavage (a, c, & d- P06NM16; b-Jk01-58-H1).

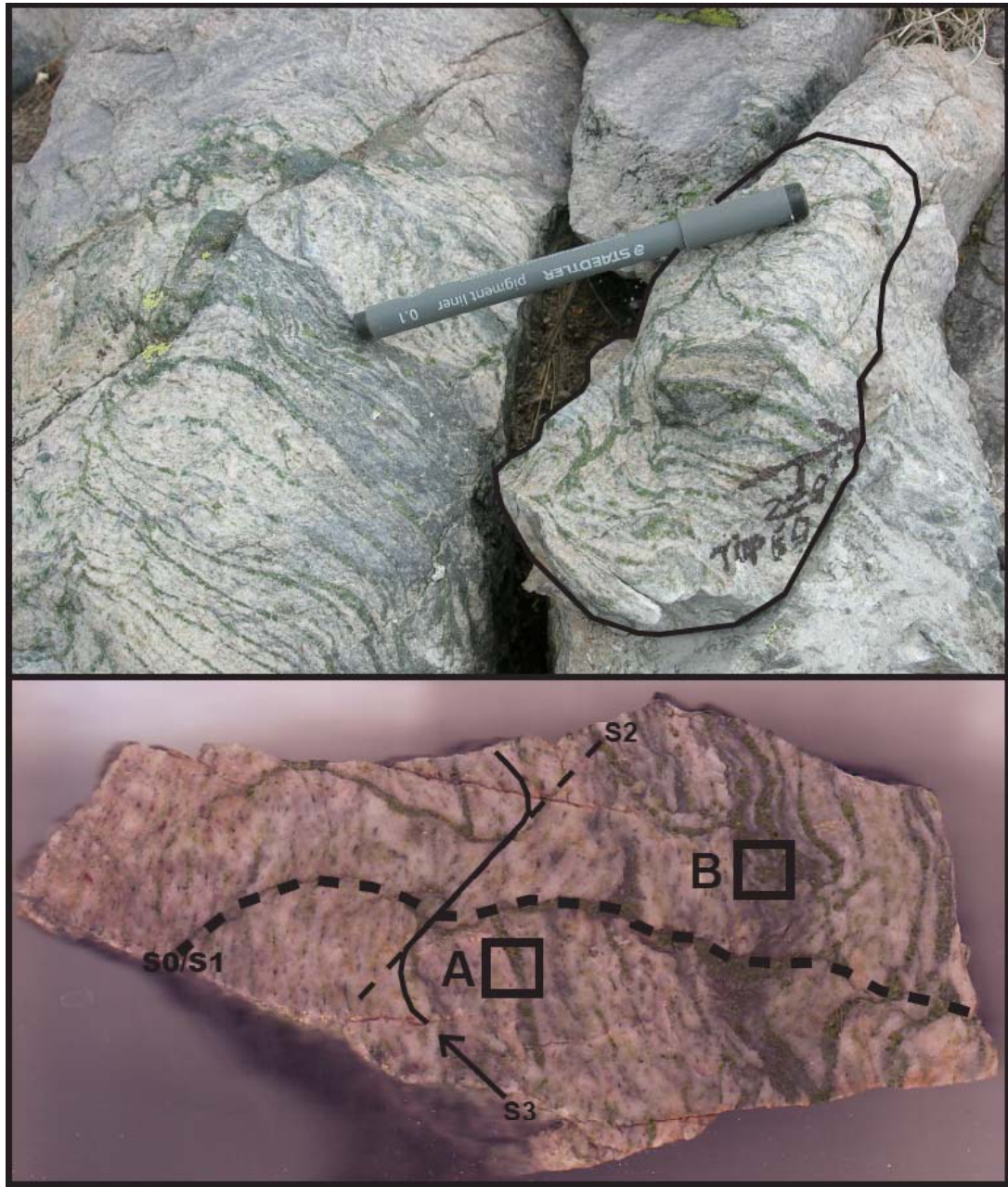


Figure 6.18. The heterogeneous distribution of D3 strain leads to the incomplete breakdown and regrowth of Mn-andalusite preserving both M2 (a) and M3 (b) Mn-andalusite in the same rock (sample- P06NM16).

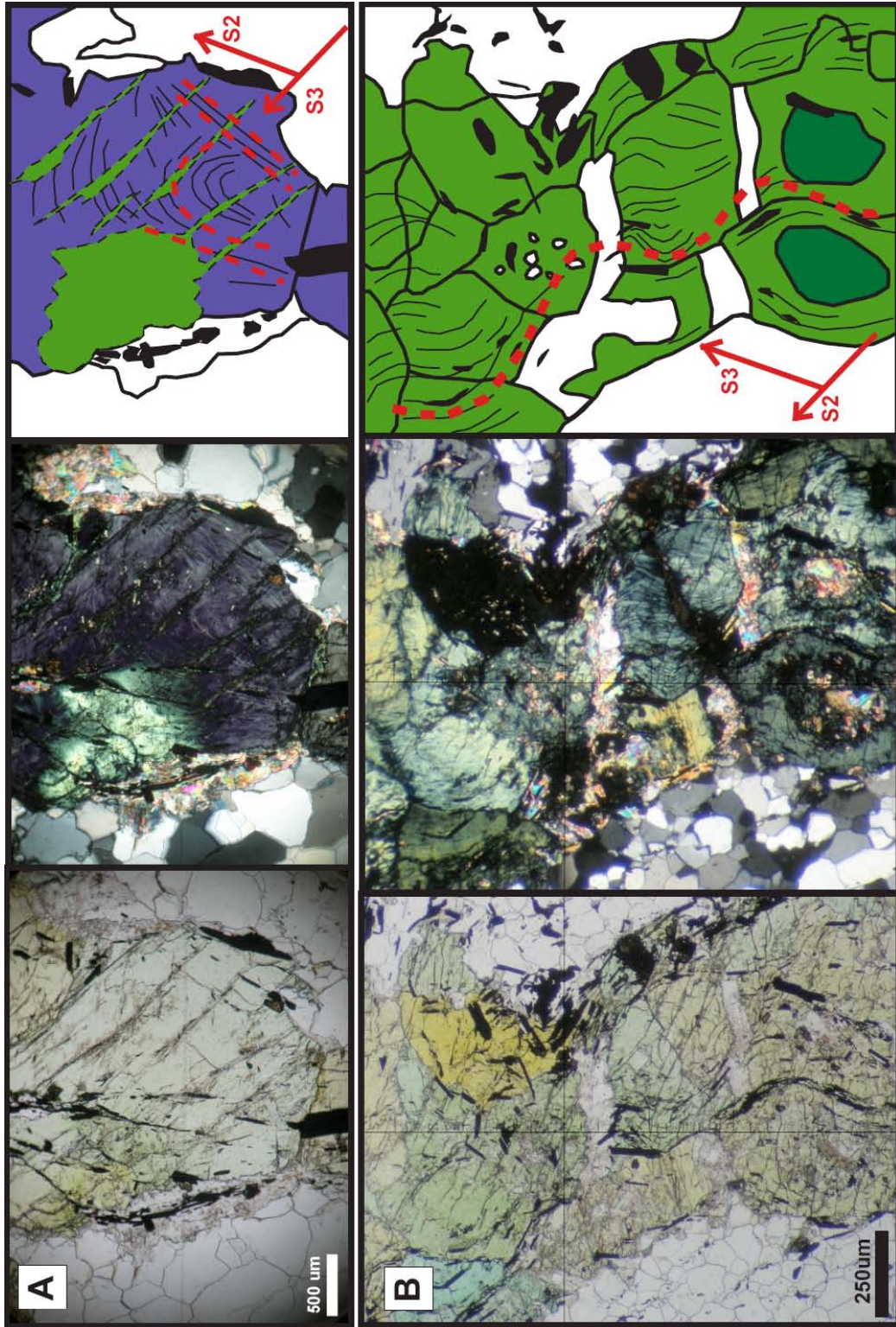


Figure 6.18. (continued).

polarizers than in the first generation of Mn-andalusite (Fig. 6.18b). Locally, the feathery texture helps to define open D3 crenulation cleavages (Stage 2-3 of Bell & Rubenach, 1983). The feathery texture of the D3 crenulation cleavage commonly wraps areas of Mn-andalusite that represent remains of the first generation of Mn-andalusite (Fig. 6.18b). Andalusite grain boundaries commonly cut across the continuous crenulation cleavage in second generation of Mn-andalusite so that the crenulation cleavage is preserved in more than one optically distinct crystal (Fig. 6.18b). The second generation of Mn-andalusite can also have a mottled appearance due to localized heterogeneity in Mn distribution and is typically found in areas of high D3 strain (Fig. 6.17c,d).

The two generations of Mn-andalusite represent two distinct periods of Mn-andalusite growth at the Hopewell anticline in the Hopewell Lake-Jawbone Mountain area. The first generation preserves a tight D2 crenulation cleavage whereas the second generation preserves a more open D3 crenulation cleavage (Fig. 6.18). This suggests that the first generation of Mn-andalusite grew syn- to post-D2 during the growth of the M2 assemblage and the second generation grew syn- to post-D3 during the growth of the M3 assemblage (Fig. 6.19). Zones of dissolution in the first generation of Mn-andalusite associated with D3 and the remnants of the first generation of Mn-andalusite included in the second support the presence of the first generation prior to D3. Differences in the overall Mn-distribution also suggest that the first type of Mn-andalusite crystal grew at a different time than the second type. The Mn-distribution in the first generation was controlled by the location of high Mn-core regions, with localized highs within a crystal of otherwise low Mn-distribution. In this case, early Mn-andalusite growth preserved what may have been the original heterogeneous distribution of Mn. The second generation of Mn-andalusite preserves a more homogenous Mn-distribution suggesting a homogenization of Mn from a starting distribution of extreme localized highs.

Evidence from the Mn-andalusite layer supports the interpretation that the Hopewell anticline was near the andalusite-pyrophyllite reaction line throughout much of its history and suggests that both M2 and M3 lead to the growth of andalusite (Fig. 6.19). Early M1 phyllosilicates were crenulated during D2 deformation. Post-D2 Mn-andalusite growth occurred

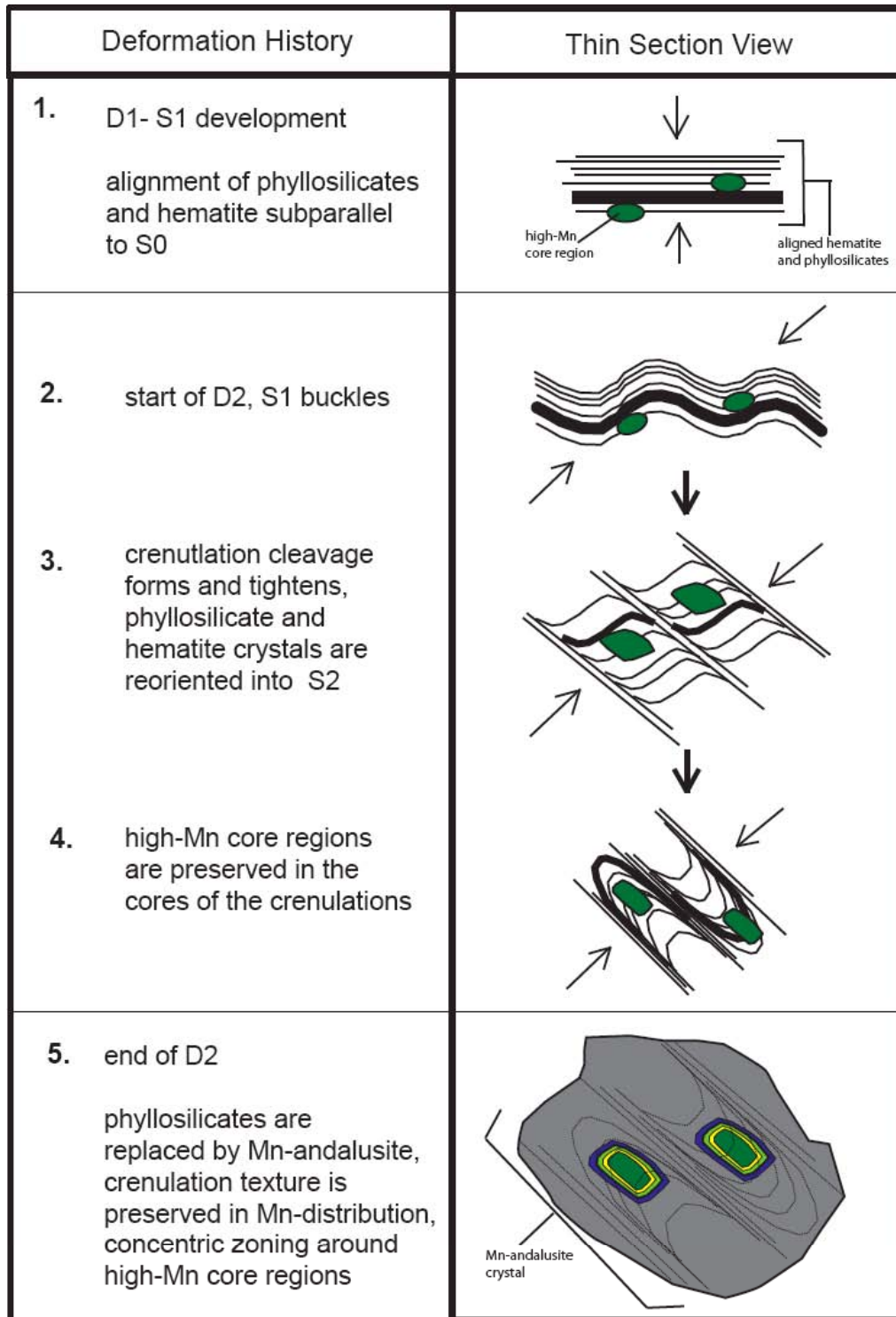


Figure 6.19. A schematic diagram showing the timing of deformation and Mn-andalusite growth in the Mn-andalusite layer of the Hopewell anticline.

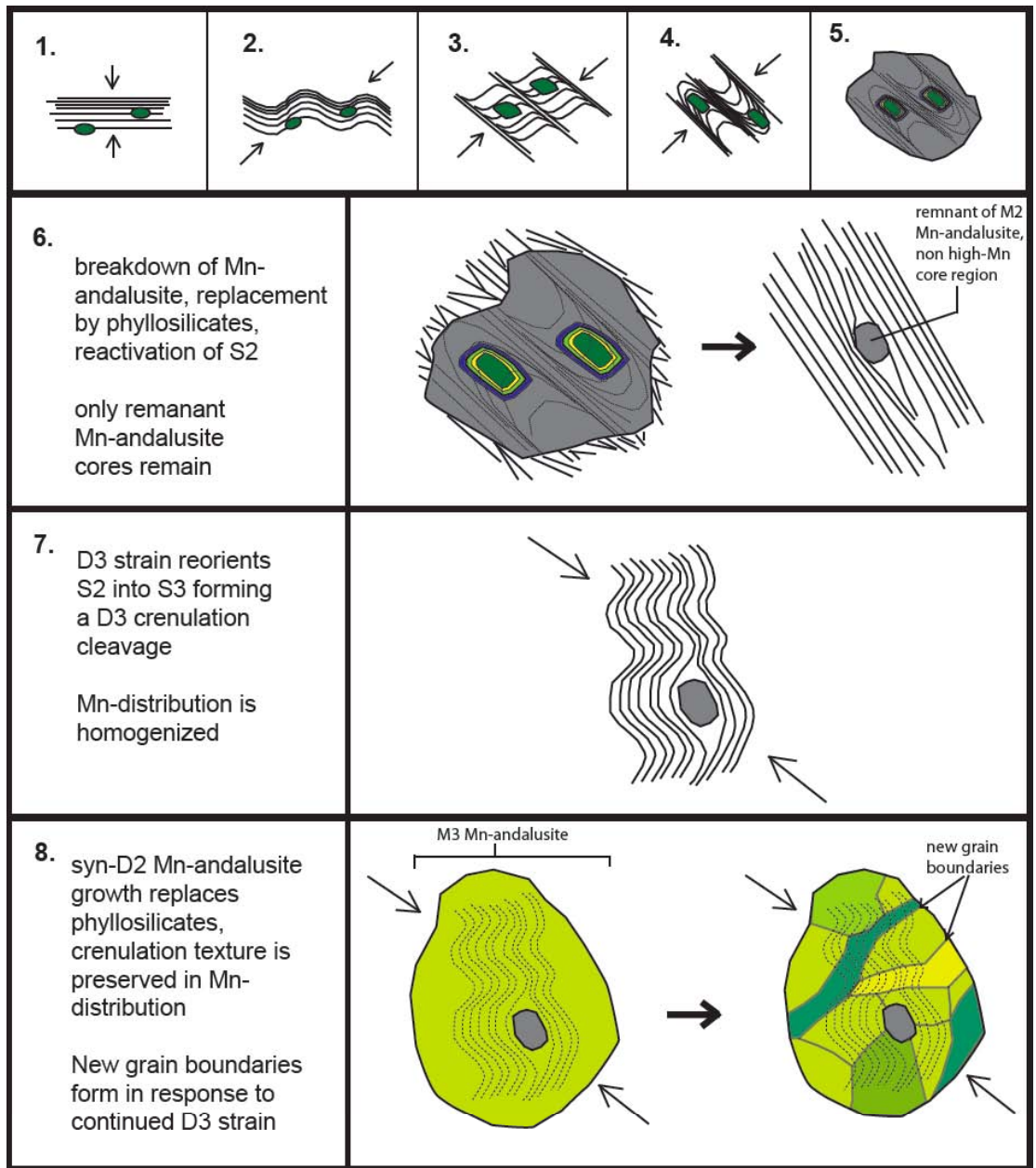


Figure 6.19. (continued).

during M2 including the high-Mn core regions and preserving the D2 crenulation cleavage in the distribution of Mn and in the alignment of hematite inclusions. A lack of undulose extinction or new grain boundaries associated with D2 in M2 Mn-andalusite supports the conclusion that M2 postdates D2. D3 led to the breakdown of M2 Mn-andalusite to phyllosilicate, dominantly pyrophyllite, in the areas where D3 strain was greatest leaving remnants of M2 Mn-andalusite and forming a D3 crenulation cleavage. M3 involved the growth of new Mn-andalusite that replaced the pyrophyllite, included the remains of M2 Mn-andalusite crystals, and preserved the D3 crenulation cleavage in the distribution of Mn and in the alignment of hematite inclusions. M3 andalusite displays new grain boundaries that cut across the D3 crenulation cleavage suggesting that M3 Mn-andalusite growth occurred syn-D3.

Both M2 and M3 Mn-andalusite can be found in the same rock making the interpretation of the timing of deformation and mineral growth complex, but the differences in character between two generations, particularly differences in Mn-distribution, are distinctive enough to make it possible to discern between M2 and M3 Mn-andalusite in thin section. The first generation (M2) is best characterized by a heterogeneous Mn-distribution and a relative lack of undulose extinction. The second generation is best characterized by a more homogeneous Mn-distribution and a deformed appearance (new grain boundaries and undulose extinction). When preserved in the birefringence pattern, the orientation and character of the crenulation cleavages easily distinguish the two generations apart, with M2 Mn-andalusite preserving a tight D2 cleavage and M3 Mn-andalusite preserving a more open D3 cleavage.

Kiowa Mountain

The Mn-andalusite at Kiowa Mountain does not preserve wide variations in Mn-content or extreme localized highs of Mn like those in the Hopewell Lake-Jawbone Mountain region. In areas where the Mn-distribution varies, the andalusite typically displays a relatively mottled appearance under crossed polarizers (Fig. 6.20 a,b,c).

Textural patterns identified in the birefringence and Mn-distribution of the Mn-andalusite crystals from Kiowa Mountain include a kyanite-Mn-andalusite intergrowth texture, high-Mn

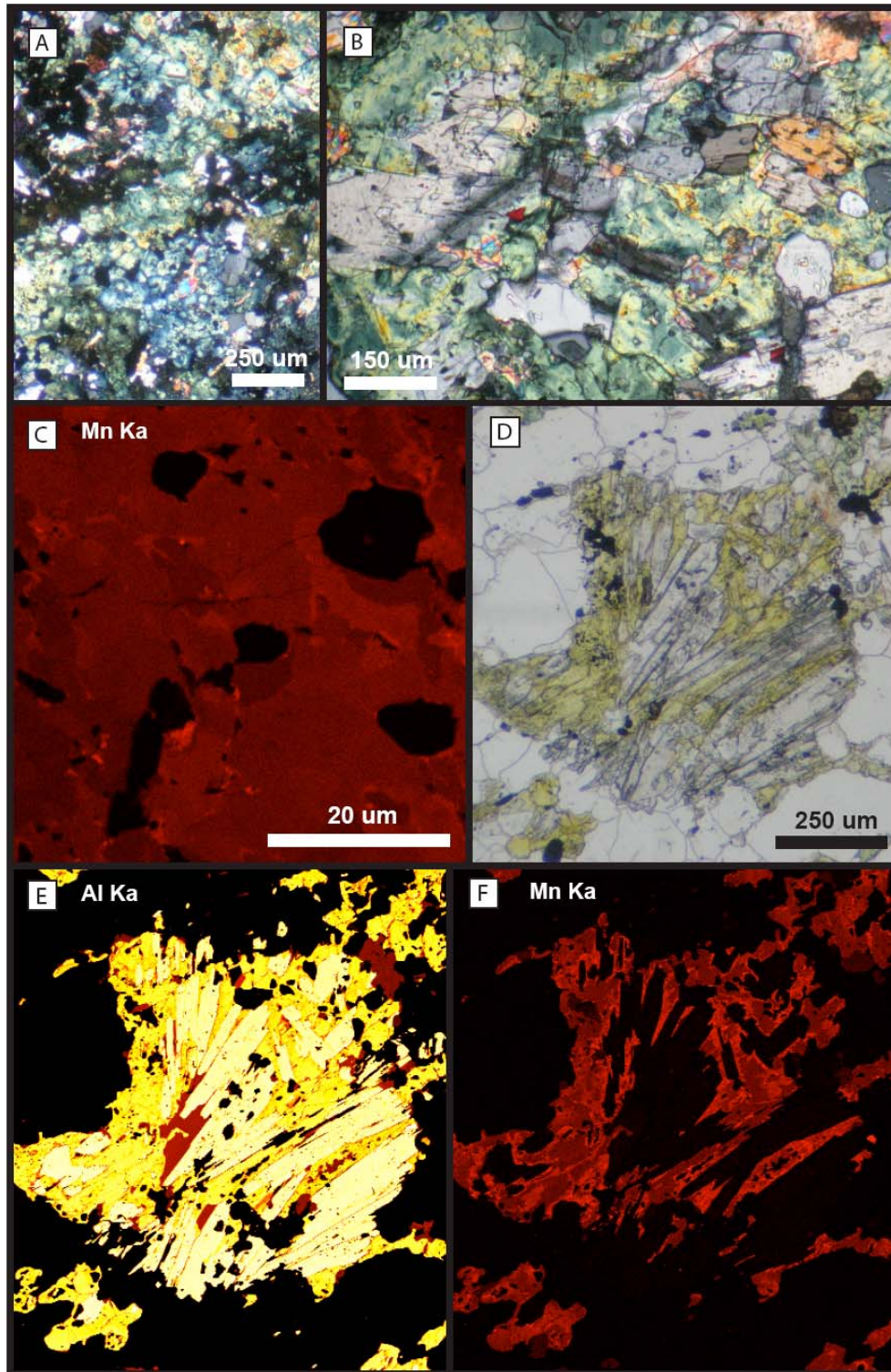


Figure 6.20. Mn-andalusite at Kiowa Mountain displays a mottled texture (a,b,c) and a kyanite-Mn-andalusite intergrowth texture (d,e,f) (EMP x-ray maps of Mn and Al).

halos around kyanite, and areas of low Mn-content that mimic crystal shapes. Mn-andalusite and kyanite appear intergrown in places with Mn-andalusite concentrated along zones subparallel to the C-axis of the kyanite crystal (Fig. 6.20d,e,f). Intergrown areas are relatively uncommon in samples from Kiowa Mountain and are associated with aluminum silicate rich S2 cleavage planes. An increase in Mn-content at the edge of some kyanite crystals included in Mn-andalusite creates high-Mn halos around the kyanite (Fig. 6.20). Additionally, areas of low Mn content mimic splintery, elongate, blocky, and/or bladed crystal shapes in some Mn-andalusite crystals (Fig. 6.16). The areas of low Mn-content (low order colors) that mimic crystal shapes are typically outlined by areas of markedly higher Mn-content (higher order colors) making them appear more defined. An otherwise randomly mottled appearance in the birefringence of Mn andalusite does not appear to conform to any specific textural patterns (Fig. 6.20a,b,c). The Mn-andalusite crystals at Kiowa Mountain do not preserve a phyllosilicate texture in the Mn-distribution like those in the Hopewell Lake-Jawbone Mountain region.

The textures preserved in the birefringence of Mn-andalusite at Kiowa Mountain suggest an early period of kyanite and Mn-andalusite growth that was followed by a period of Mn-andalusite stability. Kyanite-Mn-andalusite intergrowths are interpreted to represent an M2 assemblage due to their association with S2 and F2. The high Mn-halos would have formed during kyanite growth prior to and/or during Mn-andalusite growth and the areas of low Mn-content would be formed when Mn-andalusite replaced kyanite. Together the textures suggest a history of early kyanite growth prior to and/or during Mn-andalusite growth followed by kyanite replacement. This suggests that the rocks of Kiowa Mountain were at or near the kyanite + Mn-andalusite reaction line and moved into the Mn-andalusite only field during M2.

Fabric relationships suggest that a separate period of kyanite and Mn-andalusite growth occurred during D3 (Chapter 5). In areas where M3 aluminum silicates are present, the birefringence pattern in Mn-andalusite is too complexly mottled to identify specific textures. M2 and M3 assemblages are interpreted to have grown at similar conditions, and without fabric relationships to support periods of metamorphic mineral growth, it is difficult to identify more than one period aluminum silicate growth.

CHAPTER 7

CONCLUSIONS

The Proterozoic supracrustal rocks of the Tusas Mountain range contain a manganiferous marker horizon that is characterized by Mn-mineralization and is found in the lowermost 100m of the Ortega Formation and locally in parts of the upper Vadito Group. The layer is characterized by Mn-andalusite with quartz, hematite, rutile, zircon, monazite, phyllosilicates (dominantly pyrophyllite and some pennantite) ± kyanite and gahnite. Mn-andalusite commonly occurs with an abundance of hematite and rutile in the aluminous, hematite-bearing layers (“kaolinitic mudstone drapes” of Soegaard and Erikson, 1986), on the surface of cross-beds, concentrated in high strain zones, and on cleavage planes.

Characteristics of the Mn-andalusite layer in the Tusas Mountains include large-scale Mn zoning in Mn-andalusite and the presence of high-Mn core regions. The large-scale zoning is a result of a decrease in Mn content away from localized Mn highs and is interpreted to reflect the original distribution of Mn in the rock at the time of Mn-andalusite growth. The zoning pattern is typically associated with the high-Mn core regions. High-Mn core regions preserve some of the earliest fabrics and the highest amounts of Mn in the andalusite crystals. They differ from the surrounding crystal in texture and appearance, but are optically continuous suggesting a core-rim relationship. The high-Mn core regions are associated with sedimentary structures (i.e. cross beds and graded beds) and they may be linked to sedimentary processes.

Hematite and rutile are characteristic of the basal section of the Ortega Formation. Both hematite and rutile from the Mn-andalusite layer at the base of the Ortega Formation are rich in trace elements. Hematite contains zones of rutile that create patchy/mottled, wormy, cross-hatched, and/or banded textures within the hematite. Similar textures have been identified in hematite of the metavolcanic units of the Vadito Group and these textures could serve as a link between similar metavolcanic units (from the Vadito Group or elsewhere) and the Ortega Formation quartzite. The textures also resemble oxidation-exsolution textures in ilmenite and spinel and could be indicative of a high oxygen fugacity. There is little variation in

trace element content of the hematite and rutile within the Mn-andalusite layer and between hematite and rutile from inside and outside the Mn-andalusite layer.

The increase in Mn-content in the manganiferous horizon may be a result extensive lateritic weathering of the metavolcanic units of the Vadito Group and/or the chemical deposition of Fe and/or Mn phases in an enriched basin environment. Lateritic weathering could have lead to the formation of an Mn-Fe crust that was then locally reworked and deposited on the surface of sedimentary structures. On the other hand, the oxidation of Fe and Mn in the oxygen-stratified waters of an enriched basin environment (e.g. hydrothermal enrichment) may have lead to the deposition and accumulation of Fe and Mn oxyhydroxides.

Mn-andalusite preserves evidence for mineral paragenesis and microstructural relationships in the textures preserved in the birefringence of Mn-andalusite. The crystal chemistry of Mn-andalusite dictates that as Mn^{3+} substitutes for Al^{3+} in the andalusite crystal structure, the crystal lattice expands changing the refractive index and thus the birefringence (Gunter and Bloss, 1982). This creates a direct relationship between Mn content and interference color. A feathery texture preserved in the birefringence of Mn-andalusite crystals is interpreted to represent the crystal habit of phyllosilicate precursor minerals. The feathery texture preserves a crenulation cleavage in the birefringence of Mn-andalusite from the Hopewell Lake-Jawbone Mountain region. When considered together, high-Mn halos around kyanite and localized areas of low Mn content that mimic crystal shapes indicate areas of kyanite replacement in Mn-andalusite. These textures provide tools to help understand the timing of metamorphic mineral growth in the Mn-andalusite layer during the Proterozoic. Examples include the Mn-andalusite layer of the Hopewell Lake-Jawbone Mountain region and Kiowa Mountain.

The Proterozoic supracrustal rocks of the Tusas Mountain range preserve evidence for three periods of deformation (D1, D2, D3) with associated fabric (S1, S2, S3) and fold (F1, F2, F3) generations and the growth of three metamorphic mineral assemblages. The general tectonic histories preserved in the Mn-andalusite layer of the Hopewell Lake-Jawbone Mountain area, Quartzite Peak, and Kiowa Mountain are similar in the timing of deformation and growth of

the metamorphic assemblages (Fig. 7.1). D1 was associated with the growth of the M1 mineral assemblage and included early kyanite growth at the Jawbone syncline in the Hopewell Lake-Jawbone Mountain region, at Quartzite Peak, and at Kiowa Mountain and phyllosilicate growth (e.g. pyrophyllite) at the Hopewell anticline in the Hopewell Lake-Jawbone Mountain region. The M2 assemblage dominantly grew post D2 and involved Mn-andalusite growth and in most cases kyanite growth as well. The M3 assemblage typically involved the growth of the same mineral assemblage that was stable during M2 and occurred during D3 strain.

The Hopewell Lake-Jawbone Mountain region reserves a history that is unlike the other areas studied in the Tusas Mountains. The Hopewell anticline is dominated by Mn-andalusite that preserves a history of phyllosilicate and Mn-andalusite stability with little or no kyanite growth. The Jawbone syncline is dominated by kyanite, late M3 sillimanite, and little to no andalusite. In both the syncline and anticline, discrete D3 high strain zones provide evidence of strain partitioning during D3. A metamorphic divide between the andalusite-dominated Hopewell anticline and the kyanite-dominated Jawbone syncline suggest differences in pressure and/or temperature conditions and may involve the movement along a late-stage D3 fault at or near Route 64. Last stage juxtaposition of the Hopewell anticline with the Jawbone syncline may have involved a north side up motion sense on the fault. The growth of sillimanite at the Jawbone syncline may reflect this movement as well as may reflect a late stage increase in temperature.

The differing metamorphic and structural history between the Hopewell anticline and the Jawbone syncline suggests early detachment and separation during D1 (or at the start of D2) and late juxtaposition during or at the end of D3. Following early detachment along a D1/D2 fault (south-side-up motion sense), the structural histories of the Jawbone syncline and the Hopewell anticline deviated. The Jawbone syncline remained relatively upright, was only mildly tilted, and was relatively spared from the majority of intense D2 and D3 strain. The Hopewell anticline was tightened, greatly tilted, and was cut by well developed D3 high strain zones. The metamorphic histories also differ very early, with the Jawbone syncline at or above the kyanite-andalusite reaction line throughout most of its metamorphic history and the Hopewell anticline

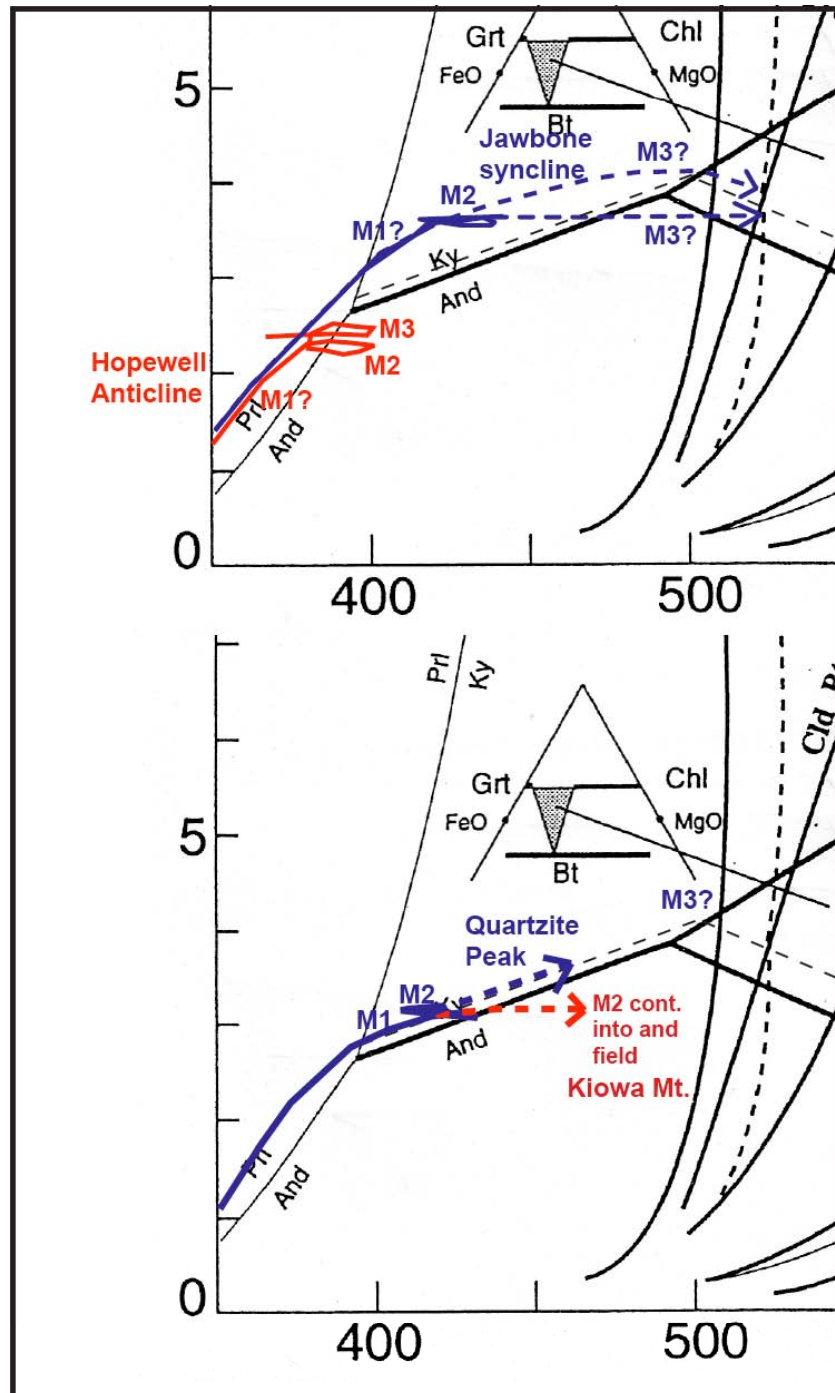


Figure 7.1. P/T diagram showing the difference in P-T paths for the Hopewell anticline and the Jawbone syncline from the Hopewell Lake-Jawbone Mountain region (top) and the deviation in P-T space of Quartzite Peak and Kiowa Mountain during D2 (bottom).

along the pyrophyllite-andalusite reaction line for most of its metamorphic history. The differences in metamorphic history persist until late in the deformational history at the end of D3 when the Hopewell anticline and the Jawbone syncline were once again juxtaposed through the north-side-down movement along a D3 fault. The location of the structural divide indicating early separation along a D1/D2 fault is at the same approximate location as the metamorphic divide that indicates late juxtaposition along a D3 fault. The overlap of the location of these faults suggests that the area between the Hopewell anticline and the Jawbone syncline along Route 64 represents a location where strain was repeatedly localized in the Proterozoic.

The metamorphic and structural histories of Quartzite Peak and Kiowa Mountain are different from the history of the Hopewell Lake-Jawbone Mountain region but are relatively similar to each other. D3 strain was uniformly distributed at both Quartzite Peak and Kiowa Mountain. In addition, intergrown Mn-andalusite and kyanite from Quartzite Peak and Kiowa Mountain that were part of the M2 assemblage provide similar estimated conditions for the start of the growth of the M2 assemblage (430C/3.2kb and 415C/2.7kb respectively). The subsequent history of M2 deviates between the two areas in that Quartzite Peak continued to have a kyanite + Mn-andalusite assemblage but Kiowa Mountain shifts to an Mn-andalusite-only assemblage. The difference between the M2 assemblages suggests a differing tectonic history between Quartzite Peak and Kiowa Mountain during M2 that may be related to movement along a fault, such as the Spring Creek Shear Zone, and/or the local emplacement of an igneous body.

The transition from a kyanite-Mn-andalusite equilibrium assemblage to an Mn-andalusite dominated assemblage in the Mn-andalusite layer of the Ortega Formation at Kiowa Mountain suggests changing P-T conditions during M2 metamorphism. Textural evidence preserved in the birefringence of Mn-andalusite crystals suggests the early growth of both kyanite and Mn-andalusite followed by significant replacement of kyanite by Mn-andalusite during M2. Changing conditions during M2 metamorphism would explain both observations. The rocks of Kiowa Mountain were at or near the kyanite + Mn-andalusite reaction line to grow

the equilibrium assemblage and probably moved into the Mn-andalusite-only field during M2 to grow Mn-andalusite and breakdown kyanite.

The Ortega Formation is well exposed in the Tusas Mountains and helps to define map-scale features. Despite this exposure, microstructural and petrologic analysis of the quartzite has been limited largely due to the difficulty in working with such a clean, well-annealed unit. The presence of kyanite and particularly Mn-andalusite within the Mn-andalusite layer provides the opportunity to study metamorphic mineral paragenesis and mineral-fabric timing relationships that would otherwise not be preserved in a quartzite. In addition, the relationship between Mn-content and birefringence in Mn-andalusite allows for the unique identification of textures that preserve the crystal habit of precursor minerals (i.e. kyanite and phyllosilicates) and that define microstructural fabrics. These textures and the information they provide help to develop a better understanding of the structural and petrologic history of Ortega Formation and the Tusas Mountains.

APPENDIX A

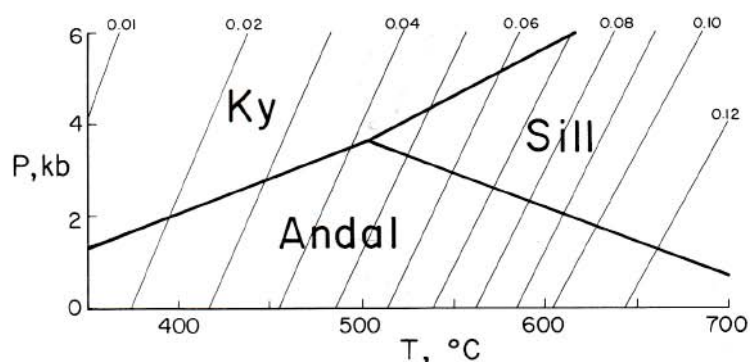
SAMPLE LOCATIONS AND DESCRIPTIONS

SAMPLE	UTM		Location	S1	S2	S3	ROCK TYPE
P06-NM-03	387406	4063498	Hopewell Lake	248, 79	315, 85	-	Burned Mt. Fm.
P06-NM-05	386854	4062472	Hopewell Lake	-	115, 75	254, 80	Ortega Fm. Mn-and layer
P06-NM-06	386360	4062855	Hopewell Lake	-	114, 74	-	Ortega Fm. Mn-and layer
P06-NM-07	386243	4062823	Hopewell Lake	-	135, 85	-	Ortega Fm.
P06-NM-09	383025	4065582	Hopewell Lake	176, 77	125, 72	075, 85	schistose metarhyolite
P06-NM-10	383230	4065795	Hopewell Lake	161, 80	306, 80	272, 73	Ortega Fm.-and layer
P06-NM-11	383309	4065788	Hopewell Lake	197, 64	159, 60	072, 60	Ortega Fm.-and layer
P06-NM-12	383310	4065788	Hopewell Lake	184, 63	150, 66	086, 84	Ortega Fm.-and layer
P06-NM-14	383743	4065068	Hopewell Lake	-	-	-	Ortega Fm. Mn-and layer
P06-NM-15	383943	4065058	Hopewell Lake	197, 60	136, 70	-	Ortega Fm. Mn-and layer
P06-NM-16	383912	4065072	Hopewell Lake	234, 35	326, 52	100, 62	Ortega Fm. Mn-and layer
P06-NM-19	387494	4062514	Hopewell Lake	-	-	-	Ortega Fm. Mn-and layer
P06-NM-20	386286	4062885	Hopewell Lake	128,72	293,63?	080, 66	Ortega Fm. Mn-and layer
P06-NM-21	384020	4064694	Hopewell Lake	119, 71	-	084, 56	Ortega Fm. Mn-and layer
P06-NM-22	388620	4064383	Jawbone Mt.	-	-	265, 84	Maquinita Fm. granodiorite
P06-NM-23	389493	4065660	Jawbone Mt.	263, 47	293, 89	-	Vadito Gp.-metaconglmt
P06-NM-24	389535	4065941	Jawbone Mt.	270, 32	~290	253, 73	Vadito Gp.- sandy schist
P06-NM-26	389179	4066718	Jawbone Mt.	206, 72	-	-	Ortega Fm. ky layer
P06-NM-27	404357	4049257	Kiowa Mt.		143, 56	285, 76	Vadito Gp.- amphibolite
P06-NM-28	403877	4050050	Kiowa Mt.	164, 50	-	-	Vadito Gp.- ms schist
P06-NM-29	401663	4050551	Kiowa Mt.	289, 81	-	-	Ortega Fm. Mn-and layer
P06-NM-30	403809	4048565	Kiowa Mt.	136, 75	328, 46	89, 68	Vadito Gp.-sandy schist
P06-NM-32	403732	4049044	Kiowa Mt.	-	-	-	Vadito Gp.- schist
P06-NM-33	403709	4049018	Kiowa Mt.	100, 43	-	-	Vadito Gp.- schist
P06-NM-35	402069	4048377	Kiowa Mt.	-	-	-	Vadito Gp.- schist
P06-NM-37	401745	4048169	Kiowa Mt.	-	-	-	Burned Mt. Fm.
P06-NM-38	402447	4048541	Kiowa Mt.	-	128, 55	-	Vadito Gp.- amphibolite
P06-NM-39	402982	4048766	Kiowa Mt.	-	140, 54	-	Vadito Gp.-bt-ms schist
P06-NM-40	396795	4053701	Quartzite Peak	-	302, 74	-	Ortega Fm. Mn-and layer
P06-NM-50	near Spring Creek		Quartzite Peak	-	-	-	Vadito Gp.-Cu-Ba layer
P06-NM-51	metarhyolite canyon		Hopewell Lake	-	-	-	Ortega Fm. Mn-and layer
P06-NM-52	396632	4053858	Quartzite Peak	-	-	-	Ortega Fm. Mn-and layer
P06-NM-53	386854	4062472	Hopewell Lake	-	-	-	Ortega Fm. Mn-and layer
P06-NM-54	Kiowa Mt. summit		Kiowa Mt.	-	-	-	amphibolite
P06-NM-56	Kiowa Mt. summit		Kiowa Mt.	-	-	-	Ortega Fm. Mn-and layer
P06-NM-58	Kiowa Mt. summit		Kiowa Mt.	-	-	-	Ortega Fm. Mn-and layer
P06-NM-59	Kiowa Mt. summit		Kiowa Mt.	-	-	-	Ortega Fm. Mn-and layer

APPENDIX B

PRESSURE-TEMPERATURE CALCULATIONS

Figure 15 (Grambling and Williams, 1985) :



Equation 4 (Grambling and Williams, 1985) :

$$\ln \left(\frac{X_{\text{Al}_2\text{SiO}_5}^{\text{A}}}{X_{\text{Al}_2\text{SiO}_5}^{\text{K or S}}} \right) \cong \frac{-\Delta \bar{V}^\circ}{RT} (P_2 - P_1)$$

Values for P-T calculations (this study):

$$R = 8.31451 \frac{\text{kb cm}^3}{\text{mol K}} \quad \Delta V = 6.85 \text{ cm}^3$$

Quartzite Peak:

$$X_{\text{Al}_2\text{SiO}_5}^{\text{and}} = 1.771 \quad X_{\text{Al}_2\text{SiO}_5}^{\text{ky}} = 1.956$$

$$X_{\text{FeAlSiO}_5}^{\text{and}} = 0.025 \quad X_{\text{FeAlSiO}_5}^{\text{ky}} = 0.017$$

Kiowa Mt.:

$$X_{\text{Al}_2\text{SiO}_5}^{\text{and}} = 1.882 \quad X_{\text{Al}_2\text{SiO}_5}^{\text{ky}} = 2.001$$

$$X_{\text{FeAlSiO}_5}^{\text{and}} = 0.023 \quad X_{\text{FeAlSiO}_5}^{\text{ky}} = 0.027$$

APPENDIX C

QUARTZITE DEPOSITION AND STRATIGRAPHY

Stratigraphic sections were produced from observations made in three areas based on the degree of outcrop exposure and the inferred location of the Mn horizon: the Hopewell Lake-Jawbone Mountain area, Quartzite Peak, and Kiowa Mountain

The Hopewell Lake-Jawbone Mountain Area

The stratigraphy across the Vadito-Hondo contact was characterized in two separate areas in the Hopewell Lake-Jawbone Mountain area: near Hopewell Lake and at Jawbone Mountain. In both sections, the Vadito Group includes the Burned Mountain Formation metarhyolite and transitional package metasediments and the Hondo Group includes the Ortega Formation quartzite (Fig. 4.1 & 4.2). In the Hopewell Lake section, the transitional metasediments include a small quartz pebble metaconglomerate unit that is overlain by a quartz-rich sandy schist unit. At the base of the Ortega Formation in the Hopewell section, a zone of high-Mn content marks the location of the Mn-marker layer, or the Mn horizon, and is characterized by Mn-andalusite mineralization. The Mn horizon abruptly transitions into an Mn-poor layer that is characterized by non-manganiferous andalusite. In the Jawbone Mountain section, the transitional metasediments include a thick quartz pebble metaconglomerate unit that is overlain by a quartz-rich sandy schist. The metaconglomerate varies in clast size and is cross-bedded in places. Concentrations of kyanite and hematite at the base of the Ortega Formation in the Jawbone Mountain section marks an Mn-poor, Al-rich zone.

Quartzite Peak

The stratigraphy across the Vadito-Hondo contact at Quartzite Peak includes the Burned Mountain Formation metarhyolite in the Vadito Group and the Ortega Formation in the Hondo Group (Fig. 4.3). The Mn horizon is located at the base of the Ortega Formation and is

Hopewell Lake

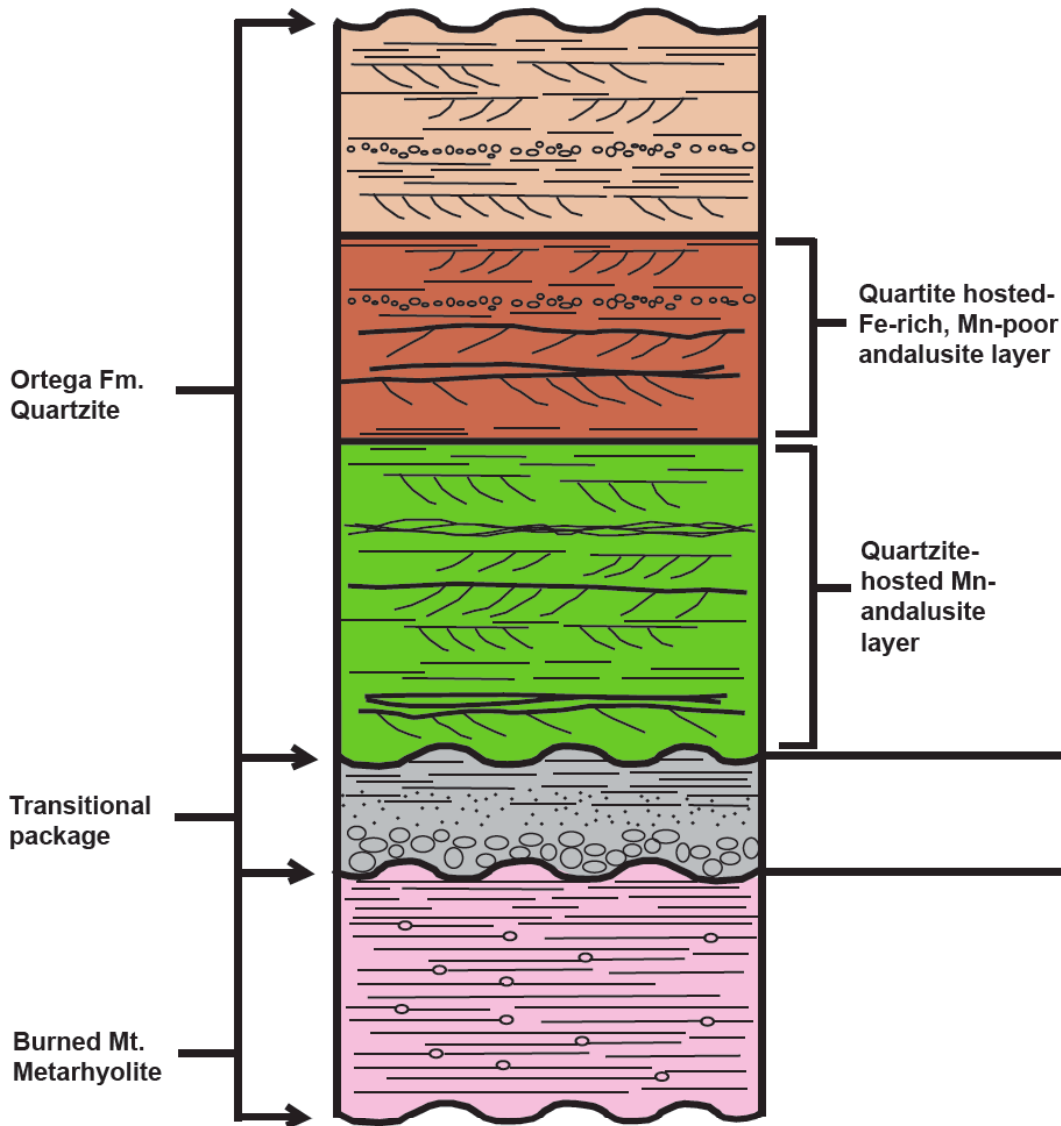


Figure C.1. The stratigraphic section from the Hopewell Lake portion of the Hopewell Lake-Jawbone Mountain area showing the upper part of the Vadito Group and the lower part of the Hondo Group. The Vadito Group includes the Burned Mountain Formation metarhyolite and the metasediments of the transitional package. The Hondo Group includes the Ortega Formation quartzite, which hosts the Mn-andalusite layer and an Mn-poor andalusite layer.

Jawbone Mt.

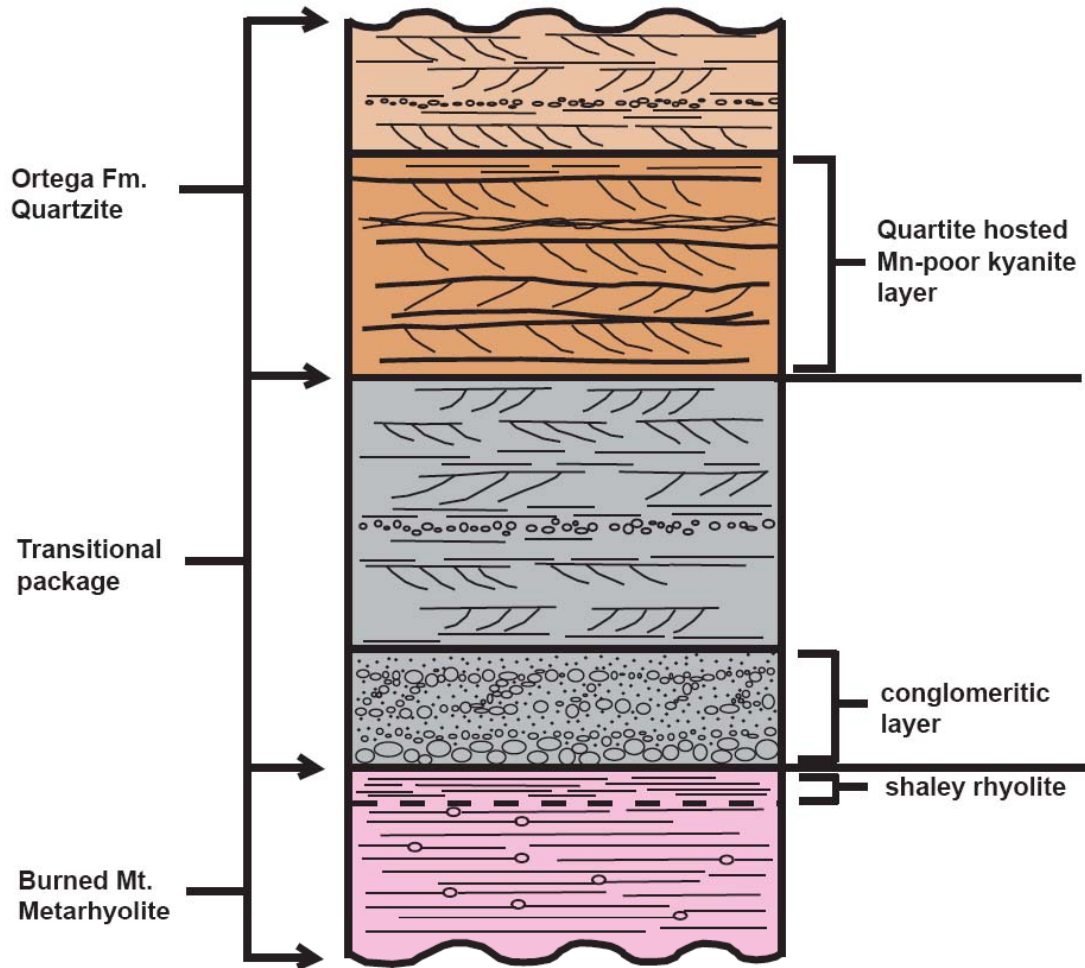


Figure C.2. The stratigraphic section from the Jawbone Mountain portion of the Hopewell Lake-Jawbone Mountain area showing the upper part of the Vadito Group and the lower part of the Hondo Group. The Vadito Group includes the Burned Mountain Formation metarhyolite and the metaconglomerate and metasediments of the transitional package. The Hondo Group includes the Ortega Formation quartzite, which hosts a kyanite and hematite-rich layer.

characterized Mn-andalusite mineralization. Quartz-rich schist float found between the Burned Mountain Formation and the Ortega Formation is interpreted to represent part of the transitional package at Quartzite Peak. The quartz-rich schist contains a thin layer of high Cu and Ba content that is characterized by malachite and barite.

Kiowa Mountain

The stratigraphy across the Vadito-Hondo contact at Kiowa Mountain includes the Burned Mountain Formation metarhyolite and a thick transitional package in the Vadito Group and the Ortega Formation in the Hondo Group (Fig. 4.3). The Mn horizon is exposed at the summit of Kiowa Mountain at the base of the Ortega Formation and is characterized by Mn-andalusite mineralization. The transitional package is composed of a thick stratigraphic succession of schists and amphibolites. A traverse of the transitional package perpendicular to bedding produced the following stratigraphic sequence: feldspar-rich schists, lower amphibolite layer, biotite-muscovite schists, upper amphibolite layer, and muscovite schists (Figure 4.5). The biotite-muscovite schists vary in biotite, muscovite, and quartz content, can be massive, layered, or contain cross-beds, and contain variable amounts of epidote and rarely feldspar. The dark amphibolite layers commonly contain chlorite and are marked by light-colored lenses and bands rich in feldspar.

Discussion

The stratigraphic sequence that spans the Vadito-Hondo contact in the Hopewell Lake-Jawbone Mountain area, at Quartzite Peak, and at Kiowa Mountain all include the Burned Mountain Formation, a transitional package, and the Ortega Formation, but vary in the thickness and types of units in the transitional package. The transitional package shown in sections from Quartzite Peak, Hopewell Lake, and Jawbone Mountain include only quartz-rich schists and/or quartz pebble metaconglomerates whereas the transitional package at Kiowa Mountain includes amphibolites and more than one type of schist.

Quartzite Peak

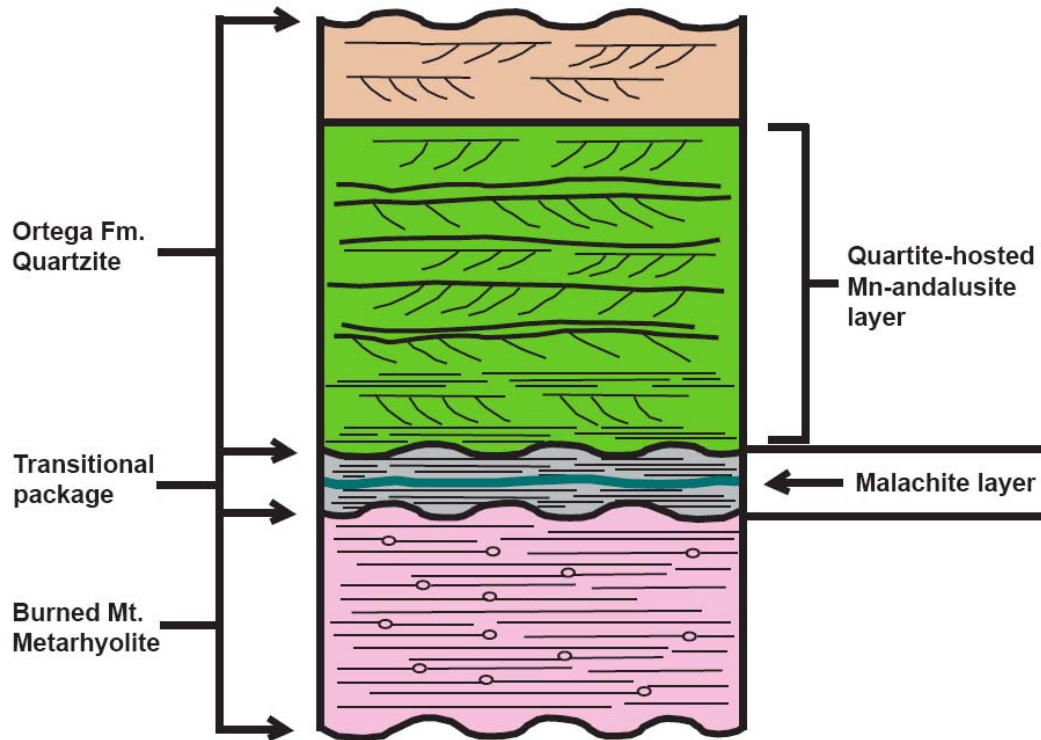


Figure C.3. The stratigraphic section from Quartzite Peak showing the upper part of the Vadito Group and the lower part of the Hondo Group. The Vadito Group includes the Burned Mountain Formation metarhyolite and the metasediments of the transitional package, which hosts a malachite layer. The Hondo Group includes the Ortega Formation quartzite, which hosts the Mn-andalusite layer.

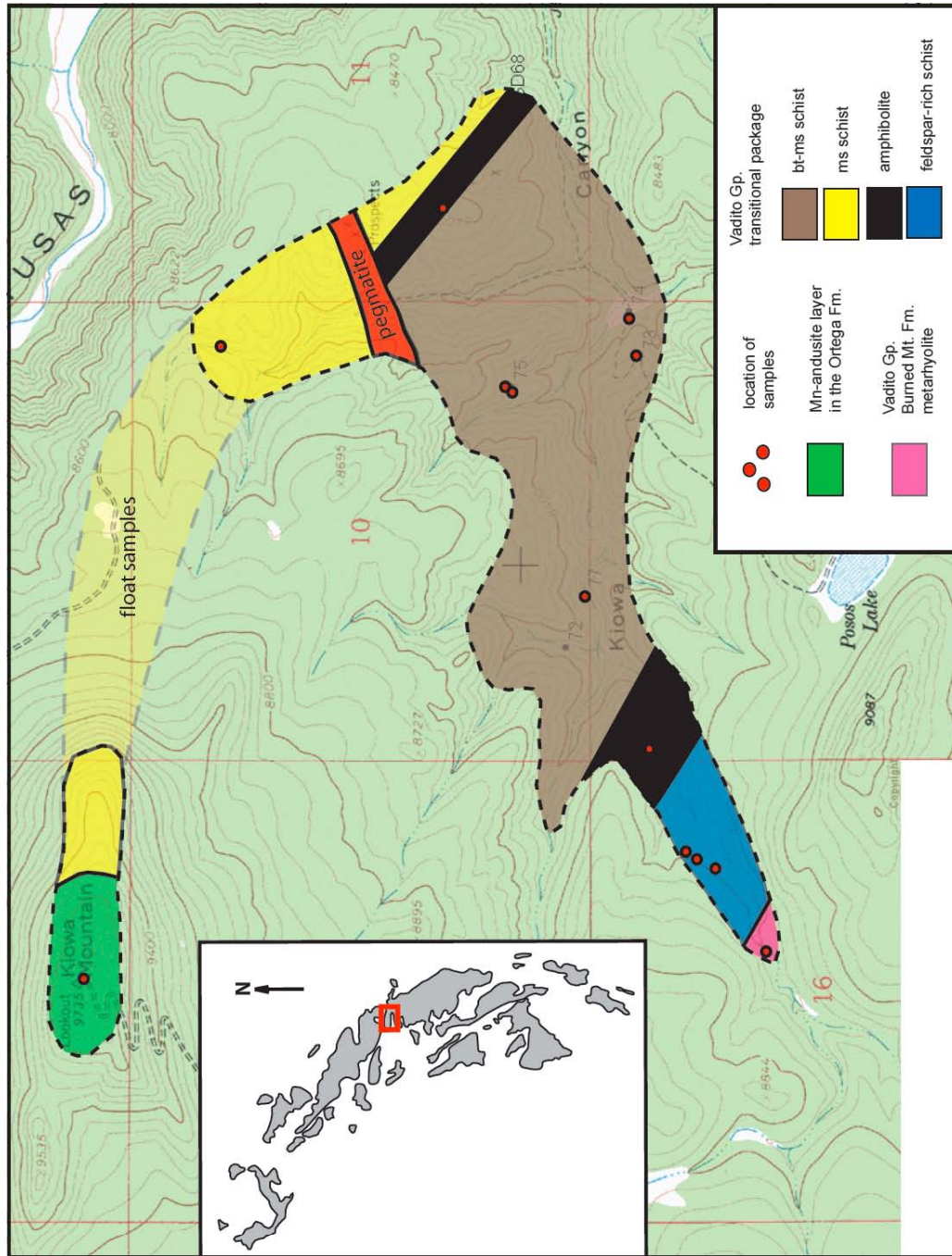


Figure C.4. A lithologic map of the Kiowa Mt. showing the location of units in the transitional package along a traverse approximately perpendicular to bedding.

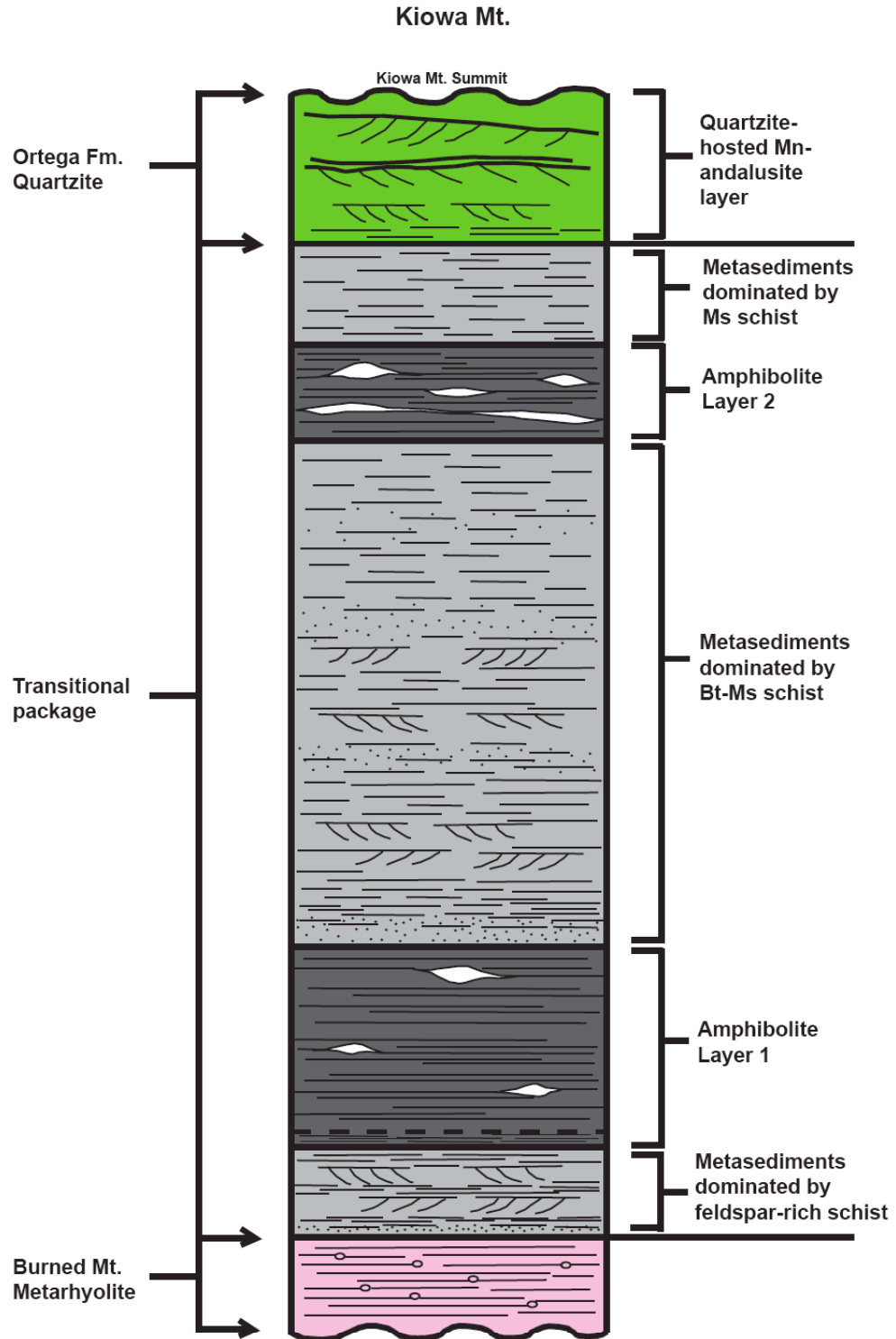


Figure C.5. The stratigraphic section from Kiowa Mountain showing the upper part of the Vadito Group and the lower part of the Hondo Group. The Vadito Group includes the Burned Mountain Formation metarhyolite and the metasediments and amphibolites of the transitional package. The Hondo Group includes the Ortega Formation, which hosts the Mn-andalusite layer.

Mn-andalusite mineralization at the base of the Ortega Formation in the Hopewell Lake, Quartzite Peak, and Kiowa Mountain sections consistently places the location of the Mn horizon in the lowermost section of the quartzite. Because the stratigraphic location of the Mn horizon is the same in all three sections, it is reasonable to conclude that the Mn horizon can serve as a point of correlation between these isolated sections. A lack of Mn-phases at the base of the Ortega Formation in the Jawbone Mountain section, however, suggests that the Mn horizon may not be present everywhere at the base of the Ortega Formation. The kyanite and hematite layer at the base of the Ortega Formation in the Jawbone Mountain section is not characterized by high levels of Mn. This leads to the conclusion that either the Mn horizon is not present at Jawbone Mountain or it is not present at the base of the Ortega Formation like at Hopewell Lake, Quartzite Peak, and Kiowa Mountain. Given that the nearby Hopewell sequence also includes an Al-rich, Mn-poor layer, it is possible that the kyanite layer at Jawbone Mountain correlates with the Mn-poor andalusite layer at Hopewell Lake and that the Mn horizon is located elsewhere in the stratigraphic section.

BIBLIOGRAPHY

- Abraham, K., and Schreyer, W., 1975, Minerals of the viridine hornfels from Darmstadt, Germany: *Contributions to Mineralogy and Petrology*, v. 49, p. 1-20.
- Abs-Wurmbach, I., Langer, K., and Schreyer, W., 1983, The influence of Mn^{3+} on the Stability Relations of the Al_2SiO_4 Polymorphs with Special Emphasis on Manganian Andalusites (Viridines), and $(Al_{1-x}Mn_x^{3+})_2(O/SiO_4)$: An Experimental Investigation: *Journal of Petrology*, v. 24, p. 48–75.
- Abs-Wurmbach, I., Langer, K., Seifert, F., and Tillmanns, E., 1981, The crystal chemistry of $(Mn^{3+}$ and $Fe^{3+})$ -substituted andalusites (viridines and kanonaite) $(Al_{1-x-y}Mn_x^{3+}Fe_y^{3+})_2(O/SiO_4)$: crystal structure refinements, Mössbauer, and polarized optical absorption spectra: *Zeitschrift Für Kristallographie*, v. 155, p. 81-113.
- Bauer, P.W., and Williams, M.L. 1989, Stratigraphic nomenclature of Proterozoic rocks, northern New Mexico,- revisions, redefinitions, and formalization: *New Mexico Geology*, v. 11, n. 3, p. 45-52.
- Bell, T.H., Rubenach, M.J., and Fleming, P.D., 1986, Porphyroblast nucleation, growth, and dissolution in regional metamorphic rocks as a function of deformation partitioning during foliation development: *Journal of Metamorphic Geology*, v. 4, p. 37-67.
- Bell, T. H., and Rubenach, M. J., 1983, Sequential porphyroblast growth and crenulation cleavage development during progressive deformation: *Tectonophysics*, v. 92, p. 171–194.
- Beukes, N.J., Dorland, H., Gutzmer, J., Nedachi, M., and Ohmoto, H., 2002, Tropical laterites, life on land, and the history of atmospheric oxygen in the Paleoproterozoic: *Geology*, v. 30, n. 6, p. 491-494.
- Bickford, M.E., and Hill, B.M., 2007, Does the arc accretion model adequately explain the Paleoproterozoic evolution of southern Laurentia? An expanded interpretation: *Geology*, v. 35, n. 2, p. 167-170.
- Bishop, J., 1997, The determination of a quantitative P-T-t-D history for Proterozoic rocks of the Cerro Colorado Area, North Central New Mexico: Unpub. M.S. Thesis, University of Massachusetts, Amherst.
- Braun, J-J, Pagel, M., Muller, J-P, Bilong, P., Michard, A., and Guillet, B., 1990, Cerium anomalies in lateritic profiles: *Geochimica et Cosmochimica Acta*, v. 54, p. 781-795.
- Cather, S.M., Karlstrom, K.E., Timmons, J.M., and Heizler, M.T., 2006, Palinspastic reconstruction of Proterozoic basement-related aeromagnetic features in north-central New Mexico: Implications for Mesoproterozoic and late Cenozoic tectonism: *Geosphere*, v. 2, n. 6, p. 299-323.
- Churakov, S.V., 2007, Structure and dynamics of the water films confined between edges of pyrophyllite: A first principle study: *Geochimica et Cosmochimica Acta*, v. 71, p. 1130–1144.
- Condie, K.C., 1982, Plate-tectonic model for Proterozoic continental accretion in the southwestern United States: *Geology*, v. 10, p. 37-42.

- Condie, K.C., 1992, Proterozoic terranes and continental accretion in the southwestern United States, in Condie, K.C., ed., Proterozoic Crustal Evolution: Elsevier, New York, pp. 447-480.
- Condie, K.C., and Chomaik, B., 1992, Continental accretion: Contrasting Mesozoic and Early Proterozoic tectonic regimes in North America: Tectonophysics, v. 265, p. 101-126.
- Cox, R., Gutmann, E.D., and Hines, P.G., 2002a, Diagenetic origin for quartz –pebble conglomerates: Geology, v. 30, n. 4, p. 323-326.
- Cox, R., Martin, M.W., Comstock, J.C., Dickerson, L.S., Ekstrom, I.L., and Sammons, J.H., 2002b, Sedimentology, stratigraphy, and geochronology of the Proterozoic Mazatzal Group, central Arizona: GSA Bulletin, v. 114, n. 12, p. 1535-1549.
- Crommelin, R.D., and Van Der Plas, L., 1961, Viridine, a rare constituent of Pleistocene sands: Geologie en Mijnbouw, v. 40, p. 189-193.
- Daniel, C.G., and Pyle, J.M., 2005, Monazite-Xenotime Thermochronometry and Al_2SiO_5 Reaction Textures in the Picuris Range, Northern New Mexico, USA: New Evidence for a 1450-1400 Orogenic Event: Journal of Petrology, v. 47, n. 1, p. 97-118.
- Dann, J. C., 1997, Pseudostratigraphy and origin of the Early Proterozoic Payson Ophiolite, central Arizona: GSA Bulletin, v. 109, p. 347-365.
- Davis, P.B., 2003, Structure, Petrology, and Geochronology of Middle Proterozoic Rocks in the Tusas Mountains of Northern New Mexico: Unpub. M.S. Thesis, University of Massachusetts, Amherst.
- Davis, R., 2006, Precambrian tidalites from the Baraboo Quartzite Wisconsin, U.S.A. Marine: Geology, v. 235, p. 247-253.
- Deer, W.,A., Howe, R.A., and Zussman, J., 1992, The Rock Forming Minerals, 2nd ed., Essex, Longman Scientific and Technical, 696 p.
- Dickinson, W.R., Beard, L.S., Brakenridge, G.R., Erjavec, J.L., Ferguson, R.C., Inman, K.F., Knepp, R.A., Lindberg, F.A., and Ryberg, P.T., 1983, Provenance of North American Phanerozoic sandstones in relation to tectonic setting: GSA Bulletin, v. 94, p. 222-235.
- Dott, J.H. Jr., 2003, The Importance of Eolian Abrasion in Supermature Quartz Sandstones and the Paradox of Weathering on Vegetation-Free Landscapes: Journal of Geology, v. 11, p. 387-405.
- Freer, R., 1981, The synthesis and some properties of Al-Fe-Mn viridines: $(\text{Al}_{2-x-y}\text{Mn}_x^{3+}\text{Fe}_y^{3+})\text{SiO}_5$: Progress in Experimental Petrology, v. 5, p. 187-190.
- Goode, J.W., and Siddoway, C.S., 1997, Mineral reactions and petrogenetic implications of Fe-Mn-andalusite, northern Wet Mountains, Colorado: Abstracts with Programs - Geological Society of America, v. 29, n. 2, p. 11.
- Gilkes, R.J., Scholz, G., and Dimmock, G.M., 1973, Lateritic deep weathering of granite: Journal of Soil Science, v. 24, n. 4, p. 523-536.
- Grambling, J.A., 1986, Crustal Thickening during Proterozoic metamorphism and deformation in New Mexico: Geology, v. 14, p. 149-152.

- Grambling, J.A., and Williams, M.L., 1985, The effects of Fe³⁺ and Mn³⁺ on aluminum silicate phase relations in north-central New Mexico, U.S.A: *Journal of Petrology*, v. 26, n. 2, p. 324-254.
- Grambling, J.A., Williams, M.L., Smith R.F., and Mawer, C.K., 1989, The role of crustal extension in the metamorphism of Proterozoic rocks in northern New Mexico, in Grambling, J.A., and Tewksbury, B.J., eds., *Proterozoic Geology of the southern Rocky Mountains: Geological Society of America Special Paper 235: Boulder, Colorado*, pp. 87-110.
- Grey, I.E., Li, C., and Watts, J.A., 1983, Hydrothermal synthesis of goethite-rutile intergrowth structures and their relationship to pseudorutile: *American Mineralogist*, v. 68, p. 981-988.
- Griffen, D.T., 1992, *Silicate Crystal Chemistry*, Oxford University Press, New York, 456p.
- Gunter, M., and Bloss, F.D., 1982, Andalusite-kanonaite series: lattice and optical parameters: *American Mineralogist*, v. 67, p. 1218-1228.
- Haggerty, S.E., 1991, Oxide textures- A mini-atlas, in Lindsley, D.H., ed., *Oxide minerals: Petrologic and magnetic significance: Mineralogical Society of America: Chelsea, Michigan*, p. 129-219.
- Heinrich, E.W., and Corey, A.F., 1959, Manganiian andalusite from Kiawa Mountain, Rio Arriba County, New Mexico: *American Mineralogist*, v. 44, p. 1261-71.
- Herbosch, A., 1968, La viridine et la braunite de Salm-Chateau: *Bulletin de la Societe Belge de Geologie, de Paleontologie et dHydrologie*, v. 76, n. 3, p. 183-202.
- Hill, B.M., and Bickford, M.E., 2001, Paleoproterozoic rocks of central Colorado: Accreted terranes or extended older crust?: *Geology*, v. 29, n. 11, p. 1015-1018.
- Hoffman, P.F., 1988, United Plates of America, the birth of a craton: *Annual Reviews of Earth and Planetary Sciences*, v. 16, p. 543-603.
- Holdaway, M.J., 1971, Stability of andalusite and the aluminum silicate phase diagram: *American Journal of Science*. v. 93, p. 138-149.
- Jessup, M.J., Karlstrom, K.E., Connelly, J., Williams, M.L., Livaccari, R., Tyson, A., and Rogers, S.A., 2005, Complex Proterozoic Crustal Assembly of Southwestern North America in an Arcuate Subduction System: the Black Canyon of the Gunnison, Southwestern Colorado, in Karlstrom, K. E., and Keller, G. R., eds., *The Rocky Mountain Region--An Evolving Lithosphere: Tectonics, Geochemistry, and Geophysics: Geophysical Monograph: American Geophysical Union, Washington, D.C.*, pp. 21-37.
- Jones, J. V., III, 2005, Timing and Style of Proterozoic Tectonism in the Southern Rocky Mountains: Constraining the evolution of an exhumed rheological transition in the middle crust: Unpub. Ph.D. Thesis, University of Texas, Austin.
- Karlstrom, K.E., Åhäll, K.I., Harlan, S.S., Williams, M.L., McLalland, J., and Geissman, J.W., 2001. Long-lived (1.8-1.0 Ga) convergent orogen in southern Laurentia, its extensions to Australia and Baltica, and implications for refining Rodinia: *Precambrian Research*, v. 11, p. 5-30.

- Karlstrom, K.E., Amato, J.M., Williams, M.L., Heizler, M., Shaw, C., Read, A., and Bauer, P., 2004, Proterozoic tectonic evolution of the New Mexico Region: a synthesis, in Mack, G.H., and Giles, K.A., eds., *The Geology of New Mexico-A Geologic History: Special Publications: New Mexico Geological Society, Las Cruces*, p.1-34.
- Karlstrom, K.E., and Bowring, S.A., 1987, Early Proterozoic assembly of tectonostratigraphic terranes in southwestern North America: *Journal of Geology*, v. 96, p. 561-576.
- Karlstrom, K.E., and the CD-ROM Working Group, 2002, Structure and evolution of the lithosphere beneath the Rocky Mountains: Initial results from the CD-ROM experiment: *GSA Today*, v. 12, p. 4-10.
- Karlstrom, K.E., Dallmeyer, D.A., and Grambling, J.A., 1997, Mesoproterozoic (1.42-1.35 Ga) regional metamorphism in New Mexico and implications for thermal evolution of lithosphere in the southwestern USA: Evidence from $^{40}\text{Ar}/^{39}\text{Ar}$ ages: *Journal of Geology*, v. 105, p. 205-223.
- Karlstrom, K.E., and Daniel, C.G., 1993, Restoration of Laramide right-lateral strike-slip in northern New Mexico by using Proterozoic piercing points: Tectonic implications from the Proterozoic to the Cenozoic: *Geology*, v. 21, n. 12, p.1139-1145.
- Karlstrom, K.E., and Houston, R.S., 1984, The Cheyenne Belt; Analysis of a Proterozoic suture in southern Wyoming: *Precambrian Research*, v. 25, p. 415-446.
- Karlstrom, K.E., Whitmeyer, S.J., Dueker, K., Williams, M.J., Bowring, S.A., Levander, A., Humphreys, E.D., Keller, R.G., and the CD-ROM Working Group., 2005, Synthesis of Results from the CD-ROM Experiment: 4-D Image of the Lithosphere Beneath the Rocky Mountains and Implications for Understanding the Evolution of the Continental Lithosphere, in Karlstrom, K. E., and Keller, G. R., eds., *The Rocky Mountain Region--An Evolving Lithosphere: Tectonics, Geochemistry, and Geophysics: Geophysical Monograph: American Geophysical Union, Washington, D.C.*, pp. 421-441.
- Kepes, G.J., 1984, Precambrian geology of the Kiowa Mountain area and Cerro Azul, north-central New Mexico: Unpub. M.S. Thesis, University of New Mexico, Albuquerque.
- Kerrick, D.M., 1990, The Al_2SiO_5 Polymorphs: *Reviews in Mineralogy*, v. 22, p. 1-46.
- Kopera, J., 2003, Monazite geochronology of the Ortega Quartzite: Documenting the extent of 1.4 Ga tectonism in northern New Mexico and across the orogen: Unpub. M.S. Thesis, University of Massachusetts, Amherst.
- Klemm, G., 1911, Uber Viridin, eine Abart des Andalusits: *Notizbl Ver Erdk Darmstadt*, v. 32, p. 4-13.
- Kramm, U., 1973, Cloritoid stability in manganese-rich low-grade metamorphic rocks, Venn-Stavelot Massif, Ardennes: *Contributions to Mineralogy and Petrology*, v. 41, p. 179-96.
- Kramm, U., 1979, Kanonaite-rich viridines from the Venn-Stavelot Massif, Belgian Ardennes: *Contributions to Mineralogy and Petrology*, v. 69, p. 387-395.
- Kugimiya, Y., Umino, S., Masuda, T., and Matsuda, Y., 2004, Kanonaite from the metamorphic sole of the Oman Ophiolite: evidence for high-f(O_2) conditions during retrograde metamorphism: *The Canadian Mineralogist*, v. 42, n. 1, p. 143-153.

- Kulish, U., 1961, Manganese-alumina rocks with viridine from the Archen of the Aldan shield (Russia). Academy of Science, USSR, Siberian Branch: Geology and Geophysics, v. 1, p. 53-65.
- Kulish, E.A., and Kulish, L.I., 1981, Viridine: Its nature, composition, and properties: *Geologiya i Geofizika*, v. 22, n. 10. p. 22-27.
- Kumar, B.N., and Hamisi, M.A., 1984, Mineral chemistry and stability relations of talc-piemontite-viridine bearing quartzite of Mautia Hill, Mpwapwa District, Tanzania and their similarity with the Konse Series rocks: International Geological Congress Abstracts, v. 27, n. 5, p. 1-19.
- Larrett, M.J.W., 1970, Contributions to Australasian Mineralogy: 1. Viridine in a beach sand from Western Australia: *Amdel Bulletin*, v. 10, p. 47-54.
- Mancheau, A., Schlegel, M.L., Musso, M., Sole, V.A., Gauthier, C., Petit, P.E., and Trolard, F., 2000, Crystal chemistry of trace elements in natural and synthetic goethite: *Geochimica et Cosmochimica Acta*, v. 64, n. 21, p. 3643-3661.
- Maynard, J.B., 2003, Manganiferous sediments, rocks, and ores, in Holland, H.D., and Turekian, eds., K.K., *Treatise on Geochemistry- vol. 7*: Elsevier, New York, p. 289-308.
- Medaris, L.G., Jr., Singer, B.S., Dott, R.H., Naymark, A., Johnson, C.M., and Scott, R.C., 2003, Late Paleoproterozoic climate, tectonics, and metamorphism in the southern Lake Superior Region and Proto-North America: Evidence from Baraboo interval quartzites: *Journal of Geology*, 111, p. 243-257.
- Nahon, D., and Parc, S., 1990, Lateritic concentrations of manganese oxyhydroxides and oxides: *Geologische Rundschau*, v. 79, n. 2, p. 319-326.
- Nakayma, T., Ishikawa, T., and Konno, T.J., 2005, Structure of titanium-doped goethite rust: *Corrosion Science*, v. 47, p. 2521-2530.
- Nelson, B.K., and DePaolo, D.J., 1985, Rapid production of continental crust 1.7-1.9 b.y. ago" Nd and Sr isotopic evidence from the basement of the North American mid-continent: *GSA Bulletin*, v. 96, p. 746-754.
- Nyman, M.W., Karlstrom, K.E., Kirby, E., and Graubard, C.M., 1994, Mesoproterozoic contractional orogeny in western North America: Evidence from ca. 1.4 Ga plutons: *Geology*, v. 22, p. 901-904.
- Odman, O.H., 1950, Manganese mineralization in the Ultevis Distrcit, Jokkmokk, North Sweden, Part 2: Mineralogical Notes: *Sveriges Geol. Undersok*, v. 44, n. 2, p. 1-28.
- Parc, S., Nahon, D., Tardy, Y., and Vieillard, P., 1989, Estimated solubility products and fields of stability for cryptometane, nsutite, birnessite, and lithophorite based on natural lateritic weathering sequences: *American Mineralogist*, v. 74, p. 466-475.
- Passchier, C.W., and Trouw, R.A.J., 2005, *Microtectonics*, 2nd ed: Berlin, Springer. 366p.
- Pedrick, J.N., 1995, Polyphase proterozoic tectonometamorphic history of the Taos Range, Northern New Mexico: Unpub. M.S. Thesis, University of New Mexico, Albuquerque.

- Pedrick, J.N. and Thompson, A.G., 1998, Anomalous tectonism and metamorphism in Proterozoic rocks at Comanche Point, Taos Range, northern New Mexico: Abstracts with Programs - Geological Society of America, v. 30, n. 7, p. 84-96.
- Pires, F.R.M., Dayan, H., and Amorim, H. S., 2000, Metasomatic kanonaite, occurrence and approach on its formation: Brazil. International Geological Congress at Serra das Bicas, Carrancas, Minas Gerais, Abstracts, v. 31.
- Prider, R.T., 1960, Viridine from Mt. Ragged, Western Australia: *The Indian Mineralogist*, v. 1, n. 1, p. 42-47.
- Roy, S., 2006, Sedimentary manganese metallogenesis in response to the evolution of the Earth system: *Earth Science Reviews*, v. 77, p. 273-305.
- Scheinhost, A.C., Stanjek, H., Schulze, D., Gasser, U., and Sparks, D., 2001, Structural environment and oxidation state of Mn in goethite-groutite solid solutions: *American Mineralogist*, v. 86, p. 139-146.
- Schreyer, W., Fransolet, A.M., and Bernhardt, H.J., 2001, Hollandite-strontiomelane solid solutions coexisting with kanonaite and braunite in late quartz veins of the Stavelot Massif, Ardennes, Belgium: *Contributions to Mineralogy and Petrology*, v. 141, p. 560-571.
- Schreyer, W., Bernhardt, H.J., Fransolet, A.M., and Armbruster, T., 2004, End-member ferrian kanonaite: an andalusite phase with one Al fully replaced by (Mn, Fe)³⁺ in a quartz vein from the Ardennes mountains, Belgium, and its origin: *Contributions to Mineralogy and Petrology*, v. 147, p. 276-287.
- Serdyuchenko, D. P., 1949, O sostave i khimicheskoi konstitutsii margantsovistykh andaluzitov: *Zapiski Vsesoyuznogo Mineralogicheskogo Obshchestva*, v. 78, p. 2133-135.
- Shaw, C., Karlstrom, K. E., and Heizler, M. T., 2005, 40Ar/39Ar Thermochronologic Record of 1.45-1.35 Ga Intracontinental Tectonism in the Southern Rocky Mountains: Interplay of Conductive and Advective Heating with Intracontinental Deformation, in Karlstrom, K. E., and Keller, G. R., eds., *The Rocky Mountain Region--An Evolving Lithosphere: Tectonics, Geochemistry, and Geophysics: Geophysical Monograph: American Geophysical Union, Washington, D.C.*, p. 163-184.
- Smith, R., 1988, Structural and metamorphic evolution of Proterozoic rocks in the Northern Taos Range, Taos County, New Mexico: Unpub. M.S. Thesis, University of New Mexico, Albuquerque.
- Soegaard, K., and Eriksson, K. A., 1985, Evidence of tide, storm, and wave interaction on a Precambrian siliciclastic shelf: the 1,700 m.y. Ortega Group, New Mexico: *Journal of Sedimentary Petrology*, v. 55, n. 5, p. 672-684.
- Soegaard, K., and Eriksson, K. A., 1986, Transition from arc volcanism to stable-shelf and subsequent convergent-margin sedimentation in northern New Mexico from 1.76Ga: *Journal of Geology*, v. 94, p. 47-66.
- Spear, F.S., 1993, *Metamorphic Phase Equilibria and Pressure-Temperature-Time Paths*, Monograph: Washington, D.C., Mineralogical Society of America, 799 p.

- Suzuki, J., Bamba, T., and Suzuki, Y., 1968, On the viridine quartz schist from the Chisaka area, Hidaka Province, Hokkaido. *Journal of the Japanese Association of Mineralogists: Petrologists and Economic Geologists*, v. 60, n. 5, p. 167-181.
- Tewksbury, B.J., 1989, Proterozoic geology of the Needle Mountains; A summary: *GSA Special Paper 235*, p. 65-73.
- Thorpe, D.G., and Burt, D.M., 1978, Viridine, otrellite, and piemontite from Squaw Peak, North Phoenix Mountains, Arizona. *Abstracts with Programs - Geological Society of America*, v. 10, n. 3, 150
- Trevena, A. S., 1979, Studies in sandstone petrology: Origin of Precambrian Mazatzal Quartzite and provenance of detrital feldspar: Unpub. Ph.D. Thesis, University of Utah, Salt Lake City.
- Whitney, D.L., and Dilek, A.Y., 1998, Metamorphism during Alpine Crustal Thickening and Extension in Central Anatolia, Turkey: The Nigde Metamorphic Core Complex: *Journal of Petrology*, v. 39, n. 7, p. 1385-1403.
- Williams, M.L., 1987, Stratigraphic, structural, and metamorphic relationships in Proterozoic rocks from northern New Mexico: Unpub. Ph.D. Thesis, University of New Mexico, Albuquerque.
- Williams, M.L., 1991, Heterogeneous deformation in a ductile fold-thrust belt: The Proterozoic structural history of the Tusas Mountains, New Mexico: *GSA Bulletin*, 103, p. 171-188.
- Williams, M.L., and Burr, J.L., 1994, Preservation and evolution of quartz phenocrysts in deformed rhyolites from the Proterozoic of southwestern North America: *Journal of Structural Geology*, v. 16, p. 203-221.
- Williams, M. L., and Jercinovic, M. J., 2002, Microprobe monazite geochronology: putting absolute time into microstructural analysis: *Journal of Structural Geology*, v. 24, p. 1013-1028.
- Williams, M. L., Jercinovic, M. J., Gonclaves, P., and Mahan, K., 2006, Format and philosophy for collecting, compiling, and reporting microprobe monazite ages: *Chemical Geology*, v. 225, p. 1-15.
- Williams, M. L., and Karlstrom, K. E., 1996, Looping P-T paths and high-T, low-P middle crustal metamorphism: Proterozoic evolution of the southwestern United States: *Geology*, v. 24, n. 12, p. 1119-1122.
- Williams, M. L., Karlstrom, K. E., Lanzirrotti, A., Read, A. S., Bishop, J. L., Lombardi, C. E., Pedrick, J. N., and Wingsted, M. B., 1999, New Mexico middle crustal cross sections: 1.65-Ga macroscopic geometry, 1.4-Ga thermal structure, and continued problems in understanding crustal evolution: *Rocky Mountain Geology*, v. 34, n. 1, p. 53-66.
- Wingsted, M.B., 1997, Microstructural history of the southern Picuris Range, North-Central New Mexico: Implications for the nature and timing of tectonism in the southwestern United States: Unpub. M.S. Thesis, University of Massachusetts, Amherst.
- Valeton, I., 1994, Element concentration and formation of ore deposits by weathering: *Catena*, v. 21, p. 99-129.

Vrana, S., Rieder, M., and Podlaha, J., 1978, Kanonaite, $(\text{Mn}^{3+}_{0.76}\text{Al}_{0.23}\text{Fe}^{3+}_{0.02})^{(6)}\text{Al}^{(5)}(\text{O}/\text{SiO}_4)$, a new mineral isotypic with andalusite: Contributions to Mineralogy and Petrology, v. 66, p. 325-332.